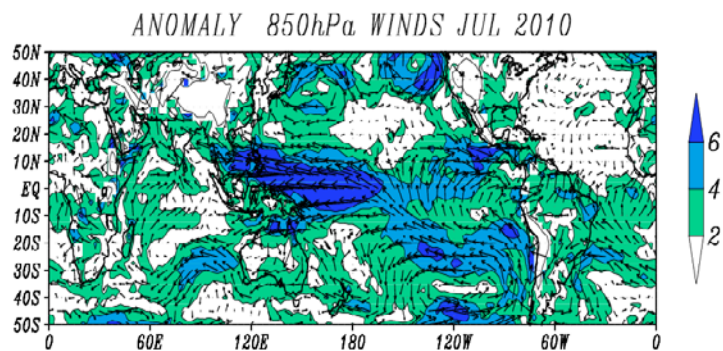
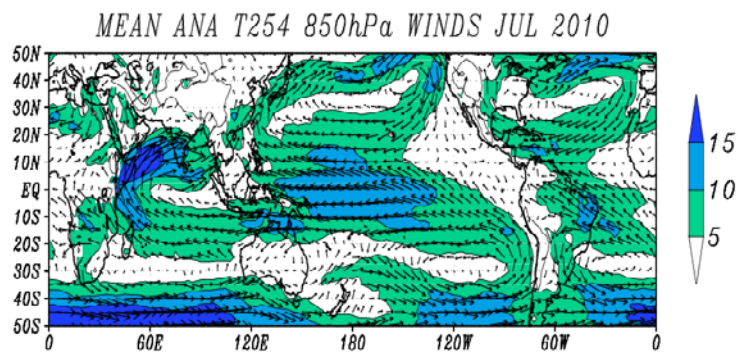


Monsoon-2010: Performance of T254L64 and T382L64 Global Assimilation – Forecast System



May, 2011

Please cite this report as given below:

NCMRWF, Ministry of Earth Sciences (MoES), Government of India, (May 2011):
'MONSOON-2010: Performance of the T254L64 and T382L64 Global Assimilation Forecast System', Report no. NMRF/MR/01/2011, with 177 pages,
Published by NCMRWF (MoES), A- 50 Institutional Area.

Disclaimer:

The geographical boundaries shown in this report do not necessarily correspond to political boundaries. The contents published in this report have been checked and authenticity assured within limitations of human errors. Short extracts may be reproduced, however the source should be clearly indicated.

Front Cover:

Geographical distribution of mean wind field (a) and anomaly (b) at 850 hPa; for July 2010. The anomalies are departures from the 1979-95 base period monthly means of NCEP reanalysis. [Units: m/s, Contour interval: 5m/s for analyses and 2m/s for anomalies]

This report was compiled by:

D. Rajan and G.R. Iyengar
NCMRWF/MoES

Acknowledgements:

Acknowledgement is also due to NCEP/NOAA for providing the GFS assimilation- forecast system codes and their support for its implementation in 2007 and 2010. Observed rainfall data was provided by India Meteorological Department.

For other details about NCMRWF see the website www.ncmrwf.gov.in



सत्यमेव जयते

डॉ. शैलेश नायक
DR. SHAILESH NAYAK




FOREWORD

The primary mandate of the Earth System Science Organisation, Ministry of Earth Sciences (MoES) is to provide the nation with best possible services in forecasting the monsoons, various weather/climate parameters, ocean state, earthquakes, tsunamis and other phenomena related to the earth system. Public/private/government demand for accurate prediction of weather and climate at short, seasonal and local scales are increasingly becoming a routine affair, more so due to the increased awareness of possible impacts of global climate change on extreme weather events. Improved and reliable forecast of weather and climate requiring routine integrations as well as research and development using very high resolution dynamical models with high complexity (e.g. coupled ocean-atmosphere-biosphere-cryosphere models) are thus becoming increasingly important.

The impact of meteorological services on society in general, and on safety of life and property in particular, is profound in terms of financial and social value. Weather services currently engage the India Meteorological Department (IMD), National Centre for Medium Range Weather Forecasting (NCMRWF), and the Indian Institute of Tropical Meteorology (IITM) in an integrated manner. While IMD is the National Weather Service, IITM is the specialized centre for basic research in meteorology and climate. NCMRWF is a specialized Centre undertaking developmental work in the field of numerical weather and climate modeling for improved weather and climate services of the country, with special emphasis on monsoon.

The science pertaining to monsoon has progressed substantially in the last two decades due to enhanced observations available from ground, ocean and space-based instruments along with the availability of necessary computing power for running numerical models in various spatial and temporal ranges. NCMRWF has vast experience in global and regional modeling and data-assimilation. The centre is making efforts to constantly imbibe the latest technologies in terms of data assimilation, improved resolution, better physics, and modeling techniques to capture the monsoon system in a most realistic manner. Towards this end, detailed performance of the models along with inter-comparison studies with major leading international NWP centres become important.

I am happy that NCMRWF has brought out this performance verification report titled "Monsoon-2010: Performance of T254L64 and T382L64 Global Assimilation-Forecast System". I am sure that this report will be of use to meteorological community at large, and forecast centres and researchers in particular. I wish NCMRWF scientists all success in their endeavor towards attaining skillful forecasts for the benefit of the society.


Shailesh Nayak



डॉ. स्वाति बासु
निदेशक

Dr. SWATI BASU
Director

email: swati@ncmrwf.gov.in
swati.basu@nic.in

भारत सरकार

(पृथ्वी विज्ञान मंत्रालय)

राष्ट्रीय मध्यम अवधि मौसम पूर्वानुमान केन्द्र

ए-50, इंस्टिट्यूशनल एरिया, फेज-II

सेक्टर-62, नोएडा-201309, उ.प्र.

GOVERNMENT OF INDIA

(Ministry of Earth Sciences)

National Centre for Medium Range Weather Forecasting

A-50, Institutional Area, Phase-II

Sector-62, NOIDA-201307 (UP)

PREFACE

Deterministic medium range weather prediction over Asian summer monsoon region remains a challenging task and needs specialized research and development efforts. The primary mission of NCMRWF is to provide accurate and reliable weather forecasts over India and neighboring regions using deterministic dynamical techniques. Advance information on weather especially in the medium range scale is of great utility for the scientific management primarily for agriculture and water resources apart from other user sectors of the country.

In order to enhance the performance and skill of forecasts there is a need for continuous improvement in the analysis forecast system that can be achieved through enhanced resolution of the numerical models, improved parameterization techniques of various physical processes and optimal utilization of data in the assimilation from various observation platforms. In this context it is important to benchmark models used for development vis-a-vis operational forecasting.

The present report evaluates the performance of NCMRWF global models during the year 2010. Results of an in-house examination of the performance of the two analysis-forecasts system at different horizontal resolutions, viz., 50 km and 35 km during the year 2010 are presented in the report. This will provide useful information to the researchers, scientists, academicians and operational forecasters engaged in monsoon prediction and research studies.

(SWATI BASU)

Earth System Science Organisation
National Centre for Medium Range Weather Forecasting (NCMRWF)
Document Control Data Sheet

S. No.		
1	Name of the Institute	National Centre for Medium Range Weather Forecasting (NCMRWF)
2	Document Number	NMRF/MR/01/2011
3	Date of publication	May, 2011
4	Title of the document	Monsoon - 2010: Performance of T254L64 and T382L64 Global Assimilation - Forecast System
5	Type of Document	Monsoon Report (MR), Scientific
6	No. of pages & figures	Pages 177 & Figures 82
7	Number of References	References 113
8	Author (S)	G.R Iyengar, E.N. Rajagopal, Saji Mohandas, A.K. Mitra, M. Das Gupta, R. Ashrit, D. Rajan, Ashok Kumar, Aditi, J.P. George, V.S. Prasad, J.V. Singh, Ranjeet Singh, M. Chourasia and T. Patnaik
9	Originating Unit	National Centre for Medium Range Weather Forecasting (NCMRWF), Ministry of Earth Sciences (MoES), Government of India, Noida
10	Abstract(100 words)	The Asian summer monsoon affects the lives and the economies of countries in the region. The primary mission of NCMRWF is to make available accurate and reliable weather forecasts over India using deterministic dynamical techniques. Prediction and simulation of Indian monsoon with NWP models still remains a very challenging scientific problem for the professionals engaged in the field. This report is to evaluate the performance of NCMRWF global models with the resolutions T254L64 and T382L64 to predict various components of the monsoon during the year 2010. Results of an in-house examination of the performance of the above analysis-forecasts system during the year 2010 are documented. This detailed report will provide useful information to the researchers, scientists, academicians and operational forecasters engaged in monsoon prediction and research studies.
11	Security classification	Unclassified
12	Distribution	Unrestricted
13	Key Words	Southwest Monsoon, Moisture Rainfall, Onset, Satellite, Boundary layer, Anomaly correlation, Errors, etc

EXECUTIVE SUMMARY

The most important rainy period for an agro-economically driven country like India is the 'southwest monsoon season'. The variability of the Indian summer monsoon rainfall affects the economy of the country significantly. The science pertaining to monsoon has progressed significantly in the last two decades due to an increase in the observations, improvement in understanding of underlying physical and dynamical processes and the availability of enhanced computing power.

NCMRWF constantly strives to imbibe the latest technologies in terms of data assimilation and modeling techniques to capture the monsoon system in a more realistic way. The global high-resolution assimilation-forecast system based on Global Forecast System (GFS) of National Centers for Environmental Prediction (NCEP), USA was implemented in 2007 at NCMRWF. Since then real time runs of that system are being carried out at T254L64 resolution and forecasts are generated up to 168 hours. An upgraded data assimilation and forecast model version of the NCEP GFS at T382L64 resolution was implemented in 2010. Experimental runs in real time mode were carried out during June-September 2010 period.

Verification/diagnostics of the analysis - forecast products is a crucial component of research and development activity in NCMRWF. A comprehensive set of diagnostics not only provides a summary of the model's prediction, but also indicates the suitability of the model for a variety of applications. Performance evaluation reports are being generated for comparing the skill of the NCMRWF analysis - forecast system vis-à-vis those of other major global NWP centres.

This report evaluates the performance of NCMRWF global analysis forecast systems with the resolutions T254L64 and T382L64 in predicting the various components of the monsoon during the year 2010.

Chapter 1 describes the various components of global data assimilation - forecast system like Data pre-processing and quality control, Global Data Assimilation Scheme (Gridpoint Statistical Interpolation (GSI) scheme), types and amount of observation assimilated, physics and dynamics used in the global forecast model.

Chapter 2 explains the mean circulation characteristics of this summer monsoon season along with their anomalies. Chapter 3(a) summarizes the nature and distribution of systematic error in the global T254L64 and T382L64 model forecasts and some verification scores. The T382 model forecasts feature relatively smaller RMSE as compared to the T254 model. Chapter 3(b) provides the verification statistics of the model rainfall forecasts. Both the models indicate higher forecast skill along the west coast, north-eastern states and along the foothills of Himalayas. The T382 model forecasts show marginally higher skill compared to the T254 model forecasts

The onset, advancement and withdrawal phases of the monsoon are addressed in Chapter 4. In 2010, the monsoon set in over Kerala on 31 May and covered the entire country by 6 July, earlier than its normal date of 15 July. Subsequently advancement of the monsoon across west coast was delayed by about a week time due to the formation of a very severe cyclonic storm. There was a

prolonged hiatus in the advancement of monsoon till the end of June due to the weakening of monsoon current. However, the withdrawal of monsoon from west Rajasthan was delayed and it commenced only on 27 September as compared to its normal date 1 September.

Monitoring and prediction of the position and intensity of the monsoon trough is important for assessment of monsoon activity. The characteristics of the two semi-permanent features namely Heat low and Monsoon trough as seen in the two global models analyses forecasts are examined in the Chapter 5. In general, the model forecasts tend to intensify the heat lows, compared to analysis.

The performance of the two versions of the global model's assimilation-forecasts system during the monsoon 2010 is respect of the Mascarene high, cross-equatorial flow, the low level westerly jet and the north-south pressure gradient along west coast are described briefly in Chapter 6. In general in a mean sense, the T382L64 system is seen to be slightly better than the T254L64 system in representing the monsoon low-level circulation features.

Chapter 7 documents the significant features like tropical easterly jet, location of the Tibetan anticyclone of the monsoon circulation over the Indian region at 200 hPa level and its interactions with mid-latitude disturbances as seen from model analysis and forecast during this season.

The parameterization of planetary boundary layer in atmospheric models is one of the most important aspects and needs special attention. These boundary layer height variations over a site are largely driven by the diurnal and seasonal changes in thermal instability and turbulence. The comparison of the boundary layer height in the above two models analysis-forecasts systems are discussed in the Chapter 8 of this report.

At the end of this report the skills of the location specific weather forecast for major cities and districts of India and customized forecasts based upon T254L64 and T382L64 are described in the Chapter 9 in detail.

In general in a mean sense, the T382L64 system is seen to be slightly better than the T254L64 system in representing the monsoon circulation features, rainfall prediction and other diagnostics undertaken.

Contents

S.No	Title	Page No
1	Overview of Global T254, and T382 Data Assimilation-Forecast Systems E.N.Rajagopal, M.Das Gupta, V.S.Prasad, Saji Mohandas	1
2	Mean Circulation Characteristics of the Summer Monsoon G.R.Iyengar	10
3 (a)	Systematic Errors in the Medium Range Prediction of the Summer Monsoon G.R.Iyengar	29
3 (b)	Verification of Model Rainfall Forecasts R. Ashrit, A.K.Mitra, G.R.Iyengar, Saji Mohandas, M.Chourasia	56
4 (a)	Onset and Advancement of Monsoon M. Das Gupta	66
4 (b)	Monsoon Indices: Onset, Strength and Withdrawal D. Rajan, G.R. Iyengar	74
5	Heat Low, Monsoon Trough, Lows and Depressions R.Ashrit, J.P.George, M.Chourasia	90
6	Mascarene High, Cross-Equatorial Flow, Low-Level Jet and North- South Pressure Gradient A.K.Mitra, M.Das Gupta, G.R.Iyengar	96

7	Tropical Easterly Jet, Tibetan High and Mid-Latitude Interaction	115
	Saji Mohandas	
8	Comparison of Planetary Boundary Layer (PBL) Height in T382L64 and T254L64 Analysis-Forecast Systems	126
	Aditi, E.N. Rajagopal	
9	Location Specific and Customized Weather Forecast for Cities and Districts: Evaluation of Forecast Skills	148
	Ashok Kumar, E.N.Rajagopal, J.V.Singh, Ranjeet Singh, Trilochan Patnaik	

1. Overview of Global Data Assimilation - Forecast System

E. N. Rajagopal, M. Das Gupta, V.S. Prasad and Saji Mohandas

1. Introduction:

The global high-resolution assimilation-forecast system based on Global Forecast System (GFS) of National Centers for Environmental Prediction (NCEP), USA was implemented on CRAY-X1E and Param Padma (IBM P5 cluster) in 2007 at NCMRWF. Since then real time runs of that system are being carried out at T254L64 resolution and forecasts are prepared up to 168 hours. The complete detail of the system was documented by Rajagopal et al. (2007).

In March 2010 a High Performance Computing (HPC) system based on IBM-p6 processor was installed at the centre. An upgraded data assimilation and forecast model package of GFS at T382L64 resolution was implemented on this system. Using this new T382L64 system, experimental runs in real time mode was carried out during June-September 2010 period.

In this report an attempt is made to verify and compare the evolutions of various weather systems and semi-permanent monsoon features during June-September 2010, in both T254L64 and T382L64 analysis-forecast systems.

2. Data Pre-Processing and Quality Control :

The meteorological observations from all over the globe and from various observing platforms are received at Regional Telecommunication Hub (RTH), New Delhi through Global Telecommunication System (GTS) and the same is made available to NCMRWF through a dedicated link at half hourly interval.

In decoding step, all the GTS bulletins are decoded from their native format and encoded into NCEP BUFR format using the various decoders. Global data assimilation system (GDAS) access the observational database at a set time each day (i.e., the data cut-off time, presently set as 6 hour), four times a day. Observations of a similar type [e.g., satellite-derived winds ("satwnd"), surface land reports ("adpsfc")] are dumped into

individual BUFR files in which, duplicate reports are removed, and upper-air report parts (i.e. AA,BB,CC,DD) are merged.

Last step of conventional data processing is the generation of "prebufr" files. This step involves the execution of series of programs designed to assemble observations dumped from a number of decoder databases, encode information about the observational error for each data type as well the background (first guess) interpolated to each data location, perform both rudimentary multi-platform quality control and more complex platform-specific quality control. Quality control of satellite radiance data is done within the global analysis scheme.

3. Global Data Assimilation Scheme:

The Gridpoint Statistical Interpolation (GSI) [Wu et al. 2002] replaced Spectral Statistical Interpolation (SSI) in the operational global suite with effect from 1 January 2009. Some positive impacts of GSI were seen in the parallel analysis system experiment conducted in August 2008 using NCMRWF's T254L64 model (Rajagopal et al., 2008) and hence it was decided to make GSI operational from January 2009.

GSI replaces spectral definition for background errors with grid point version based on recursive filters. Diagonal background error covariance in spectral space allows little control over the spatial variation of the error statistics as the structure function is limited to being geographically homogeneous and isotropic about its center (Parrish and Derber 1992; Courtier et al. 1998). GSI allows greater flexibility in terms of inhomogeneity and anisotropy for background error statistics. The major improvement of GSI over SSI analysis scheme is its latitude-dependent structure functions and has more appropriate background errors in the tropics. The background error covariances are isotropic and homogenous in the zonal direction. It has the advantage of being capable of use with forecast systems in both global and regional scale. It also has capability to assimilate newer satellite, radar, profiler and surface data. Assimilation capability of cosmic GPS – Radio Occultation, Doppler radial velocities and reflectivity, precipitation, cloud and ozone observations are the scientific advancement in GSI over SSI. A detailed description of GSI code and its usage can be found in GSI User's Guide (DTC, 2009)

The analysis variables in GSI are stream function, surface pressure, unbalanced velocity potential, unbalanced virtual temperature, unbalanced surface pressure, relative humidity, surface skin temperature, ozone mixing ratio and cloud condensate mixing ratio. Horizontal resolution of the analysis system is quadratic T254 Gaussian grid (approximately 0.5 x 0.5 degree). The analysis is performed directly in the model's vertical coordinate system. This sigma ($\sigma = p/p_s$) coordinate system extends over 64 levels from the surface (~997.3 hPa) to top of the atmosphere at about 0.27hPa. This domain is divided into 64 layers with enhanced resolution near the bottom and the top, with 15 levels is below 800 hPa, and 24 levels are above 100 hPa.

Meteorological observations from various types of observing platforms that were assimilated into both T254L64 and T382L64 global analysis schemes at NCMRWF are shown Table 3.

Satellite Radiance Data Processing

The NOAA level 1b radiance data sets obtained from NESDIS/NOAA contain raw instrument counts, calibration coefficients and navigation parameters. The data is in a packed format and all the band data exists in a 10 bit format. The data product, in addition to video data, contains ancillary information like Earth Location Points (ELPs), solar zenith angle and calibration. The raw counts in the level 1b files are transformed using the calibration coefficients in the data file to antenna temperatures and then to brightness temperatures (for AMSU-A data) using the algorithm of Mo (1999). The geometrical and channel brightness temperature data extracted from orbital data are then binned in 6 hour periods (+/-3hrs) of the analysis time for use in the assimilation system. The use of the level 1b data requires the application of quality control, bias correction, and the appropriate radiative transfer model (Derber & Wu, 1998; McNally et al., 1999). The radiative transfer model (CRTM) uses the OPTRAN transmittance model to calculate instrument radiances and brightness temperatures and their Jacobians.

In the case of T254, satellite radiances (level 1b) from AMSU-A, AMSU-B/MHS & HIRS on board NOAA-15, 16, 18, Metop-A and SBUV ozone profiles from NOAA-16 & 17 were downloaded from NOAA/NESDIS ftp server. The same are processed and encoded in NCEP BUFR. As NCMRWF does not have access to the radiance (level 1b) data of NOAA-19 and other latest satellites (namely, GPSRO, AIRS, AMSRE, Precipitation rates from SSM/I and TRMM), all the processed radiance data of NCEP's

GFS system were downloaded and used in T382 system. As a consequence more satellite radiance data were assimilated into T382 system in comparison to T254.

Table 3: Observations used in T254L64 and T383L64 systems

<i>Observation type</i>	<i>Variables</i>
Radiosonde	u, v, T, q, p _s
Pibal winds	u, v
Wind profilers	u, v
Surface land observations	p _s
Surface ship and buoy observations	u, v, T, q, p _s
Conventional Aircraft observations (AIREP)	u, v, T
AMDAR Aircraft observations	u, v, T
ACARS Aircraft observations	u, v, T
GMS/MTSAT AMV (BUFR)	u, v, T
INSAT AMV (SATOB)	u, v, T
METEOSAT AMV (BUFR)	u, v, T
GOES (BUFR)	u, v, T
SSM/I	Surface wind speed
AMSU-A radiance	Bright. Temp.
AMSU-B radiance	Bright. Temp.
HIRS radiance	Bright. Tem
SBUV ozone	Total Ozone

Upgrades to GSI from T254 to T382

- Upgraded to NCEP's latest version of GSI. Incremental improvement due to addition of new data types.
- Inclusion of AIRS data; Use of variational qc; Addition of background error covariance input file; Reduction of number of airs water vapor angels used
- Change in land/snow/ice skin temperature variance
- Flow dependent re-weighting of background error variances

- Use of new version and coefficients for community radiative transfer model
- Modification of height assignment for height based wind observations;
Modification of surface land use file to remove a few permanent (~12) glacial points to improve surface temperature forecasts over those points.

4. Global Forecast Model:

The forecast model is a primitive equation spectral global model with state of art dynamics and physics (Kanamitsu 1989, Kanamitsu et al. 1991, Kalnay et al. 1990, Moorthi et al., 2001, EMC, 2003). Model horizontal and vertical resolution & representation are same as described in analysis scheme. The main time integration is leapfrog for nonlinear advection terms. Semi-implicit method is used for gravity waves and for zonal advection of vorticity and moisture. An Asselin (1972) time filter is used to reduce computational modes. With a spectral truncation of T254 waves in the zonal direction the size of Gaussian grid is 768x384 which is approximately 50 km near the equator. The model time step for T254 is 7.5 minutes for computation of dynamics and physics. The full calculation of longwave radiation is done once every 3 hours and shortwave radiation every hour (but with corrections made at every time step for diurnal variations in the shortwave fluxes and in the surface upward longwave flux). Mean orographic heights on the Gaussian grid are used. Negative atmospheric moisture values are not filled for moisture conservation, except for a ‘temporary moisture filling’ that is applied in the radiation calculation. The T254 model outputs were post-processed at 0.5 degree horizontal resolution at NCMRWF.

Various physical parameterization schemes used in both the models are summarized briefly in Table 4.

Table 4: Physical Parameterization schemes in T254L64 and T382L64

Physics	Scheme
Surface Fluxes	Monin-Obukhov similarity
Turbulent Diffusion	Non-local Closure scheme (Hong and Pan (1996))
SW Radiation	Based on Hou et al. 2002 –invoked hourly
LW Radiation	Rapid Radiative Transfer Model (RRTM) (Mlawer et al. 1997). –invoked 3 hourly
Deep Convection	SAS convection (Pan and Wu (1994))
Shallow Convection	Shallow convection Following Tiedtke (1983)
Large Scale Condensation	Large Scale Precipitation based on Zhao and Carr (1997)
Cloud Generation	Based on Xu and Randall (1996)
Rainfall Evaporation	Kessler's scheme
Land Surface Processes	NOAH LSM with 4 soil levels for temperature & moisture Soil moisture values are updated every model time step in response to forecasted land-surface forcing (precipitation, surface solar radiation, and near-surface parameters: temperature, humidity, and wind speed).
Air-Sea Interaction	Roughness length determined from the surface wind stress (Charnock (1955)) Observed SST, Thermal roughness over the ocean is based on a formulation derived from TOGA COARE (Zeng et al., 1998).
Gravity Wave Drag	Based on Alpert et al. (1988)

Upgrades to forecast model from T254 to T382

- Inclusion of new ESMF library version 3.1.0rp2)
- Hybrid sigma-pressure vertical coordinate system. In vertical 64 hybrid sigma-p levels are used. Model's lower levels are terrain following and transforming to pure pressure levels in the upper troposphere (Sela, 2009).
- Some modifications in radiation and clouds. It includes the definition of low clouds which was changed to combine the previously separately defined boundary-layer cloud and low cloud. High, Medium and Low clouds domain boundaries are adjusted for better agreement with the observations.
- With a spectral truncation of 382 waves in the zonal direction the size of Gaussian grid is 1152x576 which is approximately 35 km near the equator.
- The time step is 3 minutes and it is run for 10 days daily.
- The T382 model outputs are post-processed at 0.32 degree horizontal resolution at NCMRWF

5. Computational Performance:

In the case of T254, one cycle of analysis (GSI) took about 70 minutes of computing time on 27 MSPs (Multi-Streaming Processors) Cray X1E and the forecast model took about 120 minutes of computation time in 27 MSPs of Cray X1E for a 168-hr model forecast. T382 model takes around 30 minutes for a ten-day forecast on IBM HPC with a combination of 24 nodes and 8 processors.

References

- Alpert, J.C., S-Y Hong and Y-J Kim, 1996: Sensitivity of cyclogenesis to lower troposphere enhancement of gravity wave drag using the Environmental Modeling Center medium range model. *Proc. 11th Conference on NWP, Norfolk*, 322-323.
- Asselin, R., 1972: Frequency filter for time integrations. *Mon. Wea. Rev.*, 100, 487-490.
- Charnock, H., 1955: Wind stress on a water surface. *Quart. J. Roy. Meteor. Soc.*, 81, 639-640.
- Courtier, P., and Coauthors, 1998: "The ECMWF implementation of the three-dimensional variational assimilation (3D-Var). I: Formulation, *Quarterly Journal of Royal Meteorological Society*, 124, pp. 1783-1807.
- Derber, J. C. and W.-S. Wu, 1998: The use of TOVS cloud-cleared radiances in the NCEP SSI analysis system. *Mon. Wea. Rev.*, 126, 2287 - 2299
- Derber, J. C., D.F. Parrish and S. J. Lord, 1991: The new global operational analysis system at the National Meteorological Center. *Weather and Forecasting*, 6, 538-547.
- DTC, 2009: Gridpoint Statistical Interpolation (GSI) Version 1.0 User's Guide, NCAR/NCEP, NOAA/GSD, ESRL, NOAA, 77 p.
(http://www.dtcenter.org/com-GSI/users/docs/users_guide/GSIUserGuide_V1.0.pdf/).
- Environmental Modeling Centre, 2003: The GFS Atmospheric Model, NCEP Office Note 442, 12pp.
- Hong, S.-Y. and H.-L. Pan, 1996: Nonlocal boundary layer vertical diffusion in a medium-range forecast model. *Mon. Wea. Rev.*, 124, 2322-2339.
- Hou, Y-T, K. A. Campana and S-K Yang, 1996: Shortwave radiation calculations in the NCEP's global model. *International Radiation Symposium, IRS-96, August 19-24, Fairbanks, AL*.

- Kalnay, M. Kanamitsu, and W.E. Baker, 1990: Global numerical weather prediction at the National Meteorological Center. *Bull. Amer. Meteor. Soc.*, 71, 1410-1428.
- Kanamitsu, M., 1989: Description of the NMC global data assimilation and forecast system. *Weather and Forecasting*, 4, 335-342.
- Kanamitsu, M., J.C. Alpert, K.A. Campana, P.M. Caplan, D.G. Deaven, M. Iredell, B. Katz, H.-L. Pan, J. Sela, and G.H. White, 1991: Recent changes implemented into the global forecast system at NMC. *Weather and Forecasting*, 6, 425-435.
- McNally, A. P., J. C. Derber, W.-S. Wu and B.B. Katz, 2000: The use of TOVS level-1 radiances in the NCEP SSI analysis system. *Quart.J.Roy. Meteorol. Soc.* , 129, 689-724
- Mlawer, E.J., S.J. Taubman, P.D. Brown, M.J. Iacono, and S.A. Clough, 1997: Radiative transfer for inhomogeneous atmospheres: RRTM, a validated correlated-k model for the longwave. *J. Geophys. Res.*, 102, 16663-16682.
- Moorthi, S., H. L. Pan and P. Caplan, 2001: Changes to the 2001 NCEP operational MRF/AVN global analysis/forecast system. NWS Technical Procedures Bulletin, 484, pp14.
[Available at <http://www.nws.noaa.gov/om/tpb/484.htm>].
- Parrish, D.E. and J.C. Derber, 1992. The National Meteorological Center's spectral statistical-interpolation analysis system. *Mon. Wea. Rev.*, 120, 1747-1763.
- Pan, H.-L. and W.-S. Wu, 1995: Implementing a Mass Flux Convection Parameterization Package for the NMC Medium-Range Forecast Model. *NMC Office Note, No. 409*, 40 pp.
- Rajagopal, E.N., M. Das Gupta, Saji Mohandas, V.S. Prasad, John P. George, G.R. Iyengar and D. Preveen Kumar, 2007: Implementation of T254L64 Global Forecast System at NCMRWF, *NMRF/TR/1/2007*, 42 p.
- Rajagopal, E.N., Surya K. Dutta, V.S. Prasad, Gopal R. Iyengar and M. Das Gupta, 2008: Impact of Gridpoint Statistical Interpolation Scheme over Indian Region, *Extended Abstracts - Int'l Conf. on Progress in Weather and Climate Modelling over Indian Region, 9-12 December 2008, NCMRWF, NOIDA, 202-205*.
- Sela, J., 2009, Implementation of the sigma pressure hybrid coordinate into GFS, NCEP Office Note # 461
[Available at <http://www.emc.ncep.noaa.gov/officenotes/FullTOC.html#2000>].
- Tiedtke, M., 1983: The sensitivity of the time-mean large-scale flow to cumulus convection in the ECMWF model. *ECMWF Workshop on Convection in Large-Scale Models, 28 November-1 December 1983, Reading, England*, pp. 297-316.

- Wan-Shu Wu, R. James Purser, and David F. Parrish, 2002: Three-Dimensional Variational Analysis with Spatially Inhomogeneous Covariances. *Monthly Weather Review*, 130, 2905–2916.
- Xu, K. M., and D. A. Randall, 1996: A semiempirical cloudiness parameterization for use in climate models. *J. Atmos. Sci.*, 53, 3084-3102.
- Zeng, X., M. Zhao, and R.E. Dickinson, 1998: Intercomparison of bulk aerodynamical algorithms for the computation of sea surface fluxes using TOGA COARE and TAO data. *J. Climate*, 11, 2628-2644.
- Zhao, Q. Y., and F. H. Carr, 1997: A prognostic cloud scheme for operational NWP models. *Mon. Wea. Rev.*, 125, 1931-1953.

2. Mean Circulation Characteristics of the Summer Monsoon

G. R. Iyengar

1 Introduction

In this chapter, mean circulation characteristics of the summer monsoon season of 2010 and their anomalies are examined. The anomalies are departures of the mean analyses of the T254L64 Global Forecast system (GFS) from the 1979–95 base period monthly means of NCEP reanalysis. For brevity, the anomalies of the mean analyses of the T382L64 GFS are not discussed as the large scale circulation features in both these systems are similar.

2. Wind Fields

The geographical distribution of the mean analysed wind fields for the months of June, July, August and September at 850, 700, 500 and 200hPa from the T254L64 GFS and their monthly anomalies are shown in Fig. 1(a-b) to Fig. 16(a-b) respectively. The anomalous features identified from the mean circulation of each month of monsoon-2010 are listed below.

2.1 June

At 850 and 700 hPa levels, anomalous easterlies were seen over the peninsula and adjoining Arabian Sea. Anomalous westerlies prevailed over the northern plains in the lower levels, indicating weak monsoon conditions. This anomalous circulation feature was associated with the prolonged hiatus in the advancement of monsoon over India during the third and fourth weeks of June. At 500 hPa level, anomalous easterlies were seen over the peninsula and an anomalous cyclonic circulation was seen over the northwestern parts of India. At 200 hPa level, an anomalous cyclonic circulation was seen over the northern parts of India

2.2 July

In the lower tropospheric levels (850 - 500hPa) anomalous easterlies were seen over the northern parts of India, indicating active monsoon conditions. At 850 and 700 hPa levels, anomalous south-easterlies and southerlies were seen over peninsula and Arabian Sea. At 200 hPa level, anomalous westerlies were seen over the southern peninsular India, indicating that the Tropical Easterly Jet was weaker than normal.

2.3 August

In the lower tropospheric levels (850 and 700hPa) anomalous easterlies were seen over the entire country. Anomalous southerlies were also seen over the Arabian Sea in the lower tropospheric levels. At 200 hPa level, anomalous westerlies were seen over the southern peninsular India.

2.4 September

In the lower tropospheric levels (850 and 700hPa) anomalous southerlies were seen over the Arabian Sea and adjoining north-western parts of the country. At 500 and 200 hPa levels an anomalous cyclonic circulation was seen over the regions adjoining the north-western parts of India. The rainfall activity was considerably above normal over the north-west homogeneous region of India. At 200 hPa level, anomalous westerlies were seen over the peninsular India

Legends for figures:

Figure 1: Geographical distribution of mean wind field (a) and anomaly (b) at 850hPa; for June 2010. The anomalies are departures from the 1979–95 base period monthly means of NCEP reanalysis. [Units: m/s, Contour interval: 5m/s for analyses and 3m/s for anomalies]

Figure 2: Same as in Figure 1, but for 700hPa.

Figure 3: Same as in Figure 1, but for 500hPa.

Figure 4: Same as in Figure 1, but for 200hPa. [Units: m/s, Contour interval: 10m/s for analyses and 5m/s for anomalies]

Figure 5: Same as in Figure 1, but for July 2010.

Figure 6: Same as in Figure 2, but for July 2010.

Figure 7: Same as in Figure 3, but for July 2010.

Figure 8: Same as in Figure 4, but for July 2010.

Figure 9: Same as in Figure 1, but for August 2010.

Figure 10: Same as in Figure 2, but for August 2010.

Figure 11: Same as in Figure 3, but for August 2010.

Figure 12: Same as in Figure 4, but for August 2010.

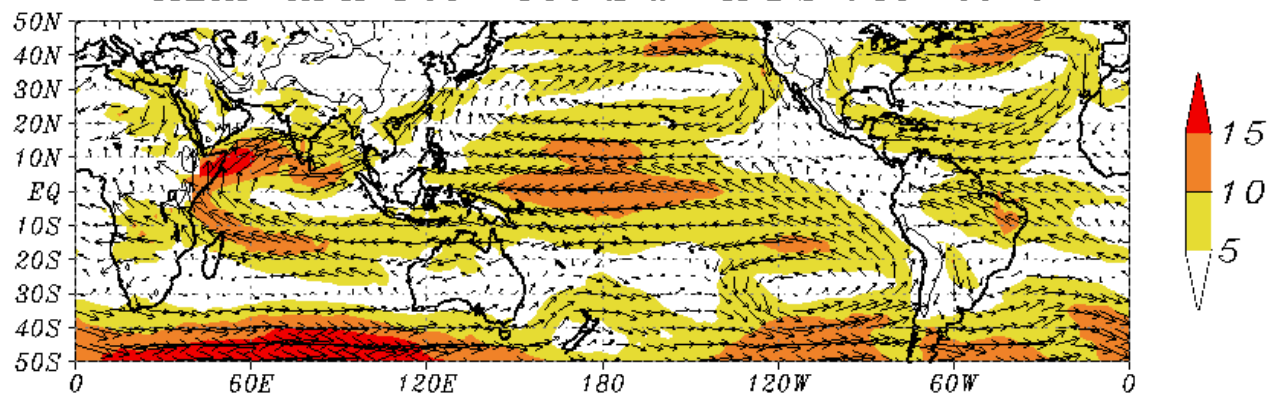
Figure 13: Same as in Figure 1, but for September 2010.

Figure 14: Same as in Figure 2, but for September 2010.

Figure 15: Same as in Figure 3, but for September 2010.

Figure 16: Same as in Figure 4, but for September 2010.

MEAN ANA T254 850hPa WINDS JUN 2010



ANOMALY 850hPa WINDS JUN 2010

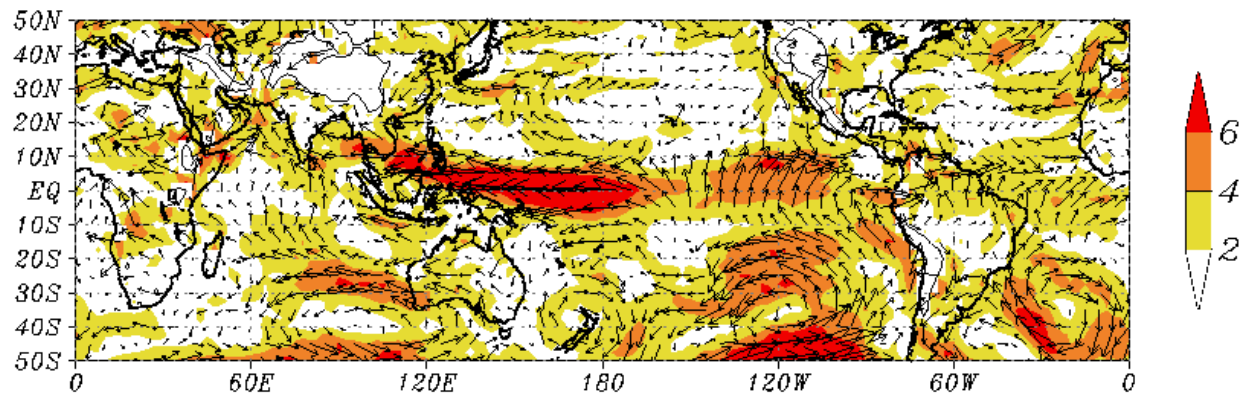
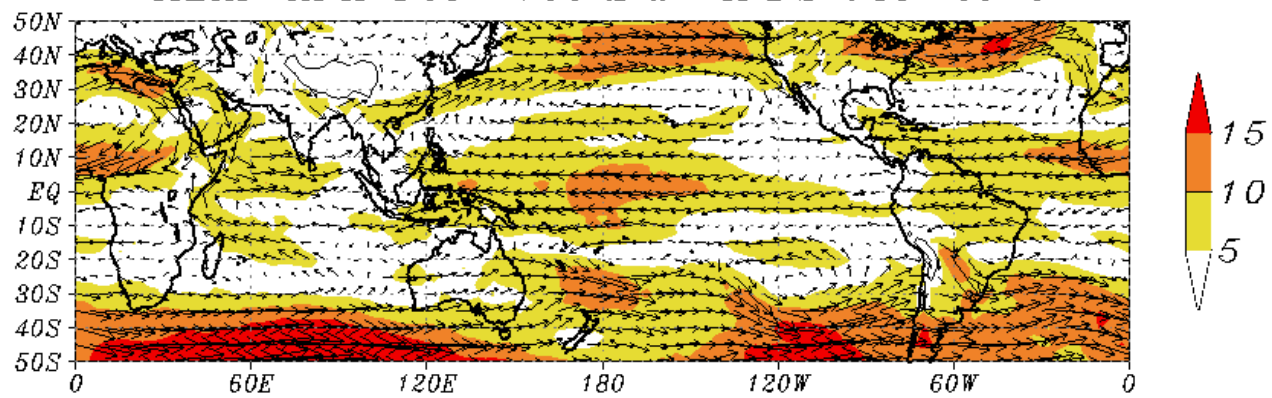


Fig. 1

MEAN ANA T254 700hPa WINDS JUN 2010



ANOMALY 700hPa WINDS JUN 2010

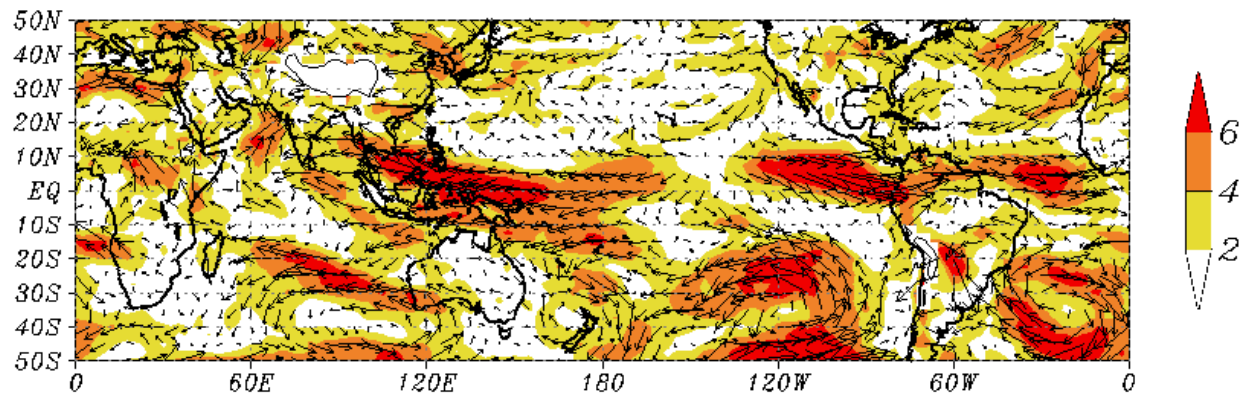
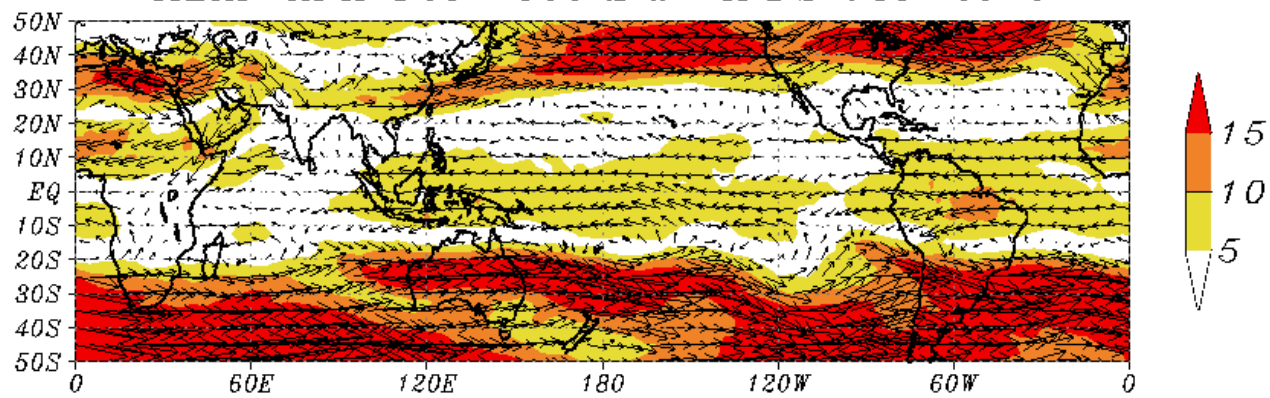


Fig. 2

MEAN ANA T254 500hPa WINDS JUN 2010



ANOMALY 500hPa WINDS JUN 2010

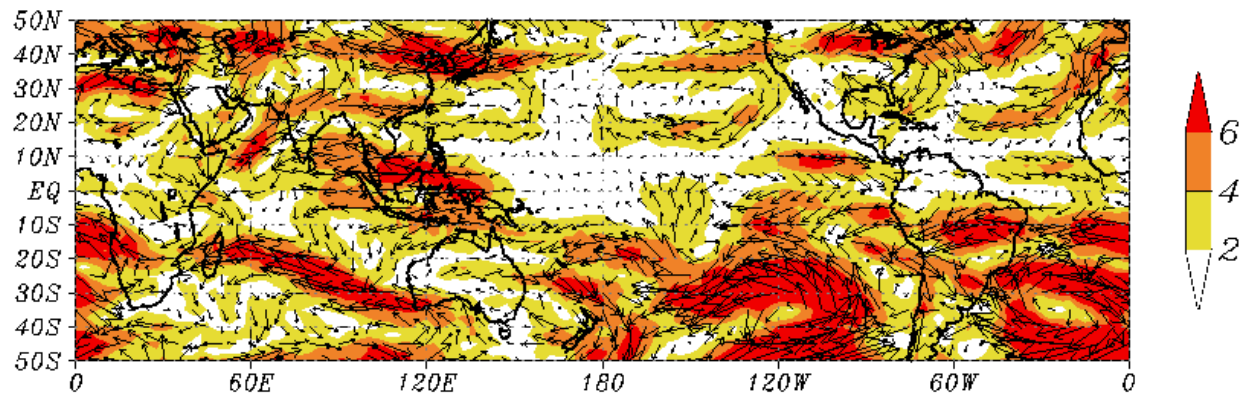
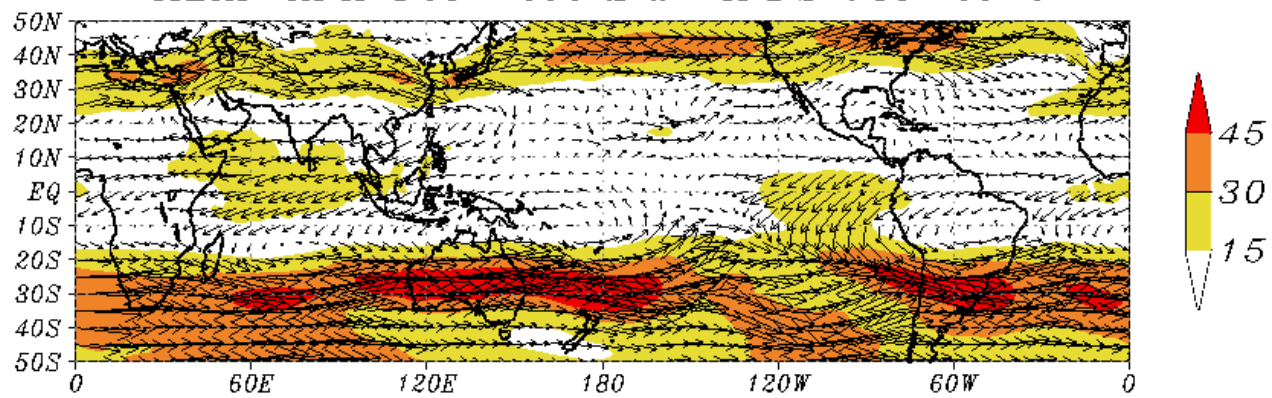


Fig. 3

MEAN ANA T254 200hPa WINDS JUN 2010



ANOMALY 200hPa WINDS JUN 2010

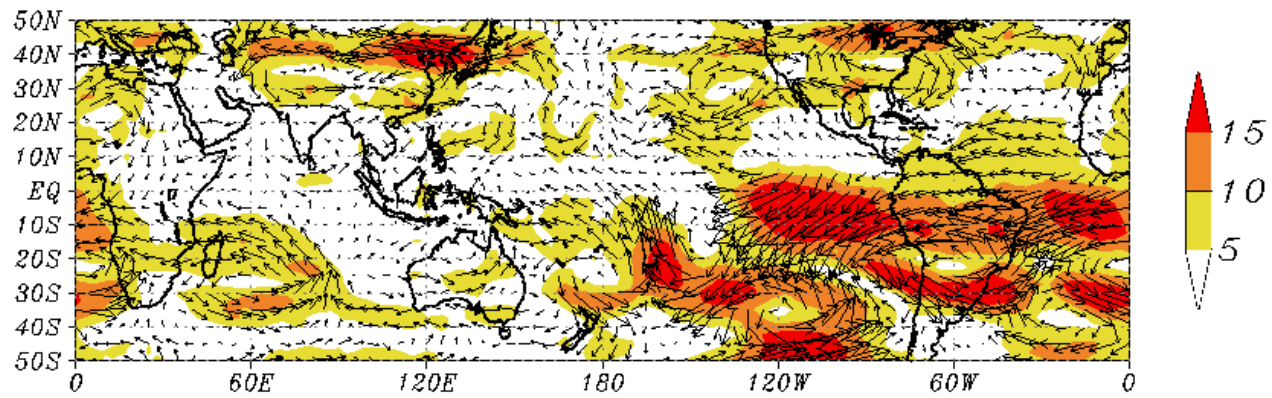
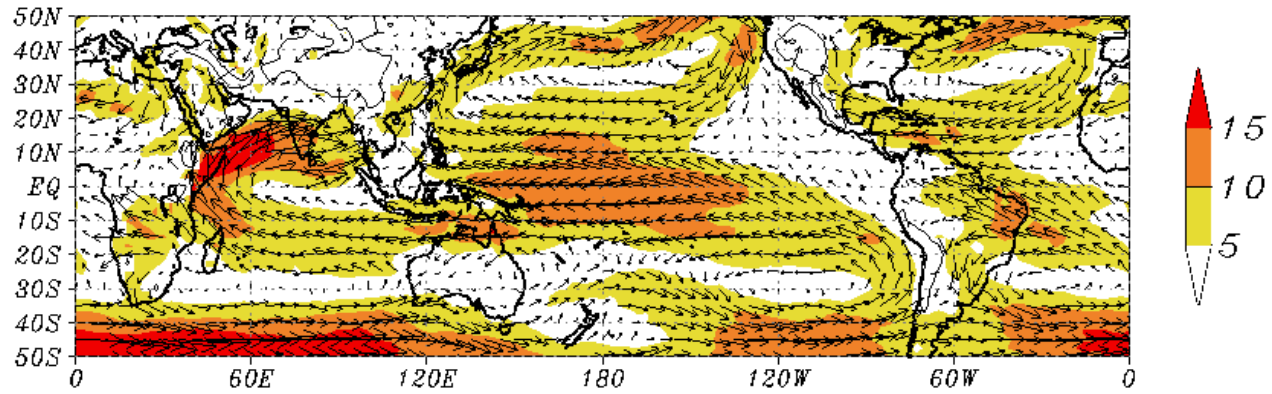


Fig. 4

MEAN ANA T254 850hPa WINDS JUL 2010



ANOMALY 850hPa WINDS JUL 2010

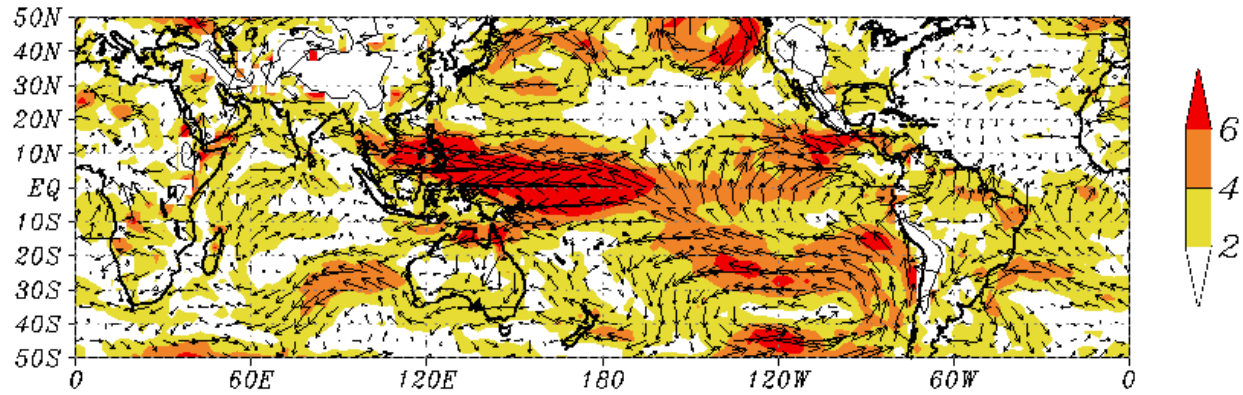
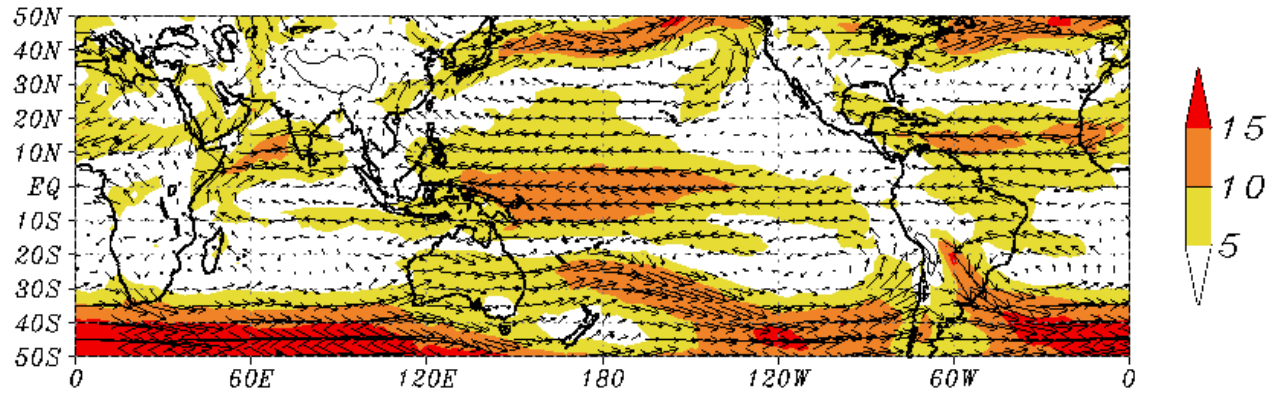


Fig. 5

MEAN ANA T254 700hPa WINDS JUL 2010



ANOMALY 700hPa WINDS JUL 2010

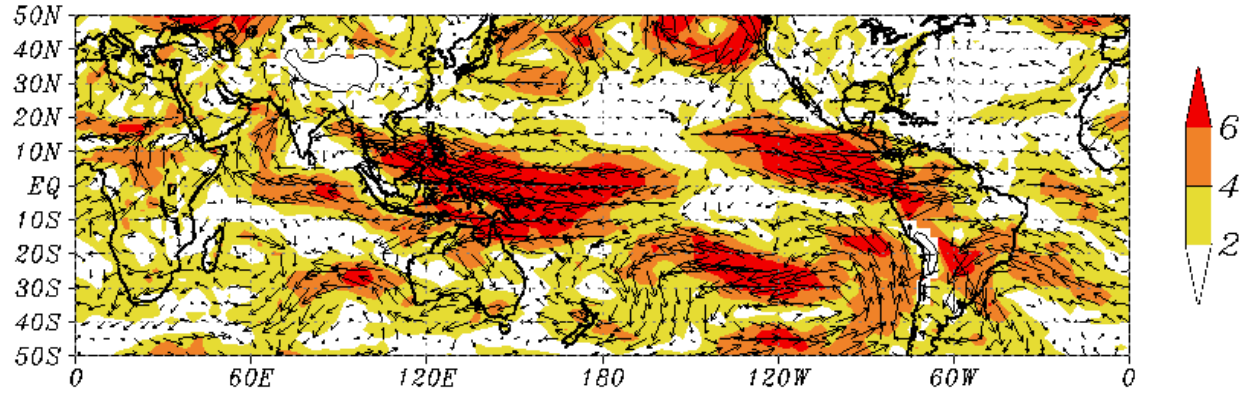
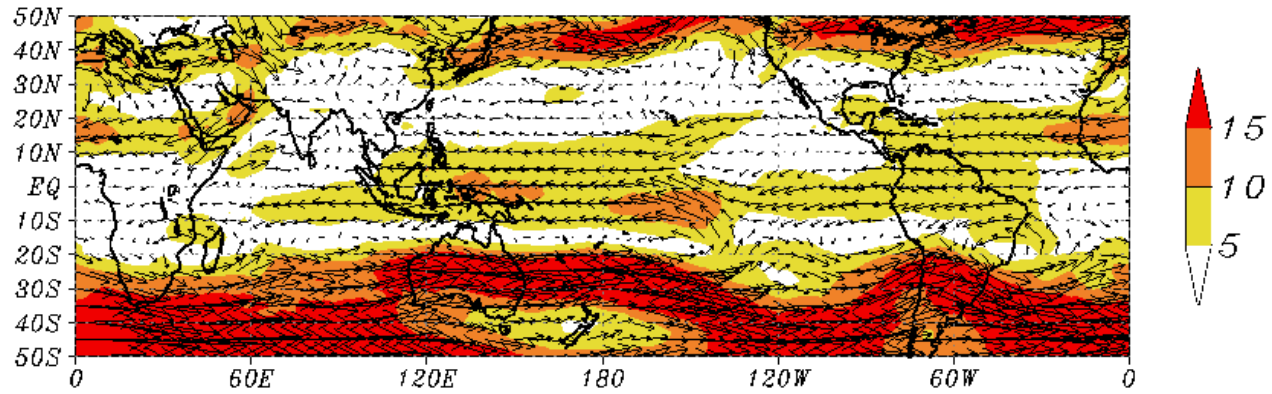


Fig. 6

MEAN ANA T254 500hPa WINDS JUL 2010



ANOMALY 500hPa WINDS JUL 2010

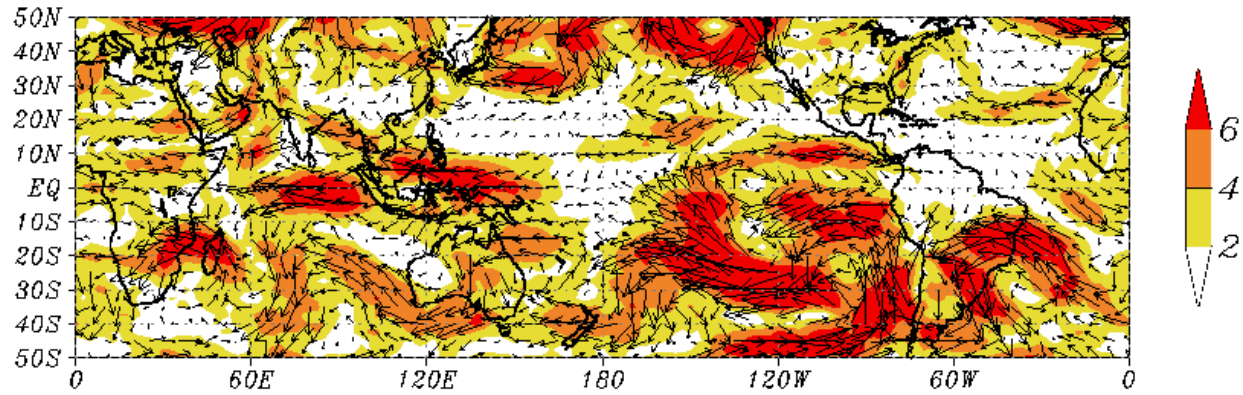
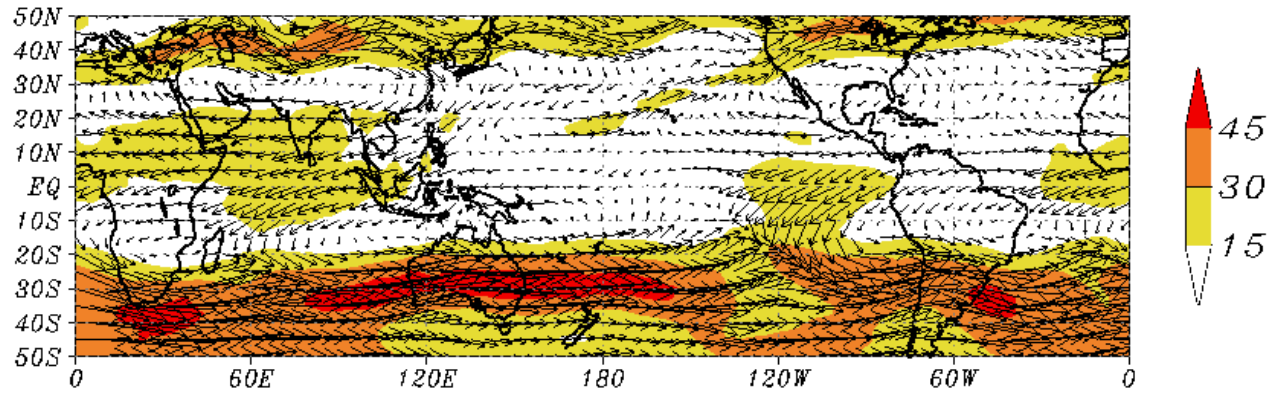


Fig. 7

MEAN ANA T254 200hPa WINDS JUL 2010



ANOMALY 200hPa WINDS JUL 2010

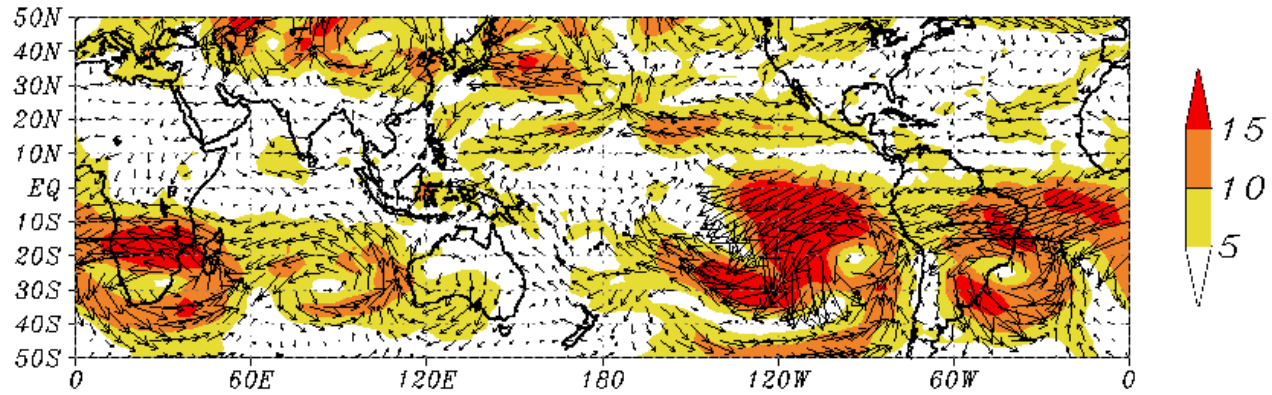
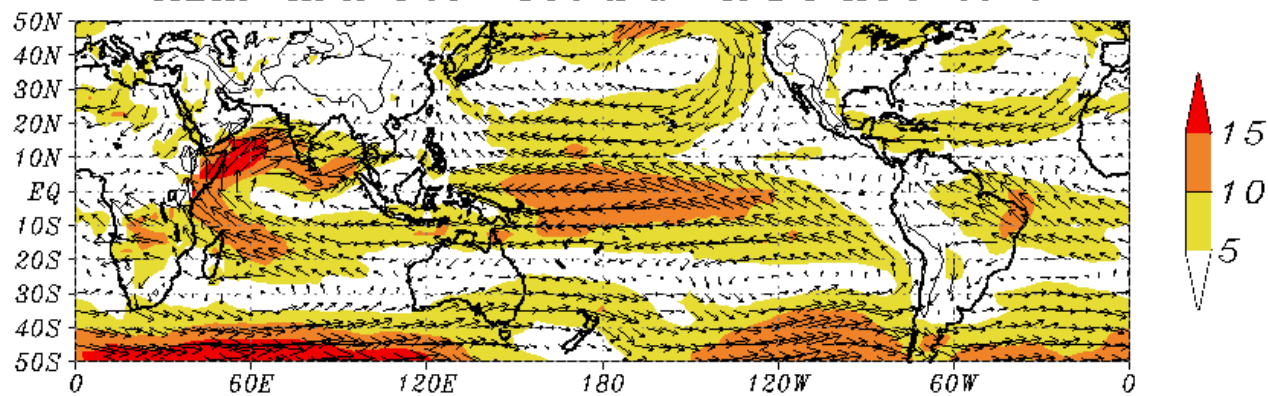


Fig. 8

MEAN ANA T254 850hPa WINDS AUG 2010



ANOMALY 850hPa WINDS AUG 2010

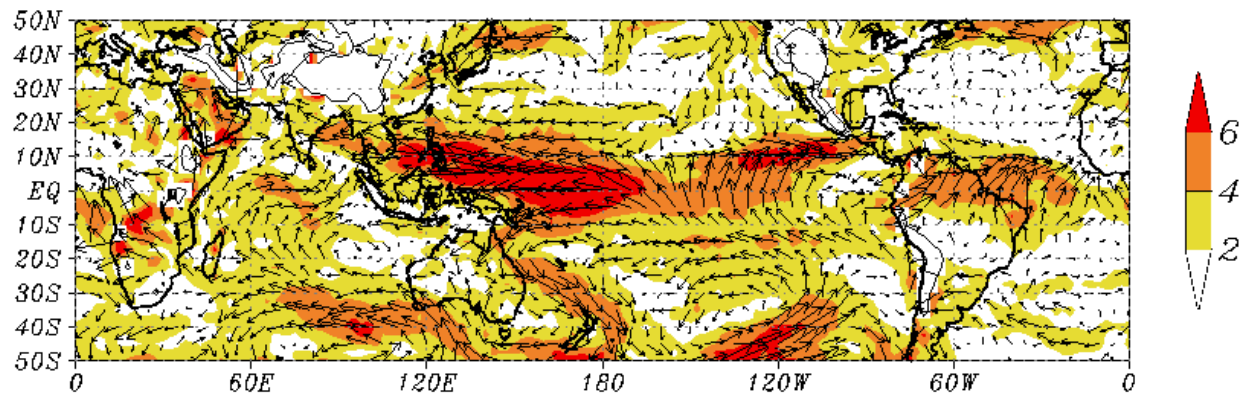
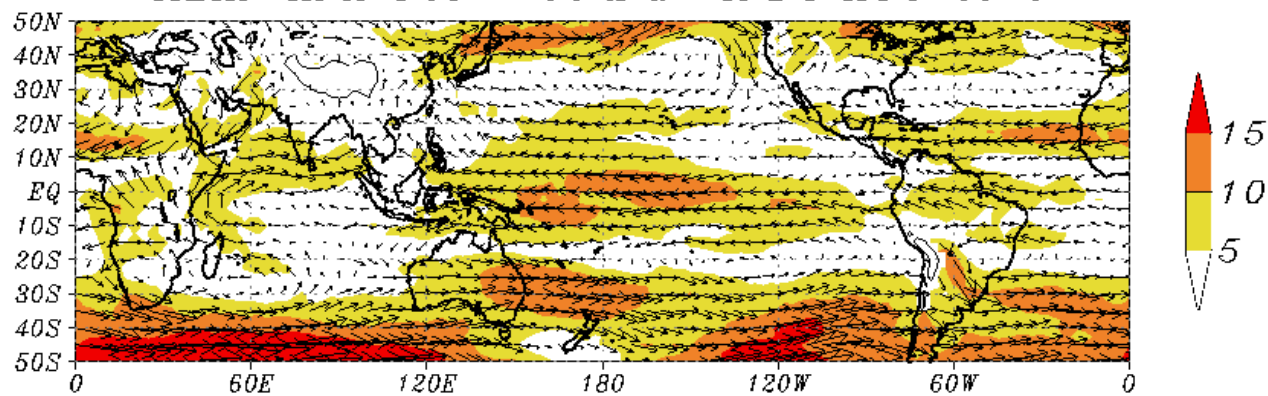


Fig. 9

MEAN ANA T254 700hPa WINDS AUG 2010



ANOMALY 700hPa WINDS AUG 2010

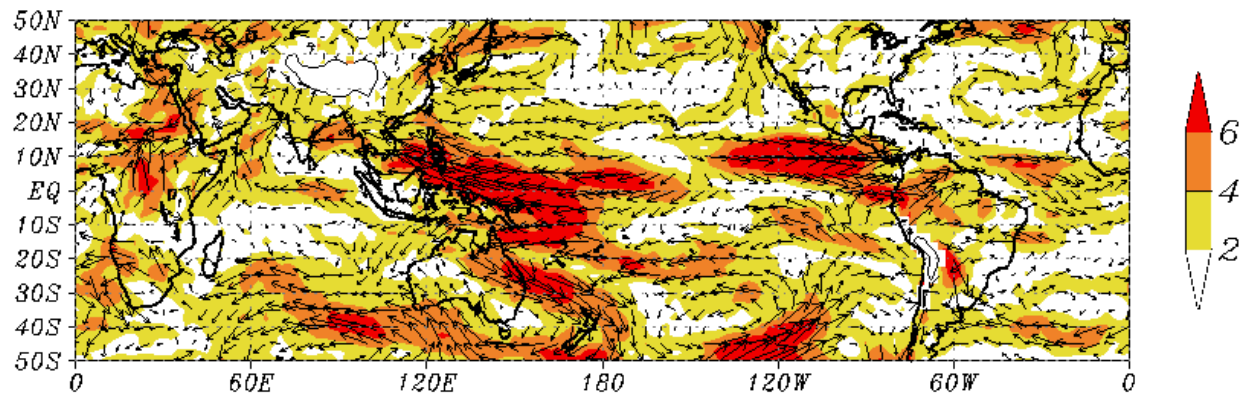
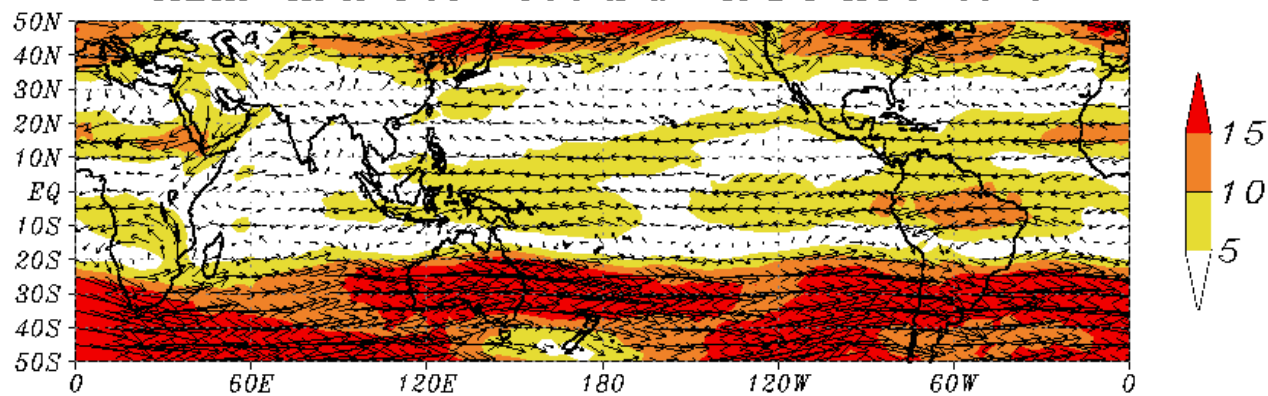


Fig. 10

MEAN ANA T254 500hPa WINDS AUG 2010



ANOMALY 500hPa WINDS AUG 2010

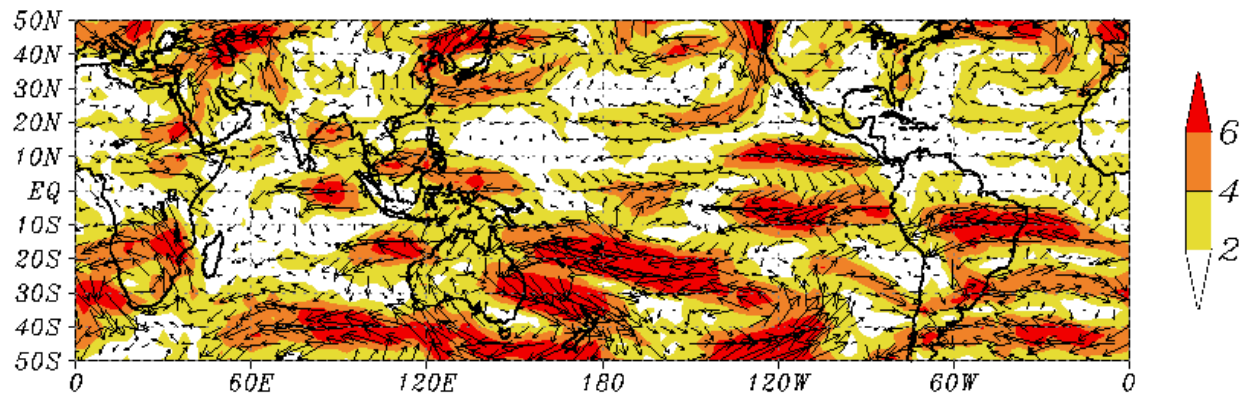
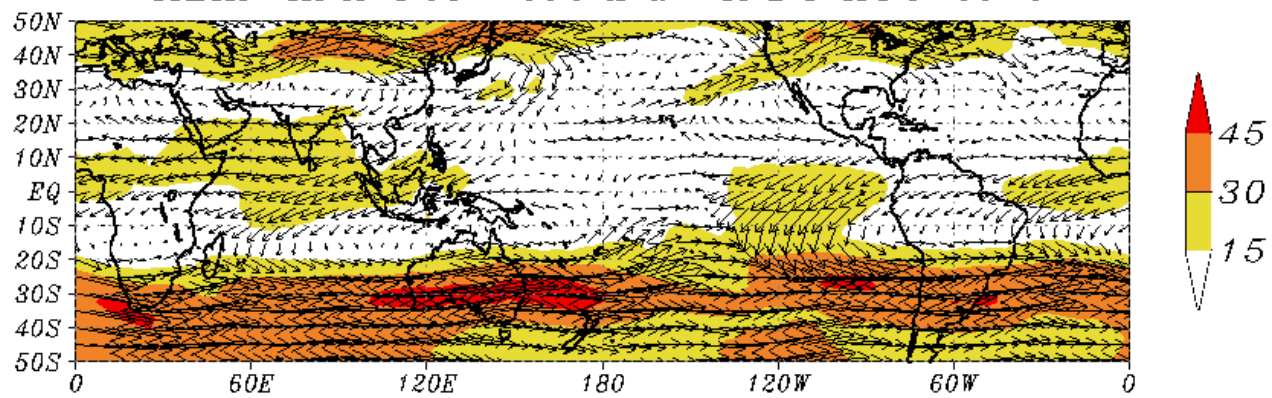


Fig. 11

MEAN ANA T254 200hPa WINDS AUG 2010



ANOMALY 200hPa WINDS AUG 2010

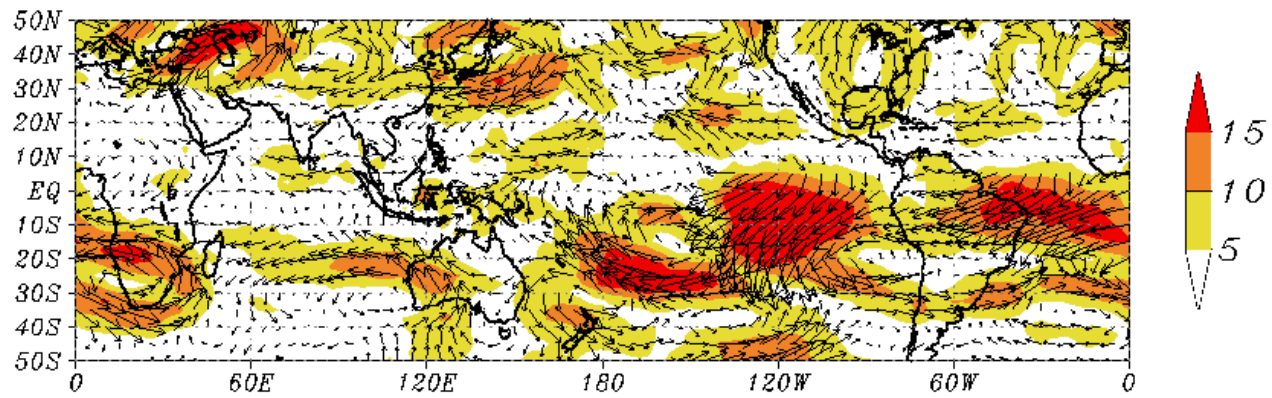
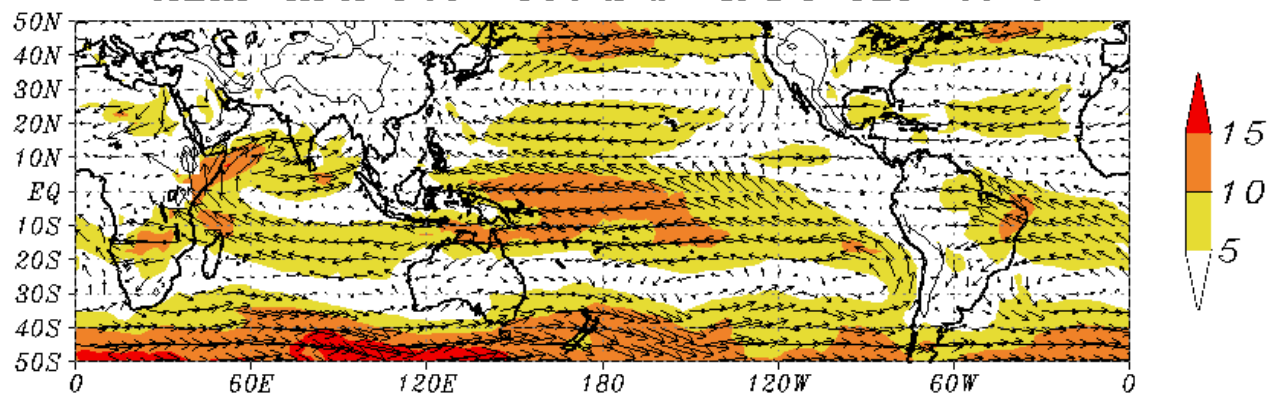


Fig. 12

MEAN ANA T254 850hPa WINDS SEP 2010



ANOMALY 850hPa WINDS SEP 2010

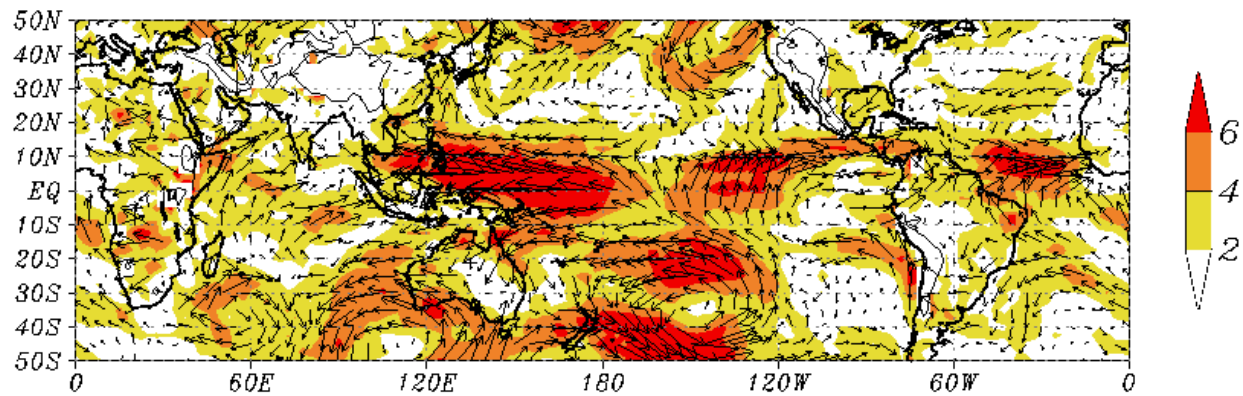
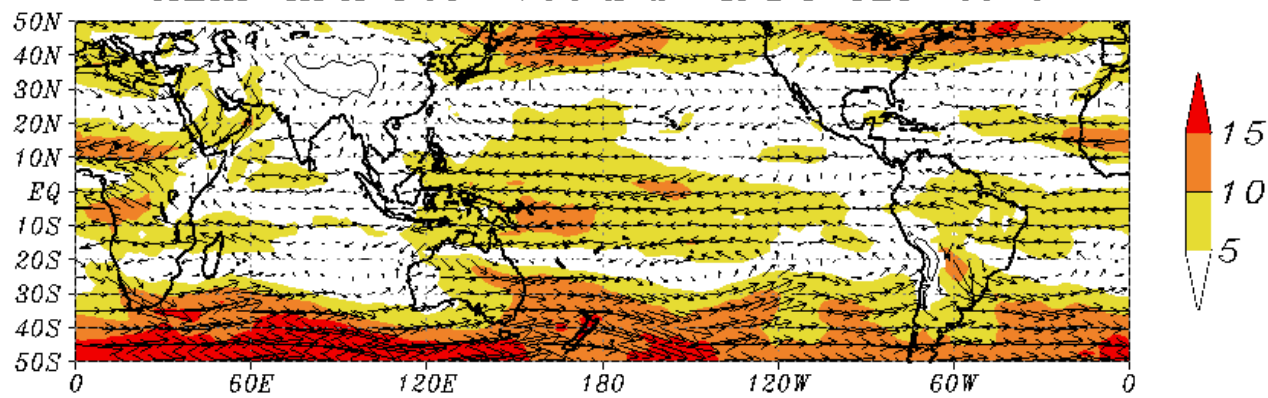


Fig. 13

MEAN ANA T254 700hPa WINDS SEP 2010



ANOMALY 700hPa WINDS SEP 2010

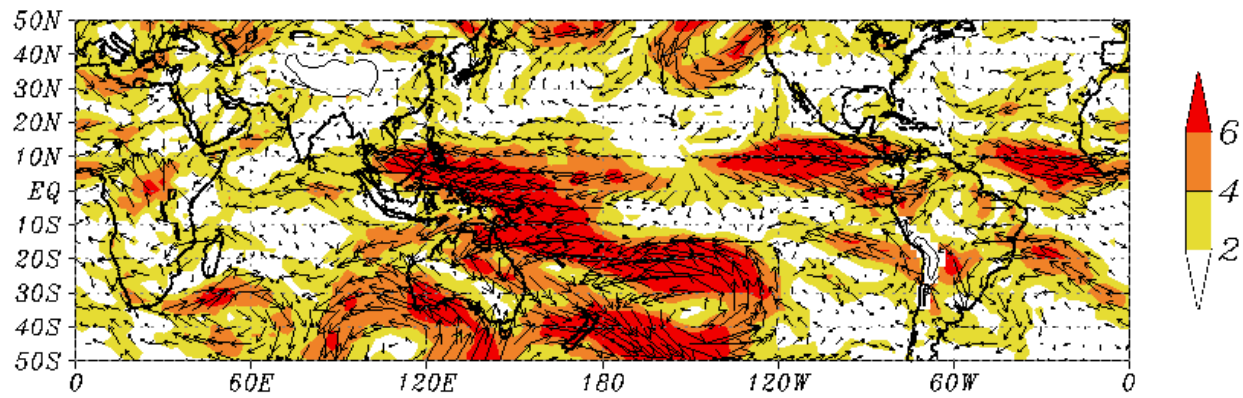
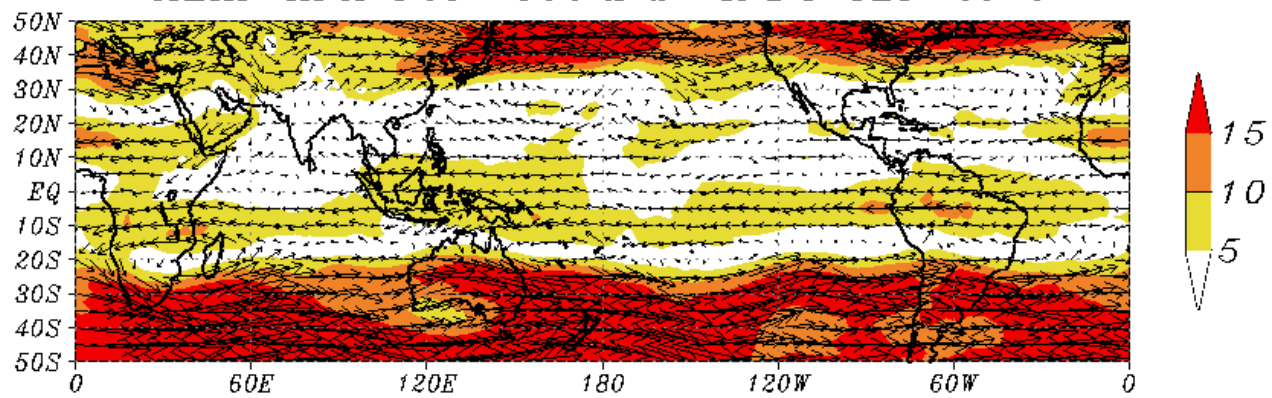


Fig. 14

MEAN ANA T254 500hPa WINDS SEP 2010



ANOMALY 500hPa WINDS SEP 2010

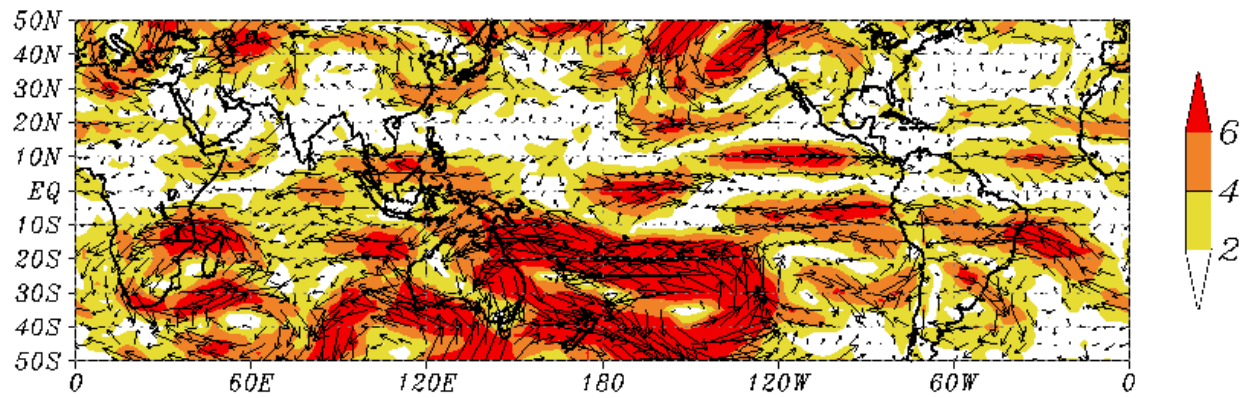
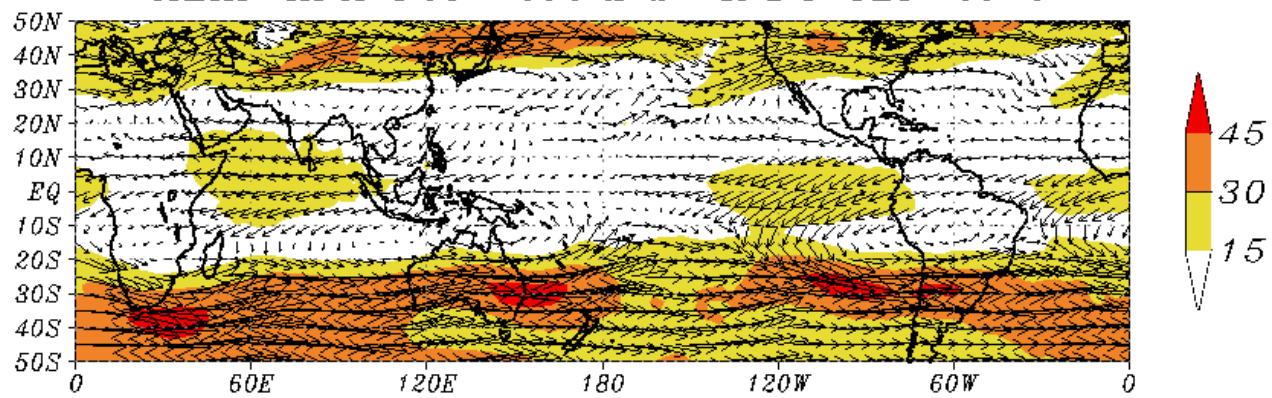


Fig. 15

MEAN ANA T254 200hPa WINDS SEP 2010



ANOMALY 200hPa WINDS SEP 2010

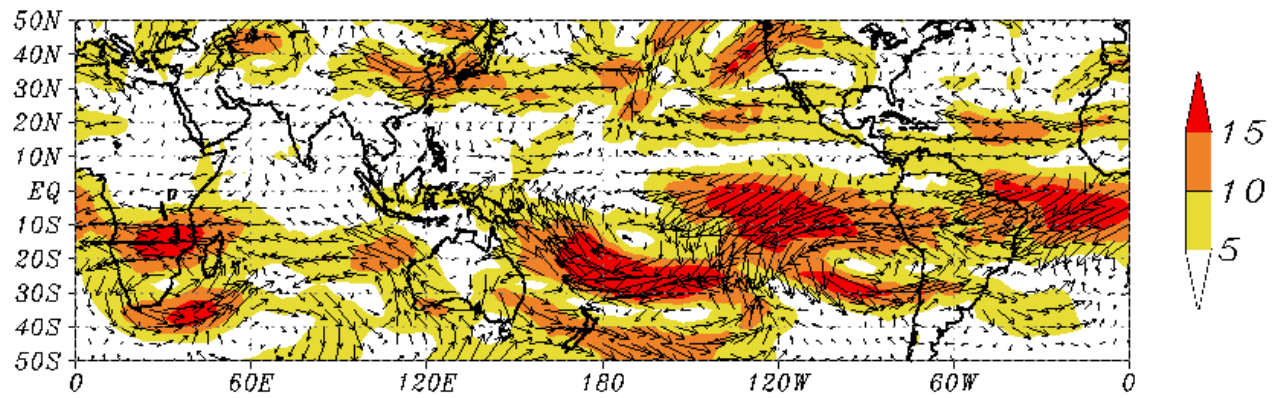


Fig. 16

3 (a). Systematic Errors in the Medium Range Prediction of the Summer Monsoon

G. R. Iyengar

1 Introduction

The nature and distribution of systematic errors seen in the NCMRWF global T254L64 and T382L64 model forecasts are discussed in this chapter using the seasonal (June-September) means of analyses and medium range (Day-1 through Day-5) forecasts.

2 Circulation Features:

Geographical distribution of the mean analysed wind field and the systematic forecast errors for the T254 and T832 model at 850hPa, 700hPa, 500hPa and 200hPa are shown in figures 1(a-d) - 4(a-d) and 11(a-d) - 14(a-d) respectively.

The notable features seen in the systematic errors of the 850hPa flow pattern of the T254 model are the anomalous southerlies over eastern parts of India and an anti-cyclonic circulation is seen over the Bay of Bengal. This feature is also seen at 700hPa level. Anomalous south-westerlies and a cyclonic circulation is also seen over the north-west parts of India and adjoining areas at 850hPa level. A westerly bias is seen over Central India extending to Southeast Asia. An easterly bias is seen over the central and eastern equatorial Indian Ocean region. An anomalous cyclonic circulation is also seen over the extreme southern peninsula and adjoining Arabian Sea. This feature is also seen at 700 and 500hPa levels. At 200hPa, the most significant feature in the systematic errors is the reduction of the return flow into the southern hemisphere. The T382 model forecasts show an increased magnitude of the anomalous south-westerlies over the north-west parts of India and adjoining areas at 850hPa level. However the magnitude of the easterly bias seen over the central and eastern equatorial Indian Ocean region in the lower levels is comparatively less in the T382 model forecasts. The reduction of the return flow into the southern hemisphere is also comparatively less in the T382 model forecasts.

The strong cross-equatorial low level jet stream with its core around 850 hPa is found to have large intraseasonal variability. Figures 5 and 15 show the Hovmöller diagram of zonal wind (U) of 850 hPa averaged over the longitude band 60–70E for the period 1 June–30 September 2010 for the T254 and T382 models respectively. The top panel in each figure shows the analysis and the middle and the lower panel depict the Day3 and Day5 forecasts respectively. The active monsoon spells are characterized by strong cores of zonal wind. The monsoon had set in over Kerala on 31st May. Subsequent advancement of the monsoon across west coast was delayed by about one week due to the formation of a very severe cyclonic storm (PHET, 31st May–2nd June). Thereafter, the monsoon covered nearly half of the country by the middle of June. There was a prolonged hiatus in the advancement of monsoon till the end of June due to weakening of monsoon current. The southwest monsoon covered the entire country by 6th July. As seen from the analysis panel of the Fig 5 the zonal wind flow was quite weak during most parts of June and in the first fortnight of July. The low level westerly flow picked up strength with a core of zonal wind of about 20 m/s in the second fortnight of July and remained so till the end of the month. This was followed by a spell of weak core of zonal wind for a period of two weeks. Another spell of strong core of zonal wind of about 15 m/s was seen in the first fortnight of September. The Day3 and Day5 forecasts of the T254 model agree reasonably well with the analysis and are able to depict the active and weak spells of the monsoon flow. However the wind strength is weaker (stronger) during the active (weak) spells in the Day5 forecasts. The T382 analyses and forecasts show similar features. The active spell in the first fortnight of September is better predicted in the T382 model.

Figures 6 and 16 show the Hovmöller diagram of zonal wind (U) of 850 hPa averaged over the longitude band 75–80E for the period 1 June–30 September 2010 for the T254 and T382 models respectively. The top panel in each figure shows the analysis and the middle and the lower panel depict the Day3 and Day5 forecasts respectively. Both the T254 and T382 analyses show a prominent northward movement of the core of zonal wind during the second fortnight of July. Two weak spells are seen in the second and third week of June and from the fourth week of August to the second week of September. The Day3 forecasts compare well with the analysis. However, the Day5

forecasts are not able to depict the northward movement of the core of zonal wind as seen in the analysis. The T382 model forecasts depict this feature comparatively better than the T254 model.

3 Temperature:

Geographical distribution of the mean systematic forecast temperature errors for the T254 (T382) models at 850hPa and 200hPa level are shown in figures 7 (17) and 8 (18) respectively. The T254 model forecasts show a warm bias in the lower troposphere over the northwest parts of India and adjoining regions which is less as compared to the T382 model. In the upper troposphere, the T254 model also shows a cold bias over the northern parts of India. The magnitude of the cold bias is much less in the T382 model.

4 Humidity:

Geographical distribution of the mean systematic forecast specific humidity errors for the T254 and T382 models at 850hPa level are shown in figures 9 and 19 respectively. The T254 and T382 model forecasts show a dry bias over the entire country, with the magnitude of the bias being comparatively more in the latter.

5 Mean Sea Level Pressure

Geographical distribution of the mean systematic forecast mean sea level pressure errors for the T254 and T382 models at 850hPa level are shown in figures 10 and 20 respectively. The T382 model forecasts show an intensification of the heat low as compared to the analyses. The T382 model forecasts also show a reduction in MSLP over the northern plains. The bias in T382 model forecasts is comparatively more as compared to the T254 model forecasts.

6. Verification of wind and temperature forecasts against analyses:

The RMSE of zonal wind, meridional wind and temperature at 850 and 200Pa levels of Day1, Day3 and Day5 forecasts from T254 and T382 models for each day have

been computed for the Indian domain of 5-38 N and 68-94 E against their respective analyses. Table 1 gives the average RMSE values corresponding for the season as a whole. The T382 model forecasts feature relatively smaller RMSE as compared to the T254 model.

7. Verification scores for wind and temperature against observations over India

Objective verification scores for the T254 and T382 model forecasts of winds and temperature against the observations valid for 00UTC at standard pressure levels (850 and 250 hPa levels) as recommended by the WMO were computed for the Indian region for the monsoon season of 2010.

Table 2 gives the average RMSE values corresponding for the season as a whole. The T382 model forecasts show marginally smaller RMSE for both winds and temperature at both 850 and 250 hPa levels

Legends for figures:

Figure 1. Mean T254 analysed wind field (a) and systematic forecast errors for Day-1 (b), Day-3 (c) and Day-5 (d) at 850 hPa. [Units: m/s, Contour interval: 5m/s for analyses and 2m/s for forecast errors]

Figure 2. Mean T254 analysed wind field (a) and systematic forecast errors for Day-1 (b), Day-3 (c) and Day-5 (d) at 700 hPa. . [Units: m/s, Contour interval: 10m/s for analyses and 5m/s for forecast errors]

Figure 3. Mean T254 analysed wind field (a) and systematic forecast errors for Day-1 (b), Day-3 (c) and Day-5 (d) at 500 hPa. [Units: m/s, Contour interval: 5m/s for analyses and 2m/s for forecast errors]

Figure 4. Mean T254 analysed wind field (a) and systematic forecast errors for Day-1 (b), Day-3 (c) and Day-5 (d) at 200 hPa. . [Units: m/s, Contour interval: 10m/s for analyses and 5m/s for forecast errors]

Figure 5. Hovmoller diagram of T254 analyses and forecast zonal wind (U) of 850 hPa averaged over the longitude band 60–70E and smoothed by a 5-day moving average for the period 1 June–30 September 2009.

Figure 6. Hovmoller diagram of T254 analyses and forecast zonal wind (U) of 850 hPa averaged over the longitude band 75–80E and smoothed by a 5-day moving average for the period 1 June–30 September 2009.

Figure 7. Mean T254 analysed temperature field (a) and systematic forecast errors for Day-1 (b), Day-3(c) and Day-5 (d) of temperature at 850 hPa.: [Units: K, Contour interval: 2 K for analyses and 1 K for forecast errors]

Figure 8. Mean T254 analysed temperature field (a) and systematic forecast errors for Day-1 (b), Day-3(c) and Day-5 (d) of temperature at 200 hPa.: [Units: K, Contour interval: 2 K for analyses and 1 K for forecast errors]

Figure 9. Mean T254 analysed specific humidity field (a) and systematic forecast errors for Day-1 (b), Day-3(c) and Day-5 (d) of specific humidity at 850 hPa.: [Units: gm/kg, Contour interval: 2 for analyses and 1 for forecast errors]

Figure 10. Mean T254 analysed MSLP field (a) and systematic forecast errors for Day-1 (b), Day-3(c) and Day-5 (d) of MSLP: [Units: hPa, Contour interval: 2 for analyses and 1 for forecast errors]

Figure 11. Mean T382 analysed wind field (a) and systematic forecast errors for Day-1 (b), Day-3 (c) and Day-5 (d) at 850 hPa. [Units: m/s, Contour interval: 5m/s for analyses and 2m/s for forecast errors]

Figure 12. Mean T382 analysed wind field (a) and systematic forecast errors for Day-1 (b), Day-3 (c) and Day-5 (d) at 700 hPa. . [Units: m/s, Contour interval: 10m/s for analyses and 5m/s for forecast errors]

Figure 13. Mean T382 analysed wind field (a) and systematic forecast errors for Day-1 (b), Day-3 (c) and Day-5 (d) at 500 hPa. [Units: m/s, Contour interval: 5m/s for analyses and 2m/s for forecast errors]

Figure 14. Mean T382 analysed wind field (a) and systematic forecast errors for Day-1 (b), Day-3 (c) and Day-5 (d) at 200 hPa. . [Units: m/s, Contour interval: 10m/s for analyses and 5m/s for forecast errors]

Figure 15. Hovmoller diagram of T382 analyses and forecast zonal wind (U) of 850 hPa averaged over the longitude band 60–70E and smoothed by a 5-day moving average for the period 1 June–30 September 2009.

Figure 16. Hovmoller diagram of T382 analyses and forecast zonal wind (U) of 850 hPa averaged over the longitude band 75–80E and smoothed by a 5-day moving average for the period 1 June–30 September 2009.

Figure 17. Mean T382 analysed temperature field (a) and systematic forecast errors for Day-1 (b), Day-3(c) and Day-5 (d) of temperature at 850 hPa.: [Units: K, Contour interval: 2 K for analyses and 1 K for forecast errors]

Figure 18. Mean T382 analysed temperature field (a) and systematic forecast errors for Day-1 (b), Day-3(c) and Day-5 (d) of temperature at 200 hPa.: [Units: K, Contour interval: 2 K for analyses and 1 K for forecast errors]

Figure 19. Mean T382 analysed specific humidity field (a) and systematic forecast errors for Day-1 (b), Day-3(c) and Day-5 (d) of specific humidity at 850 hPa.: [Units: gm/kg, Contour interval: 2 for analyses and 1 for forecast errors]

Figure 20. Mean T382 analysed MSLP field (a) and systematic forecast errors for Day-1 (b), Day-3(c) and Day-5 (d) of MSLP: [Units: hPa, Contour interval: 2 for analyses and 1 for forecast errors]

Table 1: Day1-Day5 Root Mean Square Error (RMSE) of Wind(Zonal, Meridional) and Temperature over the Indian region (68-94E,5-38N) of T254 and T382 models

T382	Day1		Day2		Day3		Day4		Day5	
	850hPa	200hPa	850hPa	200hPa	850hPa	200hPa	850hPa	200hPa	850hPa	200hPa
u(m/s)	2.8	4.2	2.6	5.3	3.9	5.8	4.2	6.1	4.6	6.5
v(m/s)	2.5	3.9	3.0	4.6	3.3	4.9	3.5	5.4	3.7	5.7
Temp(⁰ K)	0.7	0.6	0.8	0.8	0.9	0.9	1.0	1.0	1.1	1.1

T254	Day1		Day2		Day3		Day4		Day5	
	850hPa	200hPa	850hPa	200hPa	850hPa	200hPa	850hPa	200hPa	850hPa	200hPa
u(m/s)	2.9	4.6	3.6	5.45	4.0	5.8	4.4	6.2	4.8	6.6
v(m/s)	2.5	4.1	3.0	4.8	3.4	5.2	3.7	5.5	3.9	5.8
Temp(⁰ K)	0.7	0.7	0.8	0.9	0.9	1.0	1.0	1.0	1.1	1.1

Table 2: Day1-Day5 Root Mean Square Error (RMSE) of Wind and Temperature against observations over India of T254 and T382 models

T254	Day1		Day3		Day5	
	850hPa	250hPa	850hPa	250hPa	850hPa	250hPa
Wind(m/s)	5.08	6.20	5.95	6.85	6.63	7.20
Temp(⁰ K)	1.93	3.18	1.97	3.22	2.02	3.22
T382	Day1		Day3		Day5	
	850hPa	250hPa	850hPa	250hPa	850hPa	250hPa
Wind(m/s)	5.11	6.06	5.88	6.69	6.51	7.22
Temp(⁰ K)	1.92	3.14	1.97	3.10	2.00	3.10

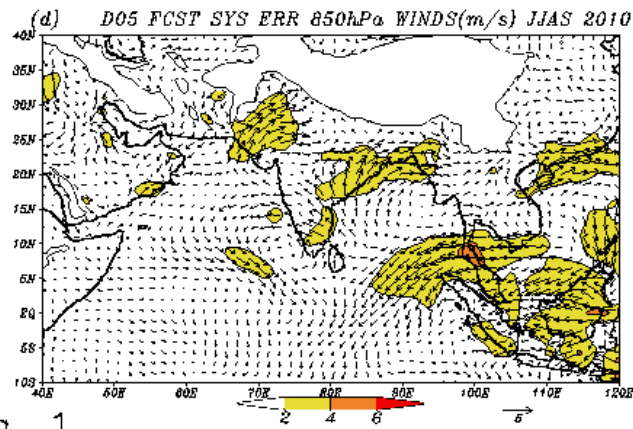
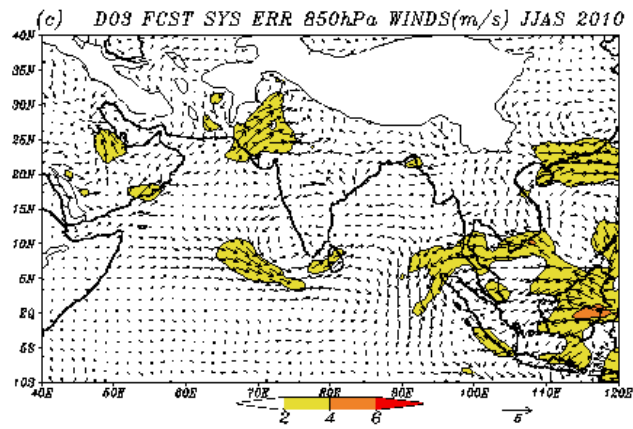
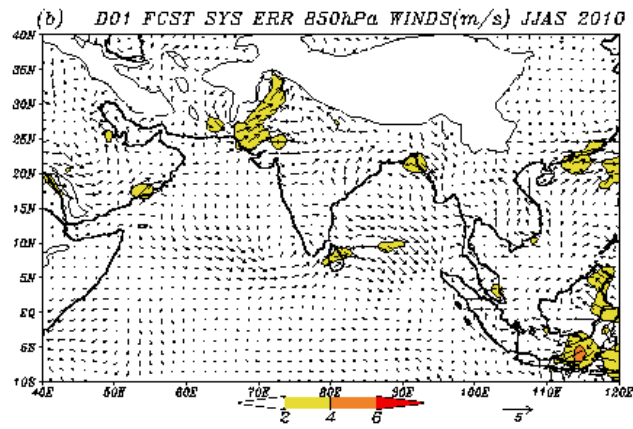
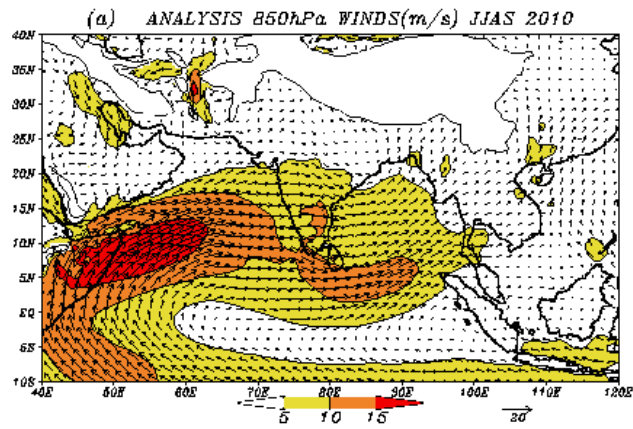


Fig. 1

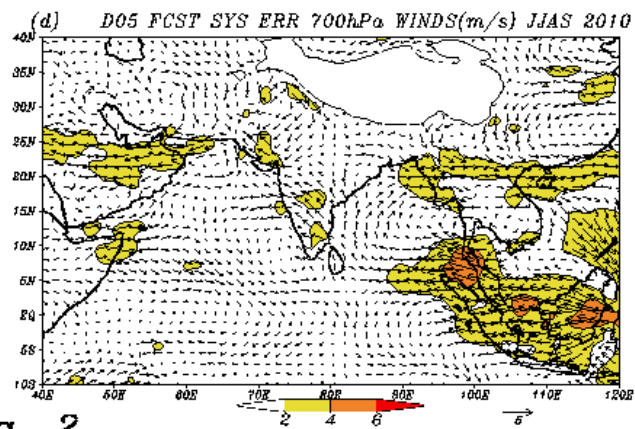
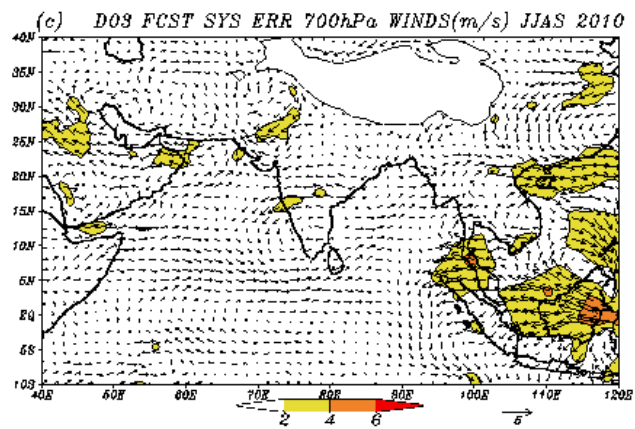
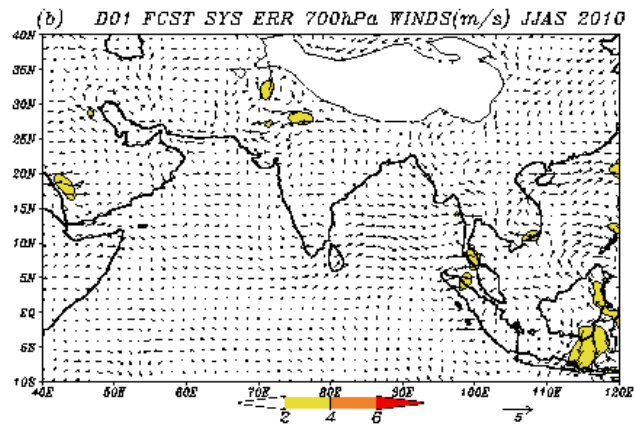
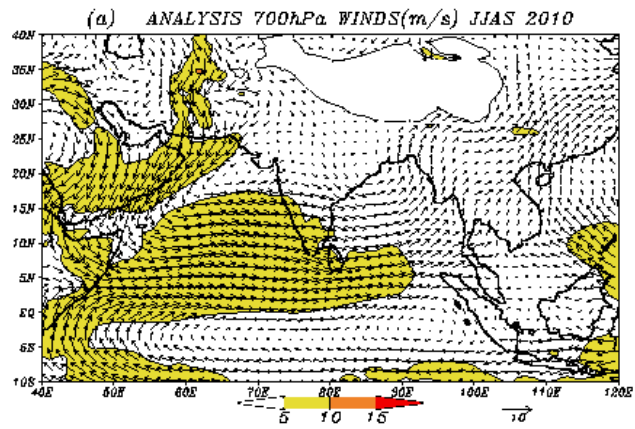


Fig. 2

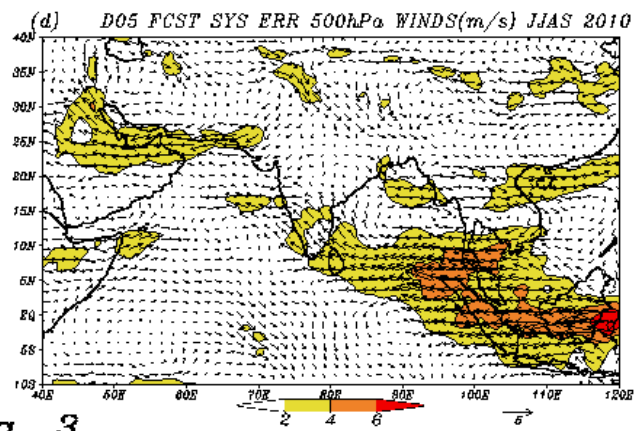
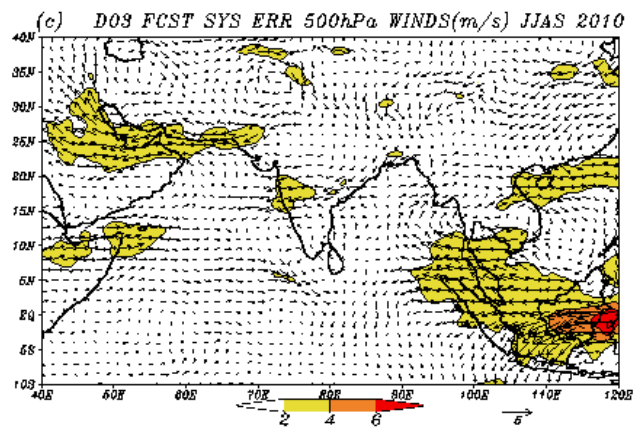
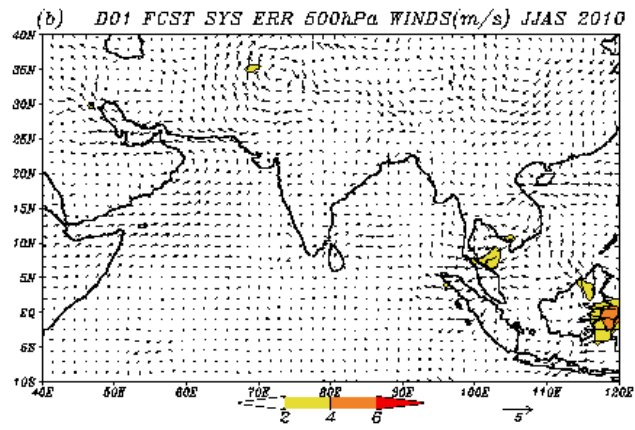
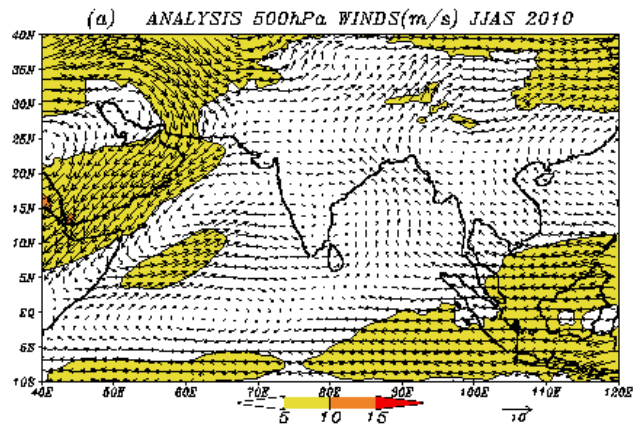


Fig. 3

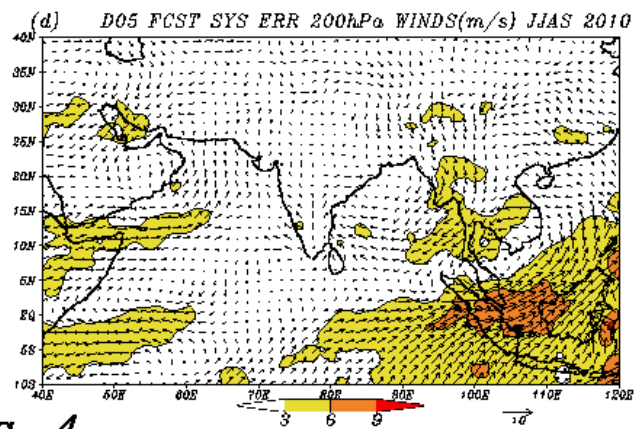
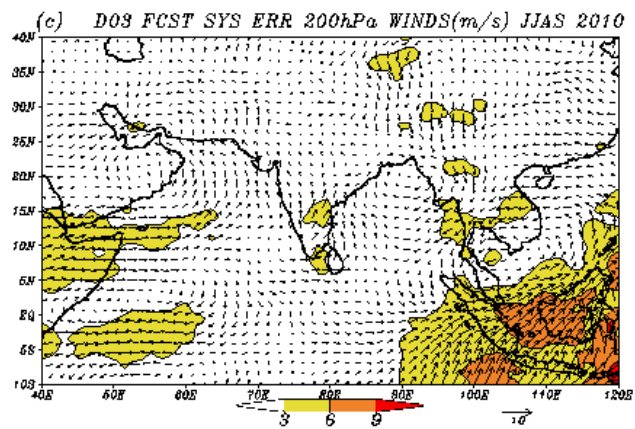
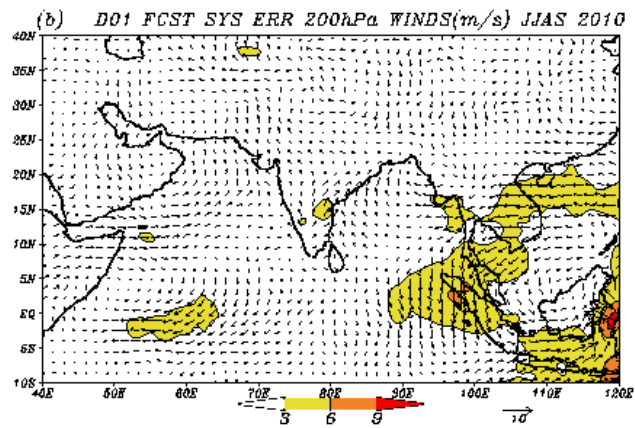
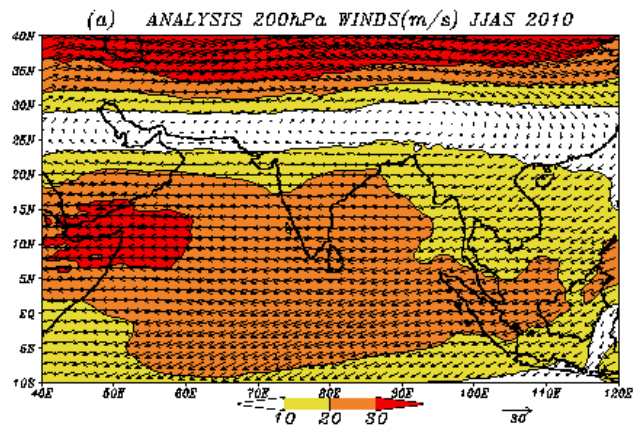


Fig. 4

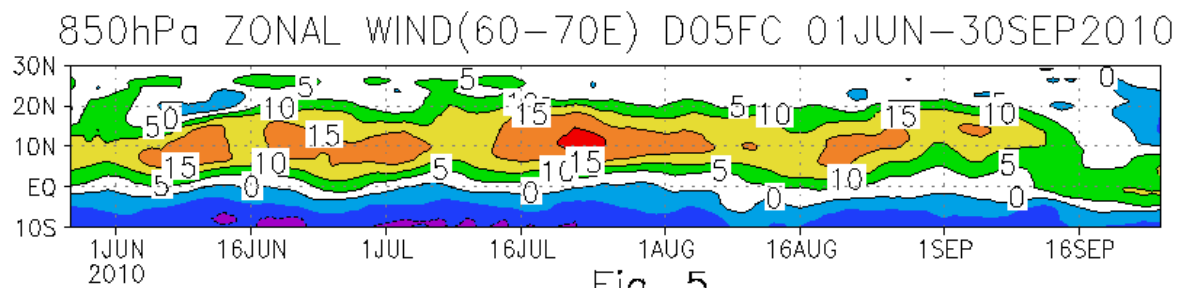
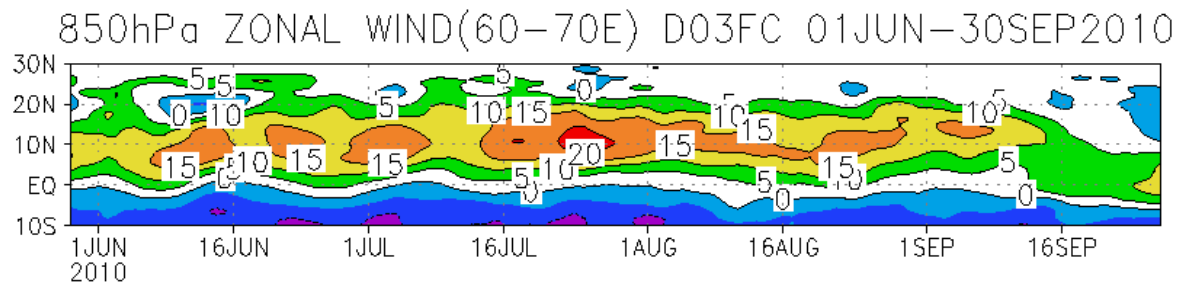
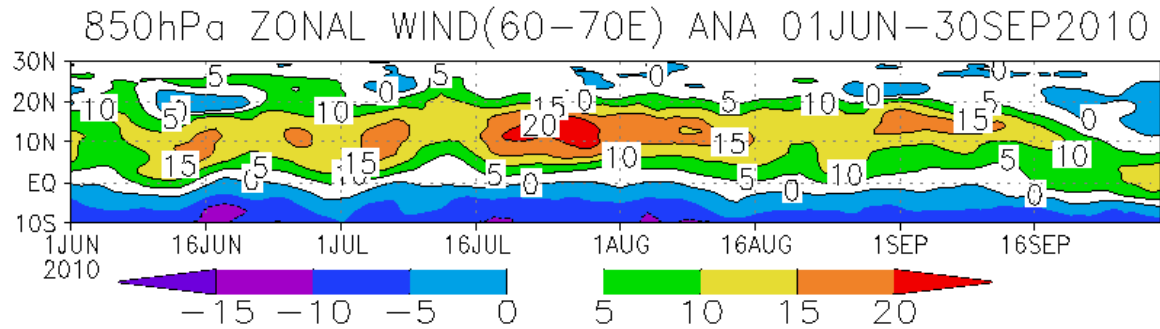


Fig. 5

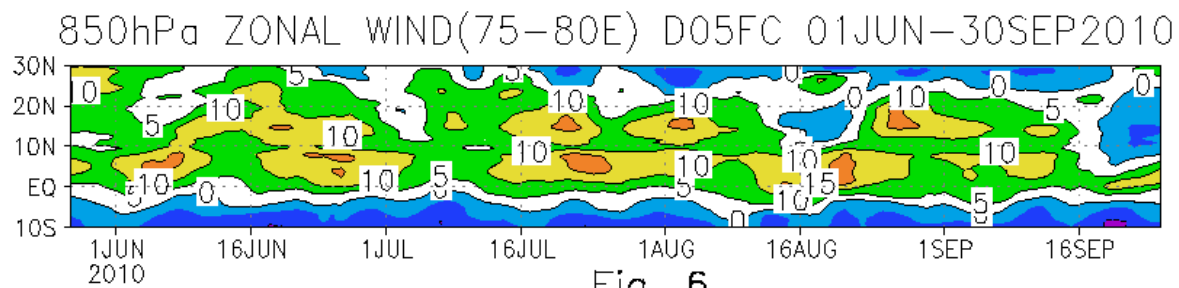
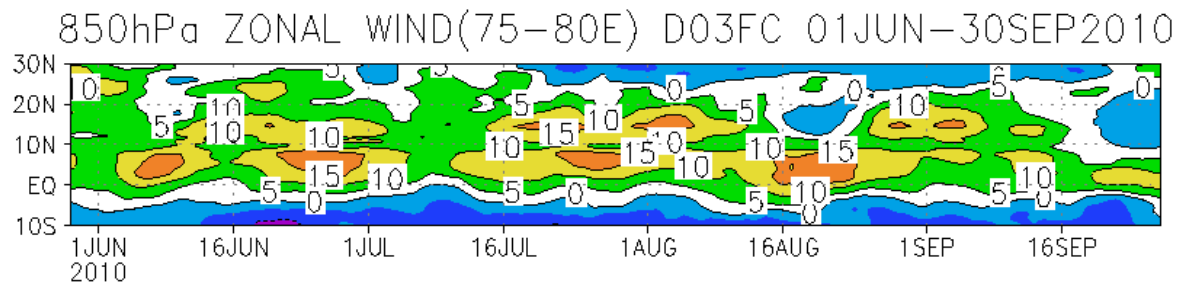
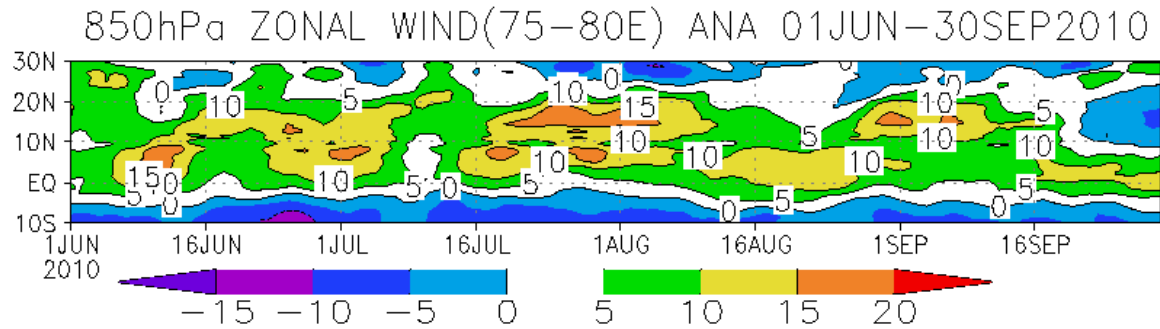
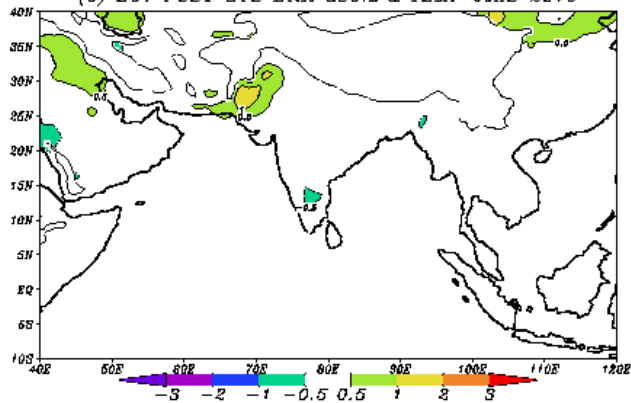
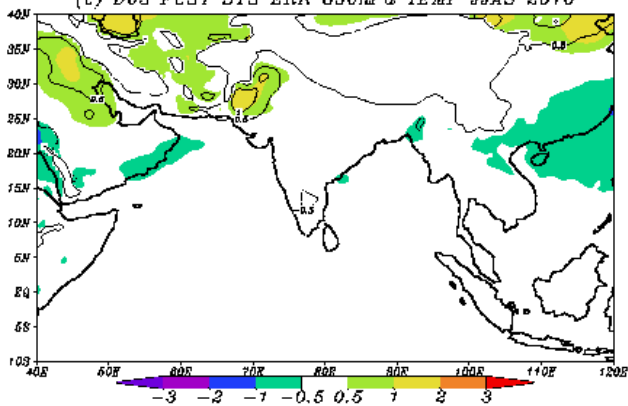


Fig. 6

(b) D01 FCST SYS ERR 850hPa TEMP JJAS 2010



(c) D03 FCST SYS ERR 850hPa TEMP JJAS 2010



(d) D05 FCST SYS ERR 850hPa TEMP JJAS 2010

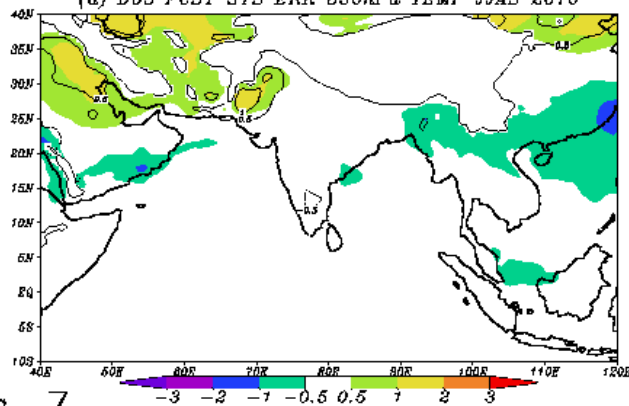
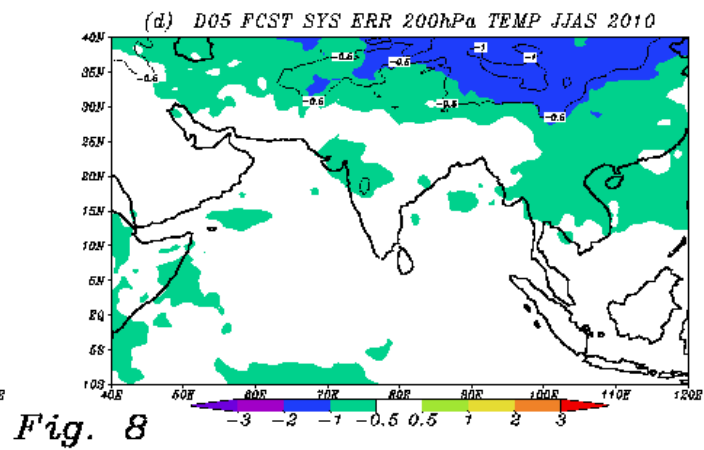
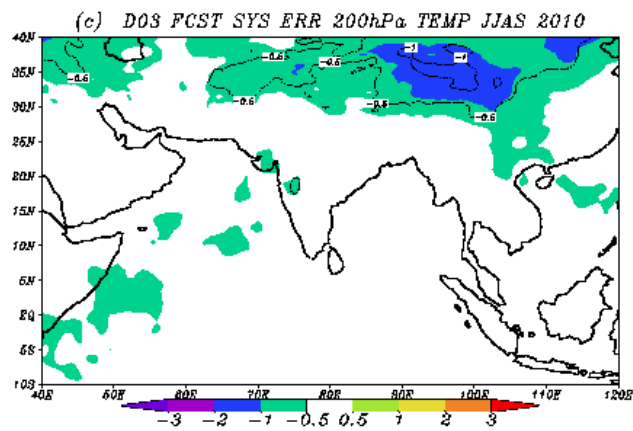
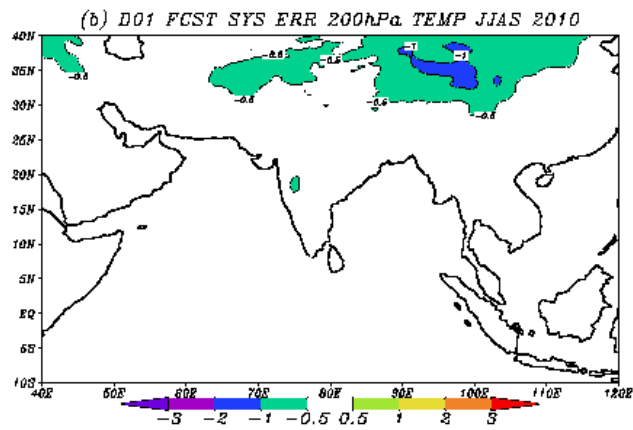


Fig. 7



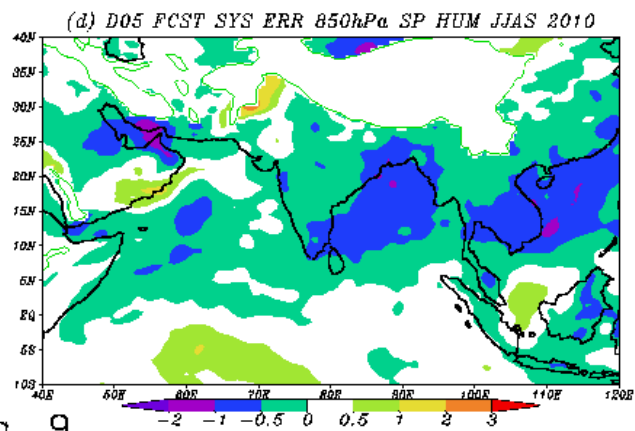
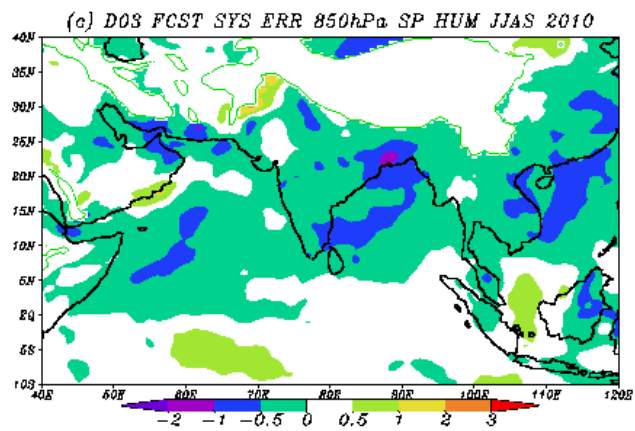
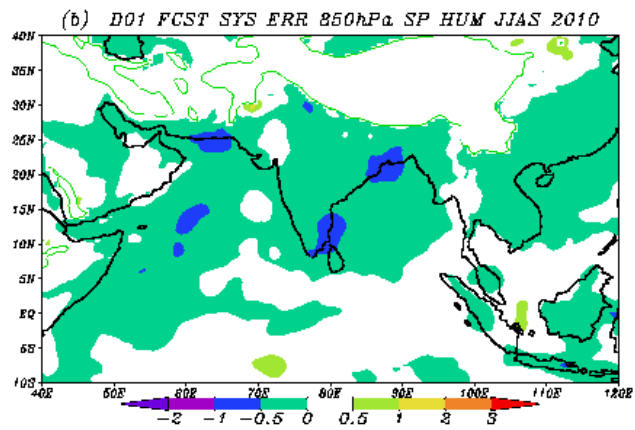


Fig. 9

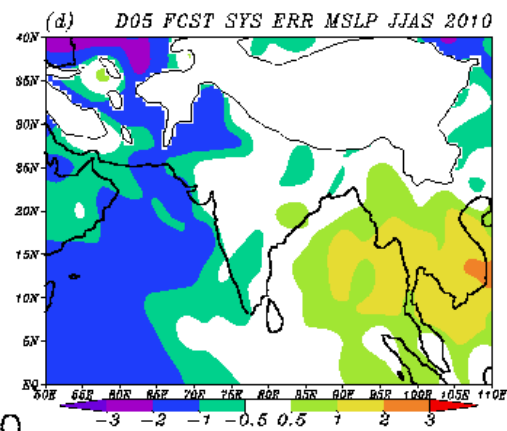
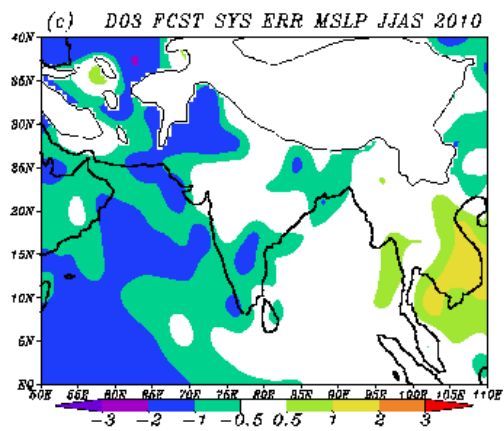
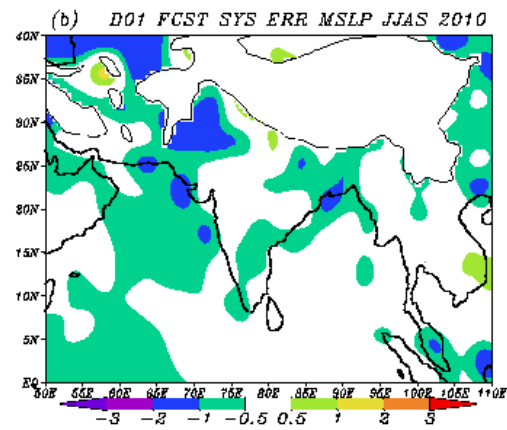
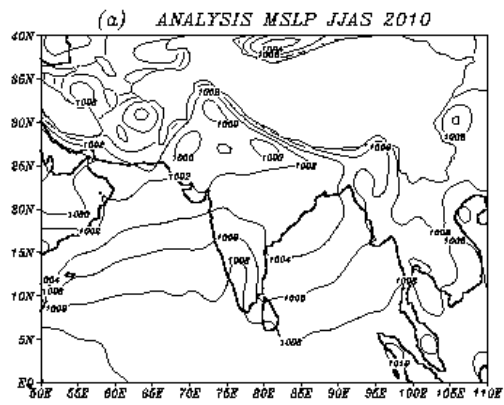


Fig. 10

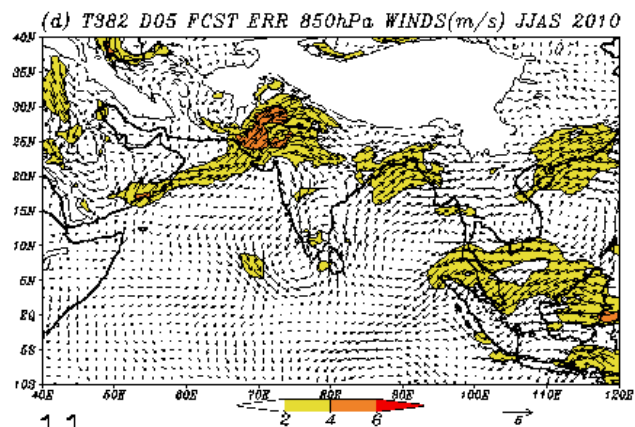
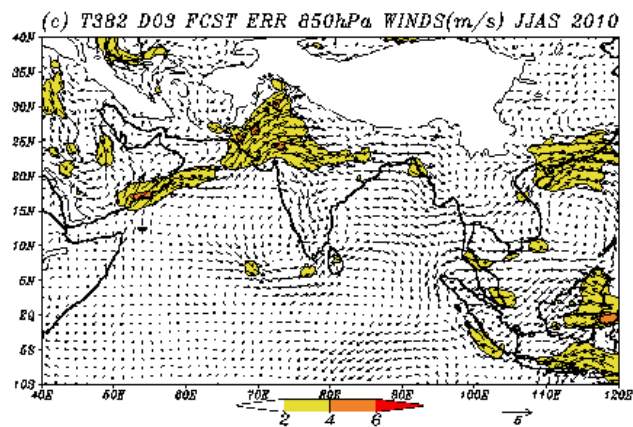
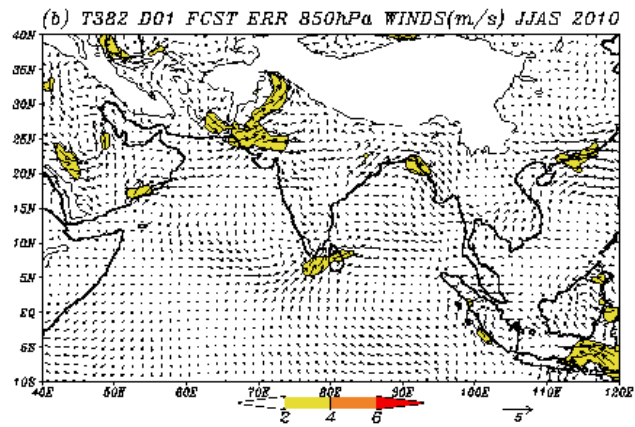
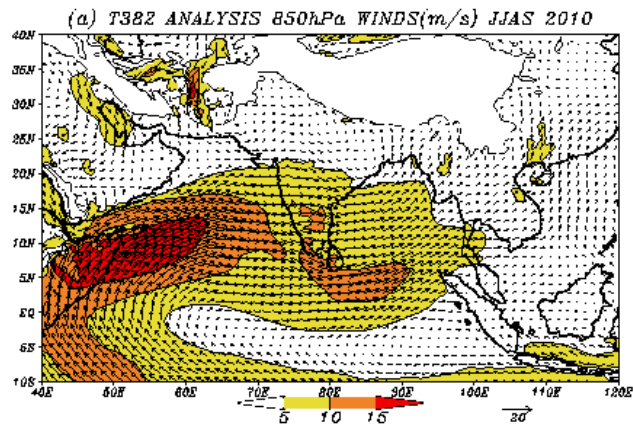


Fig. 11

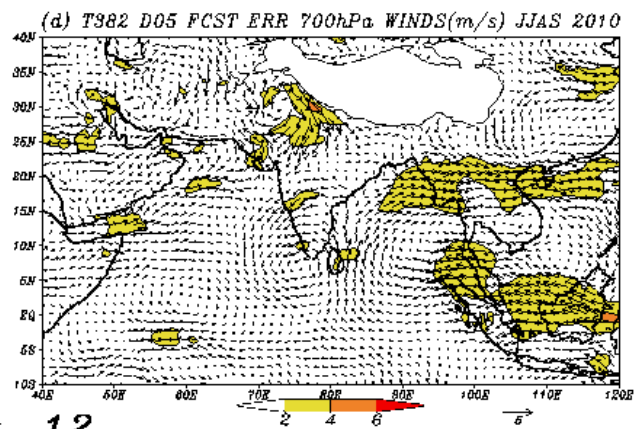
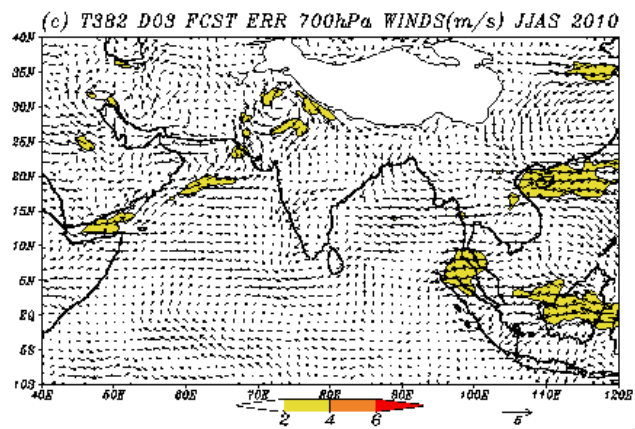
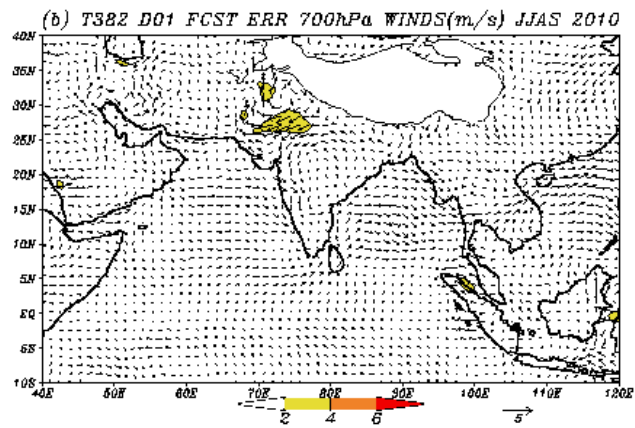
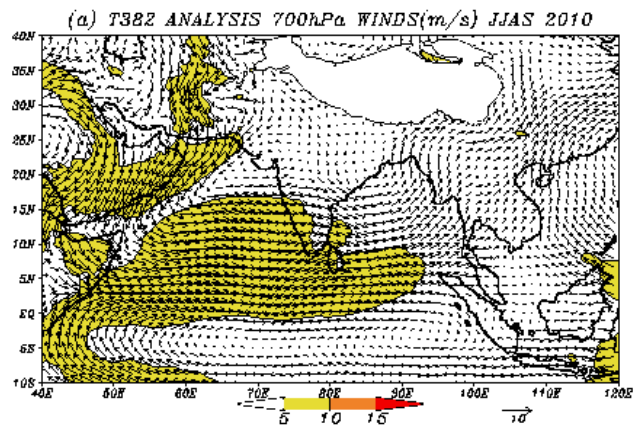


Fig. 12

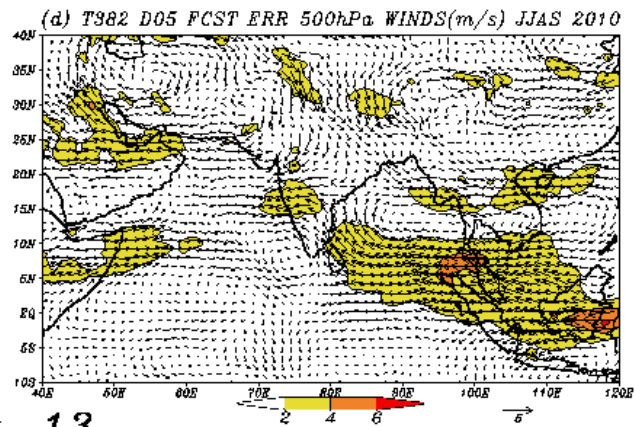
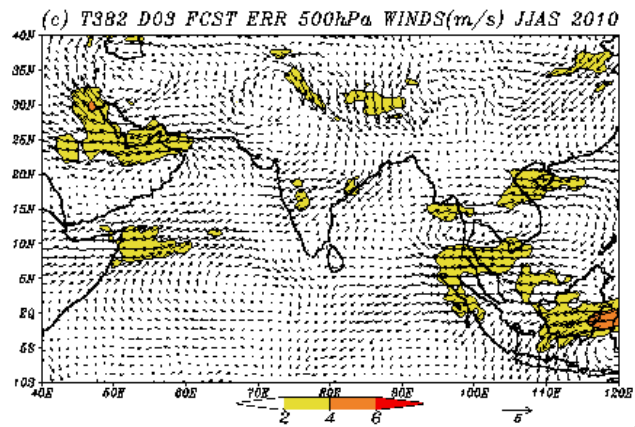
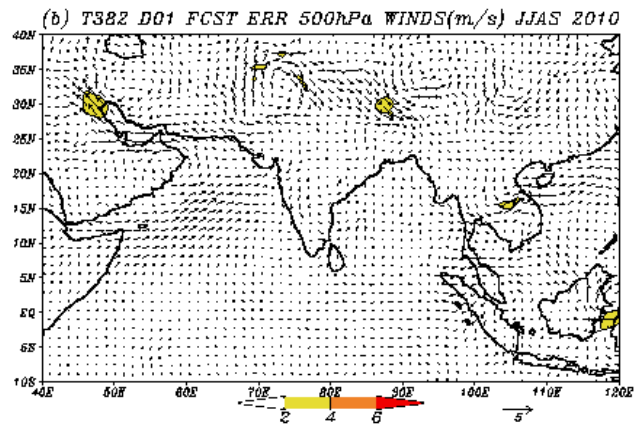
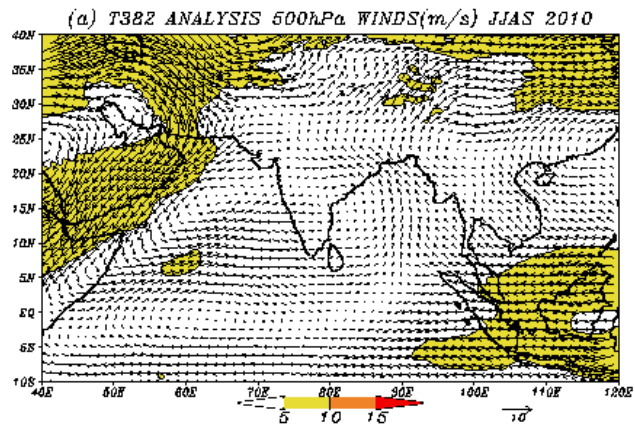


Fig. 13

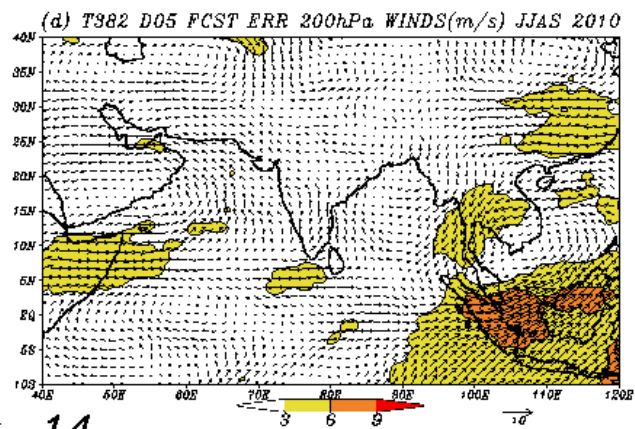
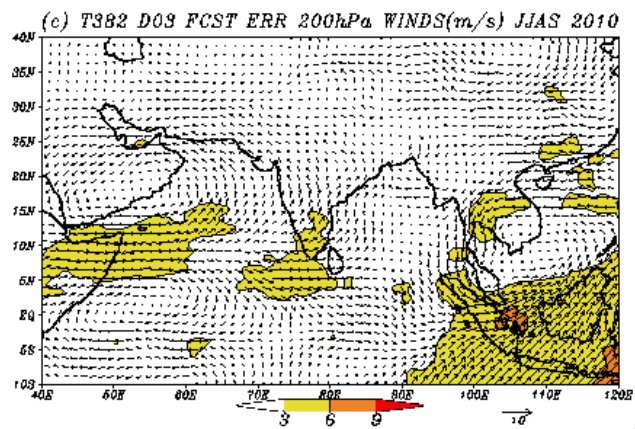
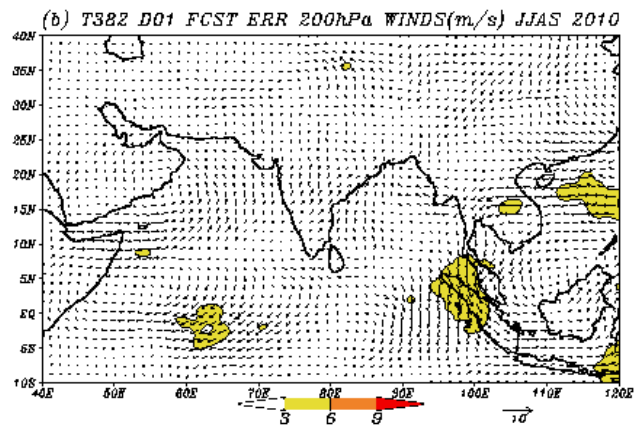
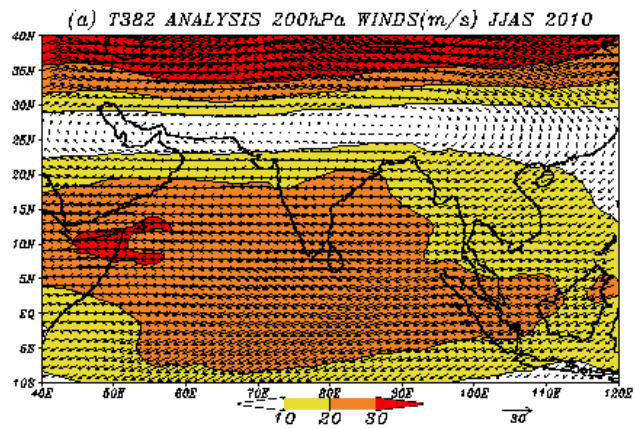
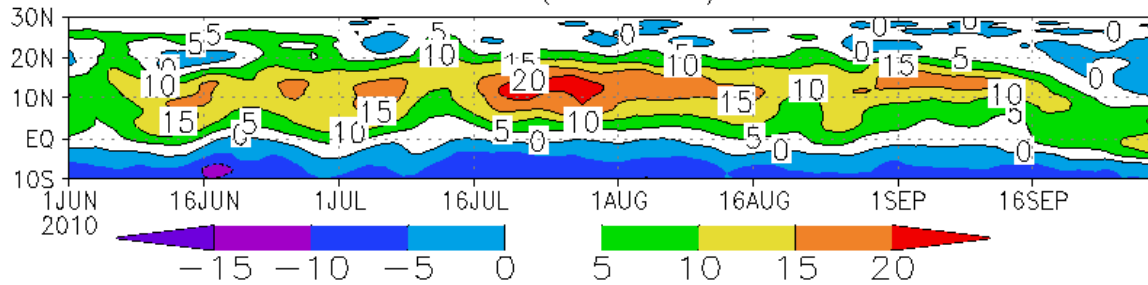
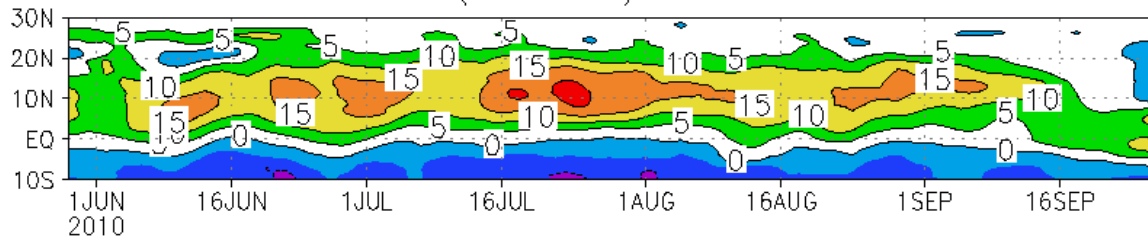


Fig. 14

T382 850hPa ZONAL WIND(60-70E) ANA 01JUN-30SEP2010



850hPa ZONAL WIND(60-70E) D03FC 01JUN-30SEP2010



850hPa ZONAL WIND(60-70E) D05FC 01JUN-30SEP2010

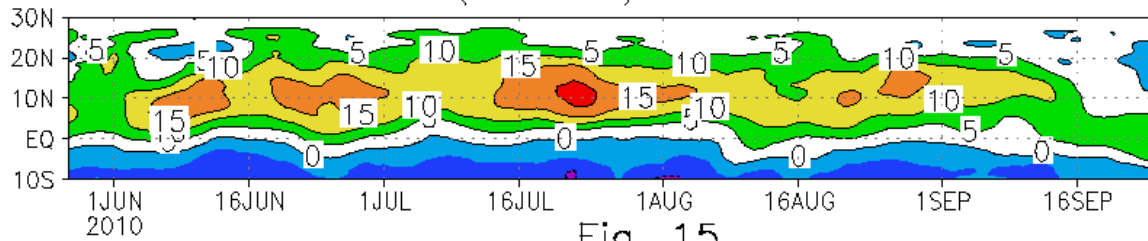
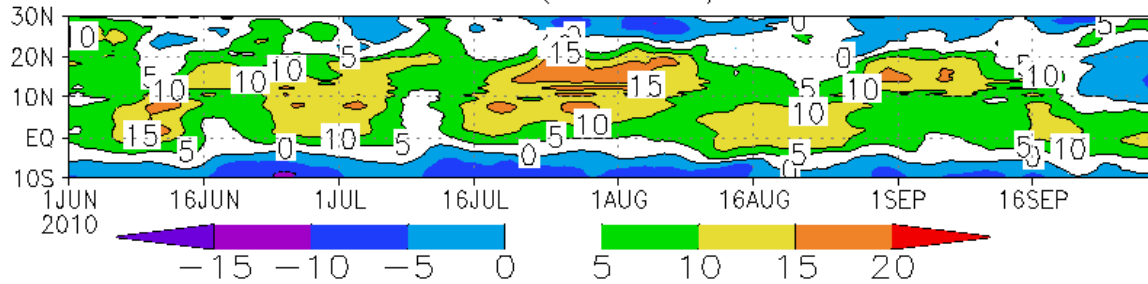
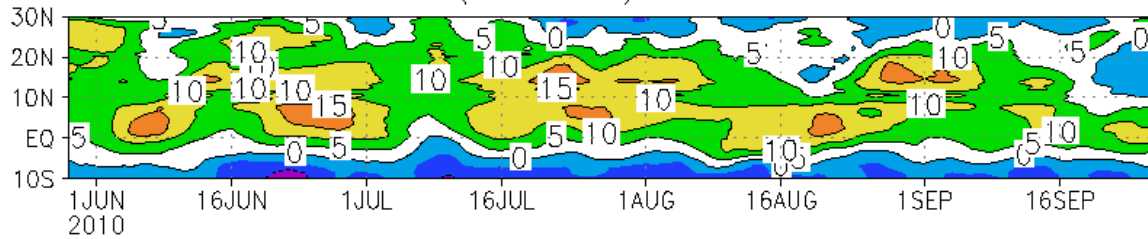


Fig. 15

T382 850hPa ZONAL WIND(75-80E) ANA 01JUN-30SEP2010



850hPa ZONAL WIND(75-80E) D03FC 01JUN-30SEP2010



850hPa ZONAL WIND(75-80E) D05FC 01JUN-30SEP2010

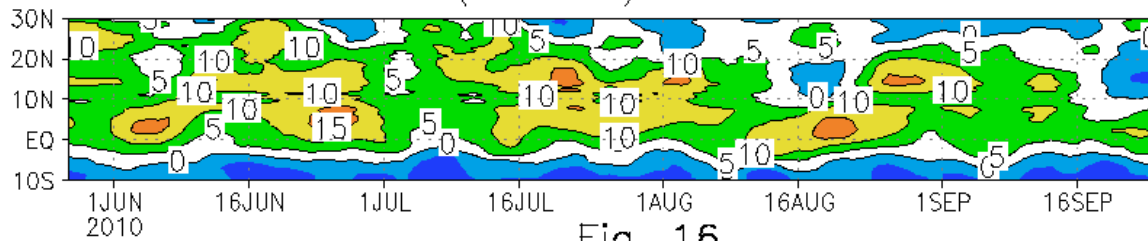
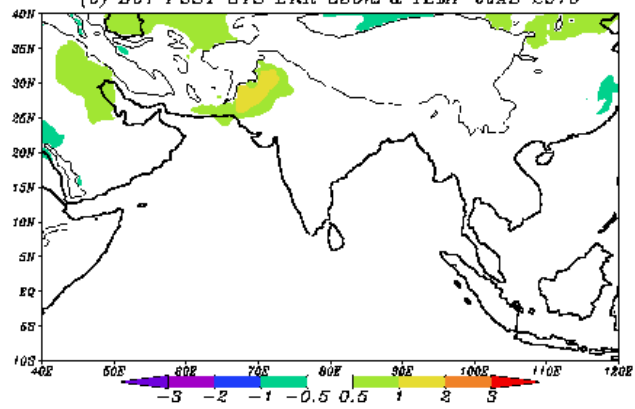
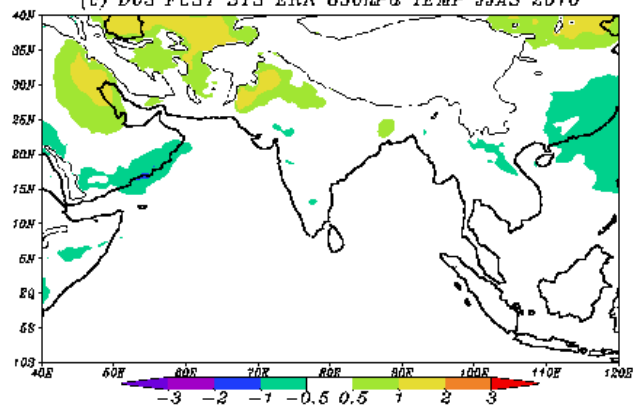


Fig. 16

(b) D01 FCST SYS ERR 850hPa TEMP JJAS 2010



(c) D03 FCST SYS ERR 850hPa TEMP JJAS 2010



(d) D05 FCST SYS ERR 850hPa TEMP JJAS 2010

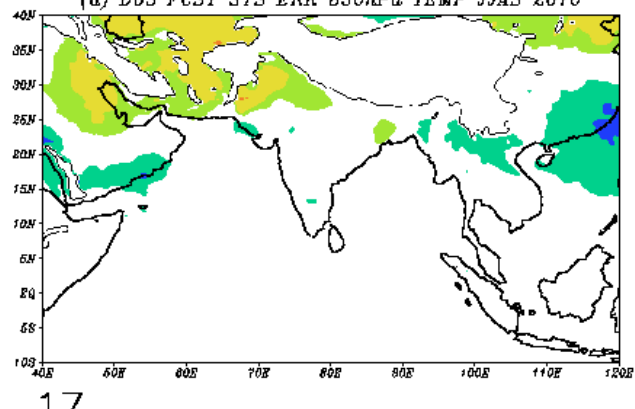


Fig. 17

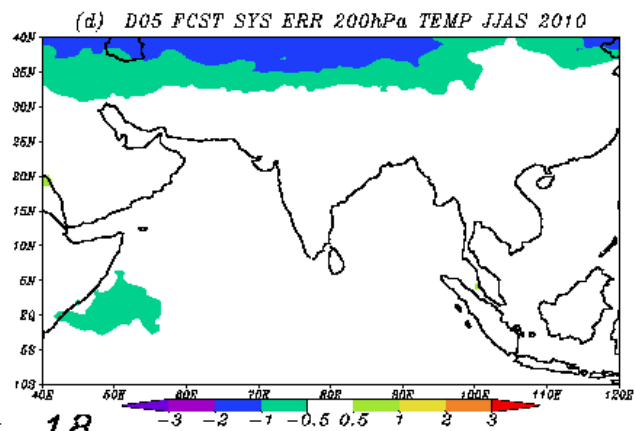
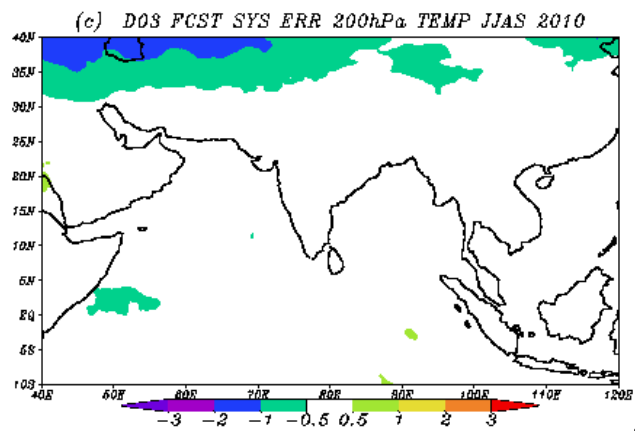
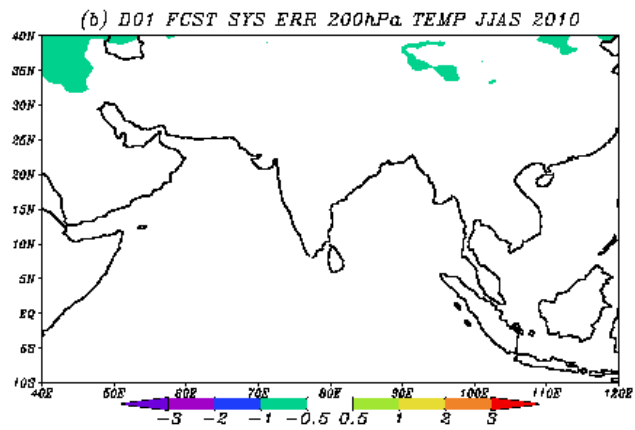
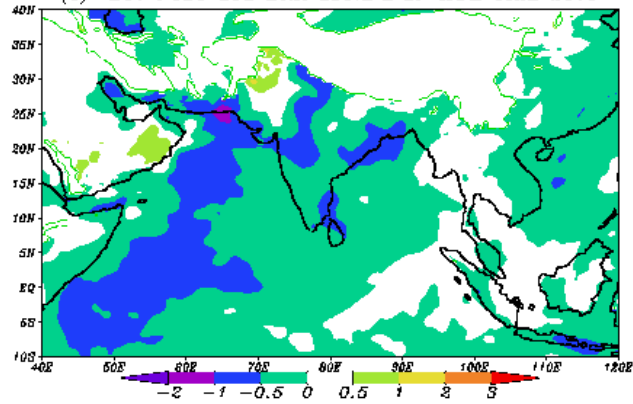
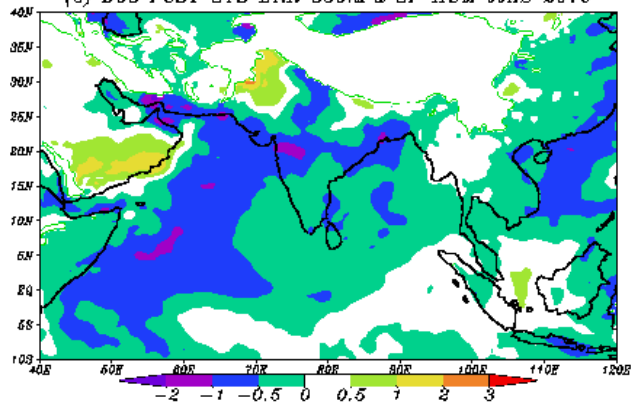


Fig. 18

(b) D01 FCST SYS ERR 850hPa SP HUM JJAS 2010



(c) D03 FCST SYS ERR 850hPa SP HUM JJAS 2010



(d) D05 FCST SYS ERR 850hPa SP HUM JJAS 2010

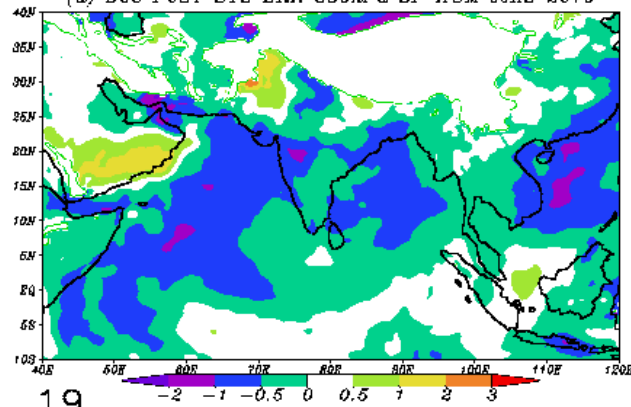


Fig. 19

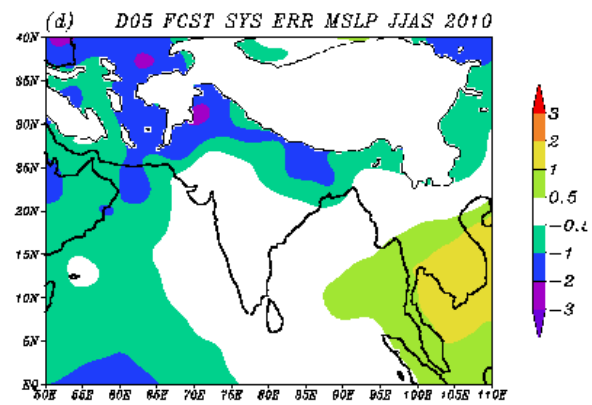
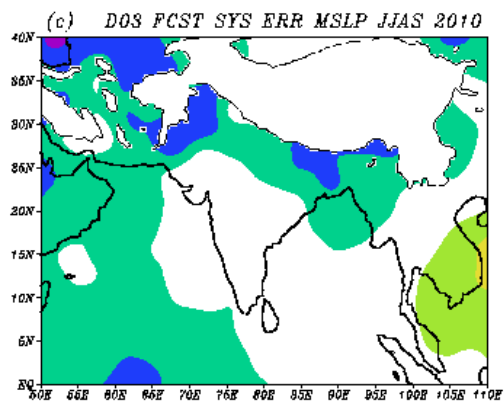
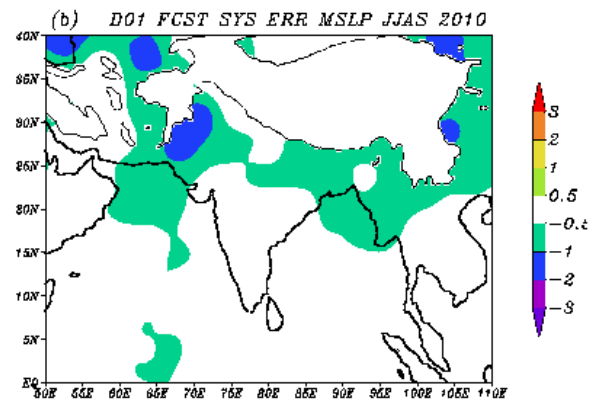
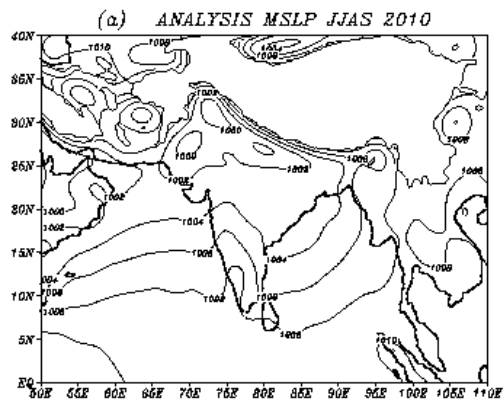


Fig. 20

3(b). Verification of Model Rainfall Forecasts

R. Ashrit, A. K. Mitra, G. R. Iyengar, Saji Mohandas and Manjusha Chourasia

For India as a whole, nearly 78% of the annual rainfall occurs during the summer monsoon season. However, the rainfall in the monsoon season over the homogenous southern peninsular of India contributes about 60% of the annual mean, and a significant amount (nearly 40% of the annual) also occurs in the post monsoon season or the north-east monsoon season. For annual as well as monsoon season rainfall, the three prominent high rainfall belts due to orographic effects are: (i) along the west coast of India and (ii) along north-east India and (iii) the foothills of the sub-Himalayan ranges. There is a general decrease of rainfall from east to west in central India and along the Gangetic plains. The rainfall over the arid regions of west Rajasthan, Saurashtra, and Kutch is less than one-third of its magnitude over the Gangetic West Bengal in the east. The monsoon season features intraseasonal variations in rainfall amount and distribution. These are mainly dictated by the active and weak cycles in the monsoon and the Bay of Bengal low pressure systems that move inland causing heavy rainfall over land regions.

1 Mean Monsoon Rainfall during JJAS 2010:

The models with high spatial resolution are expected to resolve the mesoscale processes in monsoon flow and the high resolution orography to give better rainfall prediction compared to the coarse resolution global models. In this section the performance of the two models (T254L64 and T382L64) for medium range rainfall forecasting has been examined during monsoon (JJAS) 2010. For a detailed and quantitative rainfall forecast verification, the IMD's 0.5 degree daily rainfall analysis (Rajeevan and Bhat 2008, Rajeevan et. al, 2005) is used. This is the high resolution daily gridded rainfall data set suitable for the high resolution regional evaluation. The daily rainfall data from the two models is gridded on to the observed rainfall grids over Indian land regions for the 122 days from 1st June through 30th September 2010.

The panels in Figure 1 present observed and forecast mean rainfall (cm/day) for JJAS obtained from the two models. The observed distribution of rainfall indicates the highest rainfall of up to 2 cm/day along the west coast of India surrounded by rainfall in

the range of 1-2 cm/day. Similar rainfall amounts in the range of 1-2 cm/day can be prominently seen over parts of North-east India, Gangetic plains and a large region covering West Bengal and Orissa. Over the west coast the day-1 forecasts show mean rainfall in excess of 2 cm/day at many locations surrounded by rainfall in the range on 1-2 cm/day. However, in the day-3 and day-5 forecasts the west coast features reduced rainfall amounts. Over the north east India, forecasts show high rainfall amounts comparable to the observations. The day-3 forecasts of both models show reduced rainfall amounts compared to day-1 forecasts particularly over eastern India (Orissa and surrounding areas). Over the Gangetic plains both models is over estimated rainfall particularly in Day-5 forecasts.

2 Rainfall Forecast Verification:

A detailed and quantitative rainfall forecast verification is presented in this section using the IMD's 0.5 degree daily rainfall data (Rajeevan and Bhate 2008) for the entire period of JJAS 2010. Table 1 shows the contingency table for categorical forecasts of a binary event using which the following statistics are computed. The computations take into account only the rainy days i.e., days with rainfall ≥ 0.5 cm at each grid point over land regions. The rainfall forecast verification is expressed in terms of three different scores discussed below.

2.1 Mean Error: The difference between the observed and forecast mean rainfall (Figure 2) is presented to bring out the areas of overestimated and underestimated rainfall over India. Models consistently overestimate the rainfall over the Gangetic plains. Rainfall over the dry regions of NW India is under predicted in all the forecasts. Due to reduced rainfall amounts over eastern India as well as Gangetic plains in the day-3 forecasts of both models, the mean error over these two regions is lower compared to the day1 and day-5 forecasts. In general both T254 and T382 show similar pattern and magnitude of mean error.

2.2 Equitable threat score (Gilbert skill score)-

$$ETS = \frac{hits - hits_{random}}{hits + misses + false\ alarms - hits_{random}}$$

where

$$hits_{random} = \frac{(hits + misses)(hits + false\ alarms)}{total}$$

This is a standard skill score that is being used by various weather services to evaluate their precipitation forecasts. It is frequently used to assess skill of rainfall forecasts above certain predefined thresholds of intensity of rain. ETS tells us how well did the forecast "yes" events correspond to the observed "yes" events (accounting for hits due to chance)? ETS ranges from -1/3 to 1, 0 indicates no skill and 1 meaning perfect score. Figure 3 shows the ETS computed on the forecast rainfall from both the models. Both models T254 and T382 show very similar pattern of skill in day-1, day-3 and day-5 forecasts. The gray shading in the plots indicates no skill. Large parts of peninsula shows no skill and this is true in all the forecasts. Day-1 and day-3 forecasts of both models over the central India including NW India show skill in predicting the rainy day. Similar computations for different rainfall threshold is shown in Figure 4. For lower thresholds (0.0, 0.1 and 0.6) the scores are high in the two models and there is no clear and consistent higher skill for any model. For higher rainfall amounts, the scores are low. For higher rainfall thresholds (>9cm/day) the ETS values are very small and the number of occurrences are also very low. For some of the intermediate thresholds, the T382 model forecasts show marginally higher skill compared to the T254 model forecasts.

2.3 False Alarm Ratio

$$FAR = \frac{false\ alarms}{hits + false\ alarms}$$

False Alarm ratio (FAR) is a measure of fraction of the predicted "yes" events that actually did not occur (i.e., were false alarms). This score ranges from 0 to 1 and a score of 0 implies perfect forecast. This score is sensitive to false alarms, but ignores misses. Figure 5 shows the FAR computed for the forecast rainfall for both the models. Both the models indicate higher forecast skill (lower FAR) along the west coast, north-eastern

states and along the foothills of Himalayas. Both the models show very similar patterns over dry regions with higher FAR values over the northwestern region and south-eastern tip of the peninsula.

3 All India Rainfall Verification:

The all India rainfall (AIR) variability from model (compared to observations) in time scales like daily, weekly, monthly and also in a season are useful model diagnostics, which depicts important aspects of the model skill to capture the monsoon over the Indian region in a broad sense. Several forecasters at IMD also seek (monitor) this AIR figures from the model to infer about the monsoon strength in medium range time-scale. We now examine the variability of AIR from observations and models. Figures (6-7) show the All India daily rainfall in millimeters for JJAS 2010, Seasonal rainfall, Monthly rainfall and weekly rainfall predicted by T254L64 model and figures (8-9), the corresponding charts as predicted by T382L64 model, against the observed rainfall provided by India Meteorological Department (IMD). The seasonal, monthly and weekly rainfall figures also show the long period averages (Climatology) and the weekly rainfall is the 7 days prediction from the single initial condition every week. Day-1 and Day-3 forecasts are much similar to the observations for both T254L64 and T382L64 models and there are only very minor differences between the models. However in the case of Day-5 forecasts, there is a marginal improvement in T382L64 with the intraseasonal variability better reflected by T382L64 model. The rainfall amount is over predicted by both models in Day-1. This is better observed in the seasonal total rainfall bar diagrams with Day-5 also slightly over predicting and Day-3 more comparable to the observed in both models. However, when compared between T254L64 and T382L64 systems the Day-3 rainfall is clearly closer to the observed for T382L64 compared to T254L64 model.

The monthly rainfall values suggest that July rainfall is highest followed by August, September and June, This variability is more or less reflected by the model predictions but show differences in the case of different forecast lead periods. For August and September months, generally there is more over prediction compared to the first two months. For a lead time of 3 days the predictions by T382L64 model is marginally better

than T254L64 model. In the weekly rainfall figures, the curves of observed and predicted weekly rainfall more or less coincide except for some divergences during August and September and the difference in the initial week for T254L64. T382L64 does not show the large rainfall in the first week of June and is marginally better compared to T254L64 during the rest of the period in predicting the intraseasonal variability. These weekly forecasts are made from a single initial condition once a week. The trends in AIR rainfall (changes from one week to the next during the progression of season) from global model matches well with the observed trend. However, there are some biases in values during few weeks which are obvious and consistent with the skills examined in daily scores for all India region.

4 Conclusions:

- The observed distribution of JJAS mean rainfall indicates a highest rainfall of up to 2 cm/day along the west coast of India surrounded by rainfall in the range of 1-2 cm/day. Similar rainfall amounts in the range of 1-2 cm/day can be prominently seen over parts of North-east India, Gangetic plains and a large region covering West Bengal and Orissa. Over the west coast and parts of north-eastern India the model forecasts show mean rainfall in excess of 2 cm/day surrounded by rainfall in the range on 1-2 cm/day. The forecasts clearly overestimate the observed rainfall over these two regions. Clearly the rainfall over the Gangetic plains is over estimated in both the models particularly in Day-5 forecasts. However, this overestimation is subdued in the day-3 forecasts.
- While the dry conditions of June are well captured in all forecasts of all models, the wet conditions (particularly Gangetic plains) of July, August and September are overestimated in all the forecasts.
- Both the models indicate higher forecast skill along the west coast, north-eastern states and along the foothills of Himalayas. Both the models show very similar patterns over dry regions with higher FAR values over the northwestern region and south-eastern tip of the peninsula.
- For all India rainfall, the higher resolution T382 system is marginally better compared to coarse resolution T254 system.

Table 1. Contingency table for categorical forecasts of a binary event.

Event Forecasts	Event Observed	
	Yes	No
Yes	<i>hit</i>	<i>false alarm</i>
No	<i>miss</i>	<i>correct rejection</i>

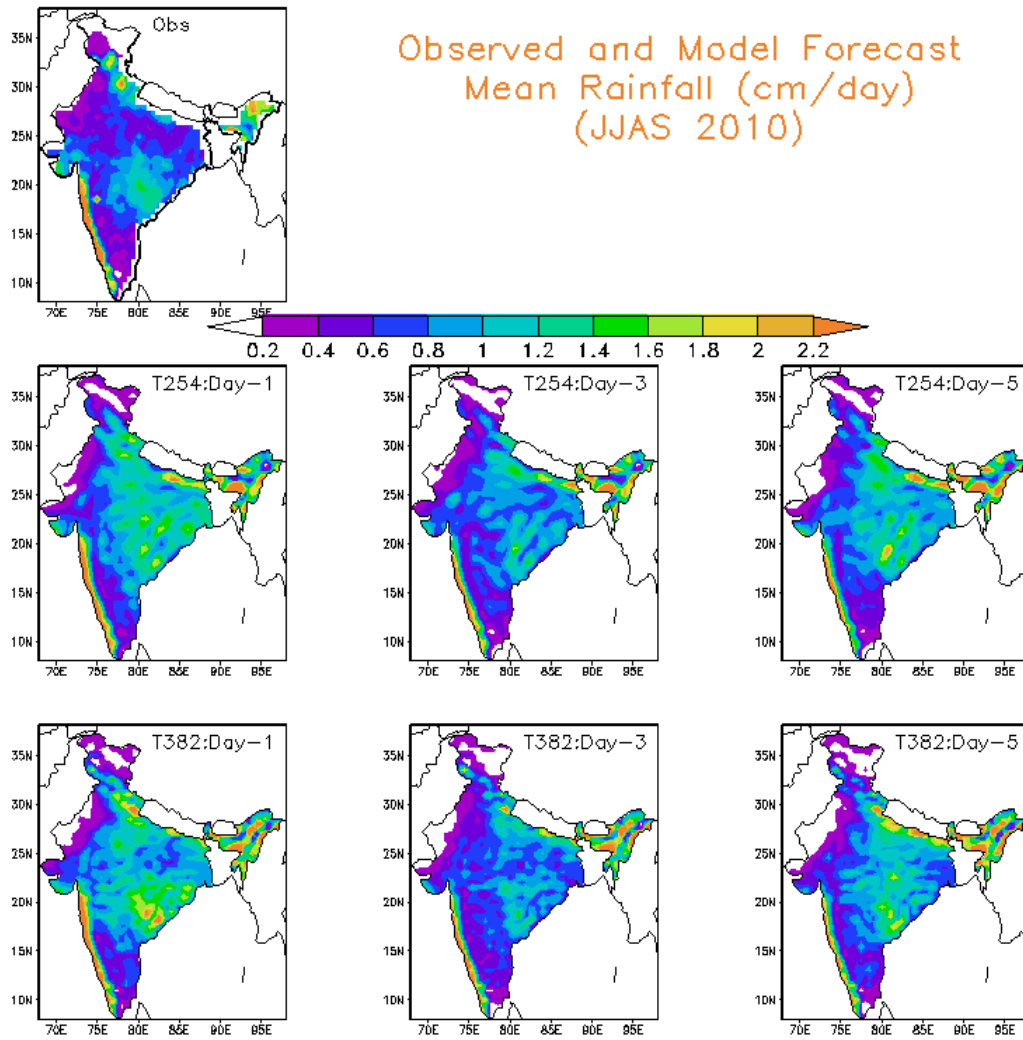


Figure 1. Observed and forecast mean rainfall during JJAS 2010.

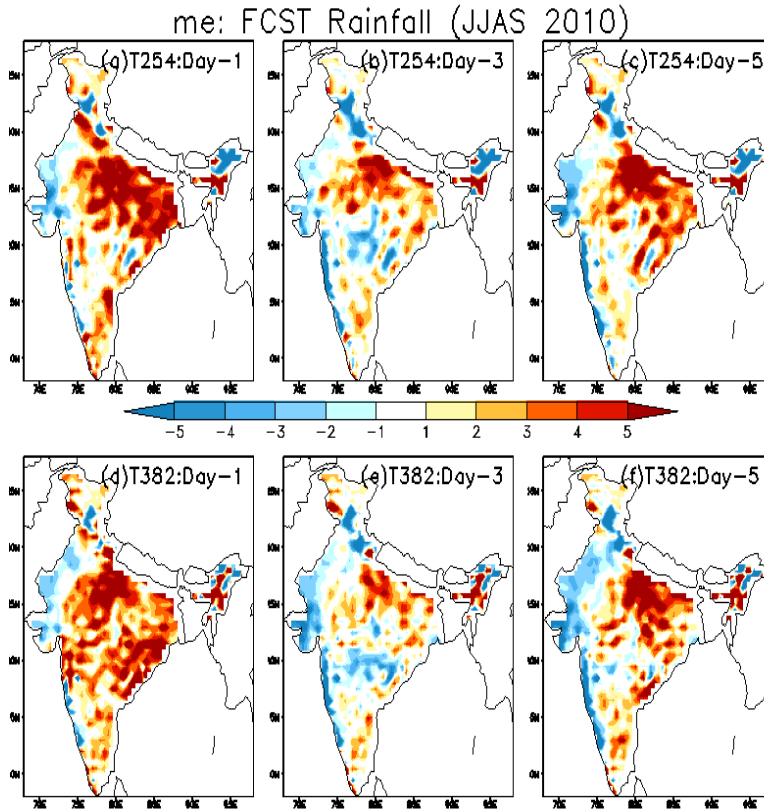


Figure 2. Mean error in the forecast rainfall during JJAS 2010.

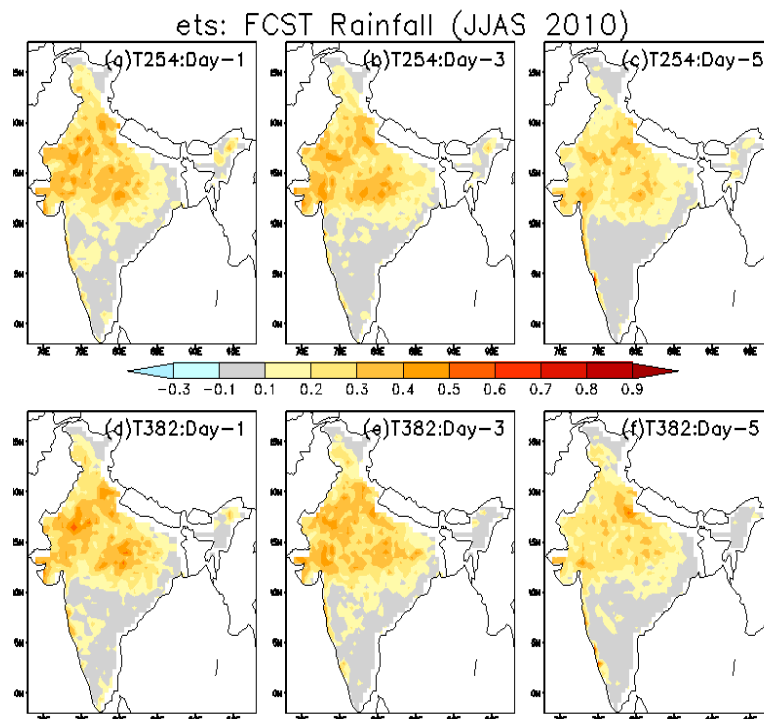


Figure 3. Equitable Threat Score for forecast of rainy day during JJAS 2010.

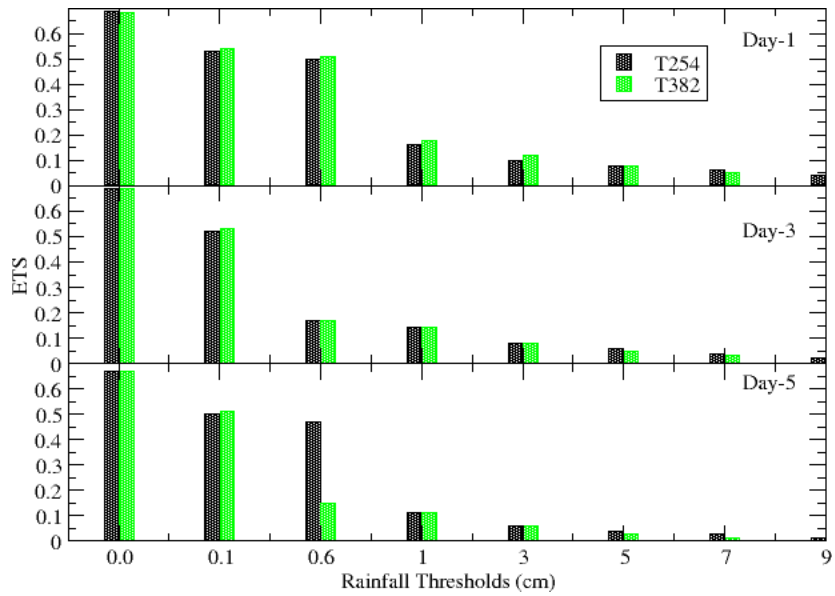


Figure 4. Equitable Threat Score for predicted rainfall exceeding different thresholds.

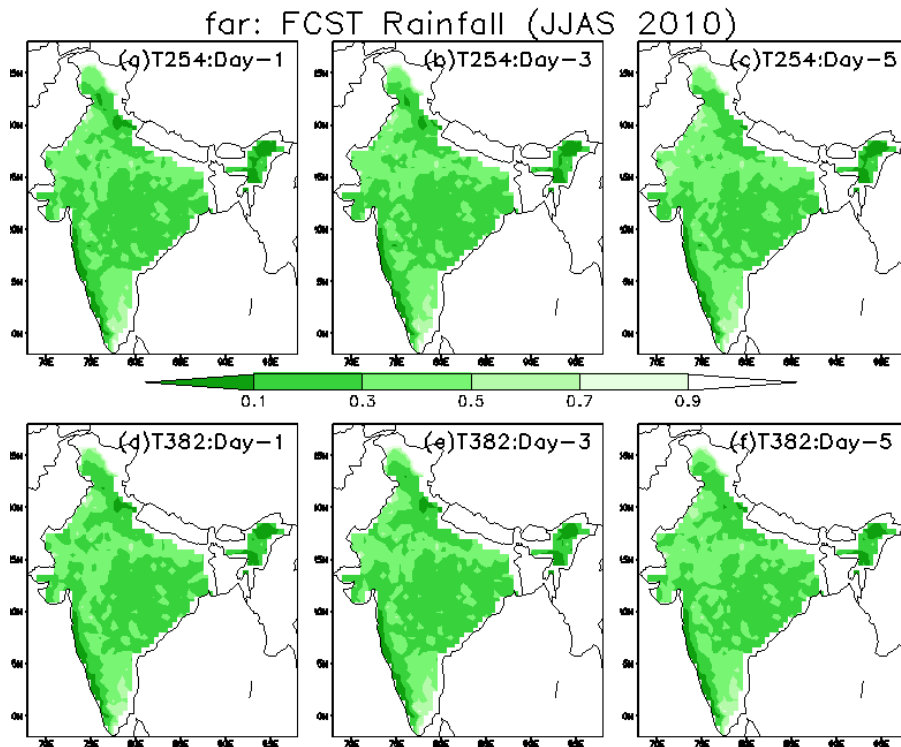


Figure 5. False Alarm ratio for forecast of rainy day during JJAS 2010

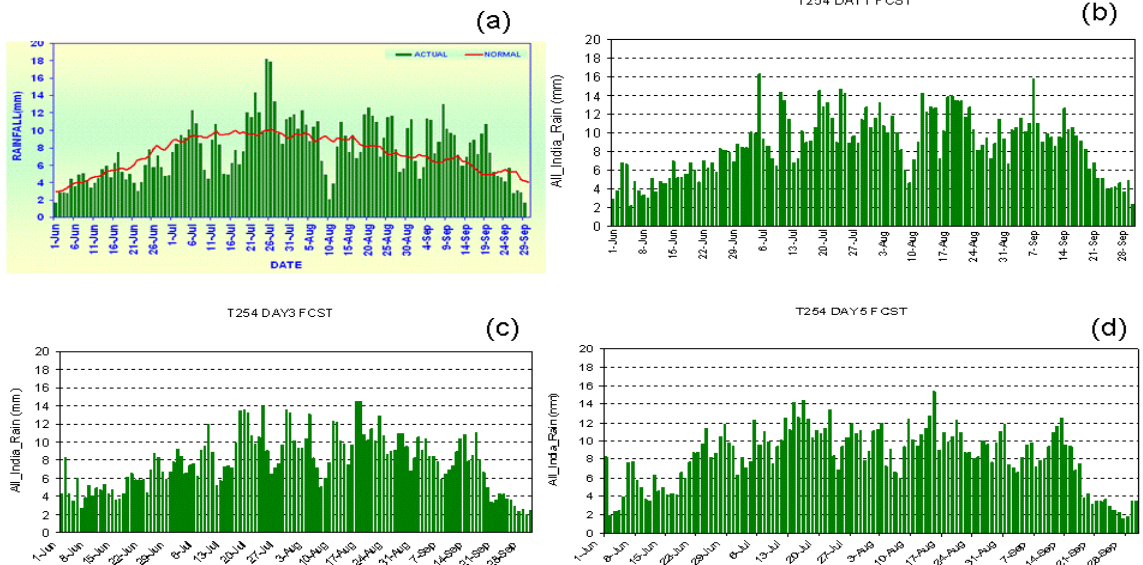


Fig. 6 All India daily rainfall (mm) for JJAS 2010; (a) observed (b) Day-1 forecast (c) Day-3 forecast and (d) Day-5 forecast by T254L64 model.

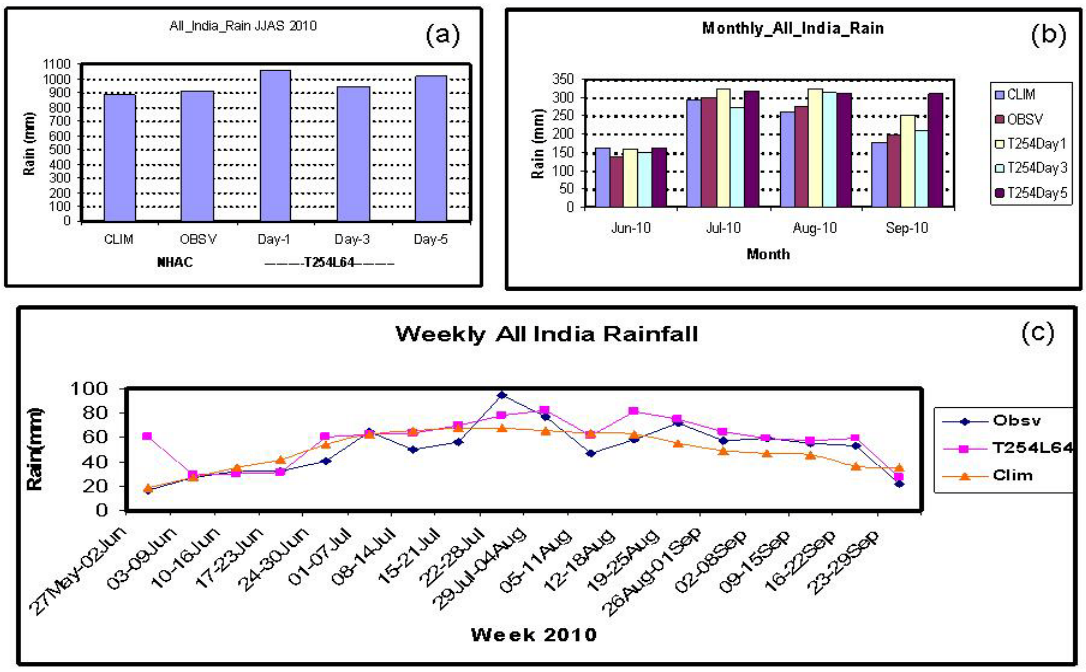


Fig. 7 Seasonal (a), Monthly (b) and weekly (c) rainfall (mm) predicted by T254L64 model for Monsoon-2010 against observed and long period average (climatology). Weekly rainfall is accumulated 7-day forecast from single initial conditions of every week.

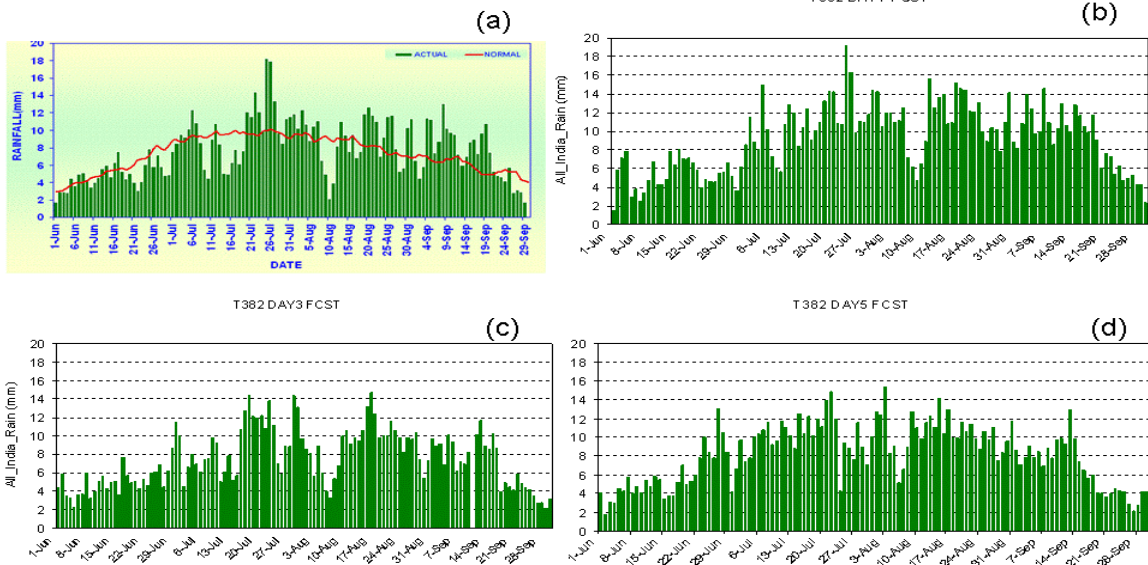


Fig. 8 All India daily rainfall (mm) for JJAS 2010; (a) observed (b) Day-1 forecast (c) Day-3 forecast and (d) Day-5 forecast by T382L64 model.

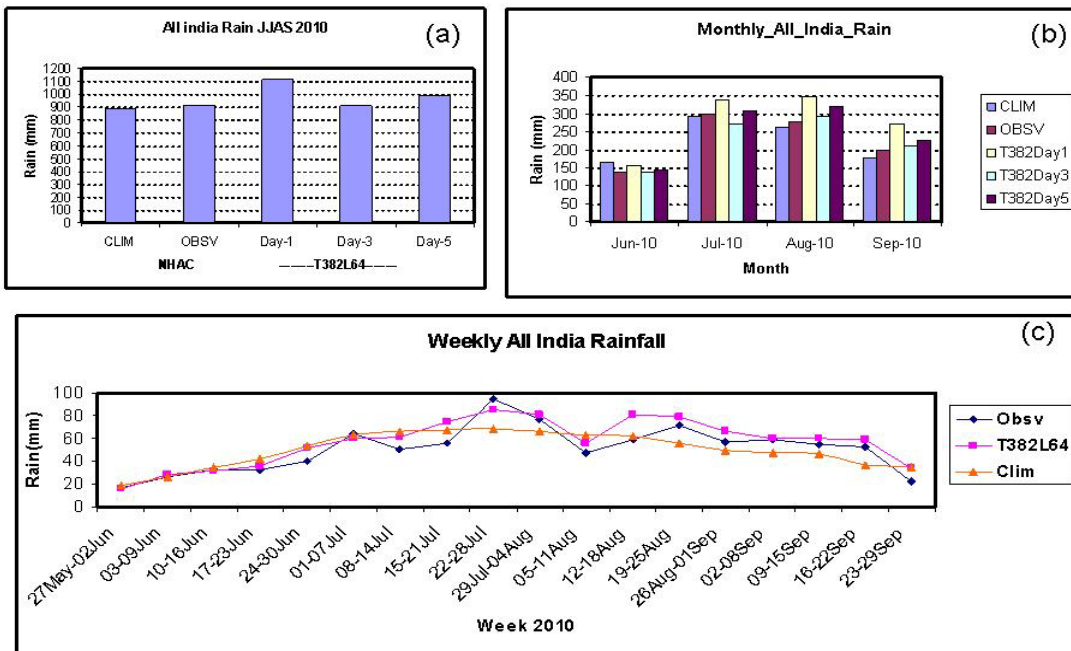


Fig. 9 Seasonal (a), Monthly (b) and weekly (c) rainfall (mm) predicted by T382L64 model for Monsoon-2010 against observed and long period average (climatology). Weekly rainfall is accumulated 7-day forecast from single initial conditions of every week.

4a. Onset and Advancement of Monsoon

M. Das Gupta

Introduction:

Southwest monsoon activity of 2010 over Indian region was normal and rainfall received was 102% of its long period average (LPA) during June to September . During monsoon 2010, the onset over Kerala was declared on 31st May (one day prior to normal date is 1st June) by India Meteorological Department(IMD). There after rapid advancement of southwest monsoon was seen and half of the country covered by middle of June. Then there was a hiatus in the advance of the monsoon during 19th to 30th June with resulting rainfall only 84% of LPA in June 2010. Rainfall activity subsequently increased in first week of July and monsoon covered the entire country by 6th of July .

The onset of Monsoon is recognized as a rapid, substantial and sustained increase in rainfall over land. However significant transitions of tropospheric circulation pattern, humidity and temperature fields are also observed. An objective method for predicting monsoon onset, advancement and withdrawal date using dynamic and thermodynamic precursors from NCMRWF T80L18 analysis-forecast system was developed (Ramesh et al. 1996, Swati et al. 1999.) and used since 1995 at NCMRWF. The same has been extended for NCMRWF T254L64 analysis-forecast system during monsoon 2008 (Das Gupta and Mitra, 2009) and subsequently to T382L64 system in 2010. The onset and advancement of monsoon, based on the above mentioned objective method from NCMRWF T382L64 and T254L64 analysis-forecast system during monsoon 2010 will be discussed here.

1. Onset over Bay of Bengal:

The advancement summer monsoon over southwest Bay of Bengal (BOB) normally takes place prior to that over Arabian Sea (ARB) around 2nd-3rd week of May. The evolution of monsoon onset was monitored routinely from the first week of May by monitoring the daily variations of the analysed and predicted value of 850 hPa kinetic energy(KE), net tropospheric (1000hPa-300hPa) moisture (NTM) and mean tropospheric (1000hPa-100hPa) temperature (MTT) computed over BOB(0°N -19.5°N,78°E-96°E). Figure 1 depict the daily variations of KE, NTM and MTT over BOB form 1st May to 21st June 2010 for 0000UTC T254L64 analysis (black line) and subsequent day-1(24hr.) to day-7(168 hr.) predictions respectively. As daily run of T382L64 at NCMRWF was started from 21st May , the plot corresponding to onset over BOB for T382L64 was not shown here. As seen from the plots the substantial increase in KE was seen on 17th May, associated with formation of tropical cyclone Laila. IMD also declared the onset over BOB on 17th May.

Daily Variation over BOB NCMRWF(T254L64)
Monsoon 2010

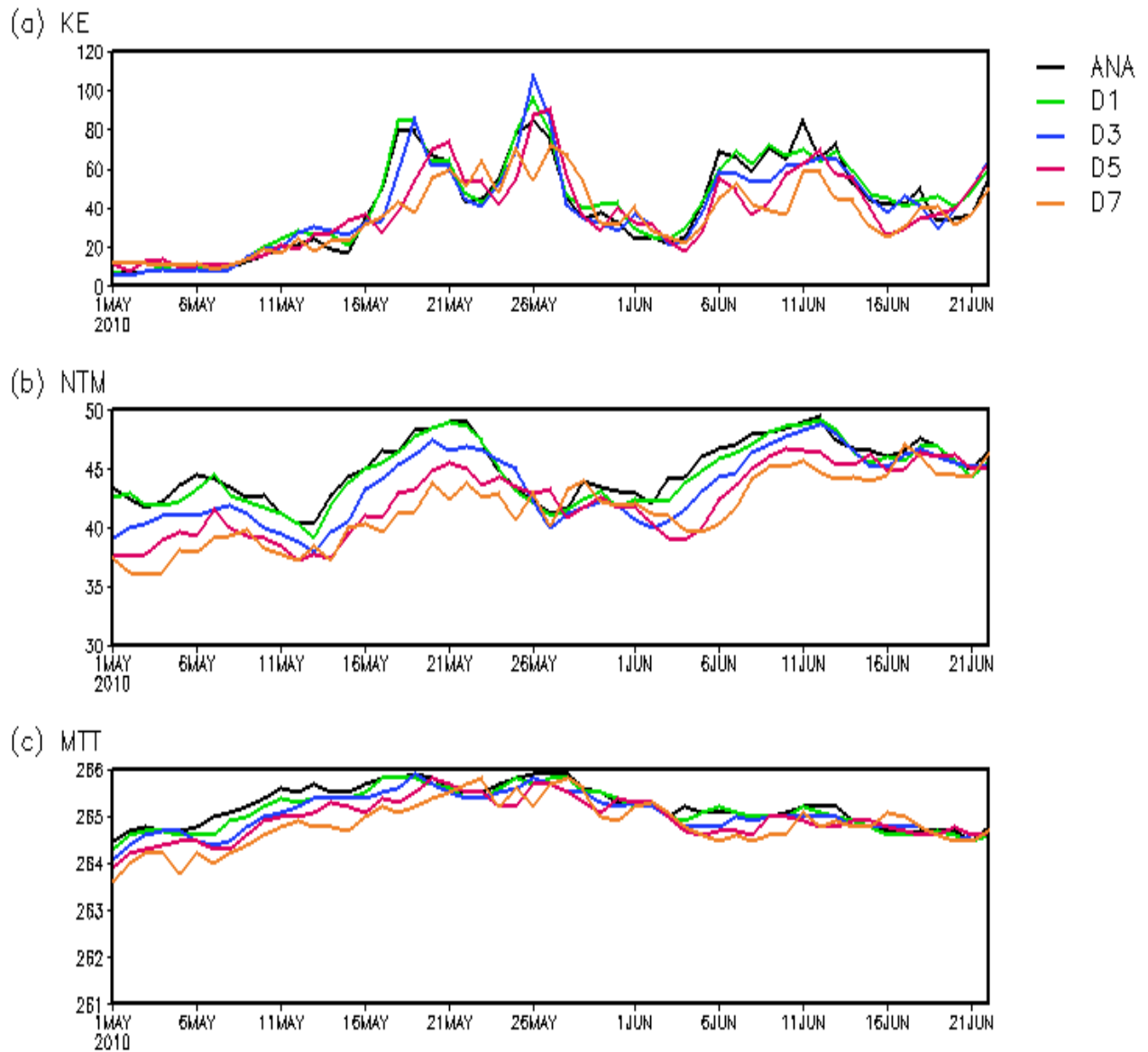


Fig.1 Daily variation of (a) Kinetic energy, (b) Net Tropospheric Moisture and (c) Mean Tropospheric Temperature over Bay of Bengal as simulated in T254L64 system during 1st May-21st June 2010

2. Onset over Kerala (Arabian Sea Branch):

The Arabian Sea branch of monsoon generally first hits the Western Ghats of the coastal state of Kerala around 1st June with standard deviation of 8 days. Figure 2 depicts the daily variations of analysed and predicted KE at 850 hPa, NTM and MTT computed over Arabian Sea (ARB) (0-19.5° N; 55.5°E-75°E) from 25th May 2010 onwards.

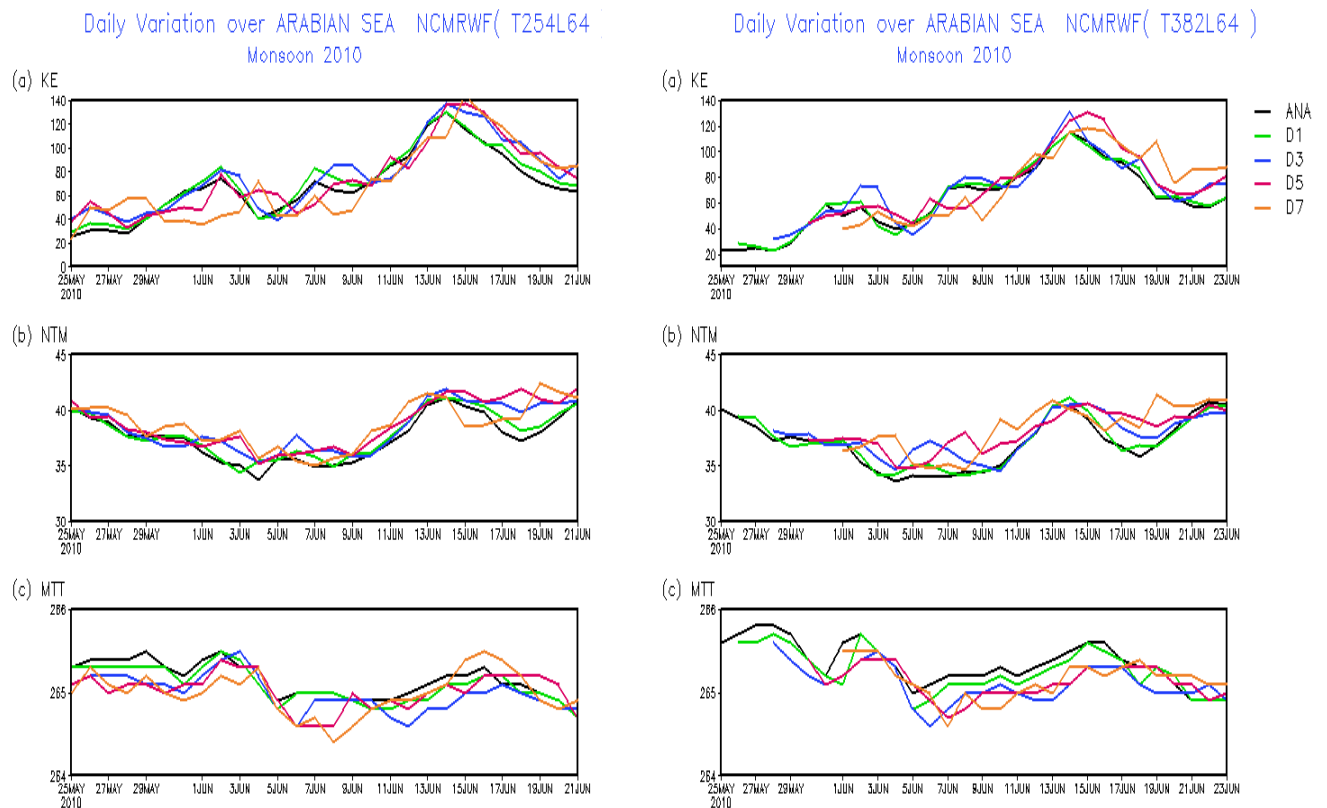


Fig.2 Daily variation of (a) Kinetic energy, (b) Net Tropospheric Moisture and (c) Mean Tropospheric Temperature over Bay Arabian Sea as simulated in T254L64 and T382L64 system during 1st May-21st June 2010

As seen from the plot that though KE was more than the threshold value $60\text{m}^2\text{s}^{-2}$ around 1st June but NTM was below 40 mm till 12th June. IMD declared the monsoon

onset over Kerala on 31st May, but NCMRWF predictions showed the onset over Kerala on 12th June (T264L64) and 14th June (T382L64) respectively, based on above said objective criterion.

3. Advancement of Monsoon:

According to objective criteria the advancement of monsoon over main land of India is determined by examining changes in NTM together with the flow characteristics at 850hPa in analyses and subsequent predictions. The criteria adopted for determining the progress of monsoon over a particular location are as follows:

- (i) Steady increase of NTM under the influence of expected wind regime at 850 hPa
- (ii) Sharp fall in the net moisture content and subsequent rise there after under the influence of same wind regime
- (iii) Date for advancing the northern limit of monsoon over a location is fixed on the day of fall in the net moisture content, which is believed to be utilized for producing the rainfall associated with the advancement of monsoon over that region

For determining the advancement of monsoon over different locations over Indian main land, NTM MTT and wind direction and speed at 850hPa in analysis and predictions are examined over 43 locations over India.

In 2010 the advancement of monsoon along the west coast was seen during 1st to 15th June. After that there was a prolonged hiatus period until 31st June and thereafter rapid advancement was seen over Gangetic plane, covering whole country within 6 days i.e. by 6th July. Figure 3 depicts the same for Mumbai during 31st May to 22nd June 2010 both for T254L64 and T382L64 system. As seen from the plot, the first occurrence of

south-westerly winds are seen around 5th June and at the same time NTM was also showing an increasing trend. But by that time the monsoon was not covered the southern part of west coast. Around 10th June wind regime changed from westerly to easterly over Mumbai indicating presence of cyclonic vorticity around 10th June. During this period NTM was also increasing and shown sudden fall on 11th June both for T254L64 and T382L64. So according to objective criterion 11th June could be fixed as onset date over Mumbai but by that time onset over Kerela was not captured in NCMRWF predictions. However, IMD declared onset over Mumbai on 11th June.

Since the advancement over Gangetic plane was very rapid during 2010 monsoon, it was not possible to predict the onset over Gangetic plane and northern parts of country using the objective criterion

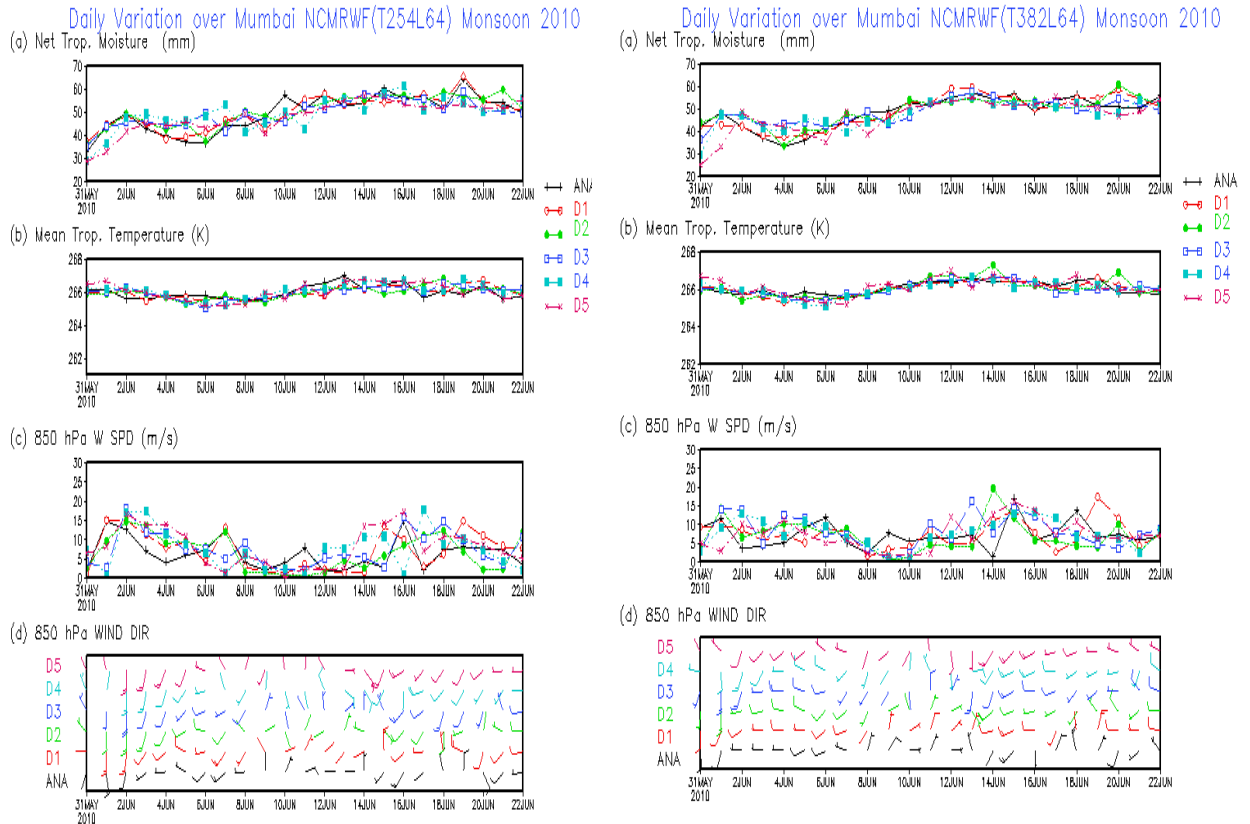


Fig.3 Daily variation of (a) NTM, (b) Net MTT (c) Wind Speed at 850 hPa and (d) Wind direction at Mumbai (IC: 31st May- 22th June 2010) for T254L64 and T382L64 respectively

4. Summary:

The objective criteria for onset/progress of monsoon was developed based on analysis and forecast data from a coarser resolution global model (T80L/18) was tested with data from a higher resolution global model (T254L64) for monsoon 2008. It was concluded that the parameters related to the objective criteria of onset and progress of monsoon over India were also well captured by analysis and the medium range predictions from higher resolution model. But during 2009, it is seen that some of these

features were not captured well by T254L64 system for southern peninsular stations. In 2010 it is seen that though onset over BOB was captured well but the onset of ARB though captured but was delayed by almost two weeks. Advancement of monsoon over land was also not captured by this technique. Mechanism for incorporating rainfall predictions from high resolution models, in the objective method could be explored in future.

References:

Das Gupta M 2010: Onset and Advancement of Monsoon, “MONSOON-2008: Performance of the T254L64 Global Assimilation Forecast System“, Report no. NMRF/MR/01/2010, 131 pages, Published by NCMRWF (MoES), A-50 Institute Area, Sector- 62, NOIDA, UP, INDIA 201 307

Das Gupta M., A. K. Mitra 2009: Onset and Advancement of Monsoon, “MONSOON-2008: Performance of the T254L64 Global Assimilation Forecast System“, Report no. NMRF/MR/01/2009, 117 pages, Published by NCMRWF (MoES), A-50 Institute Area, Sector- 62, NOIDA, UP, INDIA 201 307

Ramesh, K.J, Swati Basu, and Z.N. Begum, 1996: Objective determination of onset, Advancement and Withdrawal of the summer monsoon using large scale forecast fields of a global spectral model over India, Meteor. and atmospheric Physics,61, 137-151.

Swati Basu, K.J. Ramesh and Z.N. Begum,1999: Medium Range Prediction of summer monsoon activities over India vis-avis their correspondence with observational features, Adv. in Atmos. Sci.,16,1,133-146.

4(b). Monsoon Indices: Onset, Strength and Withdrawal

D. Rajan and G. R. Iyengar

1. Introduction:

The annual reversal of wind and rainfall regimes in monsoon is spectacular. An objective manner of declaring the onset of the south west monsoon over Indian main land is discussed in this chapter. Precipitation in India has clear seasonal variation and the onset of the Indian summer monsoon is of great interest as not only a research target but also a socio-economic factor for water resources in India. Due to distinct spatial features of monsoon and the diverse ways of representing monsoon, it is difficult to derive 'universal index' to measure the variability of the monsoon over all of Asia. The onset date of the monsoon has been defined by various methods in past research studies.

The variability of the continental tropical convergence zone and the large-scale monsoon rainfall is linked to the variability of convection over the equatorial Indian Ocean and the surrounding seas ie Arabian Sea and the Bay of Bengal. The onset and withdrawal of the broad scale Asian monsoon occur in many stages and represent significant transitions in the large-scale atmospheric and ocean circulations (Fasullo and Webster 2003), which can be examined by analyzing various monsoon indices. Useful indices provide a simple characterization of the state of the monsoon during different epochs and also the inter-annual variability. While there is no widely accepted definition of these monsoon transitions at the surface, the onset is recognized as a rapid, substantial increase in rainfall within a large scale.

1(a). Background

In 1943 for the first time the India Meteorological Department (IMD) determined the normal onset and withdrawal dates of summer monsoon with 180 rain-gauges stations across British India (present India, Pakistan, Bangladesh, Myanmar and Sri-Lanka) from 'characteristic monsoon rise/fall in pentad rainfall', and prepared charts showing normal onset and withdrawal dates across the Indian sub-continent.

The arrival of the summer monsoon over the Kerala coast is found to be reasonably regular either towards the end of May or beginning of June (Ramesh et al. 1996; Prasad and Hayashi 2005; Taniguchi and Koike 2006, Goswami and Gouda 2010). The monitoring and forecasting of the summer monsoon onset over the Indian subcontinent is very important for

the guidelines for the operational forecaster reference. This migration and location of the heat source associated with summer monsoon has important implications for the withdrawal of monsoon over South Asia. Many studies show the declaration is best when the occurrence of the onset withdrawal is abrupt and declaration is worst when it is feeble. However, to date there has been no systematic investigation of the retreat of the monsoon system despite its key contribution to total rainfall variability. But it is known that, in terms of rainfall, the onset is better defined than the withdrawal. In this section of the report NCMRWF T254L64 & T382L64 global analysis and forecast products have been used to compute various monsoon indices to monitor onset, strength and the withdrawal of the monsoon during 2010 season.

2. Monsoon circulation indices for onset, strength and withdrawal:

Kerala state, situated in the southwest part of the Indian sub-continent is the gateway for the Indian summer monsoon. Based on Kerala rainfall, the mean onset date occurs around 01 Jun and varies with a standard deviation of 8-9 days from year to year. Given the relatively small scale of Kerala that is less than 200 km in breadth, sensitivity of the declaration of onset based solely on the district's rainfall (narrow area) only; but the monsoon transitions is also likely to be large. In India at IMD the onset date is declared based on rainfall, wind, temperature, moisture, cloud pattern, and the state of the sea, etc In addition to recently re-determination of dates of onsets by taking rainfall data base from 1971- 2000 also taken place. For a forecaster it is a difficult job to declare the date of onset because all the above parameters are highly variable in space and time. It is difficult to quantify these parameters precisely and so the experience of the forecaster plays a key role in declaring the date of monsoon onset subjectively for individual years (Wang et al ., 2009).

The India Meteorological Department (IMD) has been using the qualitative method over a long period using rainfall to declare the onset date for the monsoon forecast. As per IMD's daily weather bulletins for the year 2010, the southwest monsoon set in over Andaman Sea around on 17 May, three days prior to its normal date in association with severe cyclonic storm. As per the daily bulletins it set over Kerala on 31 May, about a day earlier than the normal onset date.

Ramesh (1996) et al., suggested the following characteristics for the evolution of the onset over the Arabian Sea covering the area of $0^{\circ} - 19.5^{\circ} \text{N}$ and $55.5^{\circ}\text{E} - 75^{\circ}\text{E}$: (i) the net tropospheric (1000 – 300 hPa) moisture build-up, (ii) the mean tropospheric (1000 – 100 hPa)

temperature increase, (iii) sharp rise of the kinetic energy at 850 hPa. It is read that the above objective study most of the time computed the onset date delayed by few (8 -10) days than the declared actual date. In the pervious section of this report, onset and progress have been described with the above said criteria for monsoon 2010, which also shows onset over Kerala around 10 Jun. As per that study this year also it is noted that the onset date is seen to be around 10 Jun.

In this chapter four monsoon dynamical indices are computed using data from NCMRWF high resolution T254L64 & T382L64 analyses and forecast systems. These widely used monsoon dynamical indices of the South Asian summer monsoon are listed in the table (I) with their corresponding brief definition. These monsoon indices are based on circulation features associated with convection centers related with rainfall during the summer monsoon for the Indian region.

In 1999 Goswami et al ., defined the index based on the meridional wind (V) shear between 850 hPa and 200 hPa over the south Asian region $10^{\circ}\text{N} - 30^{\circ}\text{N}$, $70^{\circ}\text{E} - 110^{\circ}\text{E}$ which is related to the Hadley cell features. This index can be used to study the onset and advancement phases of the monsoon.

Wang et al., (2001) introduced a dynamical index based on horizontal wind (U) shear at 850 hPa called the circulation index. They recommend that the circulation index computed with the mean difference of the zonal winds (U) between the two boxes; one for southern region and the other for the northern region, i.e. $5^{\circ}\text{N} - 15^{\circ}\text{N}$, $40^{\circ}\text{E} - 80^{\circ}\text{E}$ and $20^{\circ}\text{N} - 30^{\circ}\text{N}$, $70^{\circ}\text{E} - 90^{\circ}\text{E}$ can be used as the criteria for identifying the onset date. The southern region box is taken over South Arabian Sea and the northern region box is taken over northern land region. This circulation index describes the variability of the low-level vorticity over the Indian monsoon trough, thus realistically reflecting the large scale circulation. After that Fasullo and Webster (2003) defined the onset date in terms of vertically integrated moisture transport derived from reanalysis data sets. As per their discussions the inter-annual variation in the onset date modestly agreed with reality.

Taniguchi and Koike (2006) first time emphasized the relationship between the Indian monsoon onset and abrupt strengthening of low-level wind over the Arabian sea ($7.5^{\circ}\text{N} - 20^{\circ}\text{N}$, $62.5^{\circ}\text{E} - 75^{\circ}\text{E}$). They have used three variables (i) vertically integrated water vapor (ii) moisture transport (iii) low-level wind in an objective manner to determine the onset date. This is a measure of the strength of the low-level jet over South Arabian Sea and indicates the

strength of the monsoon over India. They showed that Indian summer monsoon onset is brought mainly by enhancement of low-level wind over the Arabian Sea.

Wang et al., (2009) found that the onset date can be objectively determined by examining of the sustained 850 hPa zonal wind (U) averaged over the southern Arabian Sea ($5^{\circ}\text{N} - 15^{\circ}\text{N}$, $40^{\circ}\text{E} - 80^{\circ}\text{E}$). In the recent studies Wang et al., (2009) this criterion is referred as objective circulation index. The rapid establishment of steady westerly is excellent parameters to correlate with the abrupt commencement of the rainy season over the southern tip of the Indian peninsula. In this index, the onset date is defined as a sustained zonal westerly exceeding 6.2 m/s and persists for more than six days. This definition depends on large scale circulation feature. This circulation index clearly omits the bogus onset or multiple onset dates. The bogus or double/multiple monsoon onset develops when the strong convection in the Bay of Bengal is accompanied by the monsoon like circulation and appears in the Indian Ocean.

Syroka and Toumi (2002, 2004) also defined a similar type of circulation index by taking the box slightly towards east of Wang's (2001) case. However, to date there has been no systematic investigation of the retreat of the monsoon system despite its key contribution to total rainfall variability. A daily circulation index was defined as the difference in average 850 hPa zonal winds between a southern region $5^{\circ}\text{N} - 15^{\circ}\text{N}$, $50^{\circ}\text{E} - 80^{\circ}\text{E}$ and a northern region $20^{\circ}\text{N} - 30^{\circ}\text{N}$, $60^{\circ}\text{E} - 90^{\circ}\text{E}$. This daily circulation index is a physically sensible and practical tool to study the withdrawal of the monsoon also. According to them the date of withdrawal of the monsoon is defined as the first of seven consecutive days for which the index becomes negative. This daily circulation index can be used to define both the dates of onset and withdrawal of the Indian summer monsoon from these regions. The index changes sign, reflecting both the changing intensity of the low-level westerly monsoon flow and the vorticity associated with the monsoon trough and synoptic activity. The above index suggests that the average date of withdrawal is 16 October with a standard deviation of 7 days. In this section we have computed the above described computation for circulation indices based upon the various definitions that are tabulated in table (I).

3. Results and discussions:

We use the daily NCMRWF high resolution NCEP version of T254L64 & T382L64 analyses and forecasts (up to 120 hrs) data sets for the period May to September 2010. Details

of the NCMRWF assimilation and forecast systems are described in chapter 1 of this report. The IMD Climate Diagnostics Bulletin of India (2010) daily/seasonal reports have been referred for the observation of rainfall, flow patterns, the dates for the declaration of onsets monsoon strength and withdrawal etc during the entire period of this study.

Figures (1a1), (1a2) shows the objective circulation indices calculated by Wang et al ., (2009) for the analyses and forecasts for the length of 24 hr, 72 hr and 120 hr. From these figures it is seen that the apparent onset date (bogus onset) is noticed as 31 May, by the sustained westerly (U) exceeding 6.2 m/sec and could not persist for more than four days i.e. up to 04 Jun. This high value of U did persist beyond 05 Jun also; up-course there was a slight less westerly have been noticed during 03 - 05 Jun. From these figures T254L64 & T382L64 it is seen that the actual onset date is noticed around 05 Jun, by the sustained westerly (U) exceeding 6.2 m/sec and persisting for more than six days. Hence it is appropriate to say that the real dynamical onset occurred on 05 Jun only. The bogus onset date 31 May can be omitted safely by saying these monsoon onset criteria. In the predicted indices also broadly these features are captured well. Although in the 72 hr and 120 hr forecasts able to capture the transition of the onset. The bogus onset occurred on 31 May over Kerala coast is clearly due to the system association with the very severe cyclonic storm called '**PHET**' over the Arabian Sea whose life history was 31 May - 02 Jun. In this case cooler air is brought by the strong winds having intensity more than 6.2 m/sec at 850 hPa around the vicinity of the cyclone over the Arabian Sea. The above theory has been brought out clearly by Taniguchi et al., (2010).

Figures (1b1) and (1b2) show the circulation indices calculated by Syroka and Toumi (2002, 2004) for the onset phase. From these figures of T254L64 & T382L64 we infer that the onset date around 03 -05 Jun 2010, because on that day onwards the daily index is changing it's sign from negative to positive and maintained there after. In this case also the bogus onset seen around 28-30 May; as daily index is changing its sign from negative to positive but not maintained thereafter. The analyses and the 24 hr forecasts, 72hr forecasts, 120hr forecasts of both the resolutions show the change of sign, but with a lag of few days. Syroka and Toumi index also shown that 28- 30 May is not the actual date of onset over Kerala during this year 2010.

Figures (1c1) & (1c2) show the circulation indices/vertical shear suggested by Goswami et al., (1999) for the onset phase. This is popularly known as Goswami Hadley cell

circulation index. From these figures we infer that the onset date is seen around 03 - 05 Jun only but not on the day 31 May, because on that day onwards the daily index is changing its sign from negative to positive and maintained the positive sign there after. The analyses and the 24 hr forecasts, 72 hr forecasts, 120 hr forecasts of both the resolutions are having the same trend and are able to capture the change of sign from negative to positive with a lag of 2-3 days. Among the resolutions the T254 have clear representation than T382 in this regard.

Figures (2a1), (2a2) and (2a3) show the Wang (2001) circulation index for the 122 days of the monsoon 2010. From the IMD source it is seen that in association with monsoon onset the advance of monsoon over the northeastern states including West Bengal & Sikkim occurred earlier than normal. This year it is observed that the advance of monsoon over the northeastern states was earlier than normal. A prolonged hiatus in the advance of monsoon occurred during 19 – 30 Jun, which is clearly seen in the figures having circulation index about 5 m/sec only.

The further advance of monsoon occurred in association with the formation of a low pressure area over the North Bay of Bengal and neighborhood on 02 Jul. The monsoon covered most parts of the country except Rajasthan, on 05 Jul 2010. A prolonged hiatus occurred during 10 - 20 Jul which is clearly reflected in the index curve having minimum westerly strength as measured by Wang & Ding circulation indices.

On daily scale, rainfall for the country as a whole was generally normal to above normal on most of the days during the season, except for some days, during the end of June, middle of July, first week of August and last week of September. The seasonal rainfall was above normal over most parts of the country except parts of northeastern/eastern and adjoining central region and parts of Kerala. The above period can be very well correlated with the dates as seen from the figures (2a1), (2a2) and (2a3) as well.

As per observation, apart from the cyclonic storm '*PHET*', fourteen low pressure areas (2 in the month of June and 4 each in July, August and September) were also formed during the season. Of these, 12 low pressure areas formed over the Bay of Bengal. These low pressure areas persisted for 4 to 5 days and generally moved Westward rapidly from Bay of Bengal to western parts of the country and dissipated over the central/northern region. These low pressure areas caused good amount of rainfall over the concerned region.

As shown in the figure (2a3) there are more than six peaks with the strength of more than 10 m/sec wind speed, which can be correlated with the peaks rainfall observed Figure (2

b) during this season with some time lag. The break monsoon conditions also prevailed over the country during the middle of July. It has affected the rainfall (- 0.39 %) over the central and South peninsular India during July. The cross equatorial flow was weaker than normal during major parts of the season except for a brief period from last week of June to third week of July; which can be correlated with the rainfall observation shown in figure (2b).

The weak cross equatorial flow prevailed during most parts of June and in the first fortnight of July. Two low pressure areas formed in June over the northwest Bay of Bengal and neighborhood, one during the period 9-13 Jun and the other during 24-26 Jun. The first one dissipated in-situ and the other one was short lived and dissipated over Gangetic west Bengal and neighborhood. The observed rainfall during 21-27 Jun indicated very large negative anomaly in rainfall.

In the year 2010 the less amount of rainfall distribution was mainly due to the break monsoon condition that developed during 12 – 20 September, which can be easily correlated with the circulation index shown in figures (2a1, 2a2, 2a3).

The figures (3a1) and (3a2) show the wind circulation index as per Syroka & Toumi (2002) for the period of August – September 2010. From the IMD's climate diagnostics bulletin of India (2010) it is seen that in there was delay in the withdrawal of southwest monsoon due to rainfall activity over north India in associated with mid latitude westerly activities. In this year 2010 there is considerable delay in the withdrawal of southwest monsoon from west Rajasthan. This delay is due to the prevalence of moisture in the lower levels and favorable conditions for rainfall created by the presence of mid-latitude westerlies in the upper levels over the north western parts of the country.

From the figure it is seen that the circulation index values reduced sharply but it does not changes its positive slope to negative (dip) up to the date 27 September. So the withdrawal date can not be consider as the above date. From 22 – 30 September the index curve is near to the vicinity of the axis. It is clear that the intensity gets the minimum value around the 22 and 30 of September. Hence 27 September can be taken as withdrawal date of the southwest monsoon 2010. This date can be commented as the real withdrawal date. Thus the withdrawal of monsoon from west Rajasthan started only on 27- 28 September which is delay of more than 2 weeks time from the normal date (1 September), of withdrawal from extreme western parts of Rajasthan. In the second occasion circulation index changes its slope from positive to negative on 27 -28 September onwards; subsequently it persists for more than

5 days. This increase in the circulation index brought rainfall to the country as shown in the figure (2b). Thus the day 27 September can be regarded as the withdrawal date of southwest monsoon for the year 2010. When we consider the IMD official information on withdrawal dates it is closer to 27 September as seen in the above systems with the resolutions T254 & T382. It is reported that the withdrawal started on 27-28 September over the Rajasthan. In reality also the southwest monsoon withdrew from the entire country on 29 October 2010 (figure not shown).

4. Summary:

Several popular monsoon indices have been used to study the onset, strength and withdrawal of monsoon during 2010 season. In general, the indices are able to represent the onset, variability in strength of monsoon and the withdrawal in a reasonable way. This year bogus onset occurred on 31 May has been clearly brought out by these indices programmers. As per these indices studies, the actual date of monsoon onset over the main land is 05 Jun only. The indices when used with medium range forecast data from the global models with resolutions T254L64 & T382L64 indicate that the same could be used to forecast the changes in phases of the monsoon system within this season. The monsoon withdrew from the entire country, Bay of Bengal and Arabian Sea on 29 October and simultaneously the northeast monsoon rains commenced over the south peninsula. These indices have to be refined with more years of data from such a higher resolution system. In future use of thermodynamic parameters from the model will add value to the monitoring of monsoon by such indices.

Acknowledgement: Thanks are due to the observed rain information of IMD made available via IITM web site.

References

Climate Diagnostic Bulletin of India 2010: Special Issue No. **58**. Issued by National Climate Center office of the Additional Director General of Meteorology (Research) India Meteorological Department, Pune.

Fasullo. J. and P. J. Webster, 2003: A hydrological definition of Indian monsoon onset and withdrawal. *J. climate*, **16**(14), 3200-3211.

Goswami. B.N., V. Krishnamurthy and H. Annamalai 1999: A broad scale circulation index for interannual variability of the Indian summer monsoon. *Quart. J. Roy. Meteor. Soc.*, **125**, 611-633.

Goswami. P. and K.C. Gouda 2010: Evaluation of a dynamical basis for advanced forecasting of date of onset of monsoon rainfall over India. *Monthly Weather Review.*, (online version, February 2010)

Prasad. V S and Hayashi.T. 2005: Onset and withdrawal of Indian summer monsoon. *Geophy. Res. Lett.*, **32** L20715.

Ramesh. K J., Swati Basu and Z N Begam 1996: Objective determination of onset, advancement and withdrawal of the summer monsoon using large-scale forecast fields of a global spectral model over India. *Meteo. and Atmospheric physics*, **61**, 137-151.

Syroka, J., and R. Toumi 2002: Recent lengthening of the south Asian summer monsoon season. *Geophy. Res. Lett.*, **29**, (DOI: 10.1029/2002/ GL015053).

Syroka, J., and R. Toumi 2004: On the withdrawal of the Indian summer monsoon. *Quart. J. Roy. Meteor. Soc.*, **130**, 989-1008.

Taniguchi. K., and T. Koike 2006: Comparison of definitions of Indian summer monsoon onset: better representation of rapid transitions of atmospheric conditions. *Geo. Res. Lett.*, **33**, L02709, 5 pages.

Taniguchi. K., D. Rajan and T. Koike 2010: Effect of the variation in the lower tropospheric temperature on the wind onset of the Indian summer monsoon. *Meteorology and Atmospheric Physics*, **106**, 75-94.

Wang, B., Q. Ding and V. Joseph 2009: Objective definition of the Indian summer monsoon onset using large-scale winds. *J. Climate* **22**, 3303–3316.

Wang. B., R.Wu and K.M. Lau 2001: Interannual variability of the Asian summer monsoon: Contrasts between the Indian and Western North Pacific-East Asian monsoons. *J. Climate*, **14**, 4073-4090.

Name of the Index	Type of Index	Domain of application	Definition in terms of regions	Reference
Goswami	Meridional wind	South Asia	$V_{850} - V_{200}$ over (10°N – 30°N, 70°E – 110°E)	Goswami et al., (1999)
Wang and Wu	Circulation index	Tropical Asia	U_{850} (5°N – 15°N, 40°E – 80°E) – U_{850} (20° N – 30°N, 70°E – 90°E)	Wang et al ., 2001
Wang and Ding	Circulation zonal wind	Tropical South Asia	U_{850} averaged over (5°N – 15°N, 40°E– 80°E)	Wang et al ., 2009
Syroka and Toumi	Circulation zonal wind	Tropical Asia	U_{850} (5°N – 15°N, 50°E –80°E) – U_{850} (20°N – 30°N, 60°E –90°E)	Syroka and Toumi (2002, 2004)

Table I

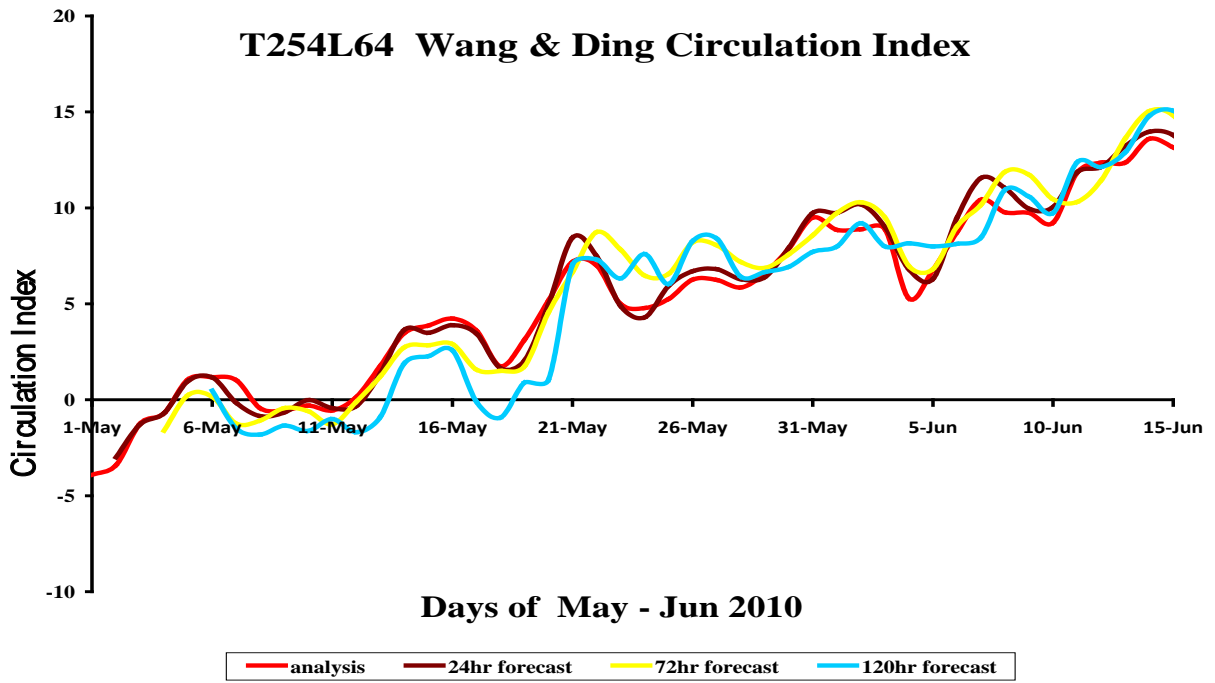


Fig. 1 (a1)

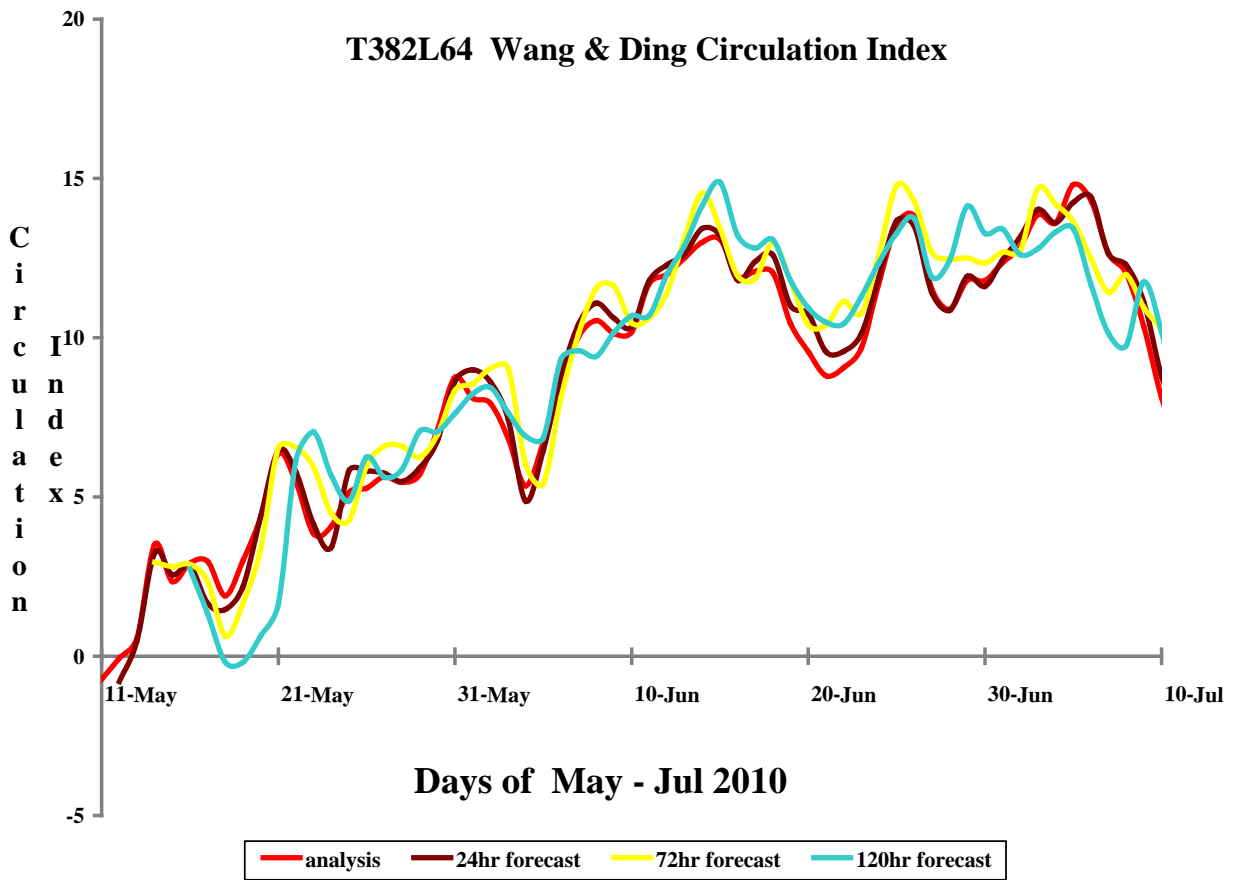


Fig. 1 (a2)

T254L64 Syroka & Toumi Circulation Index

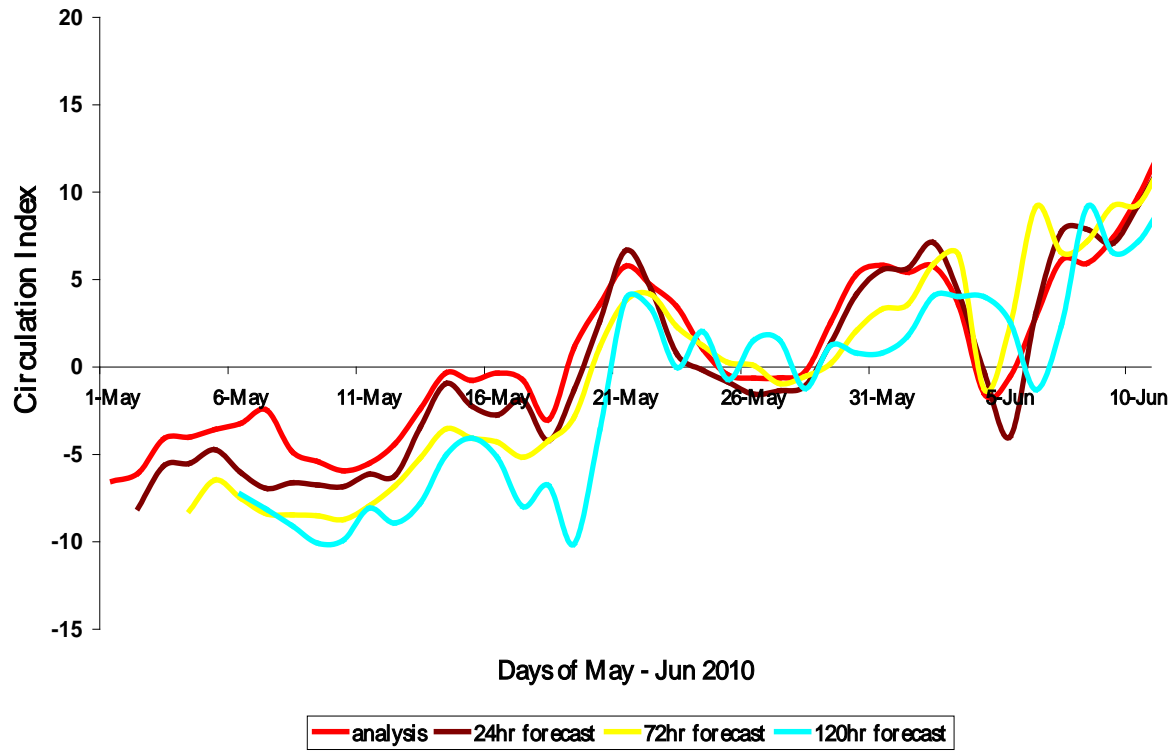


Fig 1 (b1)

T382L64 Syroka & Toumi Circulation Index

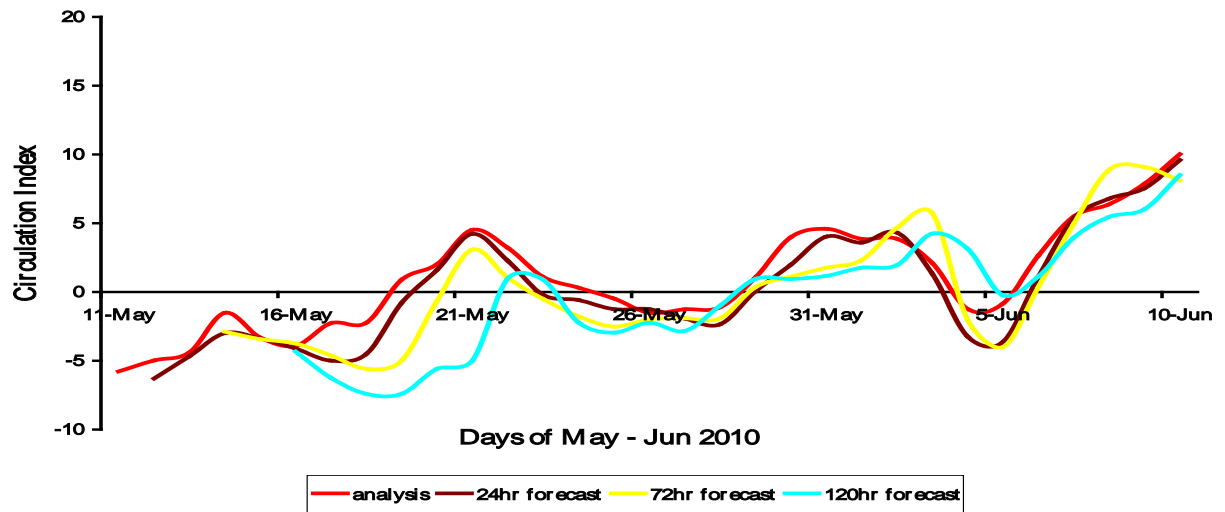


Fig 1 (b2)

T254L64 Goswami Hadley cell Index

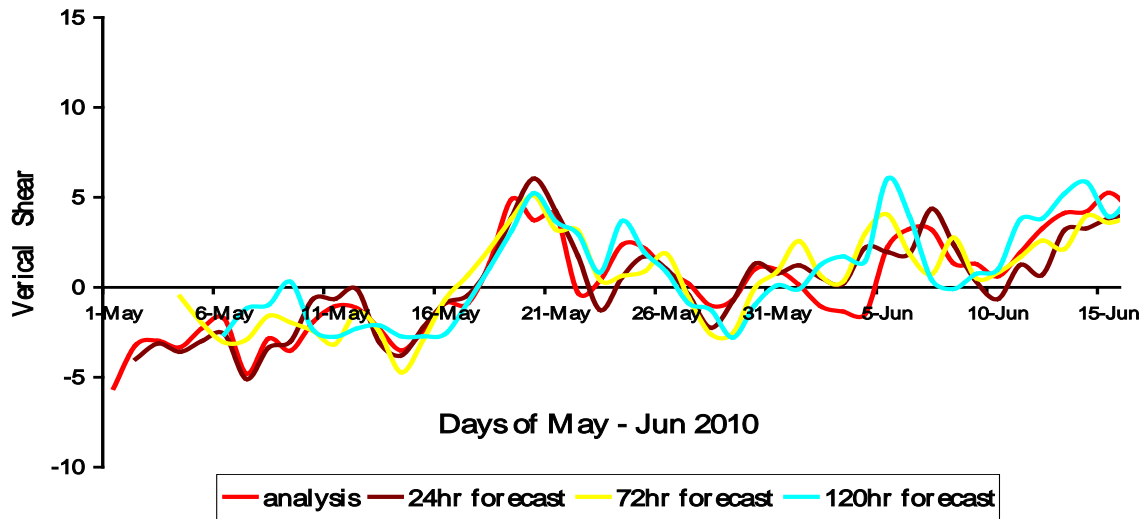


Fig. 1(c1)

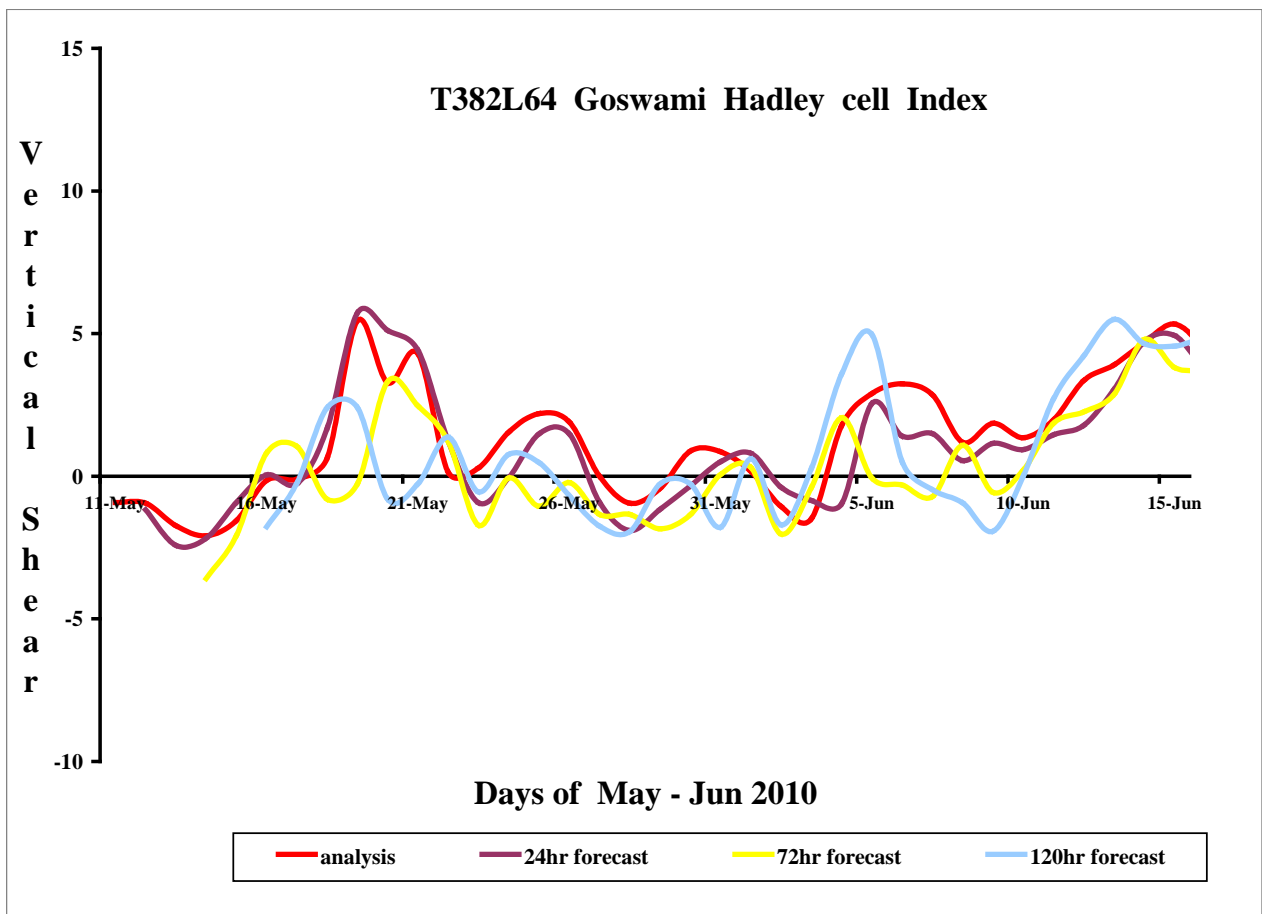


Fig. 1(c2)

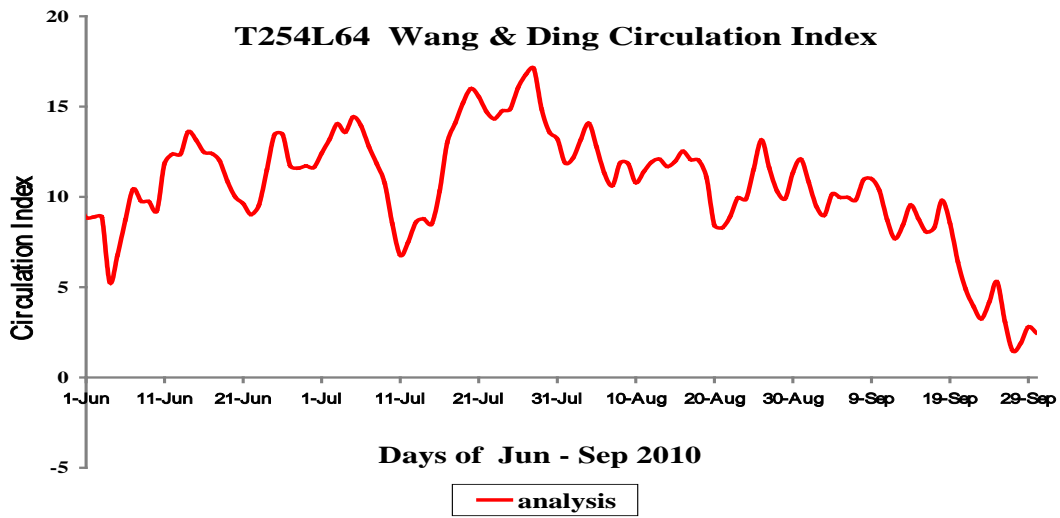


Fig. 2 (a1)

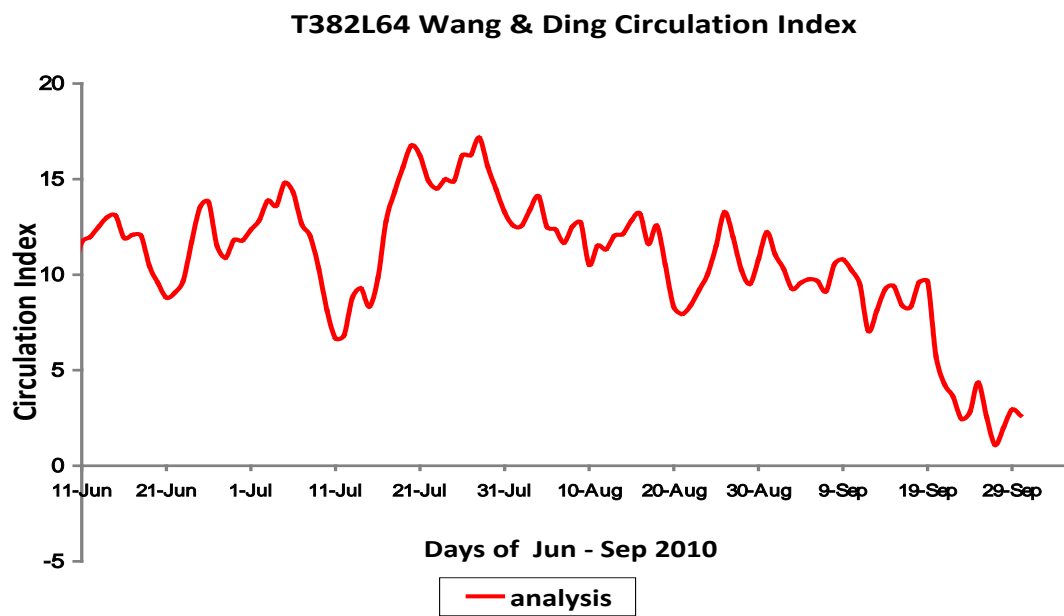


Fig. 2 (a2)

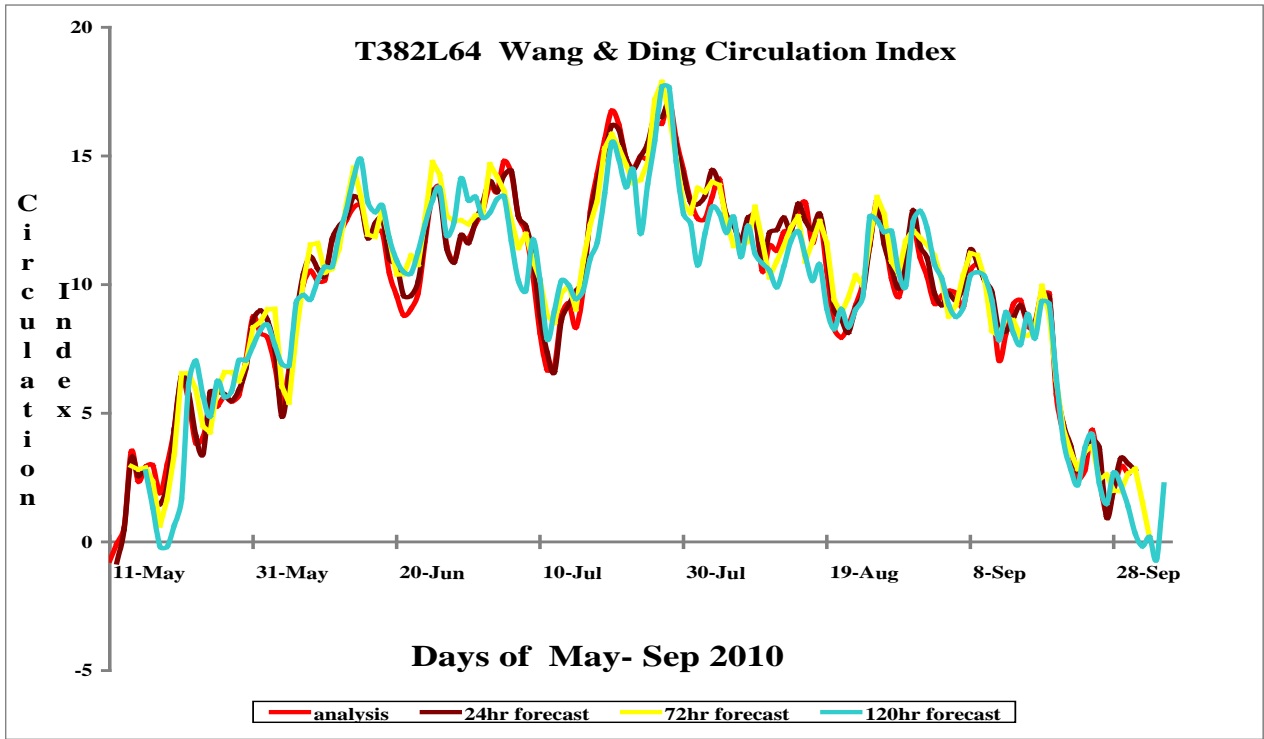


Fig. 2(a3)

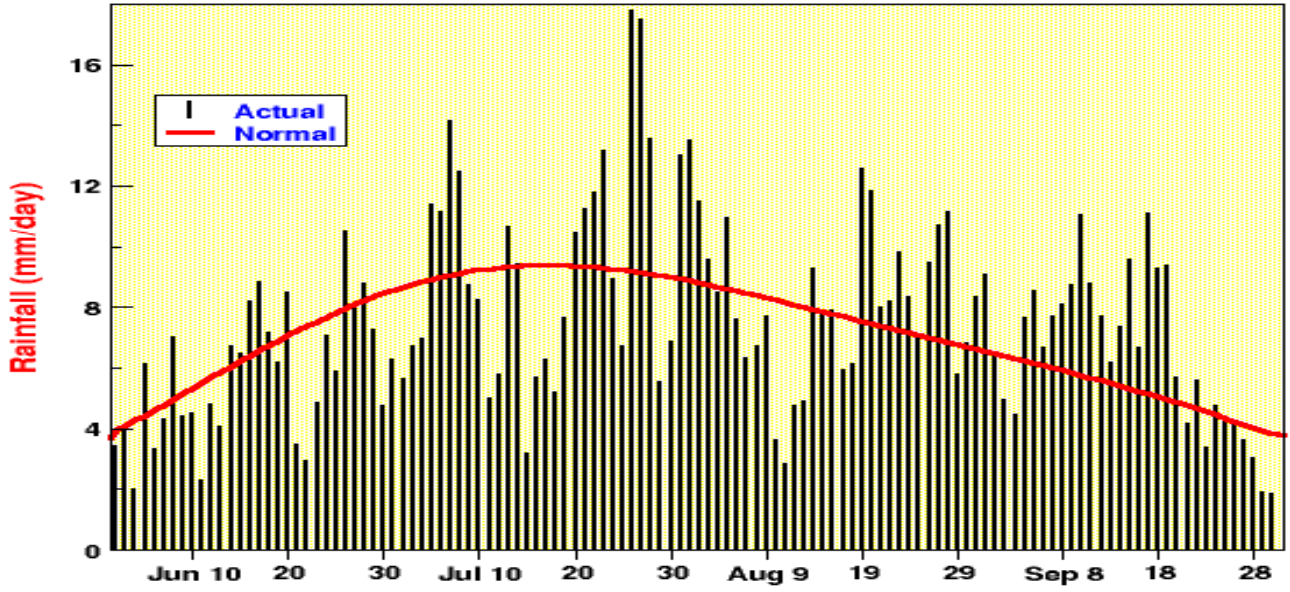


Fig. 2 (b)

T254L64 Syroka & Toumi Circulation Index

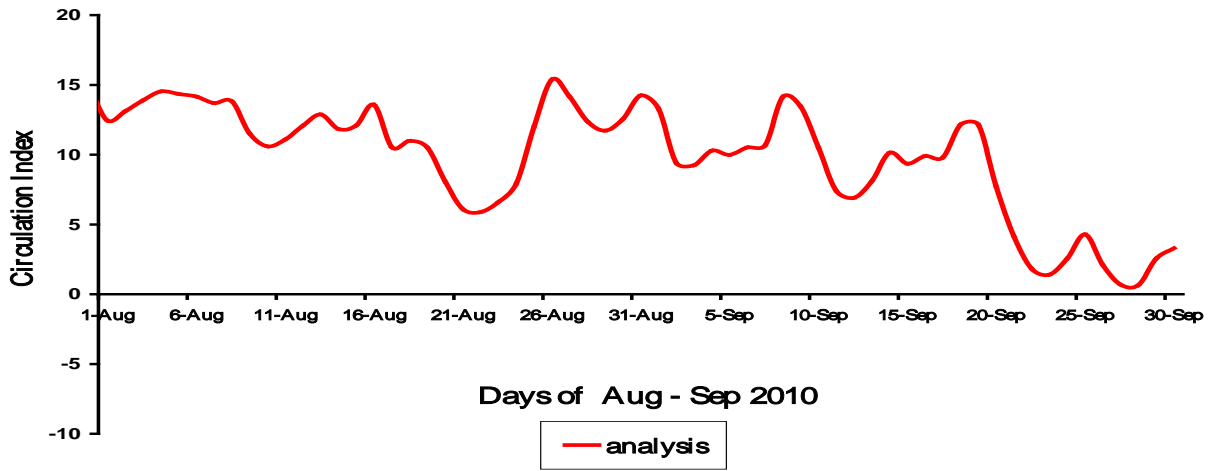


Fig. 3 (a1)

T382L64 Syroka & Toumi Circulation Index

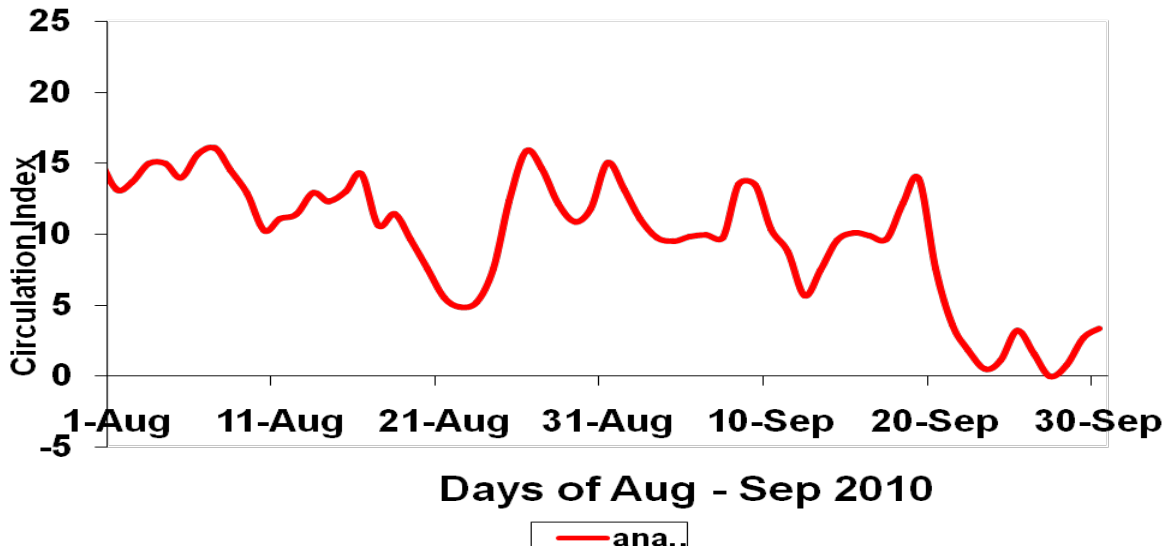


Fig. 3 (a2)

5. Heat Low and Monsoon Trough

R. Ashrit, J.P. George and Manjusha Chourasia

1. Introduction:

The Heat low over northwest of India and monsoon trough over the Gangetic plains are the two most prominent quasi-permanent near surface features of monsoon circulation and are closely related to the large scale monsoon activity over the Indian sub-continent. Due to the intense heating in summer months a low pressure belt develops over the Afro-Asian continent running from North Africa to North-West (NW) India through Arabia and Pakistan. The deepest low pressure area over Pakistan and adjoining NW India is known as the heat low. The intensity of heat low is a good indicator of the continental heating and land-sea contrast which drives the monsoon. Deep (*shallow*) heat low will usually be associated with stronger (*weaker*) North-South pressure gradient and enhanced (*subdued*) monsoon activity. The large scale monsoon activity is closely associated with the position of the monsoon trough. During the established phase of the monsoon season, the monsoon trough normally runs from Sriganaganagar in NW India to the Head Bay of Bengal. A *northward shift* (towards the foothills of Himalayas in the extreme cases) of trough is usually associated with *weak monsoon* activity over major parts of the country except over the Sub-Himalayan regions and South-East peninsula. A *southward* location of monsoon trough is favorable for *strong monsoon* activity over large parts of the country. Monitoring and prediction of the position and the intensity of the monsoon trough is thus very important for assessment of monsoon activity. The characteristics of these two semi-permanent features, viz. Heat low and monsoon trough in the two global model (T382 and T254) analysis and day-1 forecasts, day-3 forecasts and day-5 forecasts during JJAS 2010 are examined in this chapter.

2. Heat Low:

The intensity of the heat low is represented in this study by the magnitude of the innermost closed isobaric contour on a mean sea level pressure chart. By this terminology, a higher value of innermost closed isobar will mean shallow or less intense heat low. The average heat low centre pressure of the NCMRWF T382 and T254 model analyses and forecasts for different months during the monsoon season (Figure. 1) were examined to understand the behavior of the heat low during June-September 2010. The time-series presented in Figure 1 are computed over the region 24-34°N/65-75°E. During June and July, the minimum MSLP values are well below 1000 hPa in the analysis and forecasts of the models. In the month of August the lowest MSLP values over this location were well closer to 1000 hPa and in the month of September 2010 the minimum MSLP values over this location were well closer to 1000 hPa. The Day-1, Day-3 and Day-5 forecast position of the heat low for all months, except September, are close to its analysis position. In June, the lowest MSLP contour in the analysis is 993 hPa whereas in the forecasts it is lower than 990 hPa. In the month of August, the heat low becomes weak in both analysis and forecast; particularly in the second half of August. In September no heat low is seen in both analysis and forecast. It is seen that the heat low is generally more intense in model forecast as compared to the analysis. Also the Day-1 and Day-3 forecast intensity is more than that of Day-5 forecast. In general, the model forecast tends to intensify the heat lows, compared to analysis.

3. Monsoon Trough:

Monsoon trough is the most prominent semi-permanent feature of the Indian summer monsoon. Intensity and location of the monsoon trough is indicative of general monsoon condition over India and neighborhood. During JJAS of 2010 the north-south surface pressure gradient across the country was mostly weak throughout the season. The

vertical extent of monsoon trough was also very shallow and during many occasions was situated north of its normal position.

To identify the strength and position of the monsoon trough at surface level in the T382 and T254 analysis and forecast, the MSLP field is used in this study (Figure. 2 and 3). In the month of June, compared to the mean analysis, Day-1, Day-3 and Day-5 forecasts show lower MSLP values over the monsoon trough region. This feature is seen in both the models. The mean June position of the monsoon trough is the same in the analysis and the forecast, up to day-5 forecast and is over the Indo-Gangetic plains close to foot hills. The Day-5 forecast of T382 shows the monsoon trough extending to head Bay of Bengal (1000 hPa contour) which is not seen in T254 model. In July the mean analysis and forecasts of both models indicate weaker monsoon trough in terms east-west spread compared to the features in June. However both models show very similar patterns and intensity during July in the analysis and forecasts. In the month of August, the monsoon trough was weak. Both T382 and T254 forecasts also clearly show the dramatic change from July to August in terms of spatial extent. In September the monsoon trough is further weak both in analysis and in the corresponding forecasts.

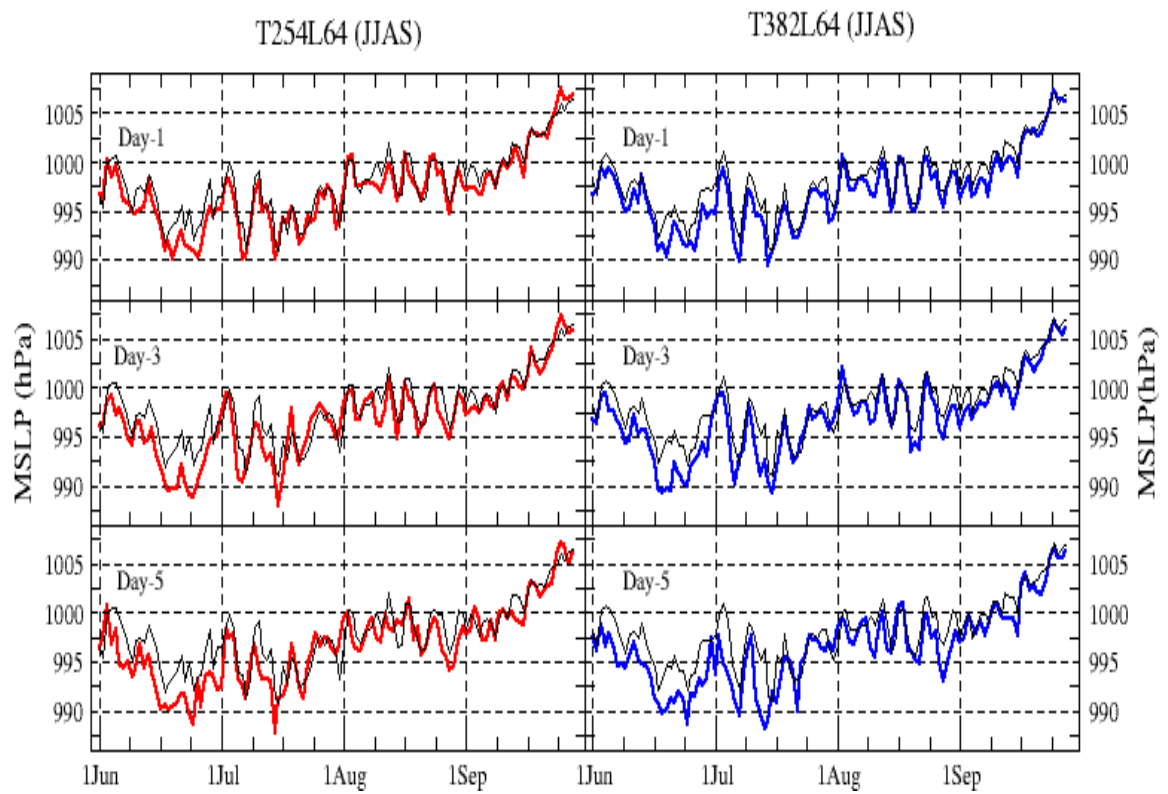


Figure 1. Time-series of the lowest SLP values in the heat low region (24-34N/65-75E) during JJAS 2010 in the analysis and forecasts of T382 and T254 models.

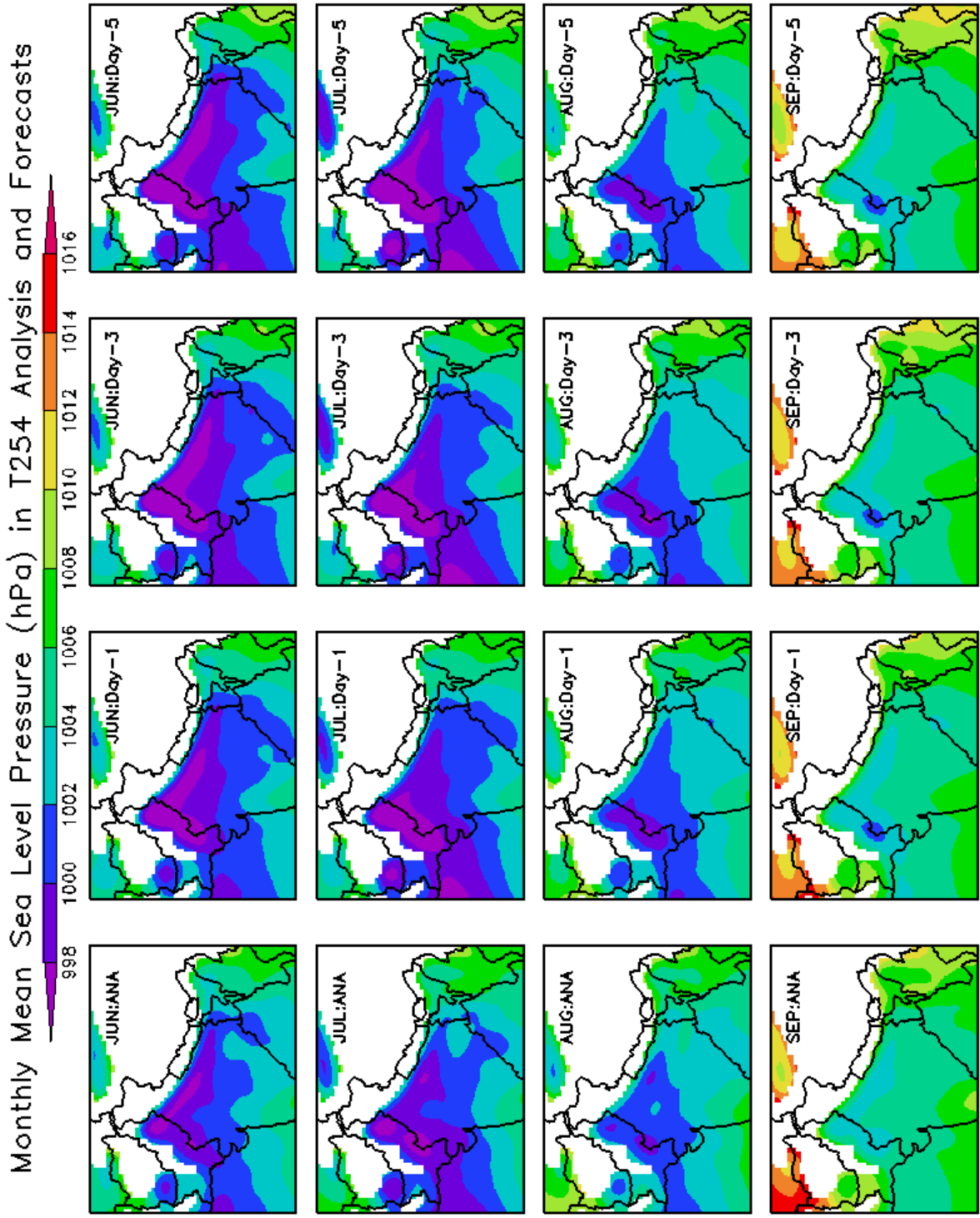


Figure 2. The monthly mean SLP (hPa) in the T382 model analysis and forecasts. The panels in the four rows correspond to the four months June-Sept 2010. Mean analysis plots are in first column and the Day-1, Day-3 and Day-5 forecasts are shown in second, third and fourth columns respectively.

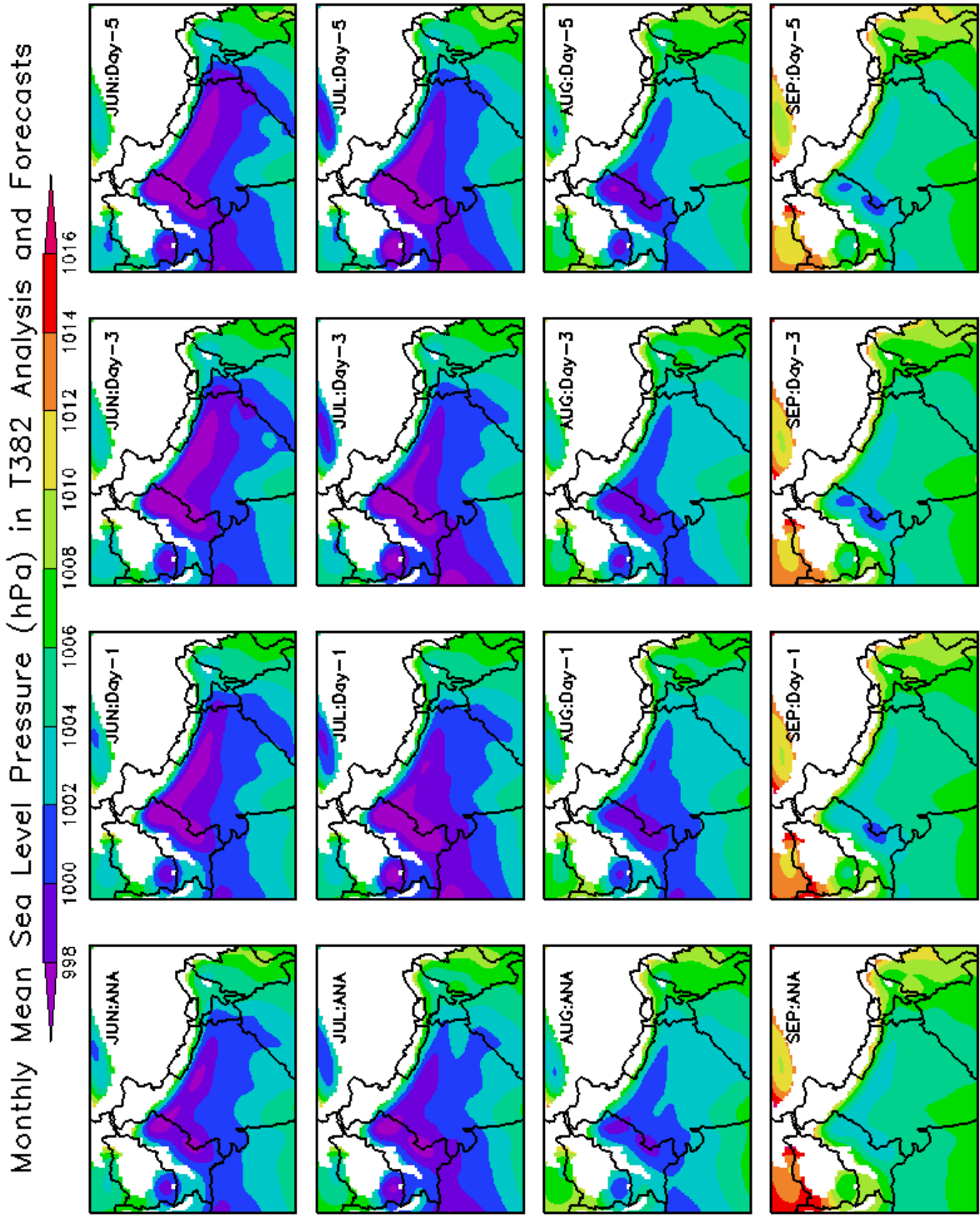


Figure 3. The monthly mean SLP (hPa) in the T254 model analysis and forecasts. The panels in the four rows correspond to the four months June-Sept 2010. Mean analysis plots are in first column and the Day-1, Day-3 and Day-5 forecasts are shown in second, third and fourth columns respectively.

6. Mascarene High, Cross-Equatorial Flow, Low-Level Westerly Jet and North-South Pressure Gradient During Monsoon 2010

A. K. Mitra, M. Das Gupta and G.R.Iyengar

1. Introduction

Low-level westerly jet is one of the most important feature of the south Asian summer monsoon system. Various features of this low level jet and associated inter-hemispheric moisture transport were documented four decades ago (Bunker, 1965; Tucker 1965; Findlatter, 1966; Joseph and Raman, 1966; Saha and Bavedkar, 1973). Through the cross-equatorial flow, southern hemisphere's Mascarene High influences the low level jet in the Arabian Sea. As this is associated with strong wind maxima offshore from Somalia, this jet is also known as Somali Jet. Indian monsoon rainfall and its active/break phases are linked to the weather systems in the southern hemisphere midlatitudes (Rodwell, 1997; Fukutomi and Yasunari, 2005). The low-level flow from the southern hemisphere interacts with the cross equatorial flow and the low level westerly jet in the Arabian Sea to shape the rainfall pattern (Anderson, 1976). Heating pattern over the southern Indian Ocean is linked to the strength/position of the East African jet, which modulates the flow over Indian monsoon region (Hoskins and Rodwell, 1995). In the southern Indian ocean significant high frequency (periods 2-6 days) transient eddy activity are seen associated with northern summer monsoon. This tropical-extratropical connection in the Indian Ocean region has to be simulated correctly by the model to represent the monsoon precipitation in the medium range time scale. The final strength of the monsoon flow is manifested in the north-south pressure gradient along the west coast of India. Arabian Sea and the Bay of Bengal are among the few regions of earth, where the low-level jets (LLJ) are seen with some regularity in the annual cycle. These jets are related to the synoptic-scale forcing and have narrow zones of high-speed flow that extend for hundreds of kilometers. These LLJs have appreciable horizontal and vertical shear. These are also important for the fluxes of temperature and moisture (both horizontal and vertical) and are generally associated with the development and evolution of deep convection over the Indian sub-continent and the neighboring regions of south Asia. The proper representation of the development and the evolution of these LLJs in a global numerical model, the physical mechanisms like the shallow baroclinicity (in PBL) interacting with other factors like the strong geostrophic forcing, the horizontal SST gradients, terrain effects are to be taken care of adequately (Stensrud, 1996; Krishnamurti et al., 1976). Surface winds, SST over Arabian Sea and other associated parameters are related to the rainfall over Indian sub-continent during monsoon

(Shukla and Misra, 1977; Raghavan et al., 1978). Similar relation of SST and low-level winds for the tropics in general was also shown in relation to the tropical deep convection (Lindzen and Nigam, 1987).

Oscillations in the strength of the components of monsoon flow have been linked to variability of monsoon rainfall. This low level jet is found to have large intraseasonal variability, affecting the moisture transport and finally the active/break conditions in convection over India and Bay of Bengal region (Joseph and Sijikumar, 2004). The splitting of the Somali Jet depends on the variable synoptic conditions, mean flow strength (dynamical feature of jet width and wavelength) and the evolving transients in the region (Thompson et al., 2008). Features of the large-scale monsoon circulation are related to the interaction of diabatic heating, orography (mountains) and their non-linear interactions with flow itself (Hoskins and Rodwell, 1995). Representations of these interactions in a model are essential to numerically simulate the low-level monsoon flow realistically (Krishnamurti et al., 1976; krishnamurti and Wong, 1979; Krishnamurti et al., 1983). The global model has to be realistic to capture the jet split. The model vertical and horizontal resolution should also be fine enough to represent adequately the forces responsible for maintenance and day-to-day variations in the strength of the low level westerly jet over the Arabian Sea. A higher resolution model is highly desirable for capturing the meso-scale convective structures in the monsoon system adequately and the associated details of monsoon rainfall distribution (Sperber et al., 1994; Martin, 1999; Teixeira, 1999). Since the low-level jet is very important in monsoon dynamics, monsoon modellers have to take adequate care to see that the low level flow and the associated deep convection and their variability are properly captured in model. This low level jet is intimately related to the cross-equatorial flow (inter hemispheric flow) deciding the moisture transport and hence the fate of the rainfall associated with Indian monsoon (Ramesh Kumar et al., 1999).

The performance of the two versions of (at different horizontal resolution and some other aspects described in chapter 1) global model (T254L64 and T382L64) assimilation-forecast system running in real-time during the monsoon 2010 in respect of the Mascarene High (MH), Cross-equatorial flow (CEF), the low level westerly jet (LLWJ) and the north-south pressure gradient along west coast is described briefly in this chapter. Description of the global modeling system with its assimilation aspects are described in chapter one of this report. These modelling systems were adapted at NCMRWF from NCEP's GFS system.

2. Performance of Model

2.1 Mascarene High (MH)

During monsoon 2010 season, the analyzed mean intensity of the Mascarene High (MH) was 1032.1 hPa and its position was approximately at 70.8° E and 35.4° S, as seen from the T254L64 system (Figure 1). From T382L64 system, the analyzed mean intensity of the MH was 1031.8 hPa and its position was approximately at 69.3° E and 35.6° S. Being a large-scale feature of the monsoon over the oceanic region, a good agreement in the intensity and position is seen between both the modeling system. The observed analysed positions from both T254L64 and T382L64 systems are slightly to the south of the long-term (80 years mean data) observed mean location of 69° E, 27° S with an intensity of 1024 hPa (Gorshkov, 1977). Intensity of MH also generally varies with time and also associated with monsoon activity over Indian region. Daily variation of MH intensity (central pressure) for analysed (lines with square marks), Day-1 and Day-5 predictions for T254L64 and T382L64 are seen in Fig. 1. The intensities predicted in Day-1 forecasts are generally in good agreement with the analyses for both T254L64 and T382L64 systems. However, in day-5 forecasts larger disagreements with respect to analyses have been noticed. Mean Analysed and predicted intensity of MH along with RMSE of predictions computed against analyses are presented in Table I. The centre of MH exhibits northeast ward propagation associated with the passage of southern hemisphere's westerly waves in day to day basis. This is clearly seen in both the system. Figure 2 and 3 depicts the analysed (lines with square marks) and Day-1 and Day-5 predicted longitudinal and latitudinal variation of MH during 1st June-30th September, 2010. For both T254L64 and T382L64 analyses, day-1 and day-5 predictions showed similar type of variation in longitude/latitude position, however the exact positions of those on a typical day are different amongst analyses from both the modeling system. Table II and III compare the mean of analyses and predictions (Day-1, Day-3 and Day-5) for longitude and latitude positions of the centre of MH respectively for both T382L64 and T254L64 systems during JJAS 2010. They also compare the root mean square error (RMSE) of predictions against respective analyses for and latitude and longitude positions of the centre of MH for both the systems. RMSEs of prediction for latitude, longitude and intensity of MH grow with prediction time, but RMSEs for T382L64 system are always less compared to T254L64 system.

2.2 Cross-Equatorial Flow (CEF)

The time mean analyzed, Day-1, Day-3 and Day-5 forecasts of the meridional wind at equator over the sector 30° E- 100° E with mean taken over the entire monsoon period (June to September 2010) are shown in figures 4(a) and 4(b) in the form of longitude-height cross-sections from T254L64 and T382L64 modelling systems respectively. In T254L64 model, the analyzed field shows prominent maxima of 15 mps around 40° E at 875 hPa representing the core of the Arabian Sea branch of the cross-equatorial flow and a secondary maxima of 4 mps between 80° E - 90° E, representing the Bay of Bengal branch. The dual core of cross-equatorial flow in the Arabian Sea is not seen in this year's analysis, which was observed during monsoon season of 1995 and 1998. This dual core was also absent in recent monsoons of 2005, 2006, 2007, 2008 and 2009 (NCMRWF Report 2006a; NCMRWF Report 2006b; NCMRWF Report 2008; NCMRWF Report 2009; NCMRWF Report 2010). Mean analysis from T382L64 system shows similar features, except the maxima of Bay of Bengal showing 3 mps. In forecasts in both the models, the core of the Arabian Sea branch of CEF is well maintained at 15 mps in a very consistent way (except day-3, where a slight intensification is seen in both models). The Bay of Bengal branch of the cross-equatorial flow is also maintained well. In T254L64 system the 3 mps contour over bay of Bengal(BoB) region is seen to descend to lower levels further, indicating a slight weakening of the BoB branch of low-level jet in terms of its vertical extent. In T382L64 system this aspect is slightly better. Overall, the skill of the models are very good during monsoon 2010, in terms of capturing and maintaining the low-level cross equatorial flow both in the Arabian Sea and the Bay of Bengal.

The mean (June to September 2010) vertical profiles of meridional wind averaged over the domain 2.5° S - 2.5° N; 39° E - 51° E from the analysed, Day-1, Day-3, and Day-5 prediction fields from T254L64 and T382L64 are shown in figures 5(a) and 5(b) respectively. It is seen that the maxima of the cross-equatorial flow occurs at around 875 hPa in the mean analysis. The intensity and location forecasts of CEF from the both models agree very well with the observations (analysis), indicating that the CEF is well maintained in the models. In both models, only marginal weakening is noticed in forecasts between 900 and 800 hPa.

2.3 Low-Level Westerly Jet (LLWJ)

The mean analyzed and predicted positions and strength of the low-level westerly jet (LLWJ) in the Arabian Sea at 850 hPa from T254L64 and T382L64 are shown in different panels

of figure 6(a) and 6(b) respectively for the whole monsoon season. This diagram brings out clearly the well maintenance of the strength and location of LLWJ during monsoon 2010 in the Arabian Sea throughout the forecast length (day-1 through day-5) in this high-resolution model, particularly in T254L64 system. The contour of 20 mps adjacent to Somalia coast in the Arabian Sea is very consistent in analysis and the forecasts in T254L64. In T382L64 system the small region covering 20 mps contour is not seen in day-1 and day-5 forecasts, however the 15 mps region is well maintained. The winds in the Bay of Bengal and peninsular India are also very well maintained in the forecasts compared to the analysis. As a result the monsoon trough over the central India is also well maintained in the forecasts.

The north-south cross-sections of seasonal mean analyzed and predicted (Day-1, Day-3 and Day-5) zonal component of wind along 54° E, a longitude which falls within the climatological location of LLWJ, from T254L64 and T382L64 models are given in figure 7(a) and 7(b) respectively. The observed core of the jet matches with the climatological location. The jet core is observed to be at 17 mps in both models. Here the second core (dual core) of 11 to 12 mps at around 14° N is also seen during 2010 monsoon. The model forecasts (Day -1 through Day -5) are matching very well with the observed jet strength and position. T382L64 system maintains this better than the T254L64 system. In T254L64 system a slight intensification (17 mps to 18 mps) is seen in day-1 and day-3 forecasts. The dual core system is very well maintained in both the models. Throughout the forecast length the LLWJ is seen to be very consistent in structure among each other and also with the observed analysis. In general, the representation and maintenance of LLWJ is very good in the high resolution model.

The latitude-height cross-sections of seasonal mean analyzed and predicted zonal wind along 75° E (a longitude where the low-level westerlies interact with the west coast orography leading to heavy rainfall) from T254L64 and T382L64 systems are given in figures 8(a) and 8(b) respectively. The maximum zonal wind at 7° N in analysis is seen to be around 9 mps in both modelling systems. The second core at 16° N represents the monsoon trough region (a very important feature of monsoon system) which is seen to be quite strong at 9 to 10 mps. During the forecast in general the strength is well maintained in T382L64 system. A slight intensification to 10/11 mps are seen in T254L64 system. The position and intensity of the monsoon trough is also well maintained in both models. This season in both T254L64 and T382L64 modelling systems the monsoon trough is seen to spread southwards slightly during the forecasts.

2.4 North-South Pressure Gradient

The daily variations of analyzed (line with square marks) and predicted (Day1 and Day5 predictions - line with diamond marks) values of north-south pressure gradient along the west coast of India, during JJAS 2010 for models T382L64 and T254L64 systems are shown in figure 9. The difference of mean sea-level surface pressure between regions 21° N; 70° E and 9° N; 77° E is considered to note the daily north-south pressure gradient near west coast of India. In T382L64 model, the day-1 predictions match very well with the corresponding analyzed values, whereas the same for T254L64 system has shown some mismatch in the beginning and end of the season. Day-5 predictions in both the system did not match very well with the corresponding analysed values during the 1st week of August, 2010. Table IV compares the mean analysed, Day-1, Day-3 and Day-5 predicted values of North-south pressure gradient along west coast of India and RMSE of predictions computed against analyses for both T382L64 and T254L64 systems during JJAS 2010. It is seen that, the errors in T382L64 system are always less than that of T254L64 system.

3. Summary

In this chapter the low-level circulation pattern and associated features seen in sea-level pressures are discussed for both T254L64 and T382L64 global modelling systems. Both these models are able to represent the low level monsoon circulation realistically. Wind pattern and their intensities associated with cross-equatorial flows, low-level westerly jet over the Arabian sea and the Bay of Bengal branch of jet are well maintained in forecasts up to day-5. The intensity of Mascarene High, and its latitude and longitude positions are well represented in both the models. However, by day-5, the errors are seen to be more compared to day-1, indicating possible impact on rainfall forecasts on Indian sub-continent in the medium range. Particularly the longitude position error of the Mascarene High by day-5 is high and needs attention. In general in a mean sense, the T382L64 system is seen to be slightly better than the T254L64 system in representing the monsoon low-level circulation features.

Legends for Figures

Fig. 1. Intensity of the Mascarene high in the analysis against Day-1 and Day-5 forecasts during monsoon 2010, from T254L64 and T382L64 global modelling systems

Fig. 2. Longitudinal position of Mascarene high in the analysis against Day-1 and Day-5 forecasts during monsoon 2010, from T254L64 and T382L64 global modelling systems

Fig. 3. Latitudinal position of Mascarene high in the analysis against Day-1 and Day-5 forecasts during monsoon 2010, from T254L64 and T382L64 global modelling systems

Fig. 4. Time mean analyzed, Day-1, Day-3 and Day-5 forecasts of meridional wind at equator over the sector 30°E - 100°E , during monsoon 2010; (a) from T254L64 (b) from T383L64

Fig. 5. Time mean vertical profiles of meridional wind averaged over the domain 2.5°S - 2.5°N and 39°E - 51°E , during monsoon 2010; (a) from T254L64 (b) from T383L64

Fig. 6. Mean analyzed, Day-1, Day-3 and Day-5 forecasts of 850 hPa flow pattern and wind speeds, during monsoon 2010; (a) from T254L64 (b) from T383L64

Fig. 7. North-south cross-section of seasonal mean analyzed, Day-1, Day-3 and Day-5 forecasts for Zonal component of wind along 54°E , during monsoon 2010; (a) from T254L64 (b) from T383L64

Fig. 8. North-south cross-section of seasonal mean analyzed, Day-1, Day-3 and Day-5 forecasts for Zonal component of wind along 75°E , during monsoon 2010; (a) from T254L64 (b) from T383L64

Fig. 9. Analyzed, Day-1 and Day-5 forecasts of North-South Pressure Gradient along west coast during monsoon 2010, from T254L64 and T382L64 global modelling systems

Reference

- Anderson,D.L.T., 1976: The low level jet as a western boundary current , MWR, 104 , 907 - 921
- Bunker,A.F., 1965: 'Interaction of the Summer Monsoon air with the Arabian Sea (preliminary analysis)', Proceedings of Symp. Meteor. Results from IIOE, July 1965, Bombay, India, 3-16
- Findlatter,J., 1966 “Cross-equatorial jet streams at low level over Kenya “, Met. Mag., 95, 353-364
- Fukutomi, Y., and Tetsuzo Yasunari, 2005, Southerly Surges on Submonthly Time Scales over the Eastern Indian Ocean during the Southern Hemisphere Winter, MWR, 133(6), 1637-1654
- Gorshkov, S.G., (Ed.), 1977: World Ocean Atlas - Atlantic and Indian Oceans, Chief Directorate of Navigation and Oceanography, Former USSR
- Hoskins, B. J., and M.J.Rodwell 1995: A model of the Asian summer Monsoon. part I : The global scale , JAS , 52 , 1329 - 1340
- Joseph P.V., and S. Sijikumar, 2004, Intraseasonal Variability of the Low-Level Jet Stream of the Asian Summer Monsoon , J Clim., 17(7), 1449–1458
- Joseph,P.V. and P.L.Raman 1966: Existence of LLWJ stream over Peninsular India during July, Ind. J. Meteor. Geophys., 17 , 407-410
- Krishnamurti, T.N.K. , V. Wong , H. L. Pan , R. Pasch , J. Molinari and P. Ardanuy 1983 : A three dimensional planetary boundary layer model for the Somali Jet , JAS , 40 , 894 - 908
- Krishnamurti, T.N.K., and V. Wong 1979: A simulation of cross-equatorial flow over the Arabian Sea, JAS, 36, 1895-1907
- Krishnamurti,T.N.K., J.Molinari and H.L.Pan 1976: Numerical Simulation of the Somali Jet, JAS, 33, 2350-2362
- Lindzen, R.S. and R.S. Nigam 1987: On the role of SST gradients in forcing low-level winds and convergence in tropics, JAS, 44, 2418-2436
- Martin, G.M., 1999: Simulation of the Asian summer monsoon, and its sensitivity to horizontal resolution, in UK Met. Office UM, QJRMS, part A, 125(557), 1499-1525
- NCMRWF, DST(GOI), January 2006a: ‘Monsoon 2005: Performance of the NCMRWF Global Assimilation Forecast System’, Report no. NMRF/MR/01/2006, 139 pages, Published by NCMRWF(DST), A-50, Institute Area, Sector – 62, UP, India 201307, chapter 5, pages 71–88
- NCMRWF, MoES(GOI), December 2006b: ‘Monsoon 2006: Performance of the NCMRWF Global Assimilation-Forecast System’, Report no. NMRF/MR/02/2006, 114 pages, Published by NCMRWF(MoES), A-50, Institute Area, Sector–62, UP, India 201307, Chapter 4, pages 51–66

- NCMRWF, MoES(GOI), January 2008: 'Monsoon 2007: Performance of T254L64 Global Assimilation-Forecast System', Report no. NMRF/MR/01/2008, 143 pages, Published by NCMRWF(MoES), A-50, Institute Area, Sector-62, UP, India 201307, Chapter 5, pages 67-93
- NCMRWF, MoES(GOI), February 2009: 'Monsoon 2008: Performance of T254L64 Global Assimilation-Forecast System', Report no. NMRF/MR/01/2009, 117 pages, Published by NCMRWF(MoES), A-50, Institute Area, Sector-62, UP, India 201307, Chapter 6, pages 81-97
- NCMRWF, MoES(GOI), March 2010: 'Monsoon 2009: Performance of T254L64 Global Assimilation-Forecast System', Report no. NMRF/MR/01/2010, 131 pages, Published by NCMRWF(MoES), A-50, Institute Area, Sector-62, UP, India 201309, Chapter 6, pages 85-102
- Raghavan,K., P.V.Puranik and V.R.Majumdar , P.Ismail and D.K.Paul 1978: Interaction between the west Arabian Sea and the Indian Monsoon, *MWR* , 106 , 719 - 724
- Ramesh Kumar M. R., S. S. C. Shenoi and P. Schluessel, 1999: On the role of the cross equatorial flow on summer monsoon rainfall over India using NCEP/NCAR reanalysis data, *MAP*, 70(3-4), 201-213
- Rodwell, M.J., 1997: Breaks in the Asian Monsoon: The influence of southern hemisphere weather systems, *JAS*, 54(22), 2597-2611
- Saha,K.R. and S.N.Bavedkar 1973: Water vapour budget and precipitation over the Arabian Sea during the northern summer,*QJRMS*,99,273-278
- Shukla,J., and B.M.Mishra 1977: Relationships between SST and wind speed over the central Arabian Sea and monsoon rainfall over India, *MWR* , 105 , 998-1002
- Sperber,K.R., S.Hameed, G.L.Potter and J.S.Boyle 1994: "Simulation of the northern summer monsoon in the ECMWF Model: Sensitivity to horizontal resolution",*MWR*,122(11),2461-2441
- Stensrud, D.J., 1996: Importance of Low-Level Jets to Climate: A Review, *J. of Climate*,8(9), 1698-1711
- Teixeira, J., 1999: The impact of increased boundary layer vertical resolution on the ECMWF forecast system. *ECMWF Tec. Mem. No268*. Feb. 1999, ECMWF, Reading, UK, pp. 55
- Thompson A, L. Stefanova and T.N. Krishnamurti, 2008, Baroclinic splitting of jets, *MAP*, 100, 257-274
- Tucker,G.B. ,1965: "The equatorial tropospheric wind regime", *QJRMS*,91,140-150

Table - I

Mean central pressure of MH (Intensity) for Analysis, Day-1, Day-3 and Day-5 Predictions along with RMSE of predictions computed against analyses for both T382L64 and T254L64 systems (JJAS 2010)

Central Pressure of MH (hpa)	Analysis	D1-FCST		D3-FCST		D5-FCST	
	Mean	Mean	RMSE	Mean	RMSE	Mean	RMSE
T382L64	1031.83	1032.04	0.64	1031.68	1.46	1031.46	2.72
T254L64	1032.18	1031.94	0.80	1031.75	1.97	1031.37	3.51

Table - II

Mean longitude position of the centre of MH for Analysis, Day-1, Day-3 and Day-5 Predictions along with RMSE of predictions computed against analyses for both T382L64 and T254L64 systems (JJAS 2010)

Longitude of the centre of MH (°)	Analysis	D1-FCST		D3-FCST		D5-FCST	
	Mean	Mean	RMSE	Mean	RMSE	Mean	RMSE
T382L64	69.31	69.54	8.18	69.76	12.19	71.61	19.75
T254L64	70.85	70.18	9.09	71.35	16.40	71.50	20.28

Table - III

Mean latitude position of the centre of MH for Analysis, Day-1, Day-3 and Day-5 Predictions along with RMSE of predictions computed against analyses for both T382L64 and T254L64 systems (JJAS 2010)

Latitude of the centre of MH (°)	Analysis	D1-FCST		D3-FCST		D5-FCST	
	Mean	Mean	RMSE	Mean	RMSE	Mean	RMSE
T382L64	-35.64	-35.48	1.51	-35.34	1.82	-35.44	2.96
T254L64	-35.43	-35.70	1.64	-35.47	2.49	-35.57	3.55

Table - IV

Mean Analysed, Day-1, Day-3 and Day-5 Predicted values of North-south pressure gradient and RMSE of predictions computed against analyses for both T382L64 and T254L64 systems (JJAS 2010)

North-south Pressure gradient (hpa)	Analysis	D1-FCST		D3-FCST		D5-FCST	
	Mean	Mean	RMSE	Mean	RMSE	Mean	RMSE
T382L64	4.87	5.12	0.92	4.45	1.32	4.54	1.82
T254L64	5.13	5.24	1.34	4.88	1.76	5.23	2.01

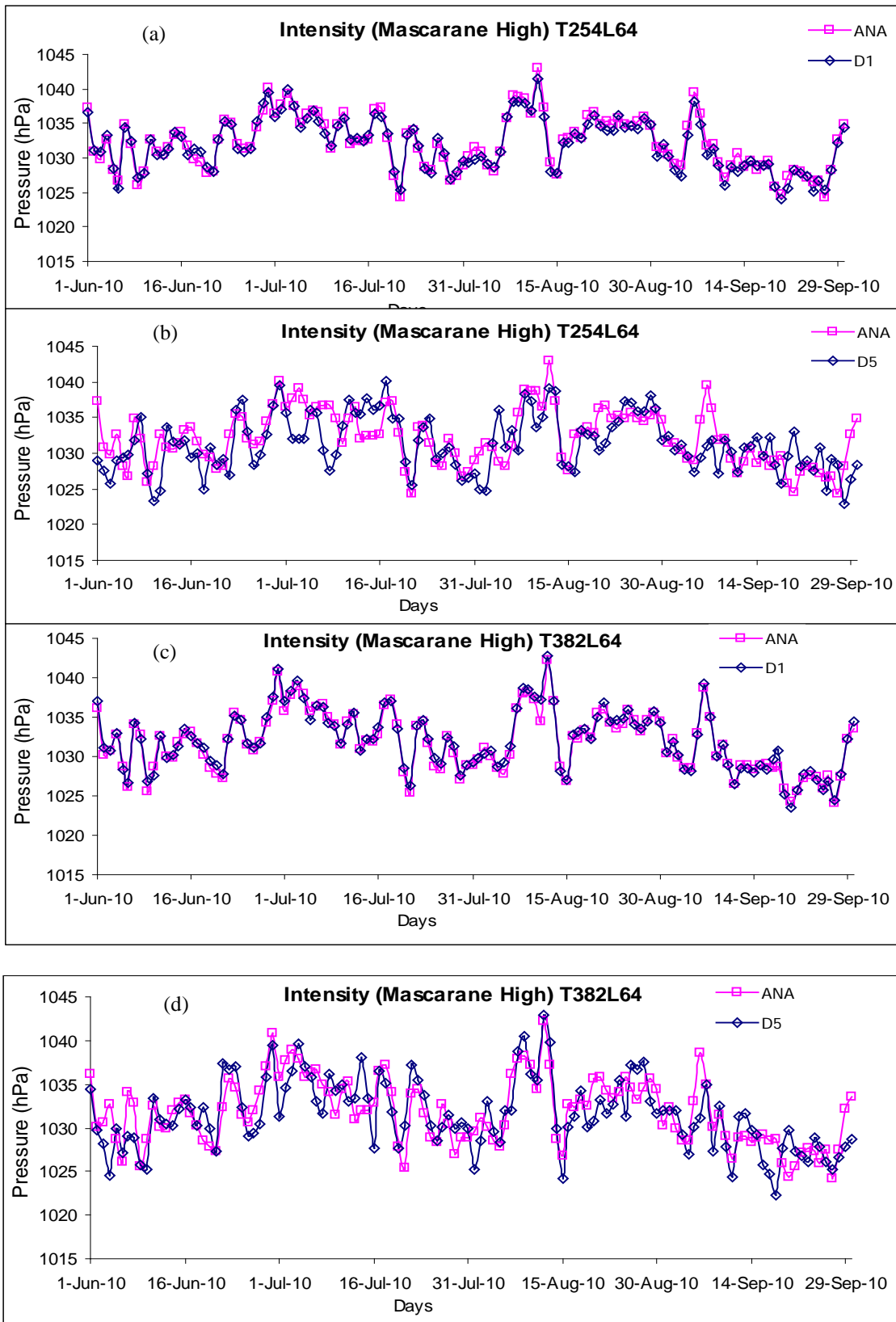


Fig 1. Daily variation of Analysed and predicted (Day-1 and Day-5) Intensity of Mascarene High during JJAS 2010
 (a) T254L64, D-1 (b) T254L64, D-5 (c) T382L64, D-1 (d) T382L64, D-5

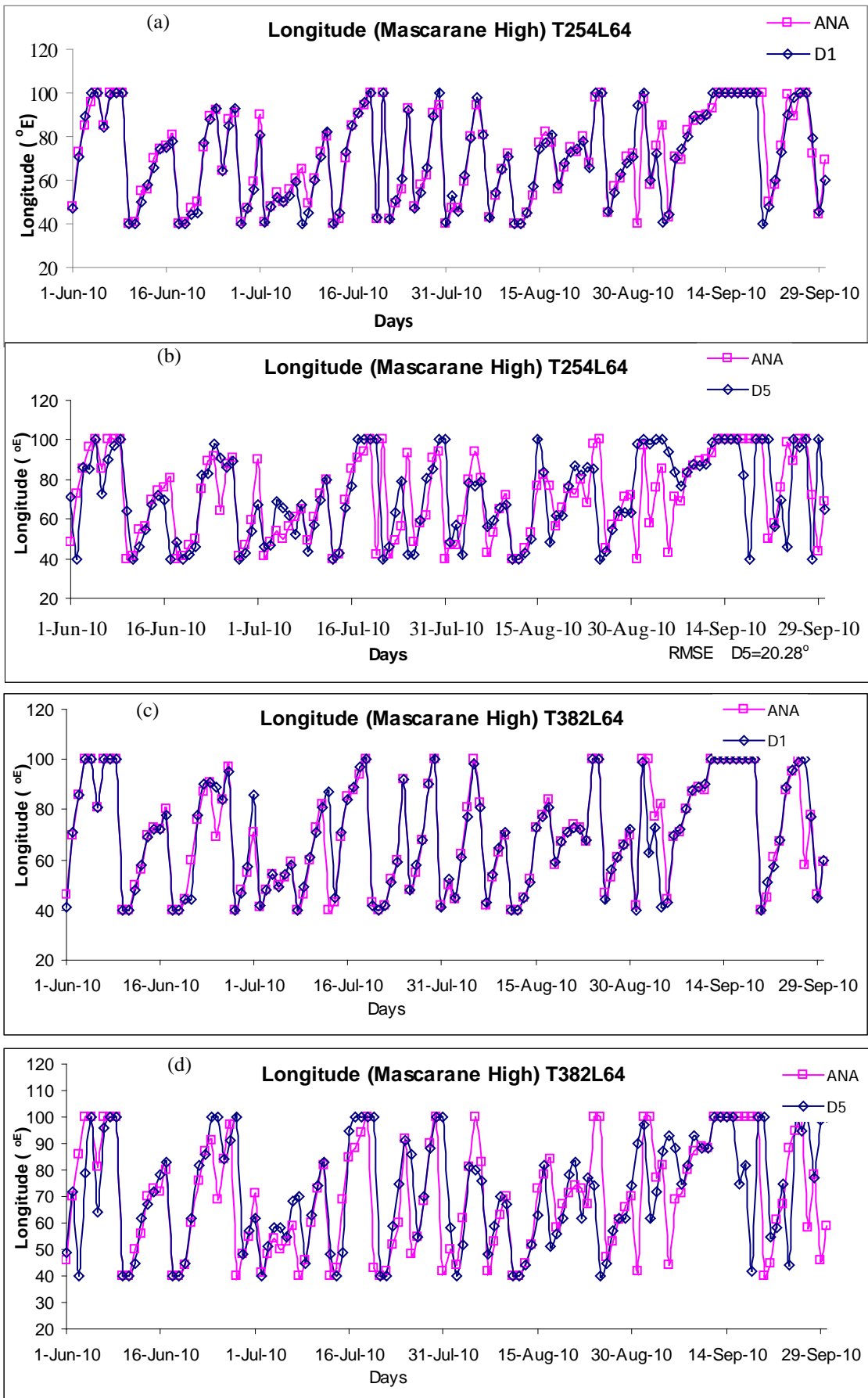


Fig 2. Daily Variation of Analysed and Predicted Longitude Position of the centre of Mascarene High during JJAS 2010
 (a) T254L64, D-1 (b) T254L64, D-5 (c) T382L64, D-1 (d) T382L64, D-5

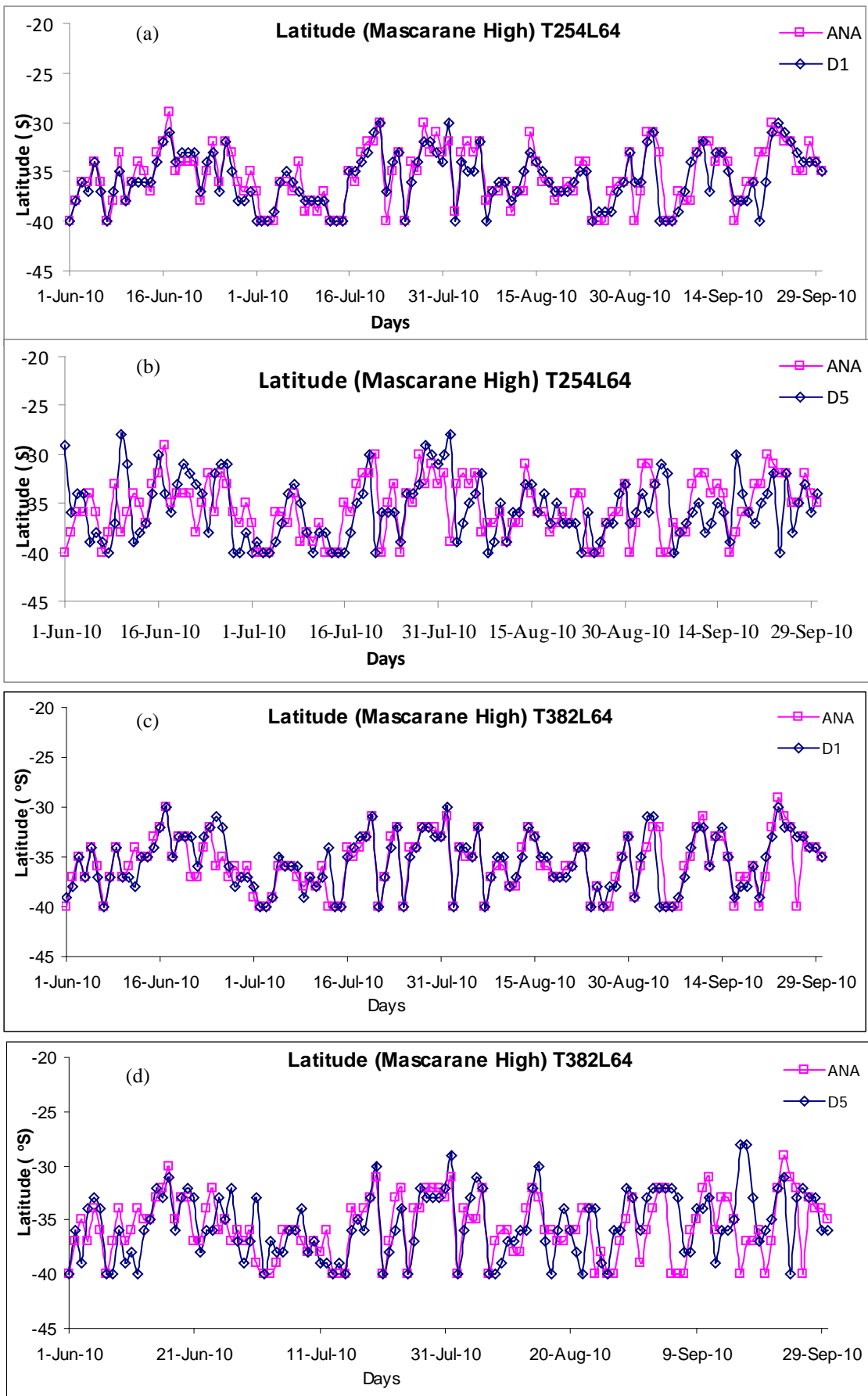


Fig 3. Daily variation of Analysed and Predicted Latitude Position of the centre of Mascarane High during JJAS 2010
 (a) T254L64, D-1 (b) T254L64, D-5 (c) T382L64, D-1 (d) T382L64, D-5

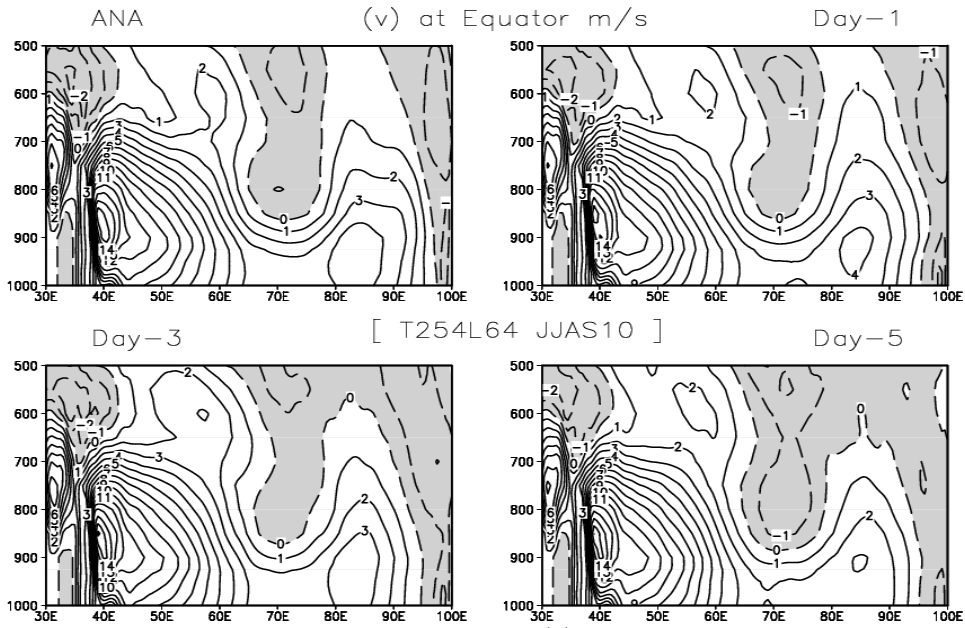


Fig. 4(a)

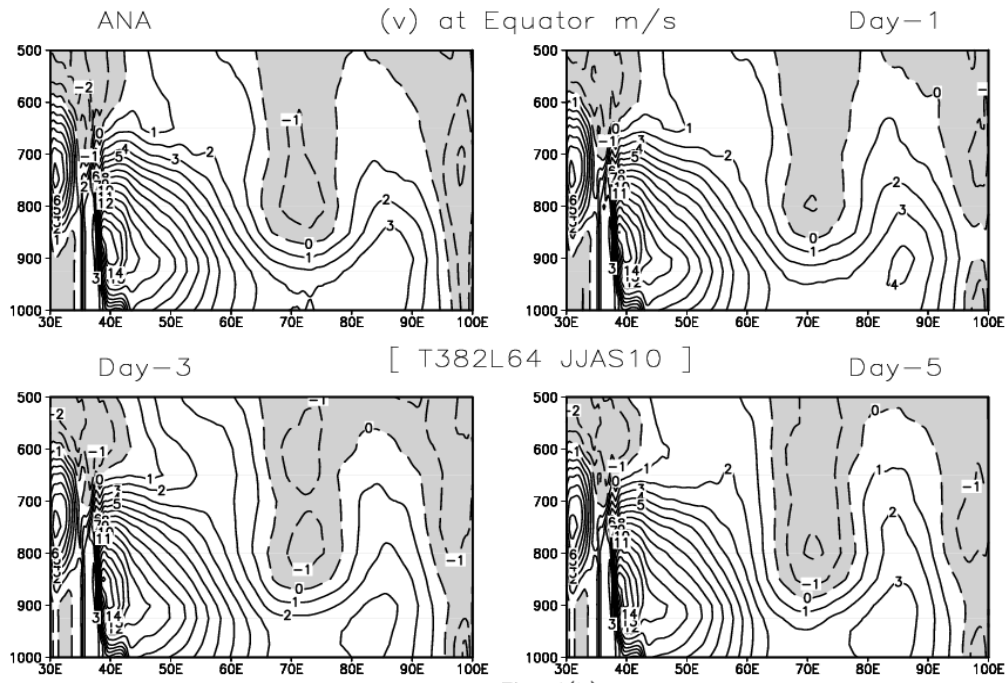


Fig. 4(b)

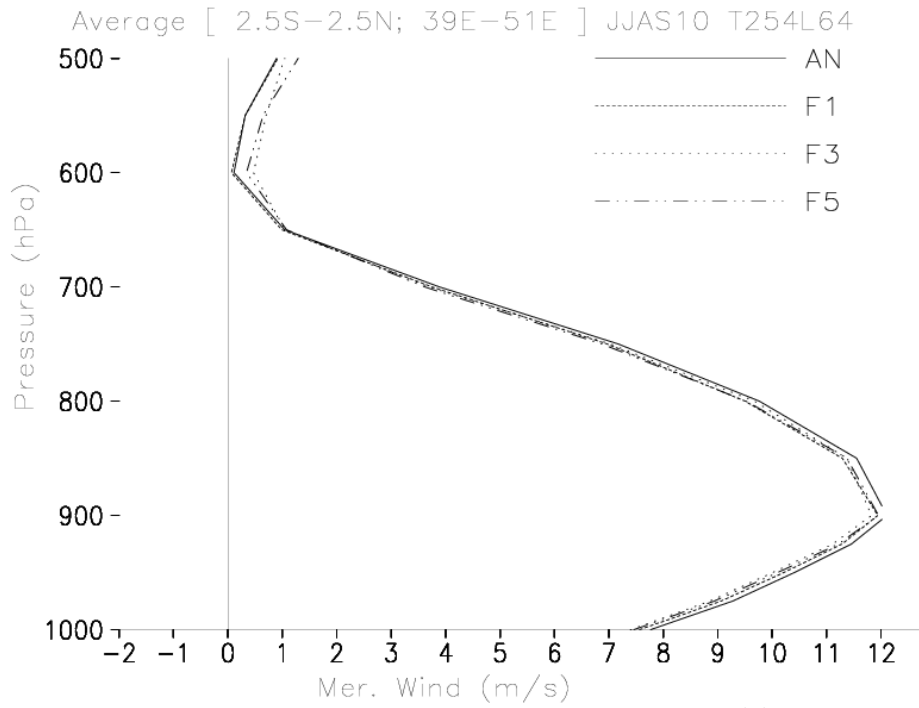


Fig. 5(a)

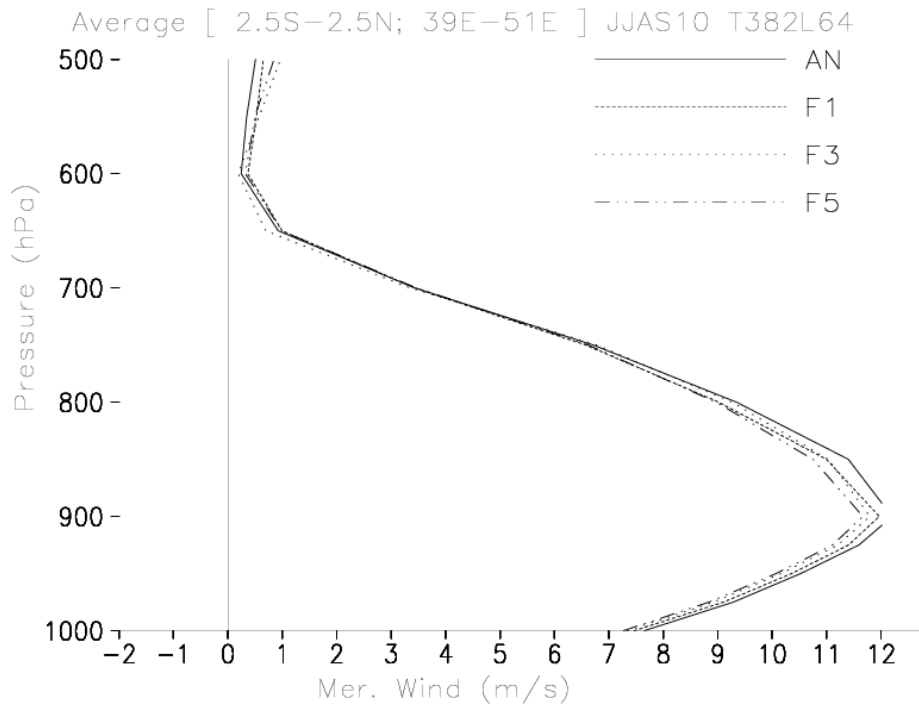
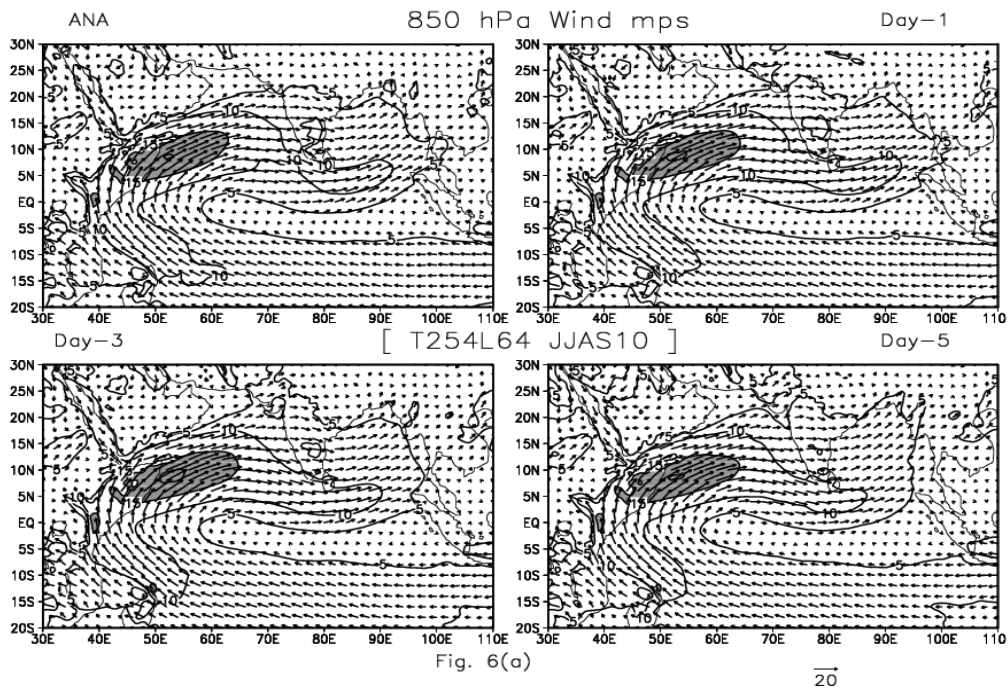
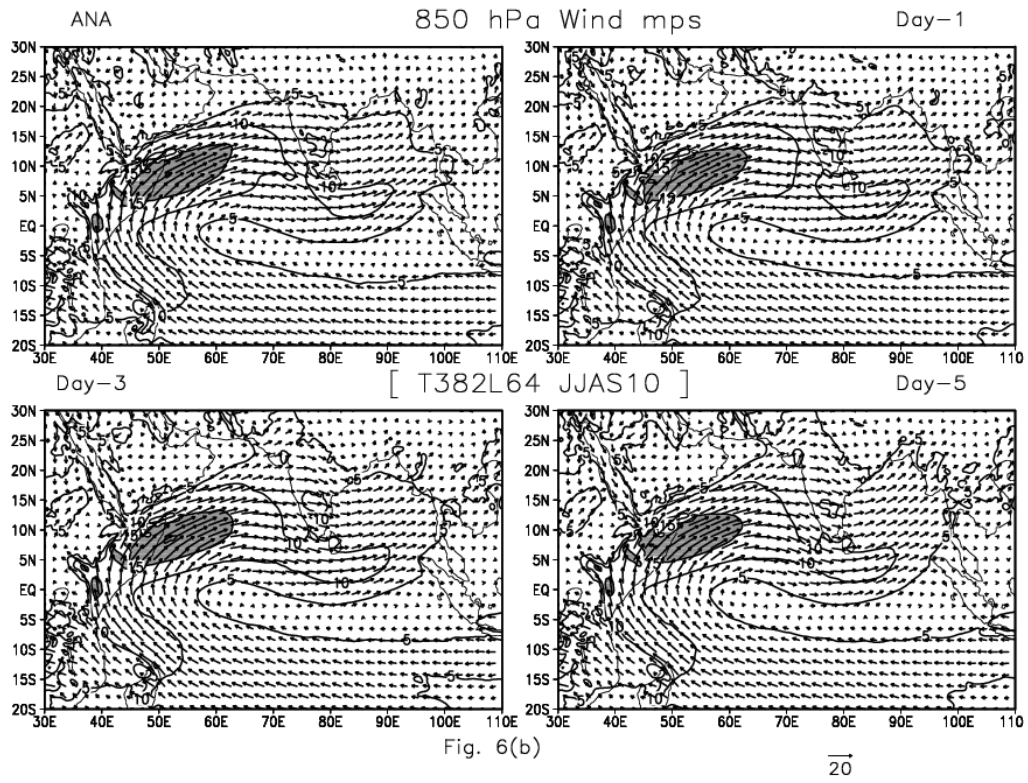


Fig. 5(b)



$\overline{20}$



$\overline{20}$

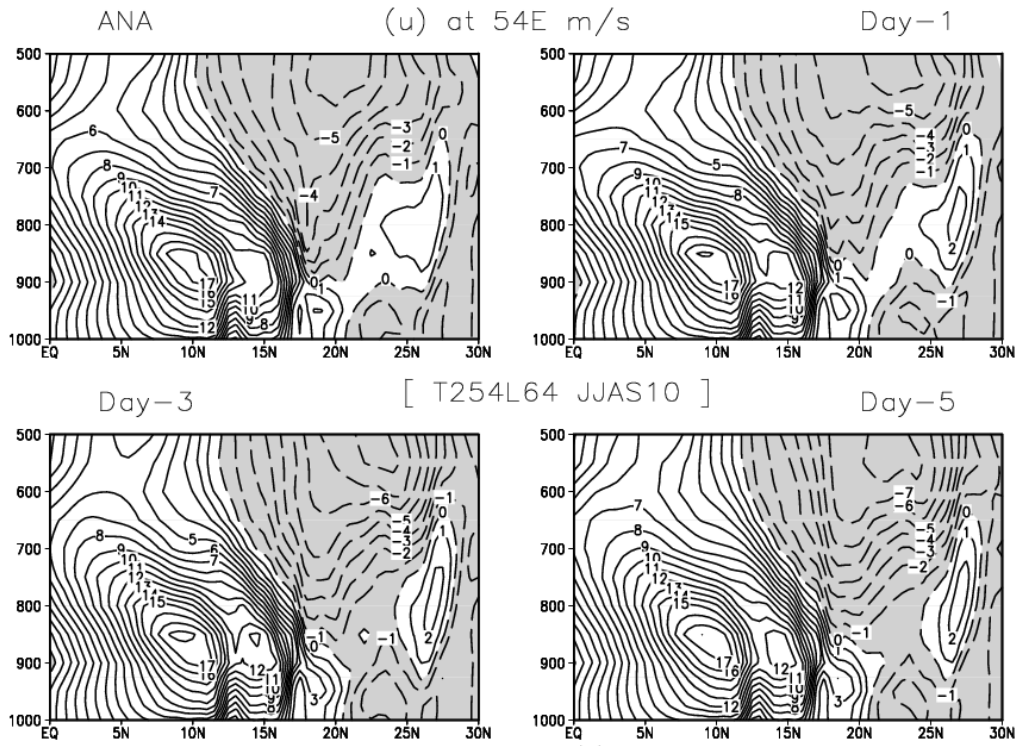


Fig. 7(o)

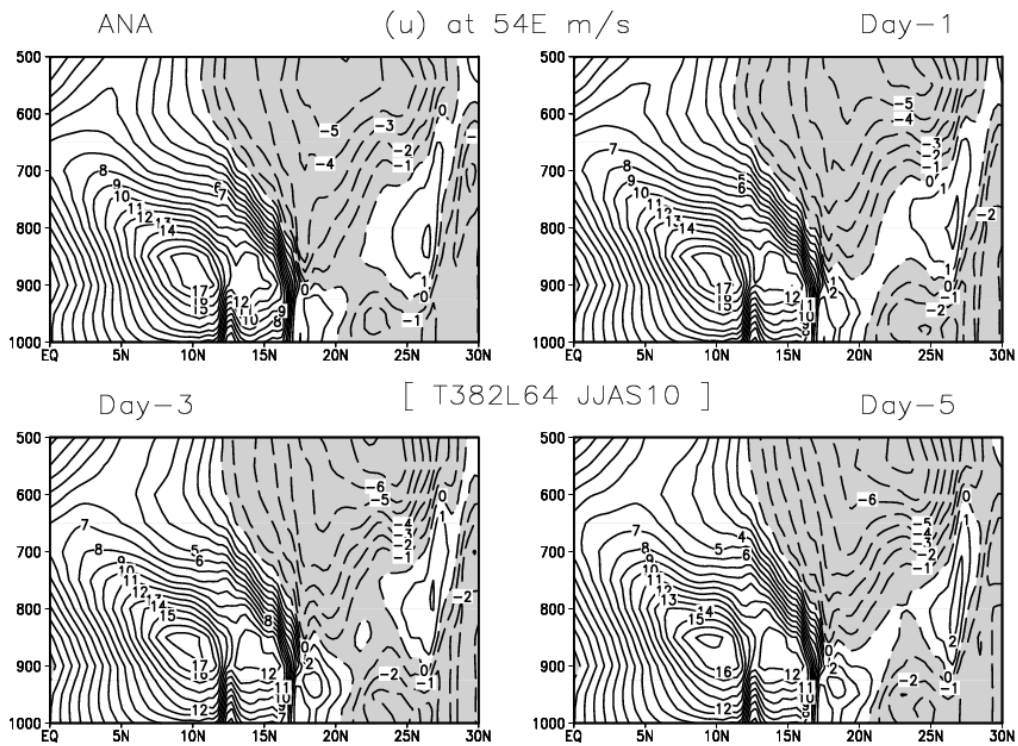


Fig. 7(b)

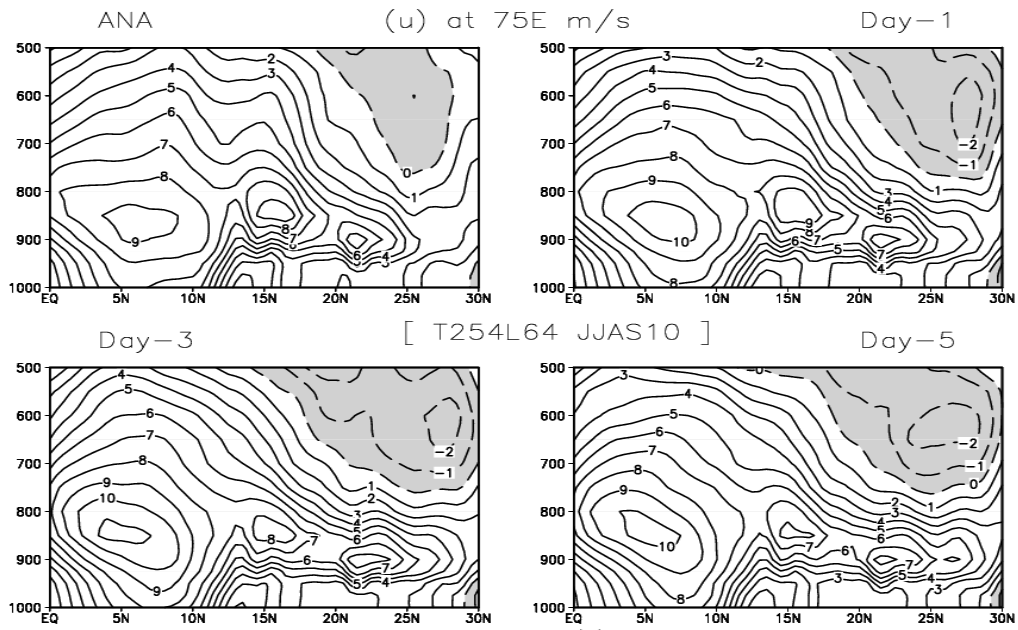


Fig. 8(a)

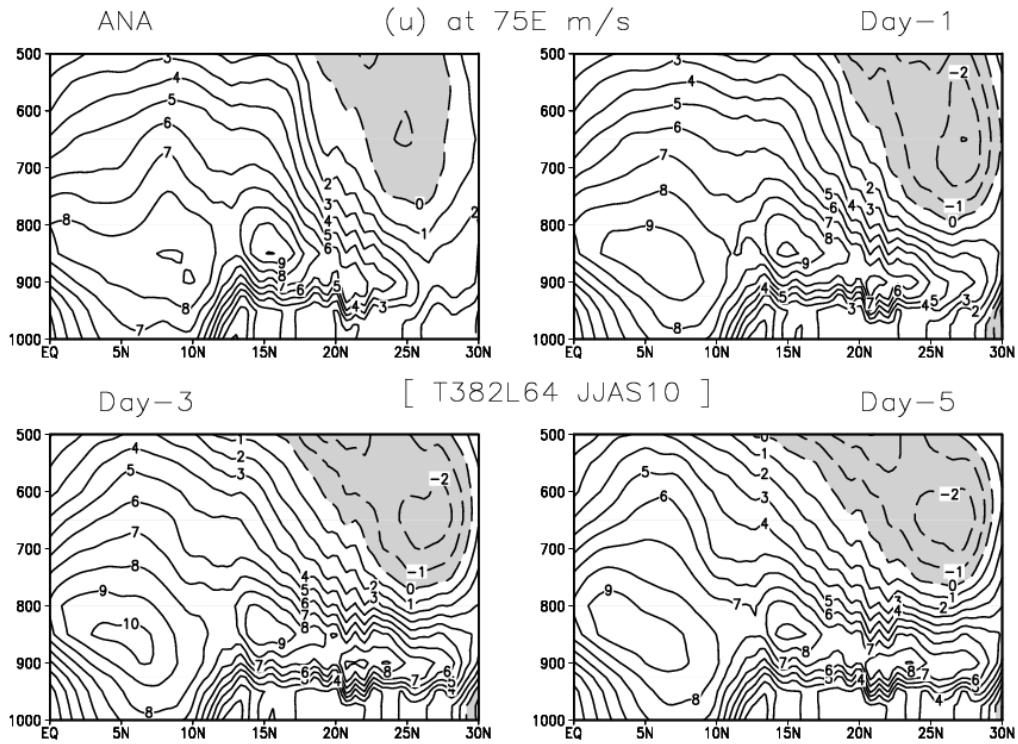


Fig. 8(b)

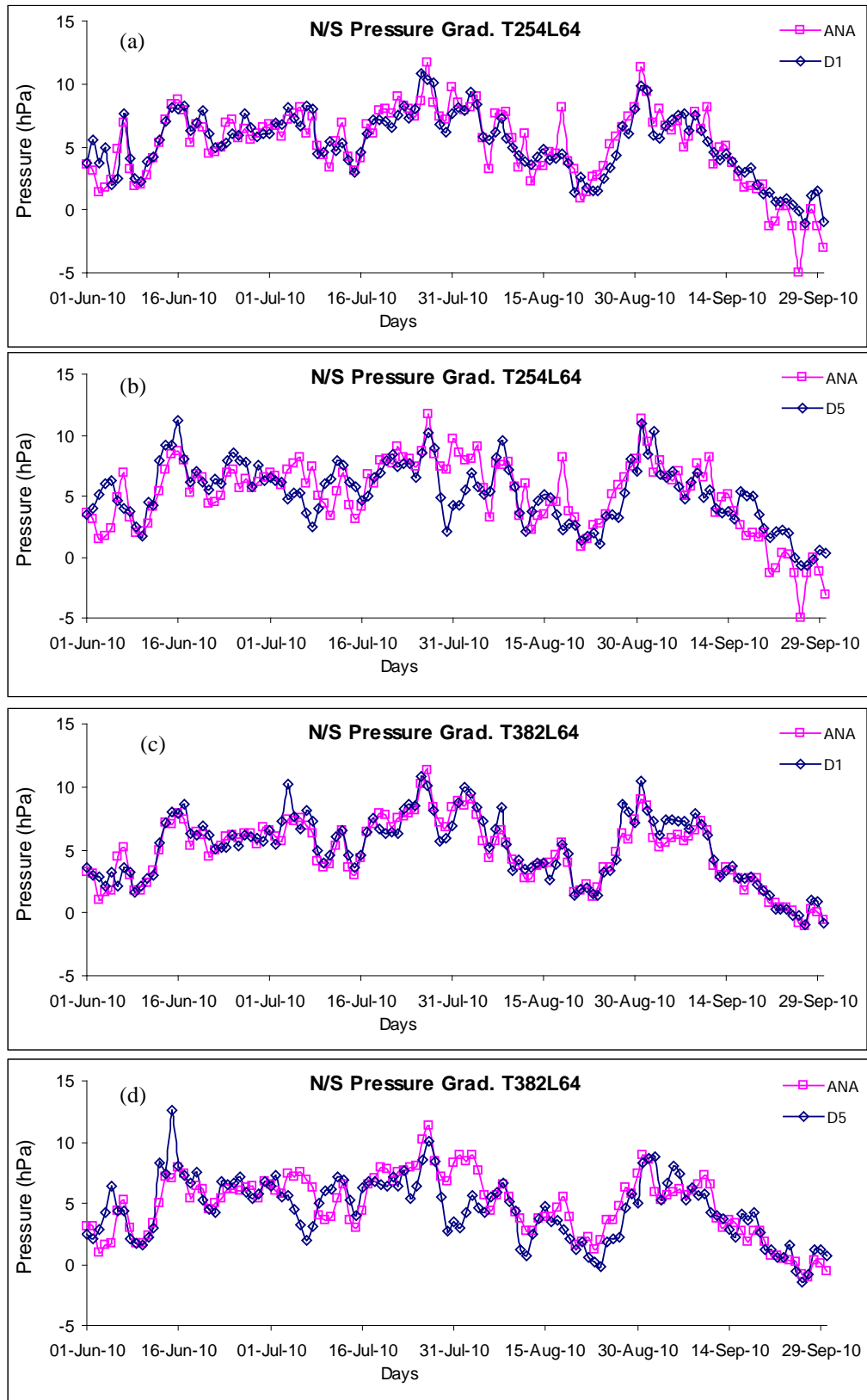


Fig 9. Daily variation of Analysed and predicted (Day-1 and Day-5) of North-South Pressure Gradient during JJAS 2010
(a) T254L64, D-1 **(b)** T254L64 , D-1 **(c)** T382L64, D-5 **(d)** T382L64, D-5

7. Tropical Easterly Jet, Tibetan High and Mid-Latitude Interaction

Saji Mohandas

1. Introduction:

Tropical Easterly Jet (TEJ) and Tibetan High are two prominent semi-permanent flow structures that exist during the Indian summer monsoon season (Koteswaram, 1958, Rao, 1976). The easterly jet is found to the south of subtropical ridge over Asia, which runs from the east coast of Vietnam to the west coast of Africa. Normally, the jet is at an accelerating stage from South China Sea to South India and decelerates thereafter, with latitudinal positions and speed fluctuating from day to day.

Tibetan High is a warm anticyclone, which gets established much later, after the onset of monsoon. Tibetan high prominently appears with its center being most marked at 300hPa level, approximately at 30 °N, 90 °E. It usually extends from 70 °E to 110 °E. There is also a ridge normally found at 700hPa level, with its axis along 40 °N, between 75 °E and 95 °E, just north of the Tibetan massif (Rao, 1976). In July another ridge also is normally observed to lie at about 700hPa and aloft, over Pakistan and northwest India to the west of 75 °E, with its axis along 30 °N. The high over Tibet from 500hPa upward, centred near Tibet at 500hPa and over Tibet at 300hPa and 200hPa levels is normally termed as Tibetan High. In June the axis of anticyclonic belt is at about 25 °N at 300hPa and 200hPa levels. In August, the anticyclone is more or less similar to July, but is shifted to more north and is slightly more intense. In September, the anticyclonic belt is near about 26°N upto 200hPa level. Ramaswamy (1965) associates well-distributed rainfall over India with well-pronounced and east-to-west oriented anticyclone over Tibet at 500hPa and 300hPa levels.

During the onset period, the position of sub-tropical high is to the south and even middle latitude westerlies may be prevailing in northern India in the upper troposphere. When the southwest monsoon is fully established over India, middle latitude westerlies prevail mostly to the north of 30 °N. However, these westerlies appear to affect the monsoon weather over north India to a considerable extend (Rao et al., 1970, Chakravorty and Basu, 1957, Mooley, 1957). Weather produced by monsoon depressions could be accentuated by extra-tropical eastward moving disturbances at a higher latitude (Malurkar, 1958). The

weather on the southern side of the high latitude disturbance may be further increased by orography near Himalayas.

In this section, the significant features of the monsoon circulation over the Indian region at 200hPa level and its interactions with mid-latitude disturbances as seen from the model analysis and forecast during southwest monsoon season of 2010 are documented. Tibetan High extends over the domain from 20°E to 140°E, with its axis along 28°N and the tropical easterly jet (TEJ) forms to the south of this anticyclone. The Tibetan anticyclone may break into two distinct cells, one close to 65°E and the other close to 85°E and oscillates about its axis. This breaking up and oscillation of the anticyclone at 200hPa may be due to the intrusion of transient mid-latitude westerly troughs over to the Indian region. In this report, the time series of the fluctuations in the location of Tibetan Anticyclone along 65°E and 85°E, the location of strong easterlies (along 75°E) and passage of westerly troughs between 65°E and 95°E as seen at 200 hPa level are documented for the monsoon season of 2010.

Comparison of two global model systems is made, namely, T254L64 and T382L64. The charts give a concise record of the variations of the features mentioned above and form the result of this work. The discussion therefore is brief.

2. Axis of the 200 hPa Anticyclone:

During the onset phase of Monsoon, seasonal anticyclone cell generally moves northwards accompanied by the northward shift of upper level westerly flow over to its northward fringes. Latitudinal positions of this 200hPa anticyclone along 65°E and 85°E are shown in the panels a & b for Day-1 (Fig. 1 & 2), Day-3 (Fig. 3 & 4) and Day-5 (Fig. 5 & 6) predictions respectively by T254L64 and T382L64 models.

It is seen that the general features of all the three forecast leading times are grossly matching. The 200 hPa ridge axis analysed by T254L64 model gradually migrated from around 20°N during the beginning of June to around 30°N by the end of June. Its position fluctuated around 30°N till the last week of August. Thereafter, it stayed between 25-28°N till the last week of September, when it migrated below 20°N. At 85°E, it is seen just below 30°N from middle of June to middle of July and then fluctuated between 30°N and 40°N till the last

week of August. After that it stayed near around 20°N till the last week of September before coming southward to 20°N. T254L64 day-1 forecast curve shows more or less good match with the analysis curve. But there are more deviations between the curves at 85°E compared to 65°E.

The T382L64 analysis shows more or less similar characteristics of intra-seasonal fluctuations of the 200 hPa ridge axes at 65 °N and 85 °N. But the corresponding curves are much smoother for both analysis and forecasts compared to T254L64 curves. The day-1 forecasts show very good agreement with the analysis. At day-3 and day-5, the correspondence diminishes and the curves are showing more deviations throughout the period. However, T382L64 shows better match between the forecasts and analysis in general, compared with the respective panels of T254L64 model at all forecast lead times.

3. Tropical Easterly Jet:

Strength of tropical easterlies at 200hPa along 75°E was monitored throughout the season as the strongest wind with speed exceeding 20 m/s (meter per second). Panels c & d of the respective figures show the latitudinal positions and strength of easterlies in the analyses and Day-1 (Figs. 1 & 2), Day-3 (Figs. 3 & 4) and Day-5 (Figs. 5 & 6) forecasts from T254L64 and T382L64 models respectively. In the figures, latitudinal positions (where the strength of easterly is maximum along 75°E) have been marked by crosses and vertical lines show the strength of easterly in m/s for the day at that position. For simplifying the plot, 20 m/s has been subtracted from the strength of easterly and in the figures, 1 m/s represents one-degree latitude of the vertical axis.

During beginning of June, the 200 hPa easterly jet at 75°E is weak and rarely attaining 20m/s at about 10°E in T254L64 analyses. With a spontaneous development of strong TEJ by the second week, it fluctuates between equator and 10°N during the rest of June. By middle of June, the easterlies of the order of 30 m/s are observed continuously for many days. By the end of June, TEJ reduced in intensity and frequency. During the first week of July, it again strengthened between equator and 5°N. However, during the second week of July, there is seen a drastic shift of easterlies towards north, fluctuating between 10°N and 20°N. By the third week of July, TEJ is again restricted mostly below 10°N. Again during the middle of

August, another episode of northward migration of TEJ is observed. By the last week of August, TEJ again shifted southward with the strongest easterly winds occurring during the last fortnight of September. By the last week of September, the activity again subsided and restricted below 10°N. T254L64 day-1 forecast predicts intra-seasonal variability fairly well in strength and position of TEJ. Day-5 forecast is also matching reasonably well with the analyses while day-3 forecast shows somewhat reduced activity compared to the analysis.

T382L64 analysis shows similar features like T254L64, but apparently with slightly higher intensity. Day-1 forecast is the best match with the analysis here also and day-3 forecast showing slightly lesser activity compared to day-1 or day-5.

4. Troughs in Upper Level Westerlies:

Panels e & f show the north south extension of the westerly troughs that passed through Indian region between 65°E and 85°E in the analyses and day-1 (Figs. 1 & 2), day-3 (Figs. 3 & 4) and day-5 (Figs. 5 & 6) forecasts respectively by T254L64 and T382L64 models. It may be noted that these figures do not show any other characteristics of the trough such as its orientation and strength. Also in these figures almost all long and smaller wave activities seen even up to 50°N are presented whereas the major activities affecting the Indian region may be related to those extending southward of 40°N. Still these may give some indication of the variations in zonal index.

200 hPa trough in T254L64 analysis is found far north at the beginning of the season. By the first week of June the troughs extend to its southernmost latitudinal positions (~20°N). During the middle of July, the activity is somewhat subdued for about two weeks. Thereafter in the last week of July, a couple of strong westerly activities are observed. August month experienced a lull in the westerly activities during most of the period. By the last week of August there is a revival of strong westerly activity. There is another lull in the activity during the first fortnight of September. By around 15th of September, a rejuvenated westerly activity with a series of episodes in quick succession till the last week of September contributed to many rainy days over north India. Day-1 forecast by T254L64 is in fair agreement with the analysis, compared to day-3 and day-5.

T382L64 analysis and forecasts show similar patterns as T254L64 but apparently with slightly less intensity and frequency.

Figure Legends

Fig. 1 Latitudinal positions of ridge axis at 200hPa level along 65 °E (a) and 85 °E (b) for both T254L64 analysis (dotted curve) and corresponding T254L64 forecasts (solid curve) for day-1. Latitudinal positions of maximum easterly wind along 75 °E at 200hPa level (marked by crosses) and the wind speed in knots above 20 knots denoted by the length of the vertical lines in terms of degrees of latitude, for analysis (c) and day-1 forecasts (d). Meridional extend in terms of degrees of latitude of the prominent trough(s) in westerlies at 200 hPa level over north India and the neighbouring parts to the north of India denoted as vertical lines for analysis (e) and day-1 forecasts (f). The x-axis is the number of days starting from 1 June, 2010 through 30 September and y-axis is latitude in degrees.

Fig. 2 Same as Fig. 1, but for day-1 forecast of T382L64.

Fig. 3 Same as Fig. 1, but for day-3 forecast of T254L64.

Fig. 4 Same as Fig. 1, but for day-3 forecast of T382L64.

Fig. 5 Same as Fig. 1, but for day-5 forecast of T254L64.

Fig. 6 Same as Fig. 1, but for day-5 forecast of T382L64.

References

Chakravorty , KC and SC Basu, 1957, The influence of western disturbances on the weather over north-east India in monsoon months, *Indian J. Met. Geophys.*, 8, 261 – 272.

Koteswaram, P, 1958, The Easterly Jet Stream in the Tropics, *Tellus*, 10, 43 – 57.

Malurkar, SL, 1958, “Monsoons of the world – India Monsoon”, *Monsoons of the World*, 92 – 100.

Mooley, DA, 1957, The role of western disturbances in the production of weather over India during different seasons, *Indian J. Met. Geophys.*, 8, 253 – 260.

Ramaswamy, C, 1965, “On synoptic methods of forecasting the vagaries of southwest monsoon over India and neighbouring countries”, *Proc. Symp., IIOE*, 317 – 326.

Rao, YP, 1976, “Southwest Monsoon”, *Meteorological Monograph, Synoptic Meteorology No. 1/1976, India Meteorological Department, June 1976*, 367pp.

Rao, YP, V Srinivasan and S Raman, 1970, “Effect of middle latitude westerly systems on Indian monsoon”, *Symp. Trop. Met., Hawaii, N IV 1 – 4*.

RIDGE, TEJ & TROUGH 200hPa JJAS2010 (T254L64)

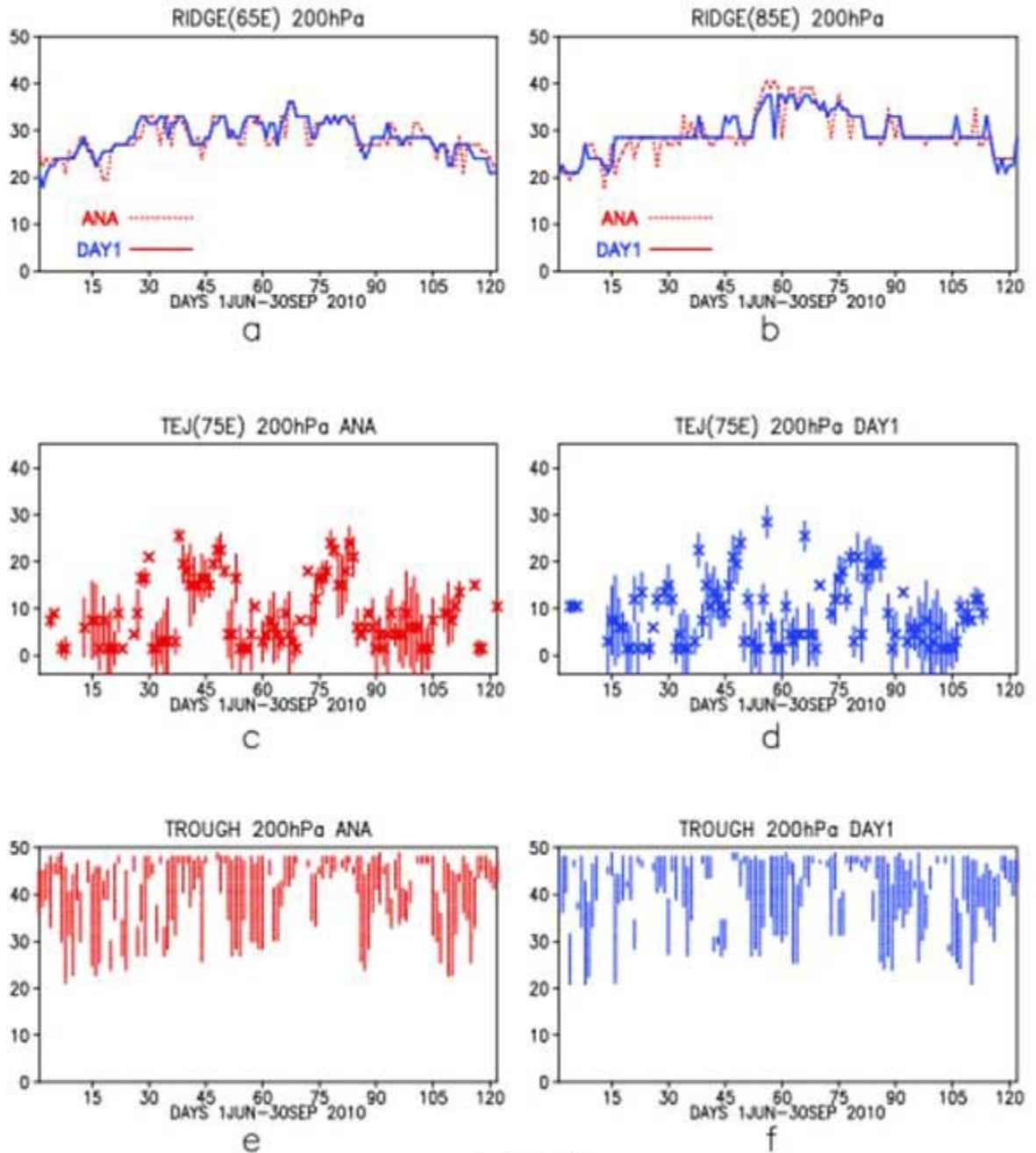


Fig. 1

RIDGE, TEJ & TROUGH 200hPa JJAS2010 (T382L64)

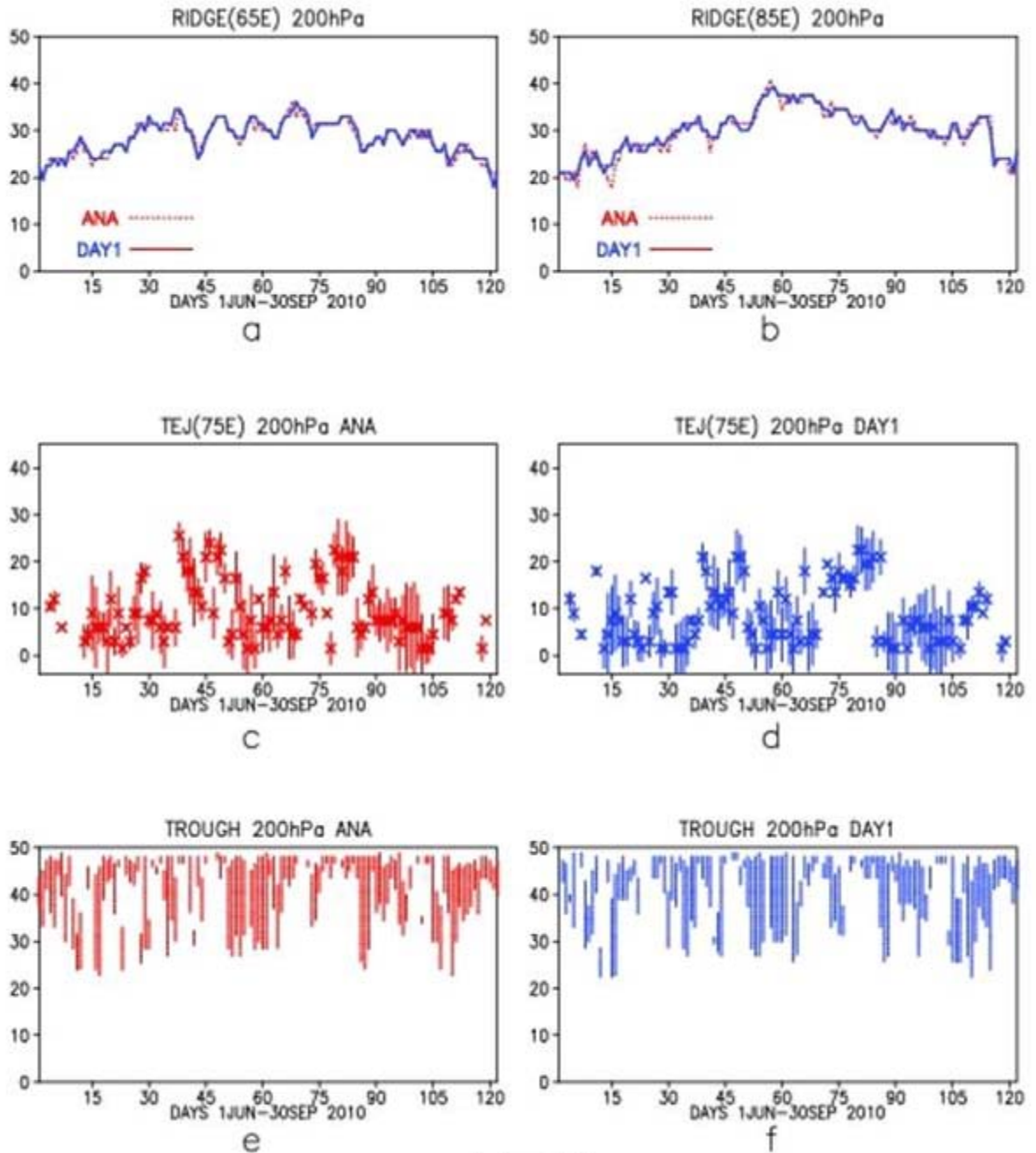


Fig. 2

RIDGE, TEJ & TROUGH 200hPa JJAS2010 (T254L64)

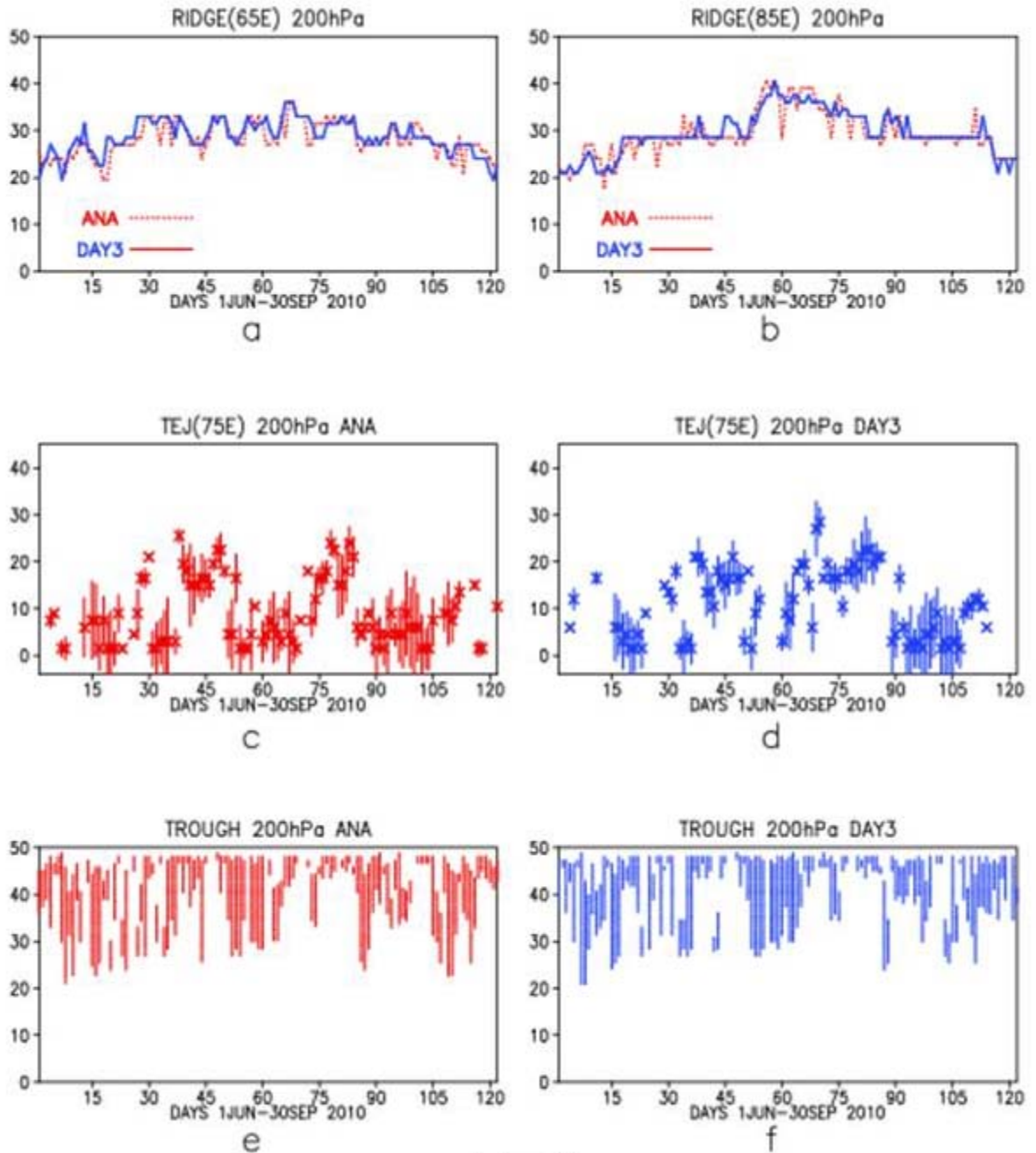


Fig. 3

RIDGE, TEJ & TROUGH 200hPa JJAS2010 (T382L64)

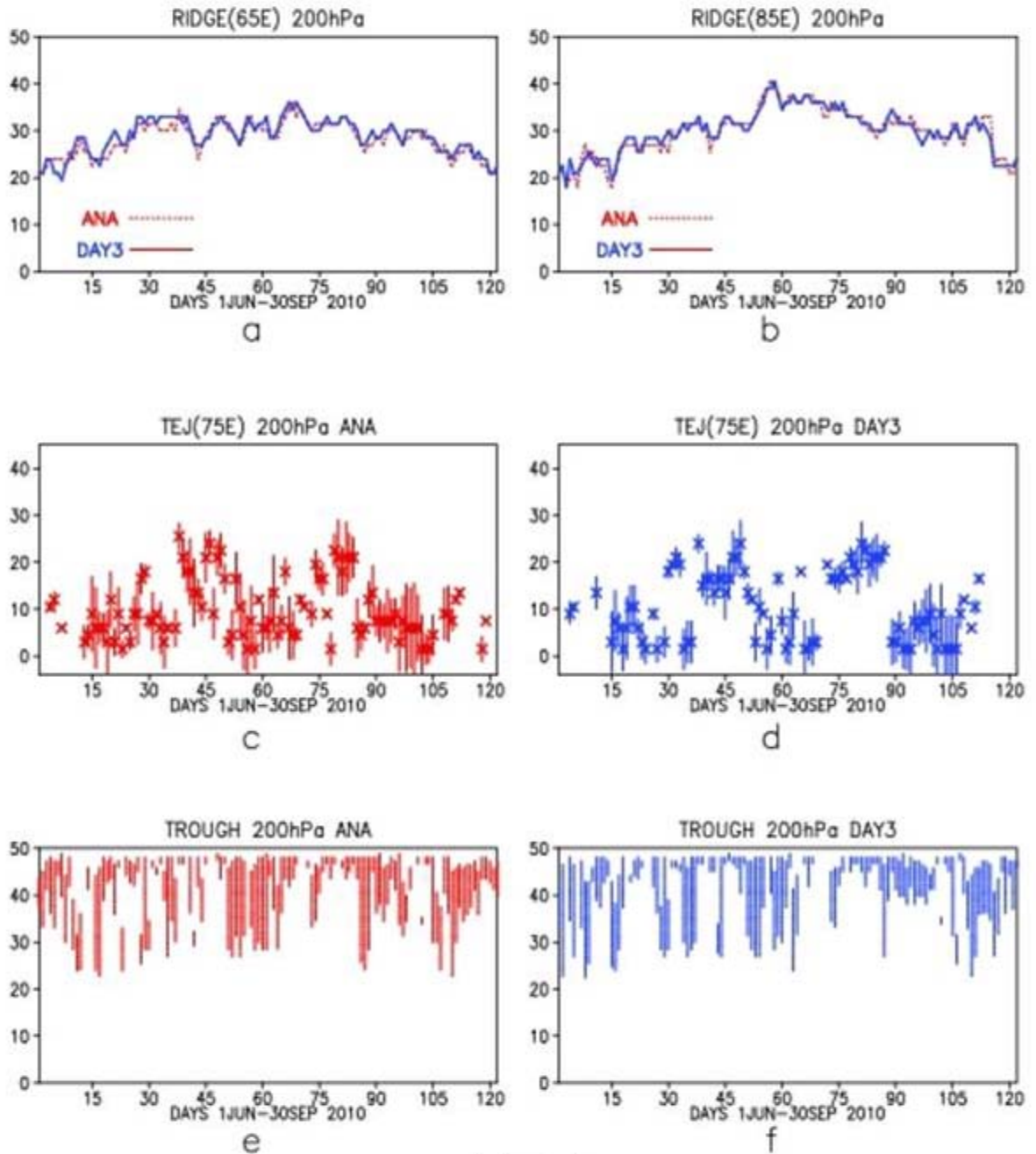


Fig. 4

RIDGE, TEJ & TROUGH 200hPa JJAS2010 (T254L64)

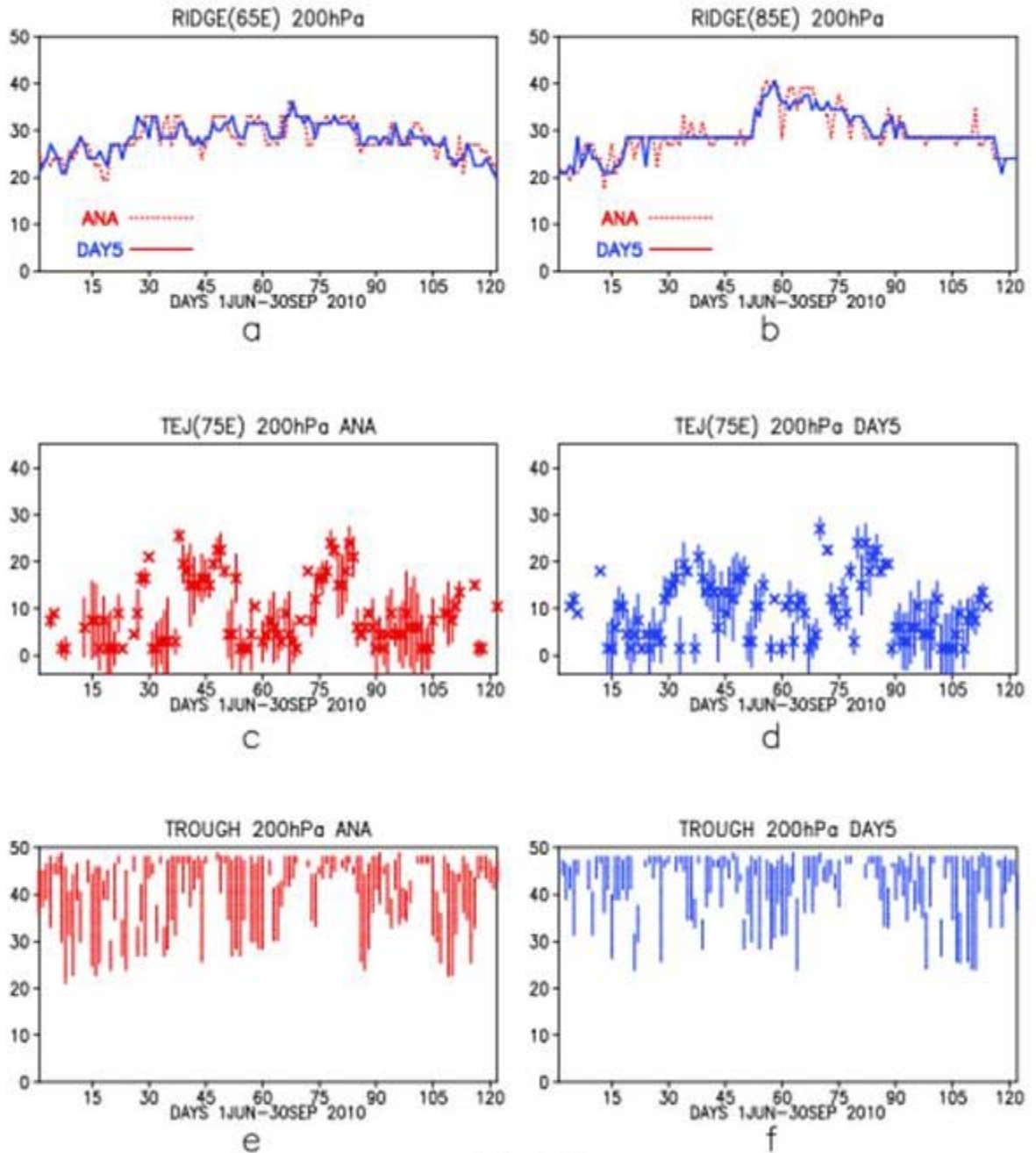


Fig. 5

RIDGE, TEJ & TROUGH 200hPa JJAS2010 (T382L64)

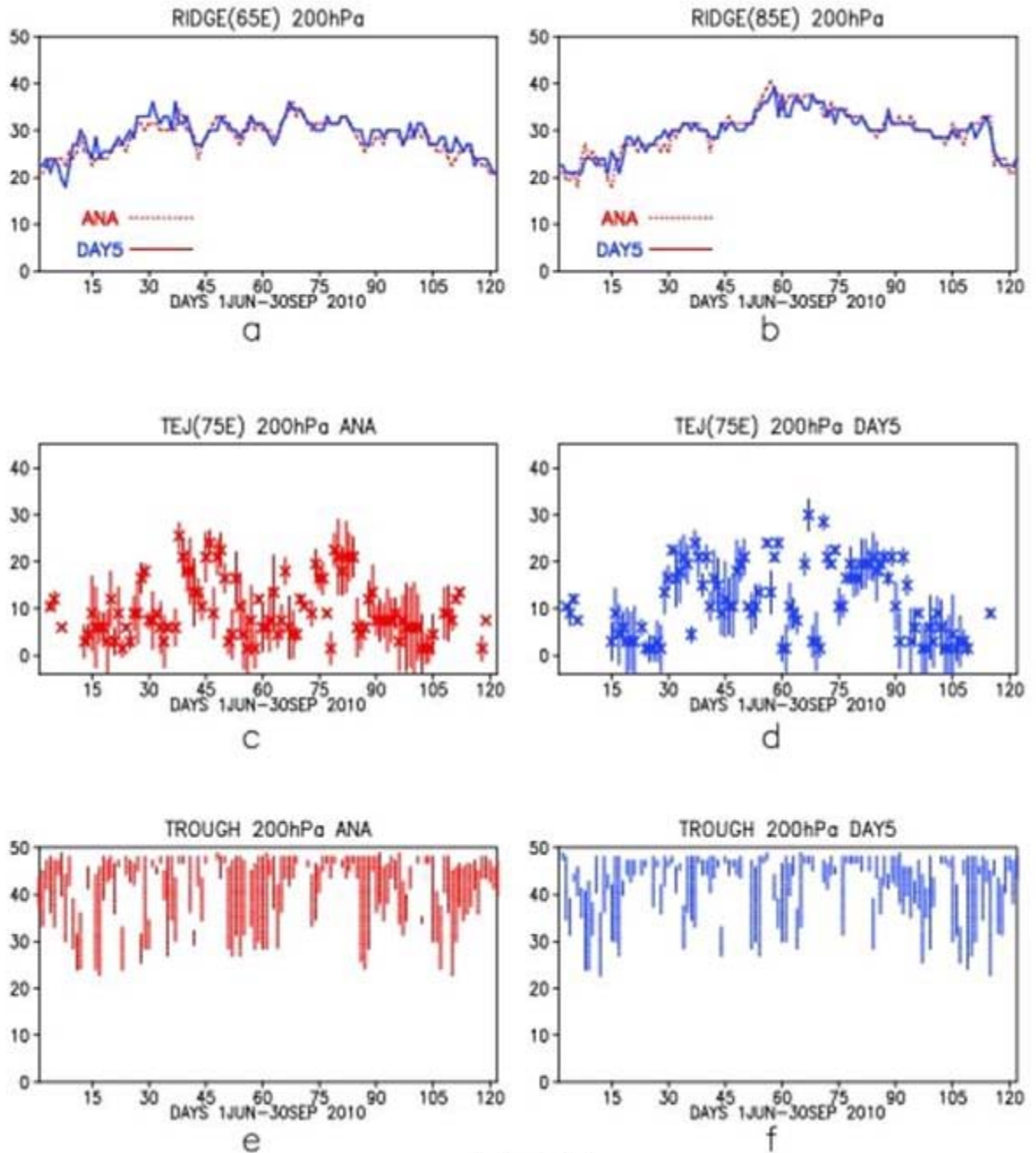


Fig. 6

8. Comparison of Planetary Boundary Layer (PBL) Height in T382L64 and T254L64 Analysis-Forecast Systems

Aditi and E.N. Rajagopal

1. Introduction:

The planetary boundary layer (PBL) is a critical component of earth's climate system. PBL has important role in both the atmospheric radiative and heat budgets as boundary layer processes are responsible for low clouds like stratocumulus and are of fundamental importance for cumulus convection. Thus, the parameterization of PBL in atmospheric models is one of the most important aspects and need special attention.

Turbulence in the PBL is responsible for mixing of heat, moisture and momentum. Due to extensive turbulent mixing, the concentration of water vapor and trace gases remain reasonably steady within the layer whose vertical thickness is referred to as the PBL/mixed layer height (Subrahmanyam et al. 2003, Alappatu et al. 2008). The height of PBL is one of the fundamental parameters that are used to characterize its structure (Gryning et al. 1987, Stull 1988, Garratt 1992). The PBL height variations over a site are largely driven by the diurnal and seasonal changes in thermal instability and turbulence (Stull 1988, Garratt 1992).

Remote sensing techniques like Lidar, Sodar and other direct measurement techniques like dropsonde and radiosonde have been used to analyze the spatial and temporal variations of PBL height in continental and marine regions (Holt and Raman 1986, Zeng et al. 1998, Subrahmanyam et al. 2003). Few long term extensive investigations were focused on the seasonal changes of PBL heights and its structure (Gamo 1984, Lee 1986, Dayan and Rodnizki 1998, Chen et al. 2001). Seasonal variation of PBL height has been studied over many places in India (Vittalmurti et al. 1980, Krishnan and Kunhikrishnan 2004). The marine PBL and its spatio-temporal variability has been analyzed during INDOEX (Indian ocean Experiment) over the Indian ocean and the Arabian sea (Subrahmanyam et al. 2003, Ramana et al. 2004).

In the present study, the performance of T254L64 and T382L64 analysis-forecast systems in respect of the prediction of PBL height is examined over Indian region during

June-September 2010. The study investigates the difference between mean analysis and mean 36 hr, 60 hr, and 108 hr forecast for PBL height for the month of June, July, August and September 2010.

2. PBL Parameterization in Atmospheric Models:

In global models, the large-scale atmospheric flow determines to a large extent the properties of the PBL and the PBL in turn reacts to these external forcings and modifies the large scale flow. Generally, the vertical diffusion scheme based on local gradients of wind and potential temperature, the so-called local K-approach, is used in atmospheric numerical models. In this scheme, the eddy diffusivities coefficients are parameterized as functions of local Richardson number. However, this scheme has certain limitations such as the transport of mass and momentum in the PBL is accomplished by largest eddies and such eddies should be modeled by bulk properties of PBL instead of local properties. Also, such a scheme is unable to represent realistically mixing in the convective boundary layer because of the counter gradient fluxes (Deardroff 1972, Troen and Mahrt 1986, Stull 1991). This may affect profiles of mean quantities especially in locations where dry convection is of importance in the PBL. One of the ways to overcome these limitations is to use higher order closure approaches developed by Mellor and Yamada (1974). The higher order closure approach was capable of representing a well mixed boundary layer structure but was computationally more expensive.

On the other hand, another type of simple diffusion scheme, the so-called nonlocal-K approach is used in weather prediction and climate models. This scheme utilizes the results of large eddy simulation research (Wyngaard and Brost 1984) and is computationally efficient. The nonlocal turbulent mixing within the PBL in atmospheric models is pioneered by the work of Troen and Mahrt (1986). The turbulent diffusivity coefficients are calculated from a prescribed profile shape as a function of boundary layer heights and scale parameters derived from similarity requirements. In addition to the advantage in matching condition between the surface-layer top and the Ekman layer bottom, it gives the ideal turbulent diffusivity profile proposed by O'Brien (1970), which is based on the physical coupling that the profile and its first derivative be continuous with height and matches the similarity requirement at the surface layer. Holtslag et. al

(1990) showed that this scheme is useful for predicting short-range weather phenomena of temperature and humidity profiles in the lower atmosphere, the structure of boundary layer, the boundary layer height and the amount of boundary layer clouds. Giorgi et al. (1993) implemented this scheme in a second generation regional climate model (RegCM2) and showed the impact on the simulated regional climate over Europe for January and June 1979. Their results showed that this scheme induced an overall increase in total precipitation amounts. Basu et. al. (2002) studied the impact of the non-local K-closure scheme for the atmospheric boundary layer using the Global Spectral Model in predicting monsoon circulation over Indian region. Their results showed a systematic improvement in the precipitation distribution over the Indian region.

Both T254L64 and T382L64 models use non-local scheme of PBL parameterization following Hong and Pan (1996). A brief description of the scheme is given in the next section.

3. Non-local Vertical Diffusion Scheme in T254L64 and T382L64 Models:

According to Deardorff (1972), Troen and Mahrt (1986), Holtslag and Moeng (1991), and Holtslag and Boville (1993), the turbulent diffusion equations for prognostic variables (C; u, v, θ , q) can be expressed by

$$\frac{\partial C}{\partial t} = \frac{\partial}{\partial z} \left[K_c \left(\frac{\partial C}{\partial z} - \gamma_c \right) \right] \quad (1)$$

Where K_c is the eddy diffusivity coefficient and γ_c is a correction to the local gradient that incorporates the contribution of the large-scale eddies to the total flux. This correction applies to potential temperature (θ) and specific humidity (q) within the mixed boundary layer. This nonlocal diffusion approach is applied only for the mixed layer diffusion. The momentum diffusivity coefficient is formulated as

$$K_{zm} = k w_s z \left(1 - \frac{z}{h} \right)^p \quad (2)$$

where p is the profile shape exponent taken to be 2, k is the von Karman constant (=0.4), z is the height from the surface, and h is the height of the PBL. The mixed-layer velocity scale is represented as

$$w_s = u_* \phi_m^{-1} \quad (3)$$

where u_* is the surface frictional velocity scale and ϕ_m is the wind profile function evaluated at the top of the surface layer. The counter gradient terms for θ and q are given by

$$\gamma_c = b \frac{\overline{(w'c')}}{w_s} \quad (4)$$

where $\overline{(w'c')}$ is the corresponding surface flux for θ and q , and b is a coefficient of proportionality. To satisfy the compatibility between the surface layer top and the bottom of the PBL, the identical profile functions to those in surface-layer physics are used. For unstable and neutral conditions $\left[\overline{(w'\theta'_v)}_0 \leq 0\right]$,

$$\phi_m = \left(1 - 16 \frac{0.1h}{L}\right)^{-1/4}, \text{ for } u \text{ and } v \quad (5)$$

$$\phi_t = \left(1 - 16 \frac{0.1h}{L}\right)^{-1/2}, \text{ for } \theta \text{ and } q$$

while for the stable regime $\left[\overline{(w'\theta'_v)}_0 > 0\right]$,

$$\phi_m = \phi_t = \left(1 + 5 \frac{0.1h}{L}\right), \quad (6)$$

where h is the boundary layer height and L is the Monin-Obukhov length scale. The top of the surface layer is estimated as $0.1h$. To determine the b factor in (4), the exponent of $-1/3$ is chosen to ensure the free-convection limit. Therefore, the following approximation is used:

$$\phi_m = \left(1 - 16 \frac{0.1h}{L}\right)^{-1/4} \approx \left(1 - 12 \frac{0.1h}{L}\right)^{-1/3} \quad (7)$$

Following the derivation of Troen and Mahrt (1986) and Holtslag et al. (1990), the right hand side of (7) leads to $b=7.8$. The boundary layer height is given by

$$h = Rib_{cr} \frac{\theta_{va} |U(h)|^2}{g(\theta_v(h) - \theta_s)}, \quad (8)$$

where Rib_{cr} is the critical bulk Richardson number, $U(h)$ is the horizontal wind speed at h , θ_{va} is the virtual potential temperature at the lowest model level, $\theta_v(h)$ is the virtual potential temperature at h , and θ_s is the appropriate temperature near the surface defined as

$$\theta_s = \theta_{va} + \theta_T \left[= b \frac{\overline{(w'\theta'_v)_0}}{w_s h} \right], \quad (9)$$

where θ_T is the scaled virtual temperature near the surface with a maximum limit of 3 K (Hong and Pan 1996).

The eddy diffusivity for temperature and moisture (K_{zt}) is computed from K_{zm} in (2) by using the relationship of the Prandtl number, which is given by

$$Pr = \left(\frac{\phi_t}{\phi_m} + bk \frac{0.1h}{h} \right), \quad (10)$$

where Pr is a constant within whole mixed boundary layer.

Numerically, the boundary layer height, h , is obtained iteratively. First h is estimated by (8) without considering the thermal excess, θ_T . This estimated h is utilized to compute the profile functions in (5)-(7), and to compute the mixed-layer velocity w_s in (3). Using w_s and θ_T in (9) h is enhanced. With the enhanced h and w_s , K_{zm} is obtained by (2), and K_{zt} by (10). The counter gradient correction terms for θ and q in (1) are also obtained by (4).

4. Data and Methodology:

In this study, model outputs of T382L64 and T254L64 for the period of June-September 2010 are used. The monthly mean PBL height of 12 UTC analyses is compared with the model's mean 36, 84 and 108 hr forecasts for June-September 2010. The PBL height at 12 UTC is much more developed as compared to 00 UTC, thus monthly mean PBL height of 12 UTC is utilized in the present study.

5. Results and Discussions:

5.1 Variation of mean PBL height in model analysis

Figs. 1 and 2 show the mean analysis of PBL height (meters, m) for June, July, August and September 2010 for T382L64 and T254L64 respectively. Mean analysis reveals that the PBL heights are highest (in north west part of India) in the month of June and it decreases from July to September for both the models. In T382L64 the mean PBL height ranges from 500-4500 m in June, 500- 3000 m in July, 500- 2000 m in August and September (Fig. 1). Similar variations in magnitude of PBL height are observed in T254L64 from June to September (Fig. 2).

The maximum value of mean PBL height is reported in June, mainly due to summer conditions. The mean PBL heights reach their maximum values in June and July, ignoring the subsiding effect of rain and loss of insolation by existing cloud cover, because of intense mixing and inability of the heat to escape beyond the cloud layer. The variations in mean PBL height are clearly seen during summer monsoon (June, July and August). A decreasing trend in the PBL height is seen in September (Figs. 1d and 2d). This can be attributed to weakening of convective activities during this month. This month also happens to be a transition period from wet south-westerly wind to drier north easterly wind.

Several attempts have been made to understand the seasonal variation of PBL height over different locations in India using the observational data. Vittalmurti et al. (1980) had shown the seasonal variation of PBL height over some urban locations in India and found that maximum PBL height is observed during April (pre-monsoon) as well as during October and January at several sites in India. Minimum values of MLH were observed during August (summer/monsoon) and October (Post-monsoon). Gamo et al. (1994) reported the day time maximum PBL height variation over Delhi and their study revealed that PBL attained highest altitude during pre-monsoon (~3000 m), low during monsoon (<2000 m), moderate during post monsoon (~2000 m) and lowest during winter (< 1000 m). Similar variation is also reported by Krishnan and Kunhikrishnan (2004) over Gadanki, a rural site in South-east India. They reported reasonably higher values of PBL height for pre-monsoon (~2200 m) and post monsoon (~1770 m) months as against slightly lower values in summer-monsoon (~1650 m) and winter months (~1500 m). Srivastava et al. (2010) investigated the seasonal variation in PBL height over Ahmedabad and found that PBL height is at maximum during summer monsoon and it is

at minimum during winter months. The differences in the estimated PBL height may be due to prevailing meteorological conditions at different location. Nonetheless, the range of PBL height is found to be somewhat similar to that obtained from mean analysis of both T382L64 and T254L64 models. In Delhi, the mean PBL height is of the order of 4000 m in June, 1500 m in July, 1000 m in August and 500 m in September as per the mean model analyses (Figs.1-2).

The changes in mean PBL height in the analysis of T382L64 and T254L64 (Figs. 1-2) are also evident in the marine boundary layer. The mean PBL height over Arabian sea is found to be of the order of 1000-1500 in June, July, August and 1000 m in September. However, over Bay of Bengal the mean PBL height is 1000 m during June and July and 500 m in August and September which is slightly lower than that over Arabian Sea. Over Indian Ocean the mean PBL height is found to be 1000-1500 m in June, July and 500-1500 m in August and 500 m in September. The values are found to be of the similar order in both the models. The model analysed values are somewhat similar to those obtained in the other observational studies. The PBL height over Indian Ocean was observed to a range of 400-1100 m (Ramana et al., 2004) during the first two campaigns (Pre-INDOEX, 1997) and First Field Phase (FFP, 1998) of the INDOEX. During the Intensive Field Phase (IFP-99) of the INDOEX campaign, Subrahamanyam et al.(2003) reported the PBL height in the range 200-900 m. Holt and Raman (1986) reported the PBL height over Bay of Bengal during monsoon about 400-500 in contrast to about 800-1500 m over Arabian Sea (Holt and Raman, 1985).

In general, the mean analysis show somewhat higher values of PBL height in all the months. This may be attributed to the fact that these values are valid for mid-afternoon hours when the PBL becomes highly convective and turbulent thereby attaining maximum values in afternoon hours. Further the height of the PBL may be really high for the year 2010.

5.2 Comparison of mean PBL height in model forecasts

The mean analysis of T382L64 for the month of June (Fig. 3a) depicts the PBL height of the order of 3000-4500 m in northwest parts of India whereas the minimum PBL height (1000-1500 m) is seen along the Western Ghats. The difference between

mean analysis and mean 36 hr, 60 hr and 108 hr forecasts designated as A-F (where A stands for analysis and F stands for forecast) are shown in Figs. 3b, 3c and 3d respectively. The difference between mean analysis and mean 36 hr forecast is positive in northern and central parts with forecast over predicting the PBL height. The difference is negative in Southern peninsular region where the 36 hr forecast is under-predicting the PBL height. The differences are found to be increasing in 60 hr and 108 hr forecasts over north and central parts whereas in peninsular region significant changes are not observed. In northwest parts the forecast is over-predicting the PBL height in 36 and 60 hr forecasts, while 108 hr forecast the under-predicts the PBL height.

The mean analysis of T254L64 for the month of June (Fig. 4a) reveals similar pattern for PBL height as in T382L64 system. The difference between mean analysis and mean 36 hr forecast (Fig. 4b) is found to be positive with the forecast over-predicting in northern and eastern parts. An under-prediction is observed in forecast in northwest and central parts. The differences are found to be increasing with 60 hr (Fig. 4c) and 108 hr forecast (Fig. 4d) over eastern parts and northwestern parts. In general, the differences are found to be smaller in T254L64 compared to T382L64.

In the month of July, the mean analysis of T382L64 (Fig. 5a) shows a decrease in magnitude of PBL height in all the parts as compared to that observed during June, with maximum (2000-3000 m) observed in north west parts and minimum 500 m over Western Ghats. The 36, 60 and 108 hr forecasts (Figs. 5b, 5c, 5d) over-predicts the PBL height in north region with magnitude increasing with forecast lead time. However, under-prediction is seen over east, west and peninsular region with highest under-prediction in 108 hr forecast.

The mean analysis of T254L64 (Fig. 6a) for July 2010 show similar PBL heights as in T382L64. The 36, 60 and 108 hr forecasts (Figs. 6b, 6c, 6d) over-predicts the PBL height in northwest parts with magnitude increasing with forecast lead time. However, under-prediction is observed in western parts. The magnitudes of differences are found to be smaller in comparison to T382L64.

The mean analysis of T382L64 for August 2010 (Fig. 7a) shows further decrease in magnitude of PBL height all over India. For most of the parts the PBL height is found to be of the order of 1000 m. PBL height is over-predicted in north, west and some parts

of east with nearly same magnitude in all the mean forecasts (Figs. 7b, 7c, 7d), however, there is an increase in the area with the forecast lead time.

The mean analysis (Fig. 8a) of T254L64 is similar to that observed for T382L64. The differences between mean analysis and mean forecasts (Figs. 8b, 8c, 8d) are not much and there is also not much difference with forecast lead time.

The PBL height is found to decrease further to 500 m in most of the parts in mean analysis of September 2010 (Fig. 9a) for T382L64. The magnitude of over-prediction in the PBL height as compared to analysis is not increasing much with forecast lead time (Figs. 9b, 9c, 9d)

The PBL height is found to show the same trend in T254L64 analysis for September (Fig.10a) as in T382L64. PBL height is over-predicted in the forecasts over west Rajasthan with magnitude not increasing much with forecast lead time (Figs. 10b, 10c, 10d)

6. Conclusions:

The high resolution T382L64 and T254L64 global models are used to analyze the variation in the PBL height over Indian region during monsoon season (JJAS) 2010. The mean analysis PBL height of the T382L64 and T254L64 forecast system at different locations over India is somewhat in agreement with those obtained from different observational studies carried over Indian continent. The differences between mean analysis and predicted PBL height are found to be decreasing from June to September with maximum in June and minimum in September. Also the differences are found to be increasing with forecast lead time in all the months from both the models.

References

- Alappattu, D.P., Subrahamanyam, D.B., Kunhikrishnan, P.K., Somayaji, K.M., Bhat, G.S., Venkateshan, R., Dutt, C.B.S., Singh, A.B., Soni, V.K., Tripathi, A.S., 2008: On the marine atmospheric boundary layer characteristics over Bay of Bengal and Arabian Sea during the Integrated Campaign for Aerosol gases and Radiation Budget (ICARB), *Journal of Earth System Science*, *117*, 281-291.
- Basu, S., G.R. Iyengar. A.K. Mitra, 2002 : Impact of a nonlocal closure scheme in a simulation of a monsoon system over India, *Monthly Weather Review*, *130*, 161-170.
- Chen, W., Kuze, H., Uchiyama, A., Suzuki, Y., Takeuchi, N., 2001: One year observation of urban mixed layer characteristics at Tsukuba, Japan using a micro pulse lidar. *Atmospheric Environment*, *35*, 4273-4280.
- Dayan, U., Rodnizki, J., 1998: The temporal behavior of the atmospheric boundary layer in Israel. *Journal of Applied Meteorology*, *38*, 4273-4280.
- Deardorff, J.W., 1972: Theoretical expression for the countergradient vertical heat flux. *J. Geophysical Research*, *77*, 5900-5904.
- Gamo, M., 1984: Seasonal change of mixed layer structure at Tsukuba. *Journal of Meteorological Society of Japan*, *63*, 60-74.
- Garratt, J.R., 1992: The Atmospheric Boundary Layer. *Cambridge University Press, Cambridge*.
- Giorgi, F., M. R. Marinucci, G.T. Bates, 1993: Development of a second-generation regional climate model (RegCM2). Part 1: Boundary layer and radiative transfer processes. *Monthly Weather Review*, *121*, 2794-2813.

- Gryning, S.E., Holtslag, A.A.M., Irwin, J.S., Sivertsen, B., 1987: Applied dispersion modelling based on meteorological scaling parameters. *Atmospheric Environment*, 21, 79-89.
- Holt, T., Raman, S., 1986: Observations of the mean and turbulence structure of the marine boundary layer over the Bay of Bengal during MONEX-79, *Monthly Weather Review*, 114, 2176-2190.
- Holtslag, A.A.M., I.F. Bruijin and H.L. Pan, 1990: A high resolution air mass transformation model for short-range weather forecasting. *Monthly Weather Review*, 118, 1561-1575.
- Holtslag, A.A.M., C.H. Moeng, 1991: Eddy diffusivity and countergradient transport in the convective atmospheric boundary layer. *Journal of Atmospheric Sciences*, 48, 1690-1698.
- Holtslag, A.A.M., B.A. Boville, 1993: Local versus nonlocal boundary layer diffusion in a global climate model. *Journal of Climate*, 6, 1825-1842.
- Krishnan, P., Kunhikrishnan, P.K., 2004: Temporal variations of ventilation coefficient at a tropical Indian station using UHF wind profiler. *Current Science*, 86, 447-451.
- Lee, C.B., 1986: Simple model and climatological aspects of structure of the convective boundary layer. *Atmospheric Environment*, 20, 705-714.
- Mellor, G.L. and T. Yamada, 1974: A hierarchy of turbulence closure models for planetary boundary layers. *Journal of Atmospheric Sciences*, 31, 1792-1806.
- Naja, M., Lal, S., 2002: Surface ozone and precursor gases at Gadanki (13.5⁰ N, 79.2⁰ E), a tropical rural site in India. *Journal of Geophysical Research*, 107 (D14), 4197.

- O'Brien, J.J., 1970: A note on the vertical structure of the eddy exchange coefficient in the planetary boundary layer. *Journal of Atmospheric Science*, 27, 1213-1215.
- Ramana, M.V., Krishnan, P., Nair, S.M. Kunhikrishnan, P.K., 2004: Thermodynamic structure of the atmospheric boundary layer over the Arabian sea and the Indian ocean during pre-INDOEX and INDOEX-FFP campaigns, *Annales Geophysicae* 22, 2679-2691.
- Stull, R. B., 1988: An Introduction to Boundary Layer Meteorology. *Kluwer Academic Publishers, UK*, pp.666.
- Stull, R. B., 1991: Static stability: An update. *Bulletin of American Meteorological Society*, 72, 1521-1529.
- Subrahamanyam, D.B., Ramchandran, R., Sen Gupta, K., Mandal, T.K., 2003: Variability of mixed layer heights over the Indian Ocean and central Arabian Sea during INDOEX, IFP-99, *Boundary Layer Meteorology*, 107, 683-695.
- Troen, I., Mahrt, L., 1986: A simple model of the atmospheric boundary layer: Sensitivity to surface evaporation. *Boundary Layer Meteorology*, 37, 129-148.
- Vitalmurti, K.P.R., Viswanadham, D.V., Sadhram, Y., 1980: Mixing heights and ventilation coefficients for urban centres in India. *Boundary Layer Meteorology*, 19, 441-451.
- Zeng, X., Zhao, M., Dickinson, R. E., 1998: Intercomparison of bulk aerodynamic algorithms for the computation of sea surface fluxes using the TOGA COARE and TAO data. *Journal of Climate*, 11, 2628-2644.

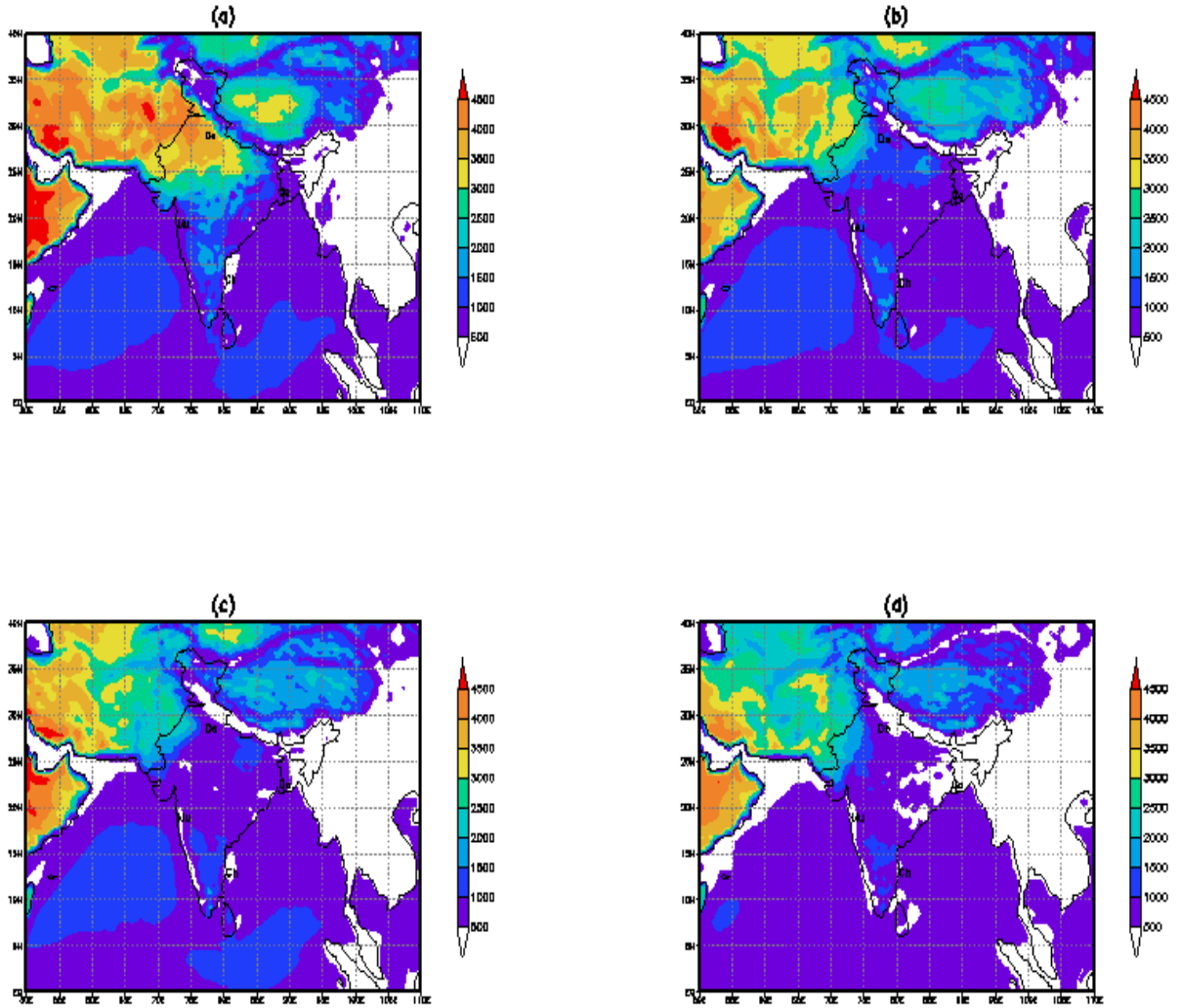


Fig 1: Mean analysis of PBL height in T382L64 for (a) June (b) July (c) August and (d) September 2010

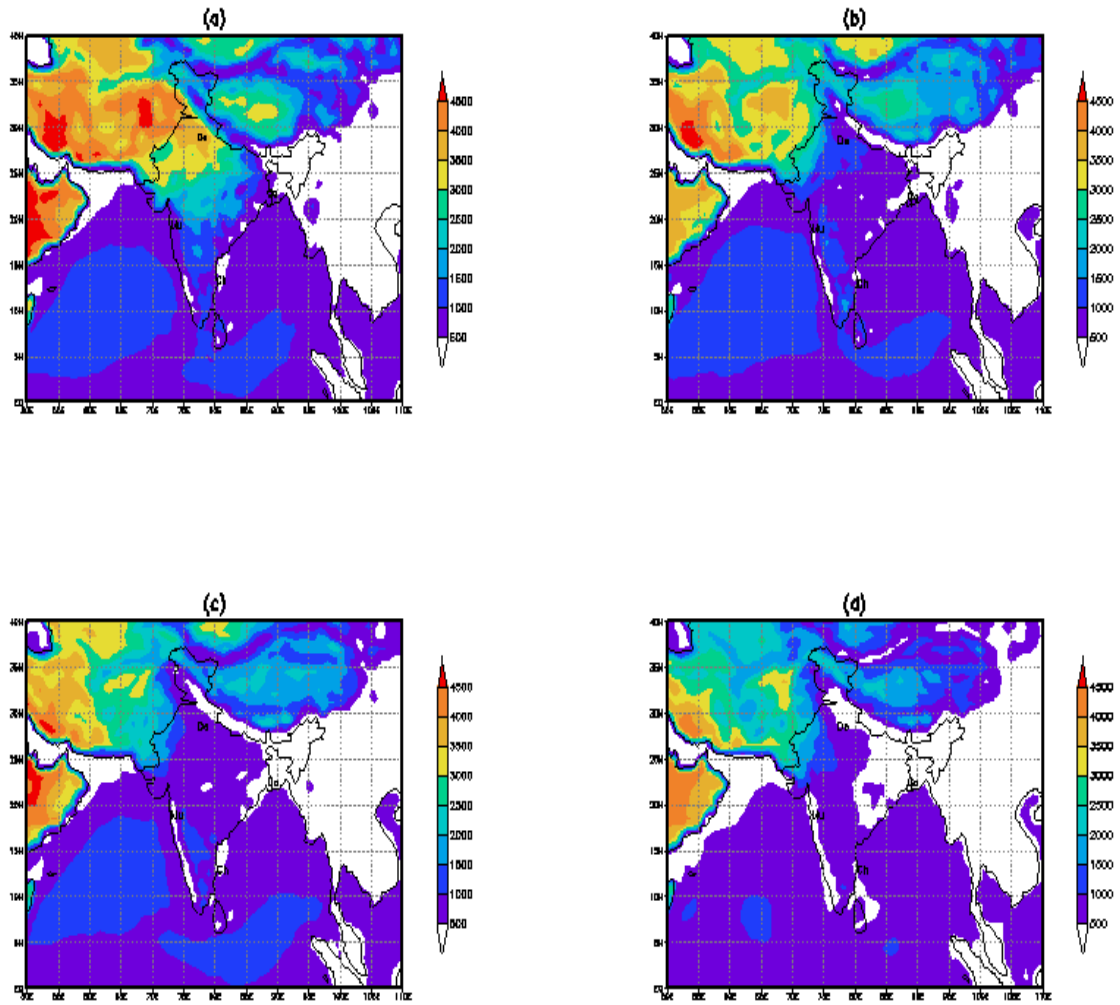


Fig 2: Mean Analysis of PBL height in T254L64 for (a) June (b) July (c) August and (d) September 2010

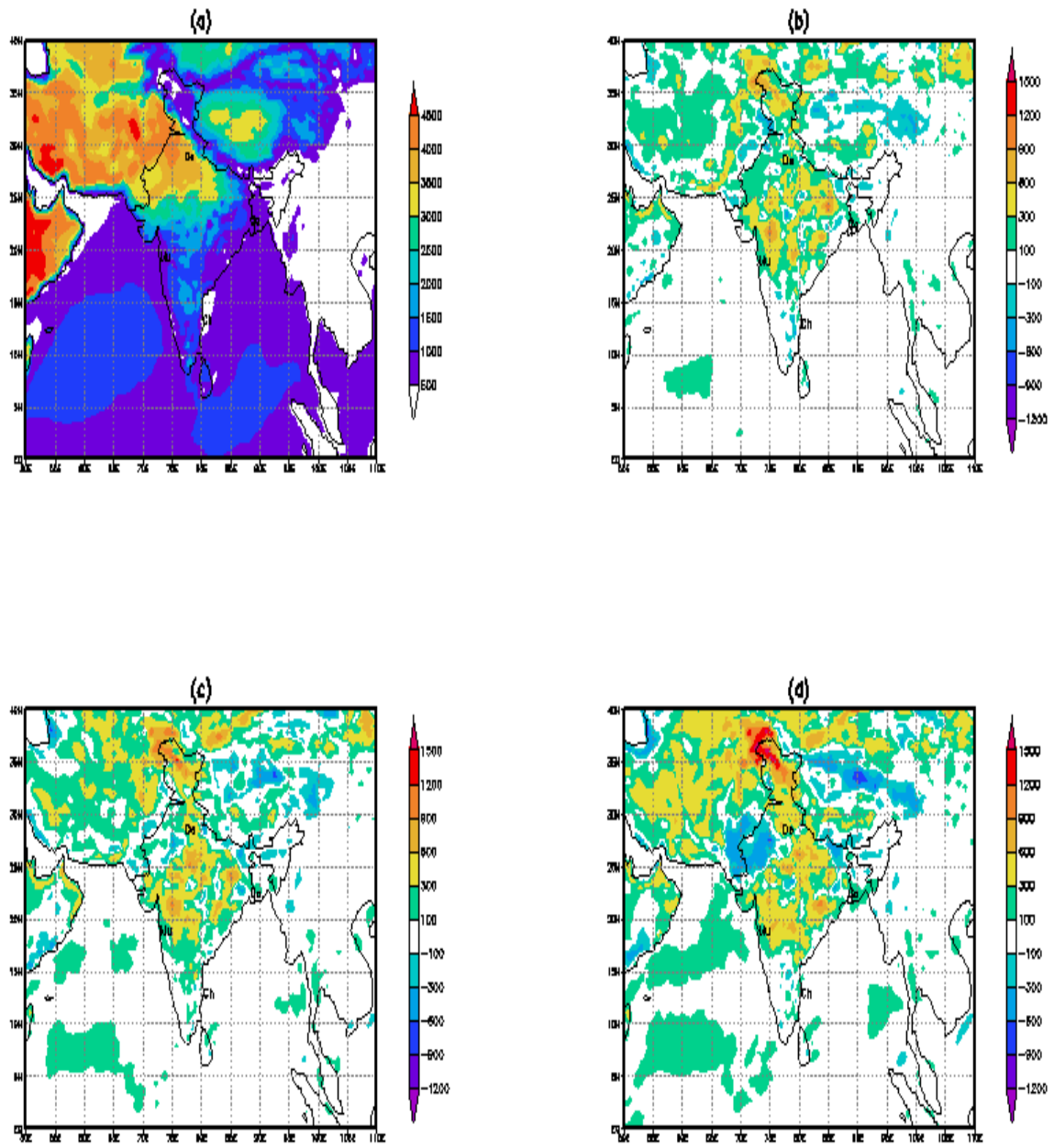


Fig. 3: Mean analysis (a) and difference between mean analysis and (b) 36 hr (c) 60 hr and (d) 108 hr mean forecasts for June 2010 for T382L64.

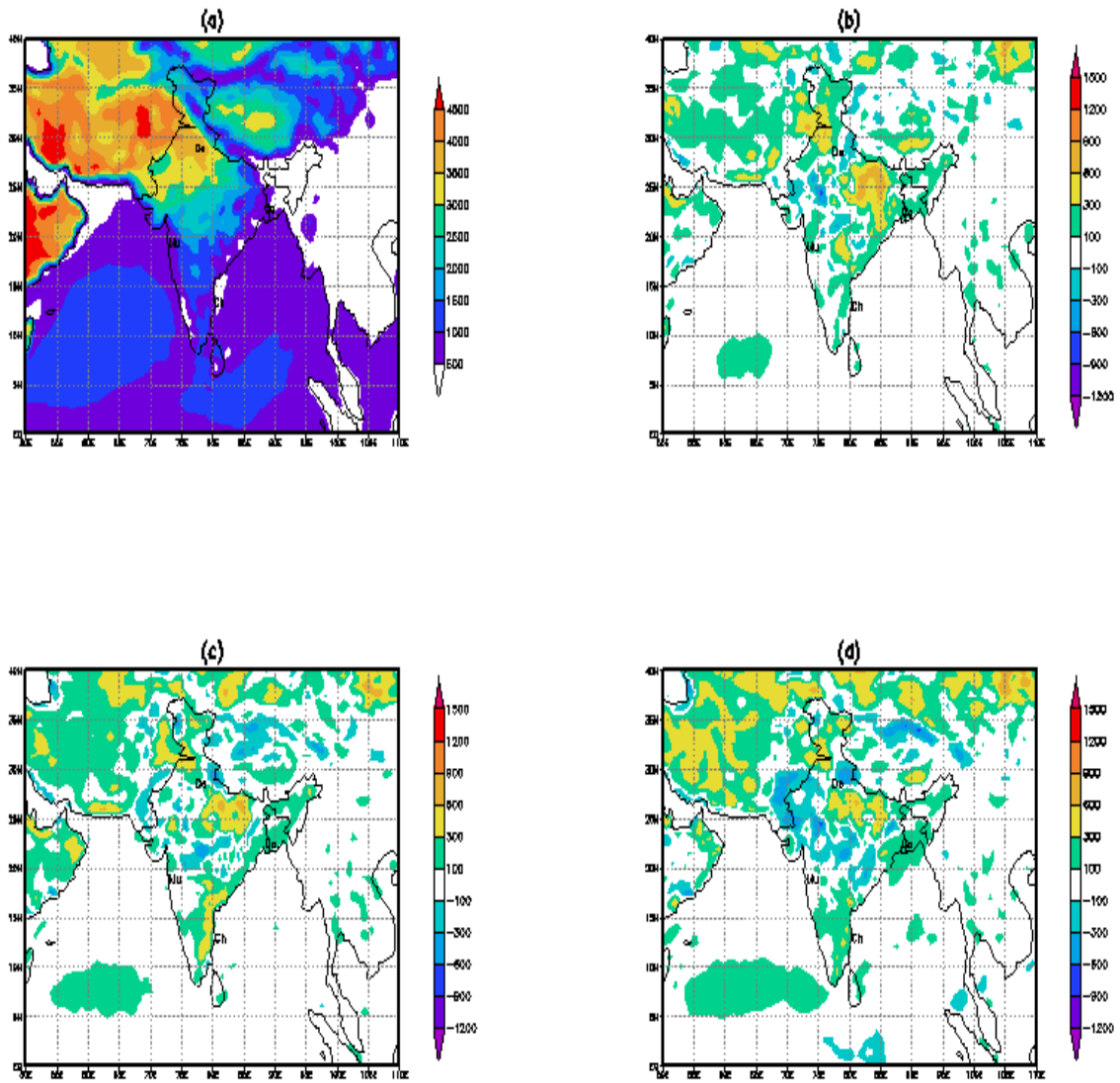


Fig. 4: Mean analysis (a) and difference between mean analysis and (b) 36 hr (c) 60 hr and (d) 108 hr mean forecasts for June 2010 for T254L64.

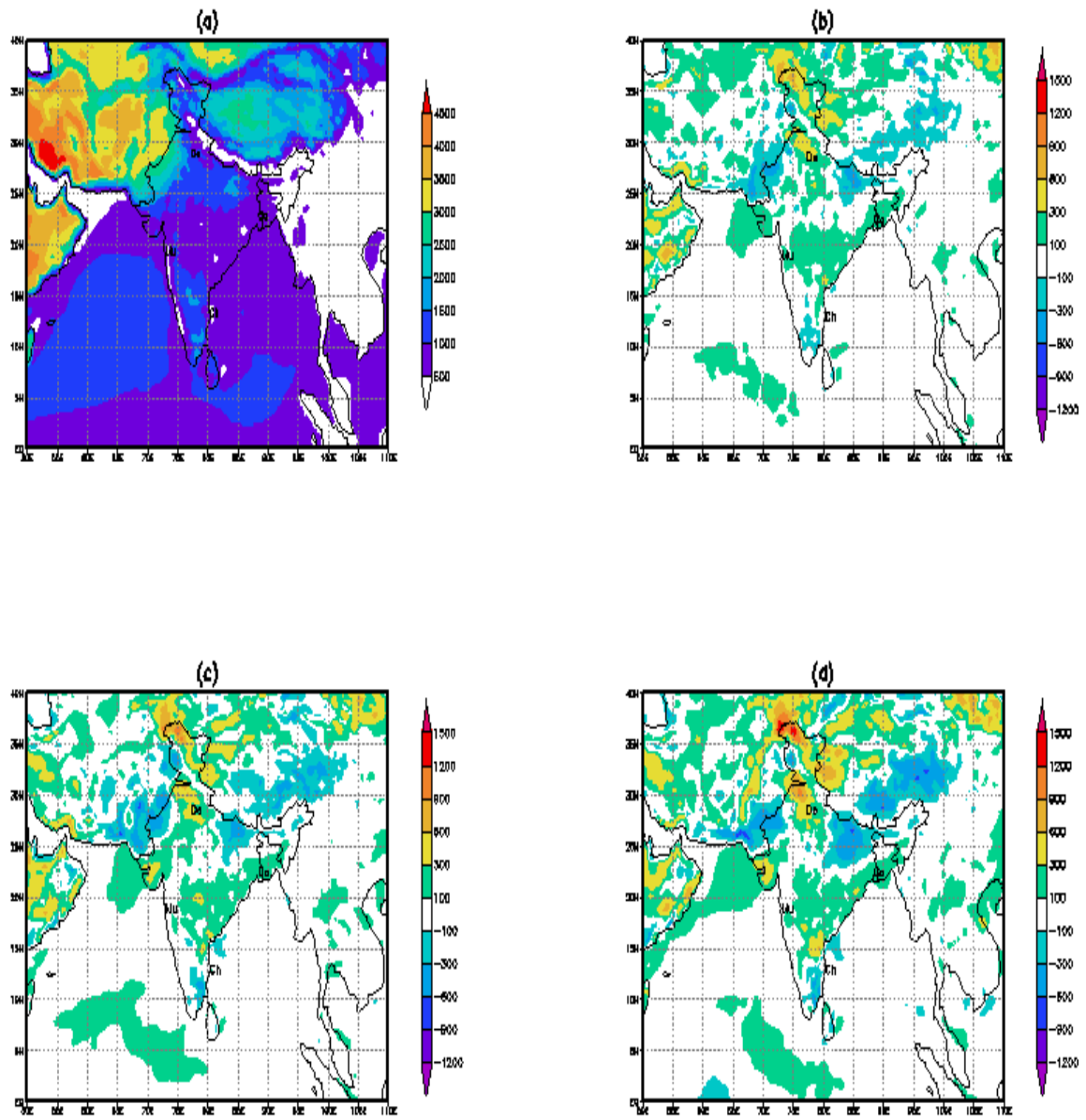


Fig. 5: Mean analysis (a) and difference between mean analysis and (b) 36 hr (c) 60 hr and (d) 108 hr mean forecasts for July 2010 for T382L64

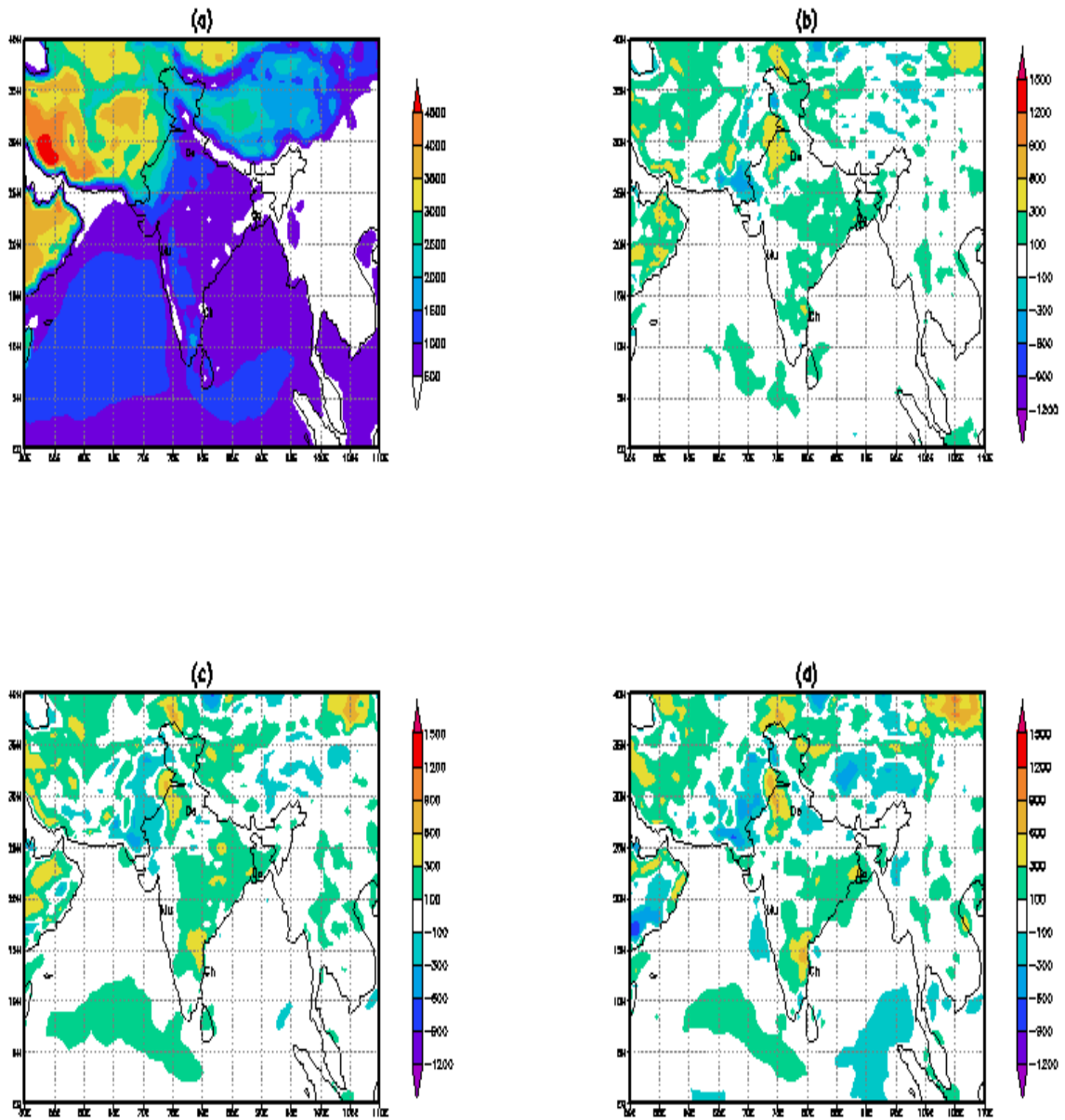


Fig. 6: Mean analysis (a) and difference between mean analysis and (b) 36 hr (c) 60 hr and (d) 108 hr mean forecasts for July 2010 for T254L64

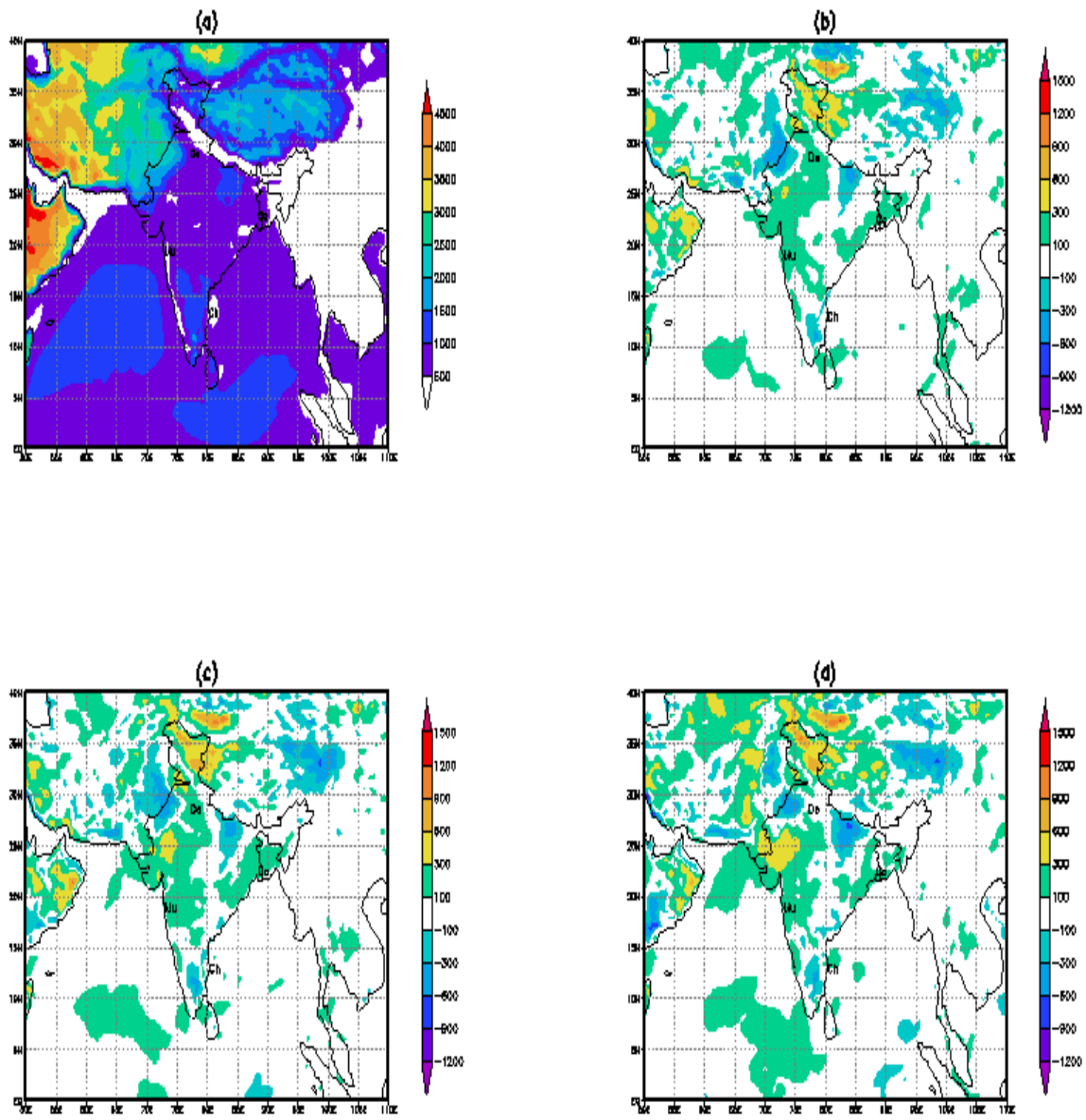


Fig. 7: Mean analysis (a) and difference between mean analysis and (b) 36 hr (c) 60 hr and (d) 108 hr mean forecasts for August 2010 for T382L64

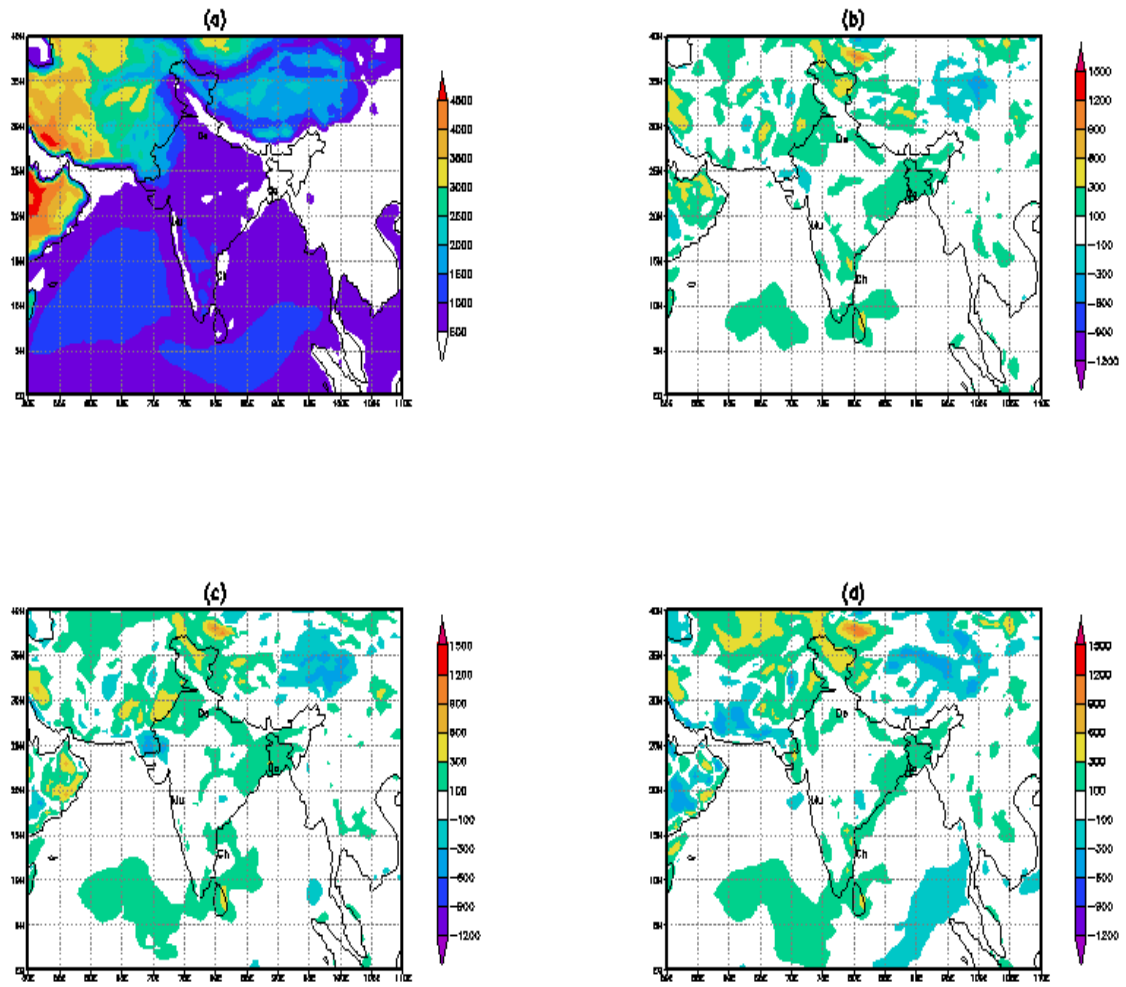


Fig. 8: Mean analysis (a) and difference between mean analysis and (b) 36 hr (c) 60 hr and (d) 108 hr mean forecasts for August 2010 for T254L64.

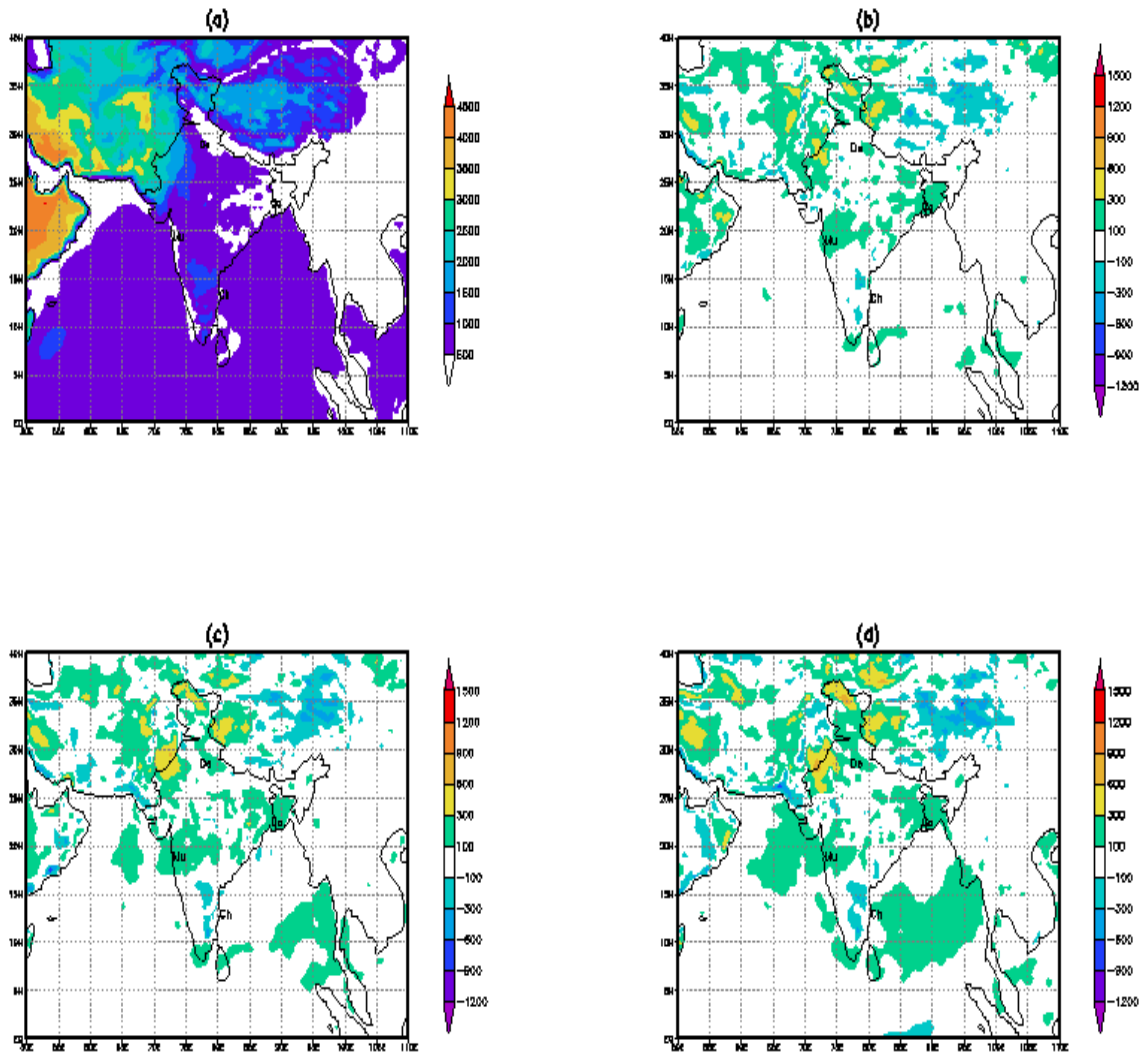


Fig 9: Mean analysis (a) and difference between mean analysis and (b) 36 hr (c) 60 hr and (d) 108 hr mean forecasts for September 2010 for T382L64.

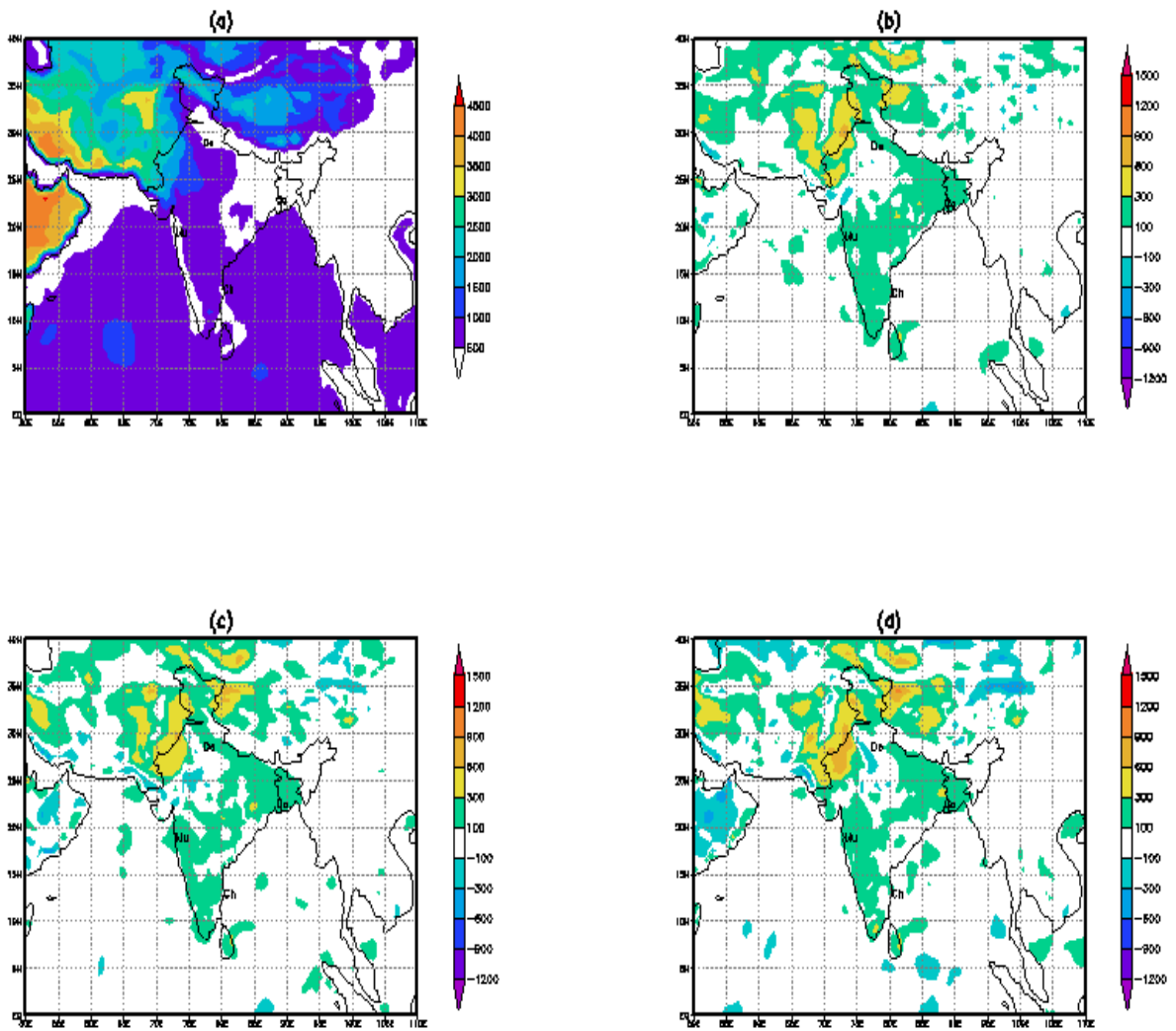


Fig 10: Mean analysis (a) and difference between mean analysis and (b) 36 hr (c) 60 hr and (d) 108 hr mean forecasts for September 2010 for T254L64.

9. Location specific weather forecast for major cities and districts of India and customized forecasts based upon T-254 and T-382 models and evaluation of forecast skills

Ashok Kumar, E.N.Rajagopal, J.V.Singh, Ranjeet Singh and Trilochan Patnaik

1. Introduction:

Location specific weather forecasts in medium range are extremely useful, as 3-5 days lead time is very essential for taking precautionary measures to save crops from bad weather in agriculture and managing other agriculture related activities.

The location specific weather forecast products are generated regularly based upon the NWP models operational at NCMRWF. Initially these products were based upon R-40, T-80 and T-170 models and now these forecasts are based upon T-254 general circulation model installed in January-2007. and T-382 general circulation installed in July-2010.

Over the years a fully operational location specific forecast system for agriculture was successfully developed on the basis of the T80L18 medium range weather forecasts. (Kumar et.al.,1996) Later on location specific weather forecast system was also developed based upon T-254 model and by monsoon 2008 it was operational for all the 127 agro advisory service units in India. The location specific weather forecasting for agriculture sector was transferred to the India Meteorological Department in 2008.

Besides this, two main location specific weather forecast products are generated every day, one is for major cities of India and other is for all the 602 districts of India and are put on NCMRWF website every day. These forecasts are easily accessible for media, general public, district authorities and farmers for planning their activities. These forecasts are obtained based upon T-254 and T-382 models. A detailed verification study for these forecasts is conducted at the end of each monsoon season and is found up to the mark almost every year. The forecast performance in monsoon 2010 is presented in the following sections.

Location specific forecasts also play an important role in managing different activities and resources in other sectors like mountain expeditions, sea expeditions, organizing games, resources in power sector, aviation and satellite launching. These forecasts are used for civil and military operations both. These special customized forecasts are issued as and when demanded by the various user departments. These forecasts had always been found matching well with the prevailing weather at the

place of work as per the information received at NCMRWF. The customized forecasts are demanded and well appreciated.

2 General circulation models(GCMs) used

A R-40 general circulation model with a resolution of $2.8^{\circ} \times 1.8^{\circ}$ was installed and made experimentally operational in 1989. The NCEP T80/L18 general circulation model is made operational in 1993 at NCMRWF. The horizontal resolution is spectral triangular truncation with 80 waves (T80). In physical space the horizontal resolution is of 256×128 grid size. This is roughly equivalent to $1.5^{\circ} \times 1.5^{\circ}$ latitude/longitude grid spacing. Forecast values are available at each time step which is 15 minutes. Hence for a particular day 96 forecast values are obtained and model is run for 7 days starting from 0000UTC initial conditions (Kumar *et. al.* 1999)

The NCMRWF T170/L28 Global Spectral Model was developed in-house, (Kar, 2002) and was made experimentally operational in 2002. It is based on the NCEP T80/L18 Model, (Kanamitsu, 1989), (Kanamitsu *et. al.* 1991), (Kalnay *et al.* 1990) and subsequent changes were made to the T80/L18 model at NCMRWF. Atmospheric dynamics are based on primitive equations with vorticity, divergence, logarithm of surface pressure, specific humidity and virtual temperature as dependent variables. In this model horizontal representation is spectral (spherical harmonic basis functions) with transformation to a Gaussian grid for calculation of nonlinear quantities and physics. The horizontal resolution is spectral triangular truncation with 170 waves (T170). In physical space the horizontal resolution is of 512×256 grid size. This is roughly equivalent to $0.7^{\circ} \times 0.7^{\circ}$ latitude/longitude grid spacing. The model has a comprehensive physics package which includes parameterisation schemes for cumulus convection, shallow convection, radiation, planetary boundary layer, surface processes and gravity wave drag due to mountains. The time integration scheme is semi-implicit. The time step is 7.5 minutes for computation of the dynamics and physics terms.

The NCMRWF T254/L64 Global Spectral Model is obtained from NCEP and is made operational at NCMRWF in January 2007, (Rajagopal *et. al.* 2007). The horizontal resolution is spectral triangular truncation with 254 waves (T254). In physical space the horizontal resolution is of 768×384 grid size. This is roughly equivalent to $0.5^{\circ} \times 0.5^{\circ}$ latitude/longitude grid spacing. The time step is 7.5 minutes for computation of dynamics and physics terms. The model has comprehensive parameterised physics package. T382/L64 Global Spectral Model is made operational

at NCMRWF in July 2010. The horizontal resolution is of 1152x576 grid size. This is roughly equivalent to 0.3125 x 0.3125 latitude/longitude grid spacing.

3. Direct model output(DMO) forecast

3.1 Nearest grid and interpolated forecast values

As the forecasts are obtained at gaussian grids and not at a particular location, hence the simplest way to get forecast at a specific location is to use the interpolated value from the four grid points surrounding it. But if the location is very near to a grid point, then the forecast at that grid point can also be taken as the forecast for the location. In order to decide as to which forecast among the two should be given more weightage for a location, it is necessary to know the distance of the location from the four grid points surrounding it. If the distance of the location from the nearest grid is less than one-fourth of the diagonal distance between any two grid points, then more importance is given to the nearest grid forecast values otherwise the interpolated value is considered, Fig 1(Kumar et.al.,1999).

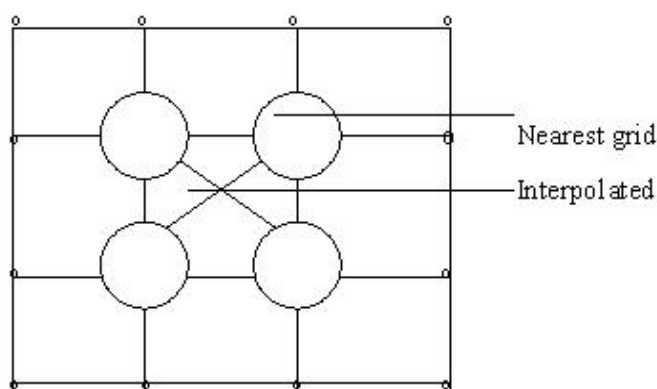


Fig. 1 Area considered around a grid point for deciding the relative importance of nearest grid and the interpolated DMO forecast values for a particular location.

3.2 DMO Forecast

DMO forecast values of both types i.e. nearest grid and interpolated, for each location of interest are obtained. Five day forecast for the following parameters is obtained by using every hour forecast values obtained from each time step values of 7.5 minutes for T-254 and T-382 models.

- Average Mean Sea Level Pressure (hPa)
- Cloud Amount (Morning and Evening) (okta)

- Rainfall (24 hours accumulated) (mm)
- Maximum Temperature(°c)
- Minimum Temperature(°c)
- Average Wind Speed (kmph)
- Predominant Wind Direction (deg)
- Maximum Relative Humidity (%)
- Minimum Relative Humidity (%)

Here, the validity of the forecast values for a particular day is for the subsequent 24 hours starting from 0003UTC(0830 hrs IST) of that day. As at NCMRWF earlier T-80 model and later on T-254 and T-382 models are run only for 7 days based on 0000UTC analysis, hence only the 24,48,72 ,96,120 hours forecasts are obtained.

The forecast thus obtained are biased and bias free forecasts are obtained for 70 major cities of India and all the districts of India, as explained in the following sections. The bias free forecasts are obtained fro the following weather parameters every day

- Rainfall (24 hours accumulated)(mm)
- Maximum Temperature (°c)
- Minimum Temperature (°c)

The meteograms are also obtained for the metropolitan cities, other important major cities every day and as and when required for the customized forecasts. In meteograms every six hourly accumulated rainfall values and six hourly wind speed and wind direction values are shown , besides this every time step or every hour values are also plotted for mean sea level pressure, maximum temperature and minimum temperature(Fig.2)

4. Bias free rainfall and Kalman filtered temperature forecast

The systematic error(bias) free forecast is obtained by using the direct model output obtained from the T-254 and T-382 general circulation models during monsoon 2010.

4.1. Bias free rainfall forecast

An optimal rainfall threshold value is set to maximise the skill score. The optimal threshold value means that if the forecasted rainfall amount is less than the threshold then the forecasted value is taken as a zero otherwise it is taken as the forecasted rainfall amount(Maini.. *et. al.* 2002). The optimal threshold is calculated as follows:

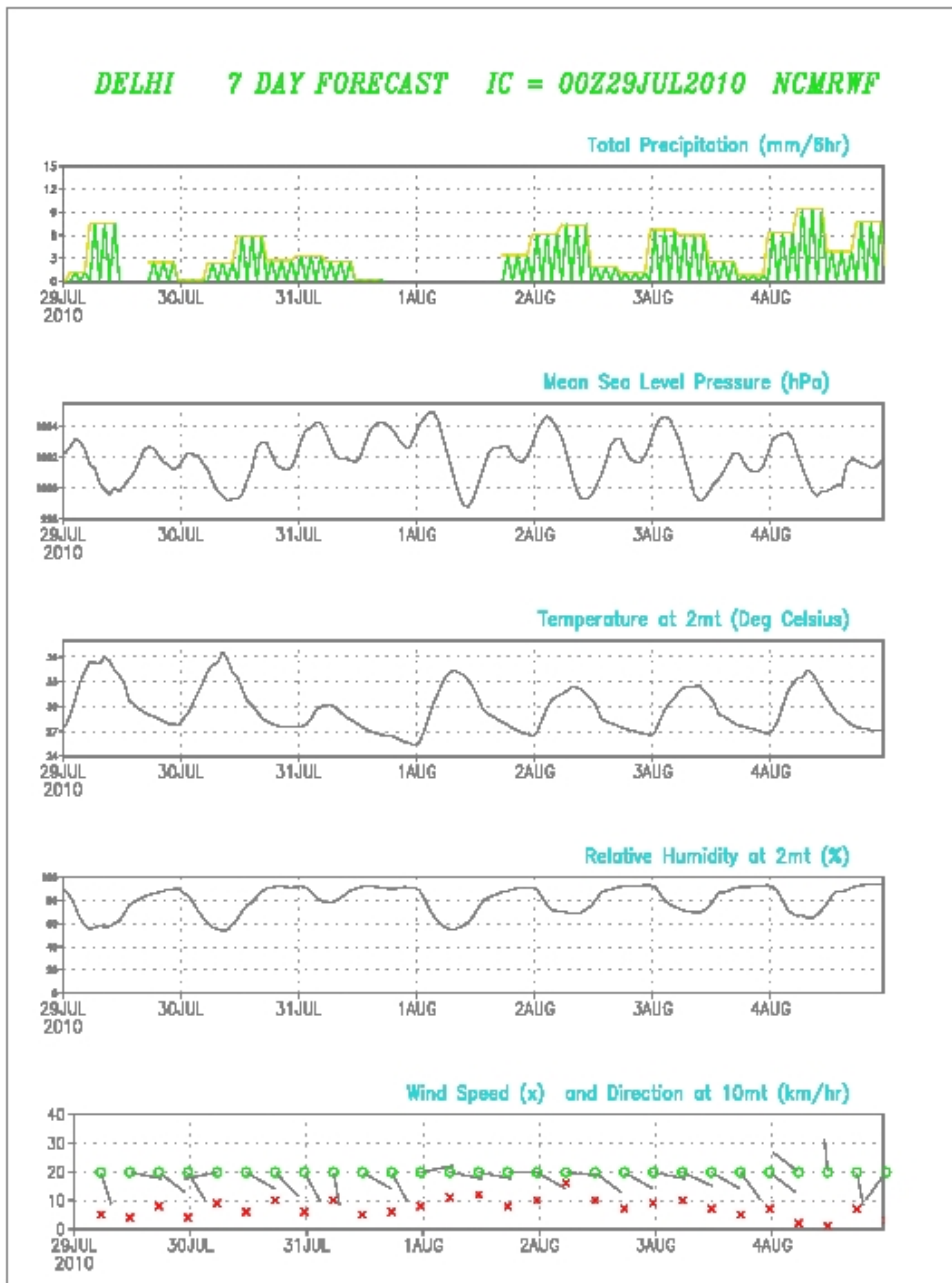


Fig 2. The meteogram for Delhi showing seven day forecast based upon initial condition of 0000UTC of 29 Jul. 2010.

Let the forecasted rainfall series during the seasons considered is denoted as R_{fi} , $i = 1, 2, \dots, n$. and Th be the threshold up to which the rainfall is taken as zero and beyond the Th value rainfall is taken as the actual value .

Then using the Th value forecasted YES/NO rainfall series is derived from the forecasted rainfall series as

if $R_{fi} \leq Th$ then no rain case i.e. 0(or N) case

and if $R_{fi} > Th$ then rainfall case i.e. 1(or Y) case

i.e value of 1(or Y) is taken for rainfall case and value of 0(or N) for no-rain case.

Similarly let the observed rainfall series during the seasons under consideration is denoted by R_{oi} , $i = 1, 2, \dots, n$; and threshold value as 0.1 mm and the observed YES/NO rainfall series is derived from the observed rainfall series using the similar logic.

As scores used for verification of the rainfall forecast are the ratio score and Hanssen and Copiers(H.K) skill score. Hence HK skill score is calculated by using the observed and forecasted YES/NO rainfall series based upon the data from the previous 2 to 3 seasons. Then HK skill score is maximized by varying the threshold(Th) value used for deriving forecasted YES/NO rainfall series. This threshold value which maximizes the HK skill score during previous seasons is applied for deriving YES/NO rainfall forecast from the DMO rainfall forecast during the current season. In the present study the thresholds correction factors are calculated based upon monsoon season (June, July, August and September) of 2003 for T-80 model. These thresholds correction factors are also calibrated and verified further using the monsoon 2005 and 2006 data for T-80 and T-170 models and these are further calibrated using monsoon 2007 and 2008 data and are used for T-254 and T-382 models. These threshold correction factors are explained further in section 5.

4.2. Basis of Kalman filtered temperature forecast (Anders o.Persson,1991)

It is a common fact that NWP models exhibit systematic errors in the forecasts of the near surface weather parameters. The 2m-temperatures for example are often systematically biased, though the magnitude of the bias varies with geographical location and time of the season. Such systematic errors may not only be due to short comings in the model but also depend on the sub-grid location of the station. Individual mountains or different parts of a large city with their specific climate can hardly be fully resolved in any NWP model.

Mathematically a correction formula for a given station and for the specific lead time can be formulated as

$$Y = X1 + X2 * \text{Temp. forc.}$$

If X1 and X2 were constant over the seasons they could be computed with good accuracy by linear regression techniques. To avoid storage of old data a recursive regression technique could be used applying weights to make more recent data have a larger impact. X1 and X2 would then reflect more recent conditions. However, in a pure statistical sense this method is only a way to smooth the data, the weights pushing the emphasis towards a more recent time. In contrast to smoothing, filtering techniques actually try to estimate today's value, in light of historical data. Thus a simple one parameter Kalman filter can be applied for removing the systematic errors in the temperature forecasts (Rashmi et al. 2009).

4.3. Kalman filter equations

The Kalman filter consists of two sets of equations, the observation equations and the system (or prognostic) equations.

The observation equation:-

Let TFC(τ) be the forecasted value and the verifying observation TOBS(τ) at a certain location and time of the year τ .

The observed forecast error is then

$$\text{TFC}(\tau) - \text{TOBS}(\tau) = Y(\tau) \quad \text{-----}(1)$$

Where Y(τ) is the time varying bias and can be assumed to be a stochastic variable, which contains noise, i.e. factors that we can not describe: errors in synoptic part of the forecast, deficiencies in the physical parametrization and unexplained small scale disturbances.

$$Y(\tau) = X1(\tau) + v(\tau) \quad \text{-----}(2)$$

Where X1(τ) is the applied correction and v(τ) is the unexplained, non-systematic noise. A part of this noise might be explained by another statistical model e.g. containing more predictors. For example the bias might seem to be dependent on the forecasted parameter, TFC(τ) or function of it:

$$Y(\tau) = X1(\tau) + X2(\tau) * \text{TFC}(\tau) + v(\tau) \quad \text{-----}(3)$$

(2) and (3) are examples of observation equations, since they relate the observed errors to the statistical error model. If there is only a bias in the forecasts, then X2 = 0. If there are only non-systematic errors both X1 and X2 will be = 0.

The System (or prognostic) equation:

So far we have only considered the static part of the Kalman filter. The “clue” of the Kalman filter is a second stochastic and dynamic model that tries to describe the time evolution of the model coefficients $X(\tau)$ in the form

$$X(\tau+1) = A(\tau)*X(\tau) + u(\tau) \text{ -----(4)}$$

Where $A(\tau)$ is a time dependent transition matrix, known a priori, describing how X evolves from one time period to the next during the season and $u(\tau)$ is a stochastic variable describing the “model noise”, i.e. those part of the model development we do not know a priori.

Since we do not know the “ideal” coefficients $X(\tau)$ and $u(\tau)$, we have to make estimates: $\hat{X}(\tau/\tau)$ and $e(\tau/\tau)$ is the corresponding co-variance of X .

In our applications $A(\tau) = 1$ for all times τ , because we lack any theory (or even empirical formulas) describing how the coefficients develop over time. In other words, we will apply estimates valid “today” as a forecast some days ahead.

All changes in X will in our examples be due to random /unexplained variations due to the noise $u(\tau)$. Both $v(\tau)$ and $u(\tau)$ as well as $e(\tau/\tau)$ are supposed to be normally distributed and uncorrelated with means 0(white noise) and standard deviations $D(\tau)$, $C(\tau)$ and $Q(\tau)$ respectively.

4.4. Kalman filter forecast

The estimates for the standard deviations is obtained based upon the data for past 30-40 days and in turn the estimates for $X_1(\tau)$ and $X_2(\tau)$ are obtained and the same estimates are used for getting the prediction for forecast error in the temperature for the next day as per the following equation;

$$Y(\tau) = X_1(\tau) + X_2(\tau)*TFC(\tau)$$

and the systematic error free temperature is forecasted.

5. Bias free rainfall and trend based temperature forecast

The direct model output forecast used for this was the forecast obtained T-170 earlier and T-254 model presently..

5.1. Bias free rainfall forecast

The technique used for getting bias free rainfall forecast is explained in section 4. The threshold values obtained here are for the forecasts obtained from T-254 and T-382 models and these are given in Table 1. These threshold values are representative of a region and are obtained as the most probable value for the stations in a particular region(Rashmi *et.al.* 2007).

5.2. Trend based temperature forecast

Let $T_f(I)$ and $T_o(I)$ be the forecasted and observed temperatures($^{\circ}C$) respectively on day I ($I = 1, \dots, n$), where n is the number of observations considered during the season. Let $T_f(I)$ and $T_o(I)$ for $I = 1, \dots, n$, are having positive correlations. Forecasted temperature values are for 24, 48, 72 and 96 hour forecast from T-170 & T-254 models.

If $Td_f(I)$ and $Td_o(I)$ are the forecasted and observed temperature trends respectively on day I ($I = 1, \dots, n$).

Then

$$Td_f(I) = T_f(I) - T_f(I-1) \quad \text{-----(1)}$$

$$Td_o(I) = T_o(I) - T_o(I-1) \quad \text{-----(2)}$$

Let Tb_f and Tb_o is the minimum value of the forecasted and observed temperatures considered respectively and Tb is the minimum of Tb_f and Tb_o . Then considering Tb as base value we can represent the forecasted and observed temperatures in terms of the new series of positive values as;

$$T_f(I) = Tb + c(I) \quad \text{-----(3)}$$

$$T_o(I) = Tb + d(I) \quad \text{-----(4)}$$

where $c(I)$ and $d(I)$ are positive for all I , $I = 1, \dots, n$ and are having positive correlations.

Then as;

$$\begin{aligned} \sum_{I=2}^n (Td_f(I) - Td_o(I))^2 &= \sum_{I=2}^n ((T_f(I) - T_f(I-1)) - (T_o(I) - T_o(I-1)))^2 \quad \text{(from 1 \& 2)} \\ &= \sum_{I=2}^n ((c(I) - c(I-1)) - (d(I) - d(I-1)))^2 \quad \text{(from 3\&4)} \end{aligned}$$

As $c(I)$ and $d(I)$ are +ve and having positive correlations, $I=1, \dots, n$. Hence it is expected that per unit rate of change in $c(I)$ and in $d(I)$ is expected to be same. Hence $(c(I) - c(I-1))$ and $(d(I) - d(I-1))$ are expected to be of same order and thus $((c(I) - c(I-1)) - (d(I) - d(I-1)))^2$ is expected to be less than or equal to $(c(I) - d(I))^2$, for $I=1, \dots, n$.

$$\begin{aligned} \text{Hence, } \sum_{I=2}^n (Td_f(I) - Td_o(I))^2 &\leq \sum_{I=1}^n (c(I) - d(I))^2 \\ &= \sum_{I=1}^n ((c(I) + Tb) - (d(I) + Tb))^2 \end{aligned}$$

$$= \sum_{I=1}^n (Tf(I) - To(I))^2 \quad \text{-----}(5) \quad \text{(from 3 \& 4)}$$

Hence from relation (5) it is clear that root mean square error for the observed and forecasted temperature trends is less than the root mean square error for the observed and forecasted temperatures having significant positive correlation (for samples of moderately large size from nearly-normal populations having significant positive correlation at a given level of confidence).

This simple relation is due to the NWP model's bias i.e. the tendency of the model to over predict or under predict the temperatures always. Hence if we use the temperature trends, such biases will get removed and will not contribute to the root mean square error.”

Hence the temperature trend forecast is obtained for maximum and minimum temperature for all the 602 districts of India based upon T-254 and T-382 models.. The user can add the present day temperature to the trends in order to get the temperature forecasts for the future days.

6. Customized forecast for user departments;

The customized forecasts had been continuously issued as and when demanded by the various user departments as per their requirements. In this direction following are worth mentioning.

- Forecast bulletins containing the forecast for rainfall, temperature, wind speed and direction had been issued along with the meteograms to various teams mainly from Army adventure wing, ITBP, National Institute of Mountaineering who had carried out expeditions to various peaks ranging from lower ranges to Mount Everest. (Fig. 3). This forecast had been issued since over last decade.

- Forecast bulletins containing the forecast for cloud, rainfall, temperature, wind speed and wind direction had been issued along with the vertical wind profile and meteograms to SHAR centre for satellite launching missions of ISRO like PSLV and GSLV. These forecasts had been issued for almost all such missions starting from the beginning.

- Forecast bulletins for location specific weather forecasts for India's first ever scientific expedition to South Pole were issued during November and December 2010.

- A forecast bulletin containing the general statements on weather systems and rainfall situation in general for Indian region and also for the different zones of the country along with the forecast table containing the objective forecast for cloud/rain, maximum and minimum temperature for 20 major cities had been continuously issued to media everyday including holidays, Saturdays and Sundays.

- Presentations during the map discussion or the statements by e.mail. in regard to forecasts from the NWP models operational NCMRWF, presently T-254 model, during the monsoon season, STORM project during pre-monsoon season and FDP-Cyclone during post-monsoon had been continuously made or sent to IMD.

- Last but not least is the district wise forecast for rainfall , maximum/minimum temperature , which is available on NCMRWF website and can be utilised by the district authorities and farmers for managing different activities at their end.

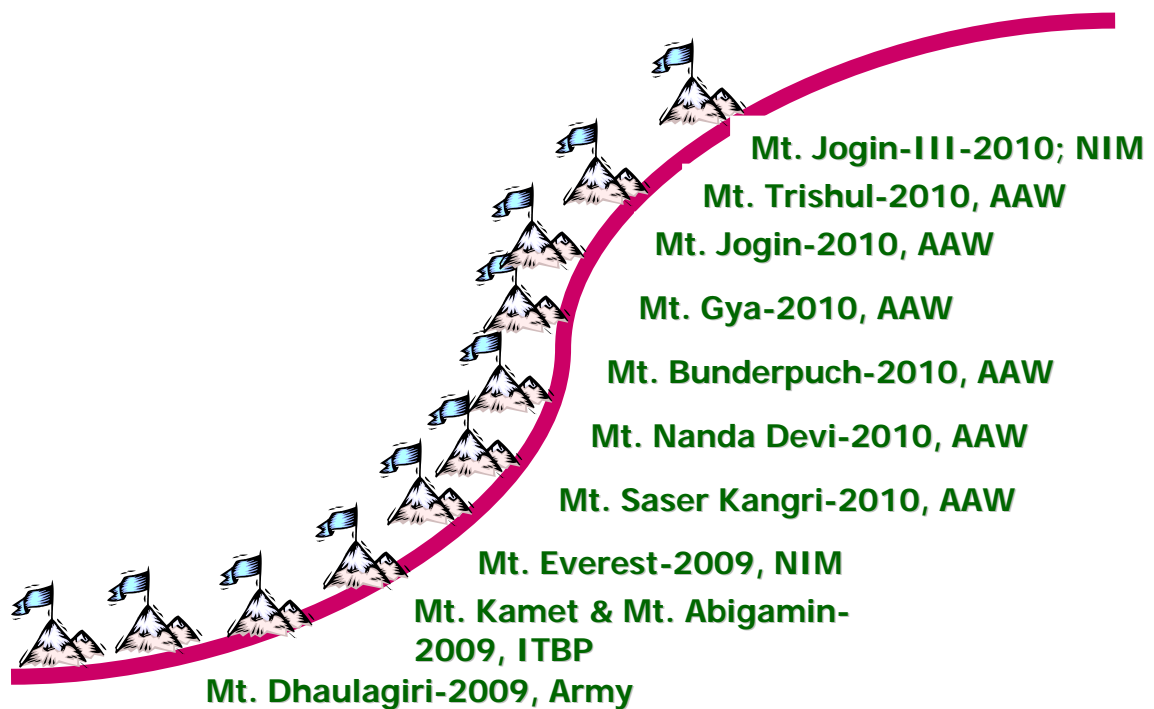


Fig. 3. NCMRWF's Customized Forecast for Mountaineering Expeditions

7. Verification of the forecast

7.1 Skill scores used for verification.

The scores used for verification of rainfall forecast are the ratio score and Hanssen and Kuipers(H.K) skill scores. The ratio score (RS) measures the percentage of correct forecasts out of total forecasts issued. The Hanssen and Kuipers' discriminant (HK) is the ratio of economic saving over climatology. H.K Score can be explained by the following contingency table.

Forecasted	Observed	
	Rain	No Rain
Rain	YY	YN
No Rain	NY	NN

$$\text{Ratio Score} = (YY+NN) / N$$

$$\text{H.K.Score} = (YY*NN-YN*NY)/(YY+YN)*(NY+NN)$$

If the H.K Score is closer to 1 then the forecasts are the best and when the H.K Score is near 0 or less than 0 then the forecasts are bad. In the case of MAX/MIN temperatures, cloud amount, wind speed and wind direction the correlation and RMSE values are calculated for evaluating the skill of the forecast.

7.2 Verification results(monson-2010)

For rainfall, minimum temperature and maximum temperature, the skill scores are calculated for bias free rainfall and Kalman filtered temperature forecast for selected major cities and for bias free rainfall and trend based temperature forecast for selected districts of India for which more data are easily available , these are a good sample representative of major cities and districts of India.

The skill scores for the 24,72 and 120 hr forecast using T-254 model output are given in Table 2 to Table 4 for major cities and for the 72,120 and 168 hr forecast using T-254 model output are given in Table 5 to Table 7 for selected districts of India.

The skill scores for the 24,72 and 120 hr forecast using T-382 model output are given in Table 8 to Table 10 for major cities and for the 72,120 and 168 hr forecast using T-382 model output are given in Table 11 to Table 13 for selected

districts of India.

The skill scores for day-3 forecasts using T-254 & T-382 models output for bias free rainfall and Kalman filtered minimum/maximum temperature are shown in Fig. 4. and that for bias free rainfall and trend based minimum/maximum temperature are shown in Fig. 5.

The skill scores are good in general. The skill for all the above mentioned forecasts decreases with prognosis hour. The skill of the forecast based upon T-254 is marginally better than that based upon T-382 model. As for maximum and minimum temperature, the correlations are comparatively less and root mean square error are comparatively more for T-382 model as compared to T-254 model for many stations. The skill scores for the forecasts for day-5 and more are giving high RMSE values especially for T-382 model as compared to T-254 model., this may be due to the problems of predicting the temperature in the tropics by using a high resolution model.

As per the information provided by the various user departments about the validity of the customized forecast issued from NCMRWF, the forecast has been reported as matching well with the prevailing weather and has been quite useful in taking strategic decisions by these departments.

8. Prospects and Future Plans:-

The forecast skill during monsoon 2010 is good in general.

There are some of the points which needs to be considered as the basis for future plans.

- District wise forecast is made operational for 602 districts, using the temperature trend and area wise estimates of the threshold value for rainfall starting from monsoon 2008 based upon T-254 model.

- Bias free forecast using kalman filter and threshold values for rainfall is obtained on operational basis for 70 major cities of India, using GTS data and T-80 initially and T-254 models output later respectively. Only last forty day data is being considered for every day run. This forecast gives the direct forecast value on a particular day, for next five days.

- The customized forecasts issued from NCMRWF had always been widely demanded and appreciated and reported to be quite useful in taking various strategic decisions by various user departments.

Following are some of the future plans;

- (i). MME forecast based upon different models for rainfall and cloud amount using Canonical variates and previous 2-3 seasons data.
- (ii) Kalman filter models based upon single best model for Max/Min Temp and Wind speed(or U & V),using online data for last 30 to 40 days for every day forecast.
- (iii) Kalman filter prediction models for rainfall based upon single best model using observed values of rainfall and forecasted values of directly related parametrical functions from NWP model using online data for last 30 to 40 days for every day forecast.
- (iv) SI forecast models based upon single best model for PoP and PoPT using previous five to six seasons data and Logistic Regression and Discriminant Analysis.

References

1. Anders O. Persson., 1991, "Kalman Filtering --- A new approach to adaptive statistical interpretation of Numerical Meteorological Forecasts" PSMP report series no. **34**, pp. XX-27 TO XX-30.
2. Ashok Kumar & Parvinder Maini 1996: Statistical interpretation of general circulation model: A prospect for automation of medium range local weather forecast in India. *Mausam (formerly Indian Journal of Meteorology, Hydrology & Geophysics)*., **47(3)**:229-236.
3. Ashok Kumar, Parvinder Maini & Singh, S. V., 1999: An operational model for forecasting probability of precipitation and YES/NO forecast. *Wea. and Forecasting*, **14**: 38-48.
4. Kalney E, Kanamitsu M, Baker WE. 1990. Global numerical weather prediction at the National Meteorological Centre. *Bull.Amer.Meteor.Soc.*,**71**,1410-1428.
5. Kanamitsu M. 1989. Description of the NMC global data assimilation and forecast system. *Weather and Forecasting*,**4**,335-342.
6. Kanamitsu M, Alpert JC, Campana KA, Caplan PM, Deaven DG, Iredell M, Katz B, Pan HL, Sela J,White GH. 1991. Recent changes implemented into the global forecast system at NMC. *Weather and Forecasting*, **6**, 425-435.
7. Kar SC. 2002. *Description of a high-resolution Global Model(T170/L28) developed at NCMRWF*. Research report, *NMRF/RR/1/2002*.
8. Maini, Parvinder, Ashok Kumar, Singh S V and L S Rathore, 2002: Statistical interpretation of NWP products in India. *Meteorol. Appl.*, **9** : 21-31.
9. Rajagopal, E.N., Munmun Das Gupta, Saji Mohandas, V.S. Prasad, John P. George, G.R. Iyengar and D. Preveen Kumar. 2007: Implementation of T254L64 Global Forecast System at NCMRWF, NCMRWF Technical Report No. NMRF/TR/1/2007.
10. Rashmi Bhardwaj, Ashok Kumar, Parvinder Maini, S.C. Kar and L.S. Rathore, 2007, 'Bias free rainfall forecast and temperature trend based temperature forecast based upon T-170 model during monsoon season' *Meteorological Applications* 14(**4**) ,pp 351-360.
11. Rashmi Bhardwaj , Ashok Kumar and Parvinder Maini, 2009, 'Evaluation of bias free rainfall forecasts and Kalman filtered temperature forecasts of T-80 model over Indian monsoon region, *Mausam*,**60**(2),pp 147-166.

Table 1**State specific threshold values for T-254/T-382 model rainfall forecasts**

SN	States/UT	Threshold rainfall values(mm) (T-254/T-382 model)
1	Andhra pradesh	5.0
2	Assam	2.0
3	Arunachal pradesh	2.0
4	Bihar	1.0
5	Chhatisgarh	2.0
	Gujarat	0.5
7	Haryana	1.0
8	Himachal pradesh	0.5
9	Jammu & Kashmir	0.0
10	Jharkhand	2.0
11	Karnataka	7.0
12	Kerala	7.0
13	Madhya pradesh	1.0
14	Maharashtra	2.0
15	Manipur	2.0
16	Meghalaya	2.0
17	Mizoram	2.0
18	Nagaland	2.0
19	Orissa	0.0
20	Punjab	1.0
21	Rajasthan	0.5
22	Sikkim	2.0
23	Tamil nadu	5.0
24	Tripura	2.0
25	Uttaranchal	0.5
26	Uttar pradesh	0.0
27	West Bengal	0.0
28	Delhi	1.0
29	Goa	2.0
30	Pondichery	2.0
31	Lakshdweep	7.0
32	Daman & Diu	2.0
33	Dadra & nagar	2.0
34	Chandigarh	1.0
35	Andaman & Nicobar	7.0

Table 2
Skill score for biasfree rainfall and Kalman filtered maximum and minimum
temperature; 24hr forecast; based upon T-254 model for major cities during
Monsoon (Jun.-Sep)-2010

Sn.	Station	Rain		Min		Max	
		Ratio	HK	RMSE	Corr	RMSE	Corr
1.	Ahmadabad	75	0.43	1.50	0.68	2.78	0.80
2.	Akola	73	0.48	1.88	0.68	3.20	0.73
3.	Allahabad	57	0.26	2.13	0.44	2.93	0.74
4.	Bangalore	63	0.26	1.11	0.22	2.51	0.56
5.	Bhopal	68	0.33	1.74	0.75	2.38	0.86
6.	Bhubaneshwar	67	0.19	1.36	0.49	3.40	0.45
7.	Coimbatore	75	0.16	1.17	0.54	2.24	0.62
8.	Dehradun	86	0.74	2.45	0.21	3.22	0.80
9.	Delhi	72	0.42	2.33	0.55	2.60	0.82
10.	Hisar	72	0.53	2.58	0.46	2.77	0.81
11.	Indore	69	0.38	1.57	0.71	2.79	0.76
12.	Jabalpur	61	0.22	1.87	0.62	3.12	0.77
13.	Jodhpur	77	0.55	1.79	0.70	3.54	0.67
14.	Jaipur	75	0.49	1.99	0.71	2.90	0.81
15.	Lucknow	68	0.36	2.25	0.32	3.43	0.60
16.	Mumbai	84	-0.08	1.81	0.23	1.84	0.56
17.	Nagpur	76	0.36	1.50	0.80	3.12	0.78
18.	Raipur	68	0.22	1.79	0.79	3.58	0.74
19.	Ranchi	68	0.27	1.25	0.75	2.18	0.80
20.	Udaipur	68	0.39	1.59	0.79	2.40	0.85
21.	Varanasi	59	0.27	2.19	0.58	3.02	0.66

Table 3
Skill score for biasfree rainfall and Kalman filtered maximum and minimum
temperature ; 72 hr forecast; based upon T-254 model for major cities during
Monsoon (Jun.-Sep)-2010

Sn.	Station	Rain		Min		Max	
		Ratio	HK	RMSE	Corr	RMSE	Corr
1.	Ahmadabad	80	0.56	1.71	0.67	3.09	0.71
2.	Akola	68	0.37	1.86	0.67	4.07	0.56
3.	Allahabad	63	0.35	2.73	0.39	3.25	0.61
4.	Bangalore	64	0.27	1.11	0.26	3.04	0.48
5.	Bhopal	70	0.37	2.32	0.60	3.54	0.73
6.	Bhubaneshwar	66	0.17	1.74	0.44	3.43	0.32
7.	Coimbatore	76	0.14	1.07	0.44	2.20	0.59
8.	Dehradun	84	0.56	2.69	0.15	3.42	0.73
9.	Delhi	71	0.39	3.58	0.34	3.89	0.70
10.	Hisar	68	0.38	2.91	0.31	5.04	0.57
11.	Indore	66	0.31	1.41	0.72	2.71	0.78
12.	Jabalpur	69	0.38	1.57	0.71	2.96	0.76
13.	Jodhpur	73	0.48	2.23	0.57	4.74	0.52
14.	Jaipur	73	0.45	2.83	0.62	3.11	0.82
15.	Lucknow	65	0.28	2.35	0.28	3.16	0.65
16.	Mumbai	89	0.23	1.97	0.14	1.88	0.53
17.	Nagpur	65	0.14	1.97	0.60	3.58	0.64
18.	Raipur	66	0.19	2.42	0.53	3.58	0.68
19.	Ranchi	67	0.24	1.71	0.62	3.02	0.64
20.	Udaipur	66	0.35	1.79	0.74	2.95	0.77
21.	Varanasi	63	0.33	1.76	0.55	2.93	0.76

Table 4
Skill score for biasfree rainfall and Kalman filtered maximum and minimum
temperature ; 120 hr forecast; based upon T-254 model for major cities during
Monsoon (Jun.-Sep)-2010

Sn.	Station	Rain		Min		Max	
		Ratio	HK	RMSE	Corr	RMSE	Corr
1.	Ahmadabad	73	0.44	1.92	0.62	4.01	0.67
2.	Akola	66	0.33	2.81	0.41	4.66	0.45
3.	Allahabad	59	0.29	2.29	0.52	4.73	0.35
4.	Bangalore	60	0.19	1.10	0.24	2.78	0.33
5.	Bhopal	65	0.25	2.14	0.62	3.40	0.70
6.	Bhubaneshwar	63	0.12	1.82	-0.04	3.87	0.00
7.	Coimbatore	75	0.10	1.22	0.21	2.73	0.31
8.	Dehradun	78	0.33	2.67	-0.02	3.43	0.68
9.	Delhi	71	0.39	3.38	0.31	5.81	0.57
10.	Hisar	60	0.24	2.76	0.23	5.93	0.52
11.	Indore	65	0.29	2.04	0.50	3.68	0.63
12.	Jabalpur	65	0.30	2.37	0.57	3.74	0.60
13.	Jodhpur	70	0.32	2.21	0.63	4.82	0.50
14.	Jaipur	69	0.38	2.08	0.70	2.70	0.83
15.	Lucknow	70	0.40	4.10	-0.09	3.62	0.50
16.	Mumbai	87	0.35	2.00	0.03	2.29	0.30
17.	Nagpur	75	0.32	2.69	0.42	4.27	0.55
18.	Raipur	70	0.27	2.51	0.59	3.38	0.64
19.	Ranchi	62	0.12	1.74	0.49	3.08	0.46
20.	Udaipur	61	0.24	1.84	0.73	3.28	0.74
21.	Varanasi	58	0.27	2.08	0.56	3.71	0.56

Table 5
Skill score for biasfree rainfall and trend based maximum and minimum
temperature; 72hr forecast; based upon T-254 model for selected districts during
Monsoon (Jun.-Sep)-2010

Sn.	Station	Rain		Min		Max	
		Ratio	HK	RMSE	Corr	RMSE	Corr
1.	Akola	64	0.32	1.40	0.79	2.85	0.80
2.	Allahabad	60	0.31	1.88	0.69	2.77	0.77
3.	Bhopal	65	0.26	1.68	0.71	2.86	0.82
4.	Chennai	54	0.08	1.52	0.35	3.48	0.30
5.	Delhi	72	0.41	1.69	0.74	3.39	0.74
6.	Hisar	62	0.32	2.06	0.69	3.70	0.73
7.	Hyderabad	69	0.19	1.33	0.69	2.91	0.67
8.	Gwalior	62	0.28	2.09	0.60	2.96	0.82
9.	Jabalpur	65	0.30	1.60	0.72	2.91	0.80
10.	Jammu	73	0.47	2.64	0.46	3.88	0.58
11.	Jaipur	68	0.35	2.06	0.72	2.96	0.83
12..	Lucknow	65	0.29	1.65	0.58	2.90	0.74
13	Ludhiana	67	0.39	1.97	0.62	4.19	0.55
14.	Madurai	53	0.07	1.22	0.48	2.50	0.48
15.	Mumbai	88	0.13	1.58	0.34	1.75	0.61
16.	Nagpur	77	0.38	1.55	0.79	3.36	0.74
17.	Pune	68	0.10	0.97	0.66	1.93	0.72
18.	Raipur	67	0.22	1.35	0.83	3.03	0.75
19.	Ranchi	65	0.20	1.11	0.76	2.30	0.79
20.	Udaipur	65	0.34	1.43	0.84	2.79	0.83
21.	Vishakhapatnam	62	0.17	1.28	0.54	2.30	0.47

Table 6
Skill score for biasfree rainfall and trend based maximum and minimum
temperature; 120hr forecast; based upon T-254 model for selected districts during
Monsoon (Jun.-Sep)-2010

Sn.	Station	Rain		Min		Max	
		Ratio	HK	RMSE	Corr	RMSE	Corr
1.	Akola	62	0.27	1.72	0.70	3.91	0.61
2.	Allahabad	59	0.29	2.09	0.57	3.44	0.67
3.	Bhopal	68	0.32	2.20	0.58	3.93	0.69
4.	Chennai	53	0.05	1.92	0.00	4.36	0.12
5.	Delhi	73	0.42	2.15	0.51	3.92	0.63
6.	Hisar	63	0.35	2.33	0.54	4.73	0.54
7.	Hyderabad	67	0.14	1.79	0.48	4.03	0.43
8.	Gwalior	61	0.28	2.63	0.41	3.49	0.76
9.	Jabalpur	65	0.30	2.20	0.54	3.88	0.65
10.	Jammu	63	0.26	3.10	0.31	4.15	0.51
11.	Jaipur	71	0.41	2.37	0.64	3.82	0.70
12..	Lucknow	65	0.29	1.94	0.39	3.50	0.66
13	Ludhiana	70	0.44	2.45	0.46	4.58	0.50
14.	Madurai	52	0.07	1.64	0.10	3.14	0.23
15.	Mumbai	88	0.33	1.96	-0.07	2.30	0.32
16.	Nagpur	70	0.23	1.65	0.76	3.74	0.65
17.	Pune	64	0.02	1.43	0.35	2.57	0.56
18.	Ranchi	65	0.18	1.34	0.68	3.13	0.56
19.	Raipur	71	0.30	1.74	0.72	3.45	0.69
20.	Udaipur	63	0.31	2.47	0.56	4.04	0.64
21.	Vishakhapatnam	61	0.14	1.63	0.22	2.96	0.21

Table 7
Skill score for biasfree rainfall and trend based maximum and minimum
temperature; 168hr forecast; based upon T-254 model for selected districts during
Monsoon (Jun.-Sep)-2010

Sn.	Station	Rain		Min		Max	
		Ratio	HK	RMSE	Corr	RMSE	Corr
1.	Akola	59	0.20	1.67	0.72	4.47	0.43
2.	Allahabad	58	0.29	2.19	0.53	3.43	0.67
3.	Bhopal	63	0.22	2.19	0.57	3.64	0.71
4.	Chennai	49	-0.01	1.90	0.07	3.99	0.12
5.	Delhi	68	0.32	2.43	0.46	4.45	0.57
6.	Hisar	61	0.29	2.80	0.30	5.27	0.41
7.	Hyderabad	66	0.15	1.89	0.37	3.75	0.45
8.	Gwalior	59	0.24	2.48	0.49	3.47	0.75
9.	Jabalpur	63	0.28	2.24	0.57	3.78	0.66
10.	Jammu	67	0.34	2.95	0.36	4.07	0.54
11.	Jaipur	62	0.24	2.73	0.53	4.41	0.59
12..	Lucknow	65	0.30	1.91	0.46	3.40	0.69
13	Ludhiana	62	0.30	2.74	0.30	5.20	0.27
14.	Madurai	58	0.19	1.43	0.22	3.54	0.17
15.	Mumbai	90	0.35	2.03	-0.13	2.39	0.24
16.	Nagpur	70	0.20	2.06	0.62	3.80	0.62
17.	Pune	66	-0.01	1.52	0.30	2.70	0.46
18.	Raipur	69	0.25	2.02	0.61	4.04	0.50
19.	Ranchi	65	0.17	1.42	0.59	2.79	0.61
20.	Udaipur	59	0.23	2.47	0.57	3.95	0.58
21.	Vishakhapatnam	54	0.01	1.58	0.24	2.82	0.13

Table 8
Skill score for biasfree rainfall and Kalman filtered maximum and minimum
temperature; 24hr forecast; based upon T-382 model for major cities during
Monsoon (Jul.-Sep)-2010

Sn.	Station	Rain		Min		Max	
		Ratio	HK	RMSE	Corr	RMSE	Corr
1.	Ahmadabad	79	0.17	1.79	0.12	3.06	0.47
2.	Akola	71	0.34	1.06	0.44	2.27	0.63
3.	Allahabad	56	0.08	2.92	0.17	4.49	0.33
4.	Bangalore	65	0.37	1.05	0.25	2.15	0.38
5.	Bhopal	65	0.05	1.46	0.26	2.27	0.54
6.	Bhubaneshwar	66	0.00	1.02	0.30	2.00	0.51
7.	Coimbatore	73	0.04	0.94	0.18	2.18	0.40
8.	Dehradun	90	0.15	1.97	0.50	3.63	0.52
9.	Delhi	74	0.30	1.67	0.61	4.01	0.40
10.	Hisar	68	0.38	1.70	0.56	3.34	0.56
11.	Indore	64	0.12	1.10	0.63	2.23	0.57
12.	Jabalpur	63	0.04	1.35	0.39	2.05	0.61
13.	Jodhpur	78	0.59	1.42	0.73	2.46	0.75
14.	Jaipur	72	0.27	1.65	0.65	2.95	0.62
15.	Lucknow	68	0.13	2.54	0.10	2.92	0.42
16.	Mumbai	95	-0.01	1.33	0.12	1.87	0.03
17.	Nagpur	79	0.06	1.73	0.14	2.60	0.47
18.	Raipur	73	0.00	1.37	0.45	2.20	0.56
19.	Ranchi	65	0.03	1.11	0.39	2.46	0.36
20.	Udaipur	67	0.26	1.30	0.59	2.31	0.64
21.	Varanasi	60	0.18	1.92	0.43	4.13	0.13

Table 9
Skill score for biasfree rainfall and Kalman filtered maximum and minimum
temperature; 72hr forecast; based upon T-382 model for major cities during
Monsoon (Jul.-Sep)-2010

Sn.	Station	Rain		Min		Max	
		Ratio	HK	RMSE	Corr	RMSE	Corr
1.	Ahmadabad	80	0.23	1.41	0.16	2.52	0.30
2.	Akola	65	0.28	1.30	0.28	2.35	0.54
3.	Allahabad	61	0.18	2.68	-0.02	3.90	0.18
4.	Bangalore	61	0.26	1.14	0.15	2.86	0.47
5.	Bhopal	65	0.12	2.31	0.22	2.46	0.51
6.	Bhubaneshwar	64	0.03	1.62	0.01	3.00	0.16
7.	Coimbatore	77	0.16	0.80	0.26	4.04	0.10
8.	Dehradun	89	0.65	2.45	0.28	3.51	0.42
9.	Delhi	73	0.28	2.32	0.35	3.56	0.41
10.	Hisar	70	0.41	2.25	0.40	3.73	0.46
11.	Indore	67	0.21	1.23	0.47	2.05	0.62
12.	Jabalpur	66	0.15	1.36	0.41	2.47	0.40
13.	Jodhpur	70	0.41	1.54	0.75	2.87	0.62
14.	Jaipur	65	0.16	1.71	0.57	2.40	0.67
15.	Lucknow	66	0.07	2.04	0.16	5.39	0.27
16.	Mumbai	95	0.57	1.56	-0.14	1.94	0.06
17.	Nagpur	75	0.09	1.61	0.30	3.07	0.30
18.	Raipur	70	0.02	1.52	0.17	2.74	0.38
19.	Ranchi	68	0.18	1.38	0.24	2.24	0.19
20.	Udaipur	71	0.37	1.79	0.21	1.93	0.59
21.	Varanasi	59	0.15	1.93	0.41	3.54	0.27

Table 10
Skill score for biasfree rainfall and Kalman filtered maximum and minimum
temperature; 120hr forecast; based upon T-382 model for major cities during
Monsoon (Jul.-Sep)-2010

Sn.	Station	Rain		Min		Max	
		Ratio	HK	RMSE	Corr	RMSE	Corr
1.	Ahmadabad	79	0.38	1.63	0.11	2.44	0.44
2.	Akola	60	0.18	1.86	0.08	4.45	-0.11
3.	Allahabad	54	0.05	1.65	0.34	2.99	0.23
4.	Bangalore	52	0.10	1.35	0.11	3.31	0.23
5.	Bhopal	70	0.26	1.83	0.27	2.49	0.45
6.	Bhubaneshwar	63	0.01	1.35	0.17	3.25	-0.19
7.	Coimbatore	80	0.23	1.01	-0.03	3.36	0.16
8.	Dehradun	79	-0.16	1.68	0.62	4.19	0.15
9.	Delhi	66	0.21	3.85	0.06	6.47	0.16
10.	Hisar	65	0.28	2.40	0.38	3.74	0.43
11.	Indore	63	0.18	1.31	0.58	3.07	0.03
12.	Jabalpur	67	0.18	1.54	0.41	3.04	-0.12
13.	Jodhpur	62	0.20	1.75	0.61	2.82	0.52
14.	Jaipur	67	0.28	1.67	0.60	3.52	0.49
15.	Lucknow	61	-0.04	1.71	0.36	4.11	0.12
16.	Mumbai	95	0.69	1.44	-0.01	1.89	0.07
17.	Nagpur	77	0.12	1.91	-0.04	4.21	0.13
18.	Raipur	74	0.17	1.75	0.11	3.44	0.09
19.	Ranchi	63	0.01	1.90	0.17	3.37	0.02
20.	Udaipur	65	0.27	2.31	0.08	2.79	0.40
21.	Varanasi	55	0.10	2.46	0.21	3.37	0.21

Table 11
Skill score for biasfree rainfall and trend based maximum and minimum
temperature; 72hr forecast; based upon T-382 model for selected districts during
Monsoon (Jun.-Sep)-2010

Sn.	Station	Rain		Min		Max	
		Ratio	HK	RMSE	Corr	RMSE	Corr
1.	Akola	54	0.14	1.31	0.83	2.73	0.83
2.	Allahabad	59	0.29	2.09	0.61	3.04	0.78
3.	Bhopal	68	0.31	1.60	0.73	2.63	0.85
4.	Chennai	54	0.10	1.56	0.37	2.80	0.40
5.	Delhi	73	0.43	1.86	0.71	3.50	0.74
6.	Hisar	53	0.12	2.55	0.49	4.45	0.56
7.	Hyderabad	68	0.11	1.63	0.52	3.75	0.44
8.	Gwalior	58	0.22	2.31	0.58	3.12	0.81
9.	Jabalpur	61	0.21	1.84	0.70	3.53	0.73
10.	Jammu	59	0.18	2.62	0.52	3.67	0.55
11.	Jaipur	60	0.19	2.58	0.61	3.76	0.71
12..	Lucknow	68	0.35	1.79	0.54	3.58	0.58
13	Ludhiana	64	0.34	2.15	0.60	4.13	0.57
14.	Madurai	61	0.21	1.30	0.45	3.01	0.39
15.	Mumbai	89	0.15	1.62	0.31	2.21	0.43
16.	Nagpur	74	0.22	2.00	0.69	3.44	0.71
17.	Pune	65	0.00	1.05	0.60	2.25	0.66
19.	Raipur	69	0.18	2.85	0.55	3.34	0.70
19.	Ranchi	65	0.16	1.24	0.73	3.25	0.62
20.	Udaipur	64	0.33	2.75	0.64	3.26	0.73
21.	Vishakhapatnam	58	0.03	1.34	0.51	2.71	0.39

Table 12
Skill score for biasfree rainfall and trend based maximum and minimum
temperature; 120hr forecast; based upon T-382 model for selected districts during
Monsoon (Jun.-Sep)-2010

Sn.	Station	Rain		Min		Max	
		Ratio	HK	RMSE	Corr	RMSE	Corr
1.	Akola	50	0.04	1.81	0.71	4.22	0.64
2.	Allahabad	59	0.30	2.21	0.61	3.85	0.71
3.	Bhopal	68	0.31	2.19	0.62	3.97	0.68
4.	Chennai	47	-0.05	1.81	0.05	3.29	0.18
5.	Delhi	75	0.46	2.54	0.58	4.13	0.65
6.	Hisar	59	0.33	2.45	0.58	4.62	0.66
7.	Hyderabad	67	0.04	1.30	0.71	3.76	0.57
8.	Gwalior	56	0.20	2.68	0.46	3.47	0.72
9.	Jabalpur	57	0.14	2.24	0.70	4.24	0.69
10.	Jammu	64	0.30	3.32	0.38	4.55	0.53
11.	Jaipur	71	0.43	2.59	0.69	3.70	0.76
12..	Lucknow	69	0.36	2.04	0.59	3.40	0.77
13	Ludhiana	69	0.43	2.33	0.51	4.47	0.53
14.	Madurai	61	0.17	1.65	0.10	3.61	0.11
15.	Mumbai	90	0.15	1.41	0.47	1.60	0.72
16.	Nagpur	67	0.08	1.99	0.75	3.63	0.74
17.	Pune	65	0.00	1.44	0.35	2.88	0.46
18.	Raipur	63	0.04	2.72	0.59	3.76	0.72
19.	Ranchi	65	0.16	1.40	0.73	3.72	0.56
20.	Udaipur	64	0.33	2.69	0.66	3.33	0.75
21.	Vishakhapatnam	57	0.02	1.65	0.22	3.26	0.33

Table 13
Skill score for biasfree rainfall and trend based maximum and minimum
temperature; 168hr forecast; based upon T-382 model for selected districts during
Monsoon (Jun.-Sep)-2010

Sn.	Station	Rain		Min		Max	
		Ratio	HK	RMSE	Corr	RMSE	Corr
1.	Akola	50	0.05	1.64	0.74	4.21	0.52
2.	Allahabad	57	0.27	2.67	0.59	3.95	0.67
3.	Bhopal	63	0.21	2.36	0.57	3.80	0.70
4.	Chennai	46	-0.08	1.91	-0.05	3.16	0.10
5.	Delhi	71	0.39	2.91	0.50	4.37	0.62
6.	Hisar	60	0.28	3.60	0.29	6.19	0.45
7.	Hyderabad	66	-0.01	2.08	0.24	5.18	0.30
8.	Gwalior	59	0.25	2.83	0.57	3.50	0.75
9.	Jabalpur	58	0.17	2.91	0.48	4.56	0.67
10.	Jammu	65	0.31	3.18	0.41	4.52	0.57
11.	Jaipur	65	0.31	3.12	0.58	5.08	0.59
12..	Lucknow	65	0.36	2.65	0.43	4.96	0.49
13	Ludhiana	65	0.36	3.17	0.32	5.05	0.40
14.	Madurai	59	0.07	1.62	0.10	4.06	0.00
15.	Mumbai	92	0.31	2.07	-0.15	2.46	0.32
16.	Nagpur	69	0.10	2.80	0.47	5.22	0.52
17.	Pune	66	-0.01	1.54	0.31	3.00	0.33
18.	Raipur	64	0.08	3.26	0.41	5.38	0.42
19.	Ranchi	58	0.01	3.00	0.33	4.91	0.35
20.	Udaipur	60	0.26	2.86	0.65	4.69	0.57
21.	Vishakhapatnam	59	0.07	1.55	0.27	3.30	0.12

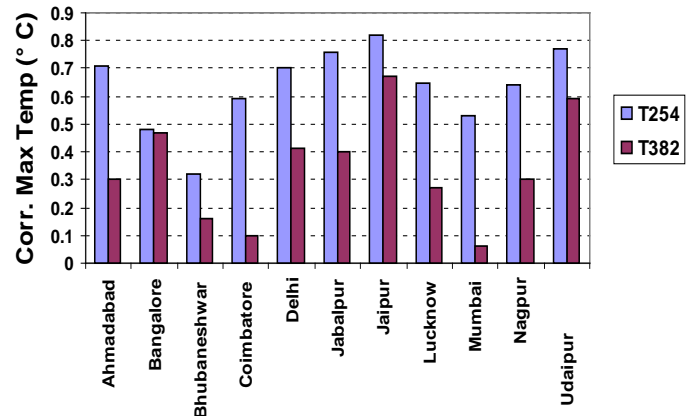
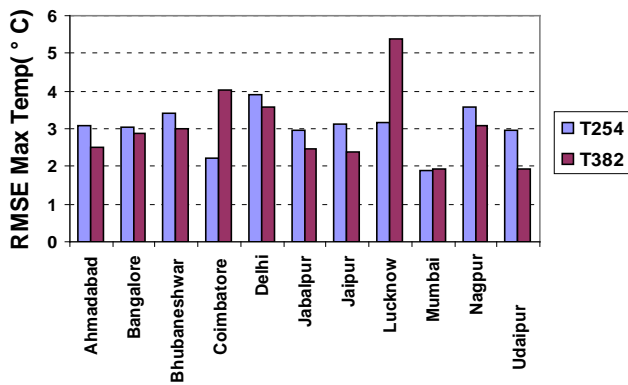
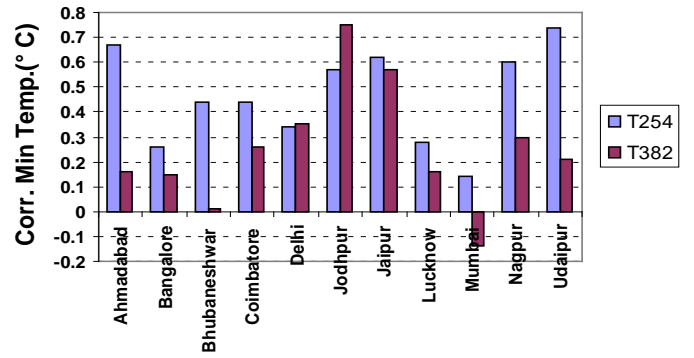
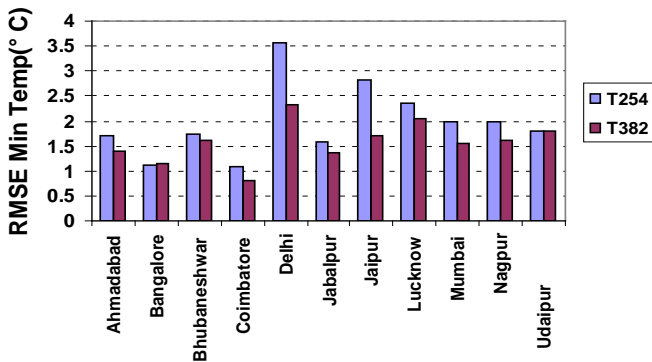
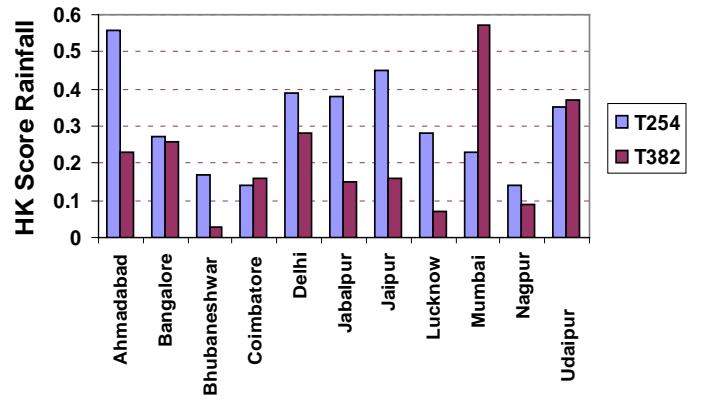
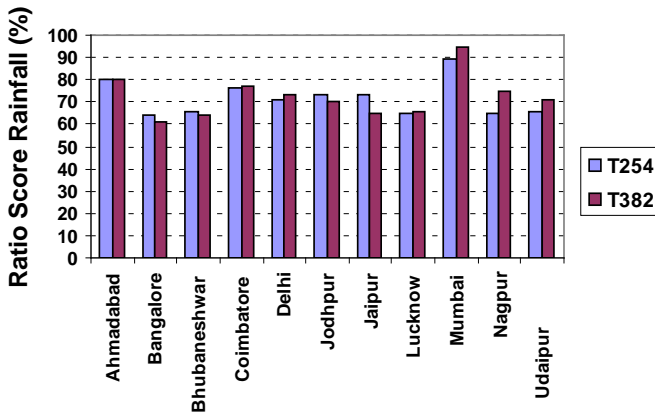


Fig-4. Skill scores for bias free rainfall and Kalman filtered minimum /maximum temperature for Day-3 forecast selected major cities of India.

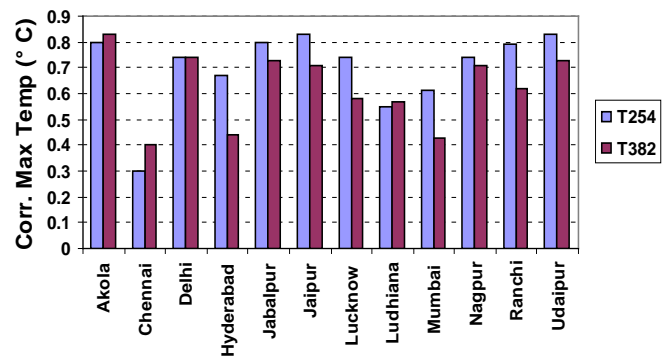
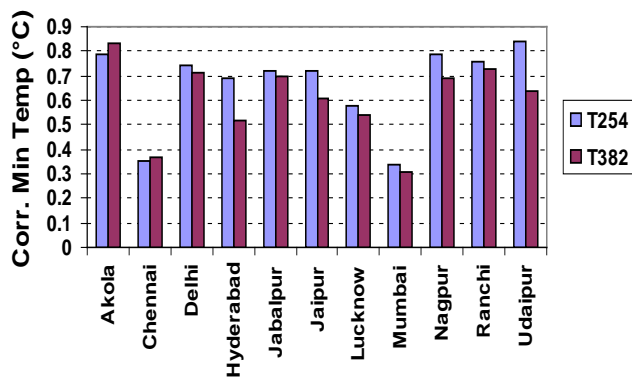
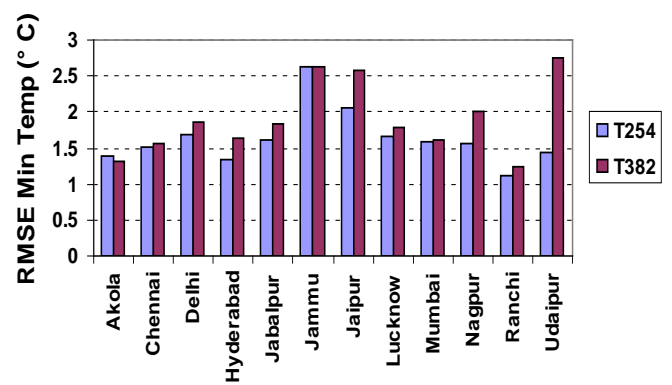
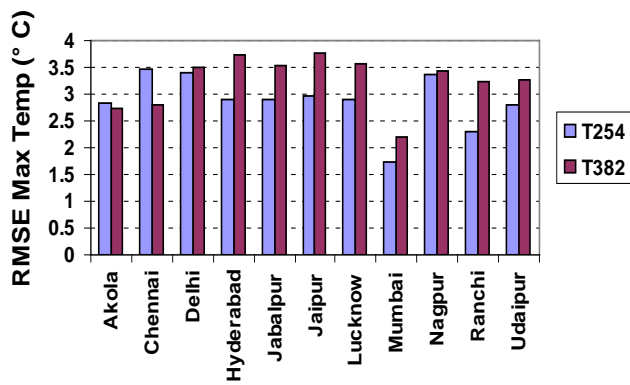
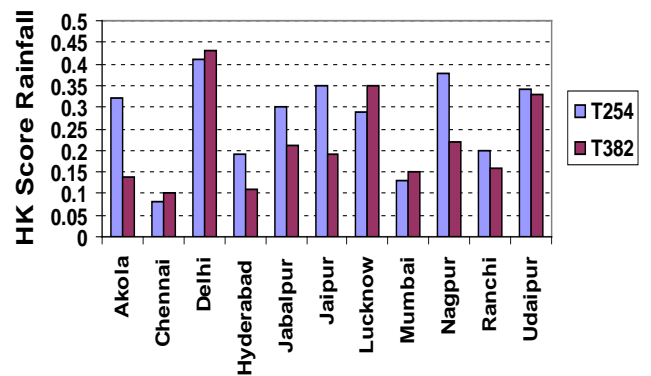
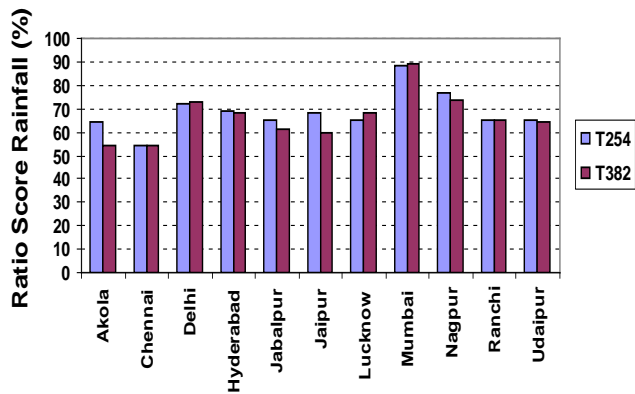


Fig-5: Skill scores for bias free rainfall and Trend based minimum/maximum temperature for Day-3 forecast of selected districts of India